Summer 2016

Modeling explosive lensing on a cylindrical body in air: A first step towards sealing an underwater offshore oil spill

Phillip R. Mulligan
Missouri University of Science and Technology, pmulligan@mst.edu

Department: Mining Engineering

MODELING EXPLOSIVE LENSING ON A CYLINDRICAL BODY IN AIR: A FIRST STEP TOWARDS SEALING AN UNDERWATER OFFSHORE OIL SPILL

By

PHILLIP RUSSELL MULLIGAN

A DISSERTATION

Presented to the Faculty of the Graduate School of the

MISSOURI UNIVERSITY OF SCIENCE AND TECHNOLOGY

In Partial Fulfillment of the Requirements for the Degree

DOCTOR OF PHILOSOPHY

In

EXPLOSIVES ENGINEERING

2016

Approved by

Dr. Jason Baird, Advisor

Dr. Paul Worsey

Dr. Grzegorz Galecki

Dr. Runar Nygaard

Dr. Braden Lusk

ABSTRACT

In 2010, the British Petroleum (BP) Deepwater Horizon accident leaked oil into the Gulf of Mexico for 87 days. A fast response method that can seal an oil pipe and stop the release of oil is needed in order to prevent future oil leaks from turning into ecological and financial disasters. Explosives can serve this need.

This research examined how a circular implosive discontinuous explosive lens interacts with a cylindrical surface. The following research was designed to study the applicability of the Method this author developed to predict the peak pressure from multiple shockwaves converging on a centrally located cylinder. This research also examined if multiple charges can impart a higher peak pressure or impulse on the centrally located cylindrical surface than a single charge of equal net weight. The experiments examined single charges in line with the signature sensor with various charge weights (0.2, 0.4, and 0.6 lb) and multiple 0.2 lb charges varying the number of charges (1-5) at different angular spacings (180, 120, 90, 60, and 40-degrees).

The Method developed throughout this research can be used to predict the pressure along the symmetry plane when $180 \geq \theta \geq 60$ degrees, for two and three 0.2 lb charges. The Peak Pressure Predictive Method is accurate to ± 4 percent. The techniques developed to predict the peak reflected pressure and impulse generated from multiple shockwaves converging on a cylindrical surface will aid in generating a rapid response system to help prevent underwater disasters similar to the Deepwater Horizon event.

ACKNOWLEDGMENTS

First and foremost, I would like to thank my wife and family for supporting me as I pursue my doctorate in Explosives Engineering. My wife Katie's love and support has been a motivation to me in more ways than she will ever know. My children's continued love and understanding of my efforts to complete my degree, will forever stay with me. My completion of this work is not only for myself, but also for them. I would also like to thank my parents and siblings for the constant encouragement

I would like to offer my sincerest gratitude to my advisor, Dr. Jason Baird, who has supported me throughout my education. I could not have completed this without his encouragement and patience. Professor Paul Worsey has been a consistent source of information and support. Without him, the testing and research could not have been completed. I would also like to thank my committee other members Dr. Galecki, Dr. Nygaard, and Dr. Lusk. Their insight, feedback, and advice was influential and essential throughout the dissertation-writing process.

I would like to than Crosstex Energy Services, LP for donating all of the cylinders used in this research. I could not have completed the testing without their help. Mike Basset was pivotal in the construction of the test material. John Tyler's innovative water jetting solutions were critical to mounting the sensors in the cylinders. Without the help of Kevin Phelps I would have had not been able to setup the test site. His sacrifice of time and effort enabled me to spend more time with my family and complete my test in a timely manner. Thank you Mike, John, and Kevin for all of your efforts. Thank you to Jimmy Taylor and Dewayne Phelps your continual support and encouragement inspired me to overcome the many obstacles that presented themselves throughout this research.

TABLE OF CONTENTS

Page

LIST OF FIGURES

Page

LIST OF TABLES

Page

NOMENCLATURE

b	Line perpendicular to cylinder surface
b'	Line tangent to cylinder surface
BP	British Petroleum
CONWEP	Conventional Weapon Effects Program
D	Cylinder diameter
D_1	Detonation velocity of material 1
D_2	Detonation velocity of material 2
Db	Decibels
DWG	Detonation Wave Generators
E_0	Ambient energy in material
E_1	Energy associated with the shockwave
EBW	Exploding Bridge Wire
EFP	Explosively Formed Projectile
EW	Effective Charge Weight
ft	Feet
I	Incident shockwave
L_0	Length the shockwave will travel in the material
L_1	Length the shockwave has traveled in the material
lb	Pounds
LSC	Linear Shaped Charge
M	Mach stem

ME	Model Error
MHz	Megahertz
Missouri S&T	Missouri University of Science and Technology
MRS	Midpoint Riemann Sum
n	Number of charges
NonEL	Non-Electric
$P_{\%}$	Percentage of reflected pressure
P_0	Ambient overpressure
P_1	Reflected pressure on cylinder surface
P_{AMP}	Pressure amplification
P_C	Pressure acting on a cylindrical surface along the symmetry plane
Pi	Incident pressure
P-I	Pressure-Impulse
P_M	Pressure from the Mach stem
P_R	Reflected pressure at signature sensor
PSI	Pounds per Square Inch
R	Reflected shockwave
Re	Reynolds Number
rho	Density of material
R_T	Line tangent to cylinder surface
S	Shockwave
sec	Seconds

u	Particle velocity
U_0	Ambient shockwave velocity = 0
U_1	Velocity of the shockwave
X,Y,Z	Axis orientation
Z_D	Scaled Distance
Z_i	Shock impedance
α	Angle between the charge plane and sensor location
β	3
θ	Angle from signature sensor to a point on the cylinder surface
θ_T	Angle from signature sensor to line tangent to cylinder surface
θ_W	Angle between horizontal plane and line tangent on cylinder surface
λ_H	Scaled height between the charge and the ground
λ_T	Scaled height of the Mach stem
λ_X	Scaled distance between the charge and the sensor
ρ_0	Density of the material prior to the shockwave interaction
ρ_1	Material density behind the shockwave
υ	Kinematic viscosity

1. INTRODUCTION TO MODELING EXPLOSIVE LENSING INTERACTION WITH A CYLINDRICAL SURFACE

This research examined how a circular implosive discontinuous explosive lens interacts with a cylindrical surface. The following research was designed to study the applicability of a symmetry plane peak pressure predictive method formulated throughout this research to predict the pressure associated with shockwaves from multiple charges converging on a centrally located cylinder. This research also examined if multiple charges can impart a higher peak pressure or impulse on the centrally located cylindrical surface than a single charge of equal net weight at the same standoff distance.

The models generated in this research will aid in predicting the peak pressure and total impulse associated with the shockwave wrapping around a cylindrical surface. Understanding the peak pressure and total impulse that multiple charges can impart on a cylindrical surface is a first step in developing a fast response system for accidents such as the Deepwater Horizon detailed below. This research serves as a platform for developing an underwater explosive lensing system that can be rapidly deployed in the event of future accidents, similar to Deepwater Horizon.

1.1. RESEARCH MOTIVATION TOWARD SEALING AN OFFSHORE UNDERWATER OIL SPILL

In 2010, the British Petroleum (BP) Deepwater Horizon accident released oil into the Gulf of Mexico for 87 days. Over the 87 days, 130 million gallons of oil were spilled into the Gulf of Mexico (Smithsonian Ocean Protal, 2015). In addition to the lost profits, BP incurred $44 billion in legal and cleanup costs (Wall Street Journal, 2015). The volume of oil released into the Gulf of Mexico is a result of the time it took to seal the leaking well. A fast response method that can seal an oil pipe and stop the release of oil is needed in

order to prevent future accidents from turning into ecological and financial disasters. Properly applied explosive charges can serve this requirement.

Using explosives as a method of sealing a leaking oil pipe is plausible; explosives have been utilized in the petroleum industry in the past to put out oil fires and perforate wells. Explosives are also used to conduct seismic exploration, rock blasting, and platform demolition. Additionally, researchers have shown cylinders can be collapsed by close proximity energetic events, but this research had not examined completely sealing a pipe.

1.2. EXPLOSIVELY DRIVEN PIPE COLLAPSE

Explosively driven pipe collapse is not a new concept. A number of researchers have examined the collapse of submerged cylinders in close proximity to an energetic event, but this research has primarily used the submerged cylinder to represent the hull of a ship. Sealing the pipe was not the focus of this type of research. An example of a submerged cylinder subjected to an energetic event can be seen in Figure 1.1; the collapse was the result of a 1-ounce explosive charge positioned 6 inches from the cylinder.

Figure 1.1. A collapsed aluminum cylinder subjected to 1-ounce of explosives at a standoff off 6 inches (Silva L. L. & Netto T. , 2010).

The resultant collapse is evident. In this experiment, Silvia and Netto were using the cylinder response to improve their modeling simulations. Sealing the cylinder was not the focus of the research. However, Figure 1.1 indicated that strategically placed charges might collapse the cylinder in a manner that would seal it.

In addition to cylinders in close proximity to an energetic event, cylinders surrounded by a contact charge have also been examined. A contact charge refers to a charge that is touching the cylinder, and the specific study referring to cylinders surrounded by contact charges is "The Collapse of Hollow Steel Cylinders by High Explosives," Neddermeyer (1943). This study examined different diameter cylinders surrounded by explosives. The cylinder thickness and explosive thicknesses were varied, and the results from one such experiment can be seen in Figure 1.2.

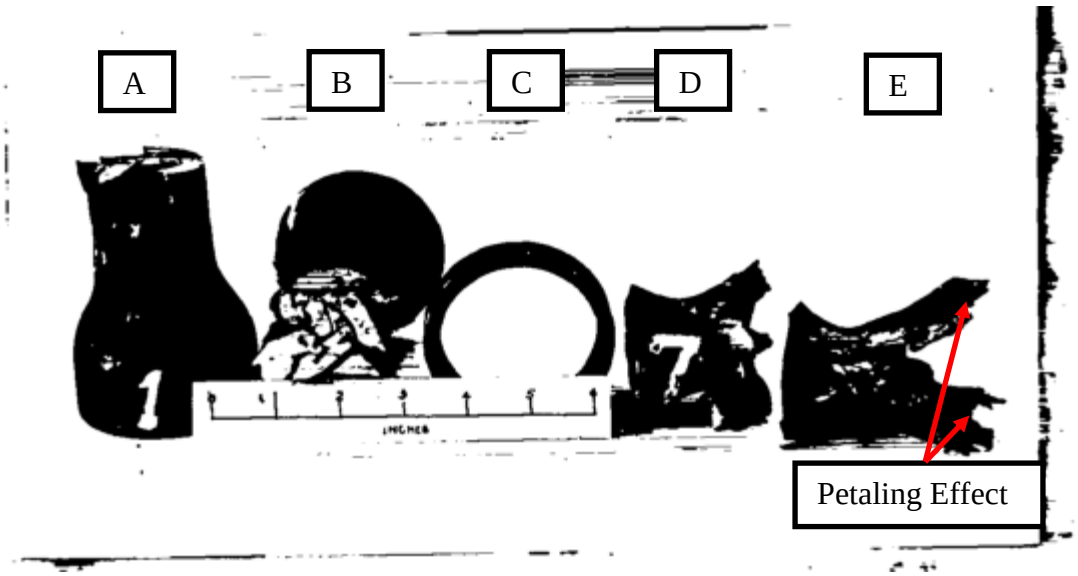

Figure 1.2. Results from three-inch diameter cylinders with 0.25-inch wall thicknesses surrounded by TNT 0.75 inches thick, three initiation points (S. Neddermeyer, H. Bradner, & J. F. Streib, 1943).

Typically, the cylinders in Neddermeyer's report suffered substantial damage. A petaling effect can be seen in Figure 1.2 A, B, D, and E. The damage observed in Neddermeyer's work indicates a standoff distance will be needed to seal the cylinder without damaging it. Therefore, this research examined a circular implosive discontinuous explosive lens focusing on a centrally located cylinder. The following section briefly explains what is explosive lensing. A more in depth description can be found in Section 2.4.2.

1.3. WHAT IS EXPLOSIVE LENSING?

An explosive lens changes the detonation wave produced by an explosive by changing the geometric conditions of the explosive (W. P. Walters, J. A. Zukas, 1989). An explosive lens can consist of air, an explosive of a different detonation velocity, and/or a metallic object imbedded into the explosive as a "wave shaper." Explosive lenses have been used in devices such as conical shaped charges (CSCs), linear shaped charges (LSCs), explosively formed projectiles (EFPs), and, most notably, the atomic bomb (Worsey, Explosive Lenses, 2012).

1.4. INFORMATION REQUIRED FOR DEVELOPING A RAPID RESPONSE SYSTEM TO SEAL AN UNDERWATER OFFSHORE OIL SPILL WITH EXPLOSIVE LENSING

Due to the complexity of sealing a cylinder underwater with explosive lensing, the process must be divided into logical steps. The steps listing in Table 1.1 were identified through the literature review process and deductive reasoning. While more steps are likely to exist, the steps listed in Table 1.1 provide insight into what is necessary to seal a cylinder underwater. The research presented herein focuses on Steps 1 and 2 in Table 1.1 (highlighted in green).

The first part of developing an explosive lensing configuration to seal a cylinder underwater is developing a configuration that will seal a cylinder in air. Developing an explosive lensing configuration to seal a cylinder in air will further define the shockwave interactions on the cylinder surface without confounding the data with the effects from the bubble dynamics or the Bjerknes force. The Bjerknes force is the force that attracts the bubble to an object (Microsystems, 2016).

Developing an explosive lensing configuration to seal a cylinder in air requires an understanding of how single and multiple shockwave interact with a cylindrical body with respect to peak pressure and impulse. Additionally, the cylinder's effect on the pressure and impulse associated with the shockwave traversing the cylinder surface must also be examined.

Future testing is needed to generate Pressure-Impulse (P-I) diagrams similar to Figure 1.3. These P-I diagrams should aim to identify the pressure and impulse combinations that induce different forms of cylinder damage. With a P-I diagram specific for the cylinder of interest the multiple shockwave and cylinder diameter information, previously discussed, can be used to develop an explosive lens to seal a cylinder in air.

After an explosive lens configuration to seal a cylinder in air has been identified, the process needs to be repeated underwater. This will allow for a comparison of the two media (air and water). The underwater testing will also enable the explosive lens to account for the bubble dynamics and Bjerknes force.

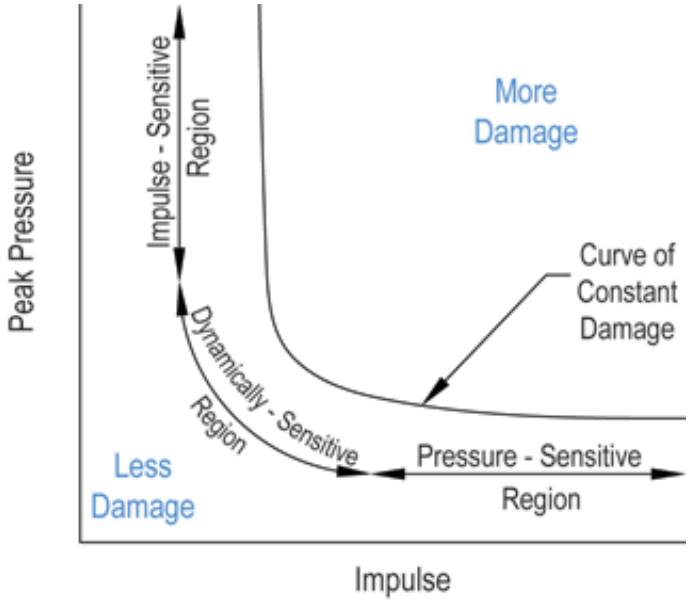

Figure 1.3. Generic P-I diagram demonstrating how the pressure and impulse imparted on an object correlate to damage (MBI, 2016).

Table 1.1. Required Research to Seal an Underwater Cylinder via Explosive Lensing.

Step	Specific Focus of Each Step	Explosive Media
1	Single Shockwave interaction with a cylindrical body.	Air
2	Multiple shockwave interactions with a cylindrical surface.	Air
3	Cylinder diameter's effect on peak pressure from the shockwave traversing the cylindrical surface.	Air
4	Dynamic loading required to collapse a centrally located cylinder.	Air
5	Single Shockwave interaction with a cylindrical surface.	Water
6	Multiple shockwave interactions with a cylindrical surface.	Water
7	Cylinder diameter's effect on peak pressure from the shockwave traversing the cylindrical surface.	Water
8	Bubble dynamics from multiple charges detonated simultaneously.	Water
9	Bjerknes force from multiple charges acting on a centrally located cylinder.	Water
10	Dynamic loading required to collapse a centrally located cylinder.	Water

The shockwave interaction with a cylinder surface (Step 1) is discussed in Section 2.3. This research used the techniques described in Section 2.3.4, to obtain a curve fit equation to predict the pressure from a single shockwave interacting with a cylindrical body. Due to time and budget constraints, this research focused on Step 2: Multiple shockwave interactions with a cylindrical surface, in Air. As a result, the objectives, theories, and tests detailed herein focus on Steps 1 and 2 in Table 1.1.

1.5. RESEARCH OBJECTIVES

The primary objective (Objective 1) of this research is to identify applicability and accuracy of the "Multiple Shockwave, Cylindrical Surface Peak Pressure Predictive Method: Along a symmetry plane." The Peak Pressure Predictive Method is the process developed, by this author, to predict the peak pressure from multiple shockwaves converging on a cylindrical surface along the symmetry plane. The Peak Pressure Predictive Method uses calculations based on a single shockwave interaction with flat reflective surfaces and Equations 7 and 8, to predict the peak pressure on a cylindrical surface from multiple shockwaves. This was accomplished with two steps. The first step was predicting the pressure from multiple shockwaves converging on the cylindrical surface using the Peak Pressure Predictive Method (Section 3). The second step was empirical testing to examine the accuracy of the predictions.

The Conventional Weapons Effects Program (CONWEP) is a widely used blast pressure predictive program. Depending on the charge size, CONWEP can have a mean model error ranging from ± 50 percent for smaller charges and ± 3 percent for larger charges. The typical mean model error from a CONWEP prediction is ± 6 percent. The research presented herein used small charges and therefore will likely have a higher mean

model error (± 25), the mean model error was calculated using Equation 1 (M. D. Netherton & M. G. Stewart, 2009).

$$\text{Blast loading model error (ME blast)} = \text{Test result/CONWEP Prediction} \quad (1)$$

Objective 2 of this research was to determine if "*Multiple charges focusing on a cylindrical surface do produce a higher peak pressure or impulse, than does a single charge of equal net charge weight."* This objective was examined by comparing the experimental results of Objective 1 (via the Bravo and Charlie tests as defined later in Section 5.3) to the peak pressure and impulse from 0.4 and 0.6 lb charges (Echo tests also defined later). An understanding of how multiple charges can impart more peak pressure or impulse on a cylindrical surface will aid future researchers in determining the appropriate charge configuration for a desired performance.

1.6. CONTRIBUTION TO SCIENCE

Accidents like BP Deepwater Horizon have a substantial economic and environmental impact. Cleanup efforts from the 2010 oil spill are still underway six years later. The Peak Pressure Predictive Method in this research serves as a first step toward developing a rapid response solution for events similar to the Deepwater Horizon accident. This research can be expanded to include different cylinder diameters.

The objectives of this dissertation provide a significant contribution to the explosives engineering industry. The Peak Pressure Method will aid in generating a controlled, explosively induced seal of a leaking oil pipe. The research presented in the

following sections provides a means of predicting the pressure and impulse associated with the shockwaves from multiple charges converging on a cylindrical surface.

Through further research, the Peak Pressure Method will be able to predict the pressures from shockwaves generated by multiple charges underwater converging on a centrally located cylinder. This can be accomplished through the 10 steps listed in Table 1.1. The Peak Pressure Method can be used to identify the explosive charge configuration required to produce the necessary peak pressure and impulse combination from the P-I diagrams, to seal a leaking pipe.

1.7. ORGANIZATION OF THIS DOCUMENT

This dissertation examines the literature (Section 2) necessary to understand the fundamental aspects of the Peak Pressure Predictive Method. Once the fundamental aspects are explained, the Peak Pressure Predictive Method (Section 3) will be described and empirical tests used to analyze its validity (Section 4). The results and accuracy of the Peak Pressure Predictive Method (Objective 1) will be discussed (Section 5). Section 5 will also review if "*Multiple charges focusing on a cylindrical surface do produce a higher peak pressure or impulse, than a single charge of equal net charge weight"* (Objective 2). Finally, the conclusions from the empirical tests will be presented (Section 5), along with the recommended future work (Section 6.2).

A number of experiments were conducted to identify equipment limitations and the experimental parameters necessary to validate the Peak Pressure Predictive Method. The results from these tests will be discussed in the body of this text, but the details of the experiments are in the corresponding appendices. Several appendices are also included that provide the necessary information for repeating the experiments described in this research.

2. LITERATURE REVIEW

2.1. ROAD MAP FOR THIS SECTION

The literature review presented in this section is important to understand how this current research was used to formulate the Peak Pressure Method discussed in Section 3. The literature review will discuss the dynamics of a shockwave generated from an explosive detonated in a free air configuration (Section 2.2). The shockwave discussion will continue through a single shockwave interaction with a cylinder surface (Section 2.3) and then the dynamics of two shockwave interactions (Section 2.4). Finally, the literature review ends with sources of blast pressure variances that can exist while attempting to record the pressure from the detonation of a free air burst explosive configuration.

2.2. SHOCKWAVE DYNAMICS FROM THE DETONATION OF AN EXPLOSIVE IN A FREE AIR CONFIGURATION

An explosion is a sudden physical or chemical change of the state of a mass, accompanied by a release of energy and by motion (Henrych, 1979). An explosion can take one of the following forms: chemical, nuclear, electrical, the burst of a steam vessel, or volcanic (Henrych, 1979). This study will focus on a chemical explosion generated shock wave. The explosion generates a shockwave when the chemical reaction propagates from a deflagration to a detonation (Cooper, 1996). A detonation is supersonic burning of material, while a deflagration is subsonic burning of material. The supersonic burn of explosive materials results in the rapid expansion of gaseous bi-products. This expansion, in turn, rapidly compresses the surrounding atmosphere (Rinehart J. S., & Pearson J., 1963). This effect is evident in Figure 2.1. Figure 2.1 was taken from the high-speed video of the experiments detailed in Appendix A.

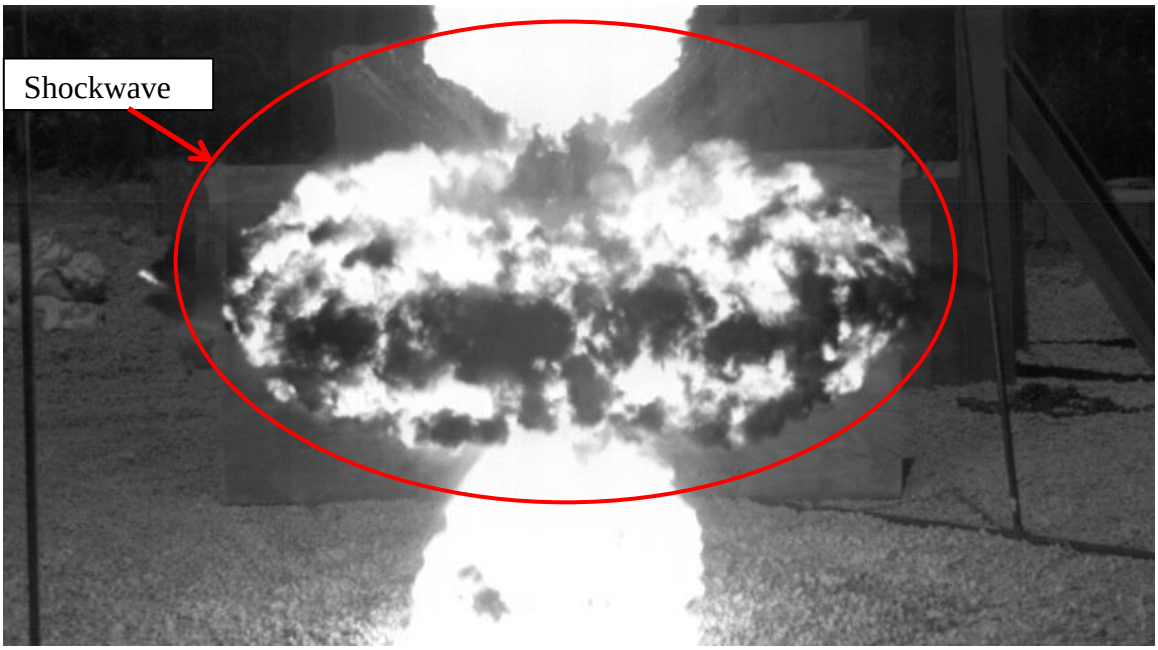

Figure 2.1. Demonstration of the shockwave expansion observed in the high-speed video.

A shockwave is a pressure wave of a finite amplitude that arises when matter is subjected to rapid compression (Ben-Dor, 1950). The media in which the shockwave traverses consists of two states: shocked and un-shocked, see Figure 2.2. These two states are due to the medium being compressed by passage of the shockwave. The ambient atmosphere in Rolla, Missouri (1,165ft) was the media of interest in this study.

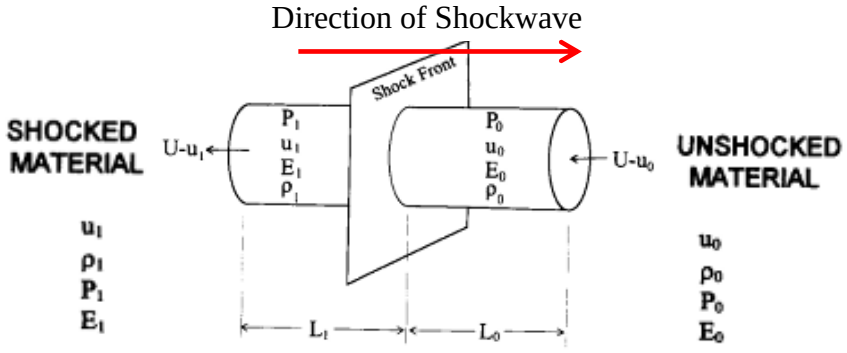

Figure 2.2. Shock parameters in front of and behind the shockwave (Cooper, 1996).

If the shockwave were to be viewed as a bubble similar to step I_1 in Figure 2.3, then upon complete detonation of the explosive the bubble would contain all gaseous by-products at a given density. As a result, when the shockwave expands an increased volume of gas at a lower density is produced. The shockwave's expansion rate is symmetrically equal to the decay rate. The increase in the specific volume reduces the pressure increase caused by the shockwave (Cooper, 1996).

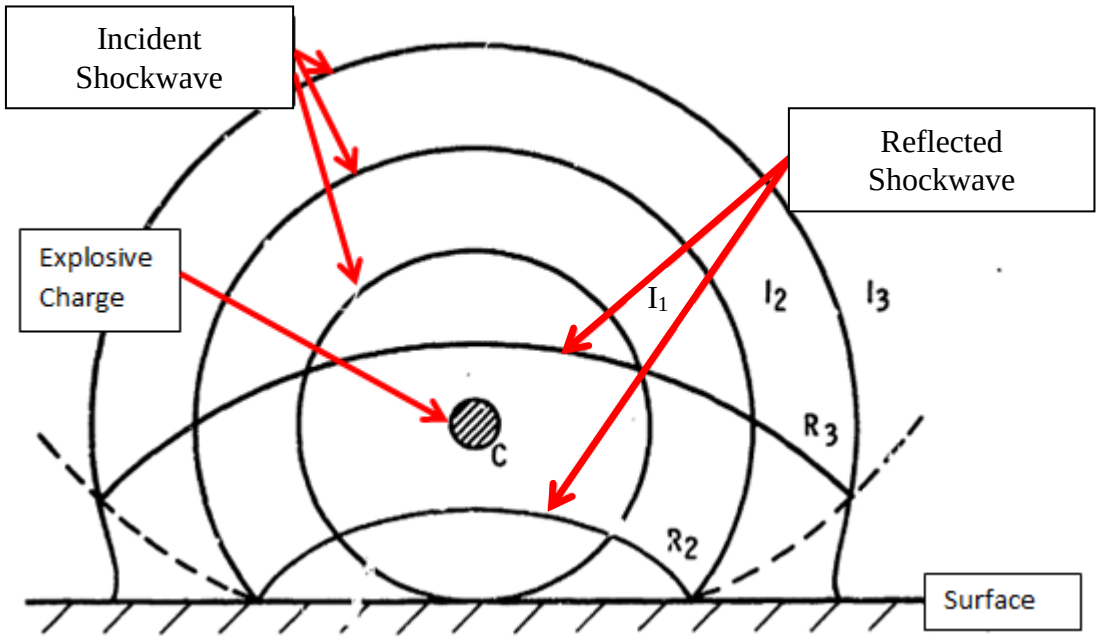

Figure 2.3. Radial expansion of the shockwave (Department of the Army, 1974).

The reflected shockwave's strength is dependent upon the impedance of the medium through which it traverses and the impedance of the medium at the boundary. The breakdown of the energy transition ratio is dependent on the impedance mismatch. When the shockwave encounters a material of different impedance, a certain fraction of the

energy is transmitted into the new material as a shockwave. The remaining fraction of the energy is reflected back into the explosive's gaseous by-product (Cooper, 1996). The shockwave both transmits and reflects in compression when going from a low impedance material into a high impedance material. The shockwave transmits in compression and reflects in tension (as a rarefaction in gases) when going from a high impedance material into a low impedance material (Cooper, 1996). Equation 2 can be used to calculate the shock impedance (Z_i) of a material where ρ_0 is the material's density (which remains constant for our purposes) and U is the shock velocity (Cooper, 1996).

$$Z_i = \rho_0 U \tag{2}$$

The incident pressure is the pressure difference between the ambient pressure and the pressure generated by the shockwave (Department of the Army, 1974). A new pressure (known as the reflected pressure) is generated when the initial shockwave interacts with a different material and a shockwave is transmitted back into the original medium (Cooper, 1996). The strength of the reflected shockwave is a result of the strength of the initial shockwave, the impedance mismatch of the material the shockwave is interacting with, and the angle in which the initial shockwave interacts with the media. The pressure behind a reflected shockwave can be as high as eight times the incident pressure (Michael M Swisdak, 1975).

A 90-degree interaction of the initial shockwave (an interaction normal to the reflected surface) will typically result in reflected pressures similar to those listed in Figure 2.4. The characteristics at the shock front corresponding to incident pressure are illustrated

in Figure 2.4. Here, the left-most column is an initial incident pressure (overpressure), and the right-most column is the estimated reflected pressure of an interaction normal to the medium's surface. For example, in Figure 2.4 a 15-psi incident pressure (highlighted with a red box) measured from a shockwave will generate approximately 42-psi of reflected pressure. In addition, the shockwave associated with the 15-psi incident pressure will have a shockwave velocity of approximately 1,493 ft/sec.

OVER PRESSURE (PSI)	SHOCK VELOCITY (FT/SEC)	PARTICLE VELOCITY (FT/SEC)	DENSITY RATIO	DYNAMIC PRESSURE (PSI)	REFLECTED PRESSURE (PSI)
.1	1090.2	5.33	1.005	2.42 E-4	.20
.15	1091.8	7.99	1.007	5.45 E-4	.30
.2	1093.4	10.63	1.010	9.69 E-4	.40
.25	1095.0	13.27	1.012	1.51 E-3	.50
.3	1096.6	15.90	1.015	2.18 E-3	.61
.4	1099.8	21.14	1.020	3.87 E-3	.81
.5	1102.9	26.35	1.024	6.04 E-3	1.01
.6	1106.1	31.53	1.029	8.69 E-3	1.22
.7	1109.2	36.68	1.034	1.18 E-2	1.43
.8	1112.4	41.81	1.039	1.54 E-2	1.64
.9	1115.5	46.90	1.044	1.95 E-2	1.85
1.0	1118.7	51.97	1.049	2.40 E-2	2.06
1.5	1134.2	76.89	1.073	5.38 E-2	3.13
2.0	1149.4	101.16	1.097	9.52 E-2	4.23
2.5	1164.5	124.81	1.120	.15	5.36
3	1179.4	147.89	1.143	.21	6.51
4	1208.7	192.42	1.189	.37	8.90
5	1237.2	235.00	1.234	.58	11.39
6	1265.1	275.79	1.279	.83	13.98
7	1292.4	314.98	1.322	1.11	16.68
8	1319.2	352.70	1.365	1.44	19.46
9	1345.4	389.08	1.407	1.81	22.34
10	1371.1	424.23	1.448	2.21	25.31
15	1493.1	584.53	1.643	4.77	41.45
20	1605.8	724.85	1.823	8.14	59.53
25	1711.2	850.51	1.988	12.22	79.33
30	1810.4	964.91	2.141	16.94	100.66
40	1994.2	1168.56	2.415	28.04	147.26
50	2162.5	1347.69	2.654	40.98	198.29
60	2318.7	1509.05	2.864	55.45	252.95
70	2465.1	1656.84	3.050	71.18	310.63
80	2603.3	1793.88	3.216	87.99	370.87
90	2734.5	1922.17	3.366	105.73	433.28
100	2859.8	2043.16	3.502	124.25	497.58
150	3418.7	2569.93	4.028	225.85	840.13

Figure 2.4. Ideal blast characteristics at the shock front (Swisdak, 1975).

An initial shockwave from the detonation of an explosive can multiply an indefinite number of times, depending on the environment in which the explosive detonates. For example, an explosive detonated in an urban environment will generate a reflected shockwave every time the initial shockwave (and each reflected shockwave) interacts with surrounding objects such as buildings, lampposts, fire hydrants, and stop signs. An explosive charge detonated in the open will not generate nearly as many reflected shockwaves as an urban explosion.

How the shockwave interacts with an object and the shape of the object affects the reflected pressure. For example, a flat plate should produce a different reflected pressure than a pipe's apex. Additionally, a shockwave that interacts with a plate at 45-degrees will have a different reflected pressure than a shockwave that collides normal to the reflective surface. The incident overpressure ratio vs the angle of interaction of the incident shockwave is illustrated in Figure 2.5. In Figure 2.5 an angle of zero degrees, positions the reflective surface perpendicular to the shockwave and 90-degrees (red box) allows the shockwave to traverse the surface relatively unimpeded. The reflected pressure equals the incident pressure as the angle of the reflective surface is increased to 90-degrees.

The reflected shockwave has a higher velocity than the incident shockwave. This is due to the reflected shock's travel through material with increased density generated from the incident shockwave. The reflected shockwave eventually overtakes the incident shockwave. When the reflected shockwave overtakes the incident shockwave a new shockwave (known as the Mach stem) occurs, see Figure 2.6. The point at which the three shockwaves (incident, reflected, and Mach stem) meet is known as the triple point.

INCIDENT OVERPRESSURE RATIO / ANGLE (degrees)	P_i/P_o 0.05	0.10	0.20	0.30	0.50	1.00	2.00	3.00	5.00	10.0	20.0
0	2.04	2.08	2.17	2.25	2.40	2.75	3.33	3.80	4.50	5.53	6.44
5	2.04	2.08	2.17	2.25	2.40	2.75	3.33	3.79	4.48	5.51	6.41
10	2.04	2.08	2.16	2.24	2.39	2.73	3.30	3.76	4.44	5.44	6.33
15	2.04	2.08	2.16	2.24	2.38	2.71	3.26	3.70	4.36	5.32	6.18
20	2.04	2.08	2.15	2.23	2.37	2.69	3.22	3.63	4.26	5.18	5.99
25	2.04	2.08	2.15	2.22	2.36	2.67	3.17	3.56	4.15	5.01	5.77
30	2.04	2.08	2.15	2.22	2.35	2.65	3.13	3.50	4.04	4.35	4.17
35	2.04	2.08	2.15	2.23	2.36	2.66	3.13	3.49	3.51	3.28	3.16
40	2.04	2.09	2.17	2.25	2.41	2.79	3.51	2.97	2.75	2.59	2.50
45	2.05	2.10	2.21	2.32	2.60	3.17	2.58	2.39	2.23	2.12	2.06
50	2.06	2.13	2.30	2.59	2.72	2.53	2.11	1.98	1.87	1.79	1.75
55	2.09	2.21	2.57	2.88	2.63	2.06	1.78	1.68	1.60	1.55	1.52
60	2.14	2.42	2.57	2.63	2.11	1.72	1.53	1.46	1.41	1.37	1.35
65	2.28	2.54	2.49	2.06	1.72	1.47	1.34	[illegible]	[illegible]	[illegible]	1.23
70	2.61	2.54	1.91	1.65	1.44	1.29	1.21	[illegible]	[illegible]	[illegible]	.14
75	2.61	1.91	1.49	1.35	1.24	1.16	1.11	1.10	1.09	1.08	1.08
80	1.77	1.39	1.21	1.15	1.10	1.07	1.05	1.04	1.04	1.03	1.03
85	1.19	1.10	1.05	1.04	1.03	1.02	1.01	1.01	1.01	1.01	1.01
90	1	1	1	1	1	1	1	1	1	1	1

Incident Pressure

Figure 2.5. Angular incident reflection vs reflection pressure (Swisdak, 1975).

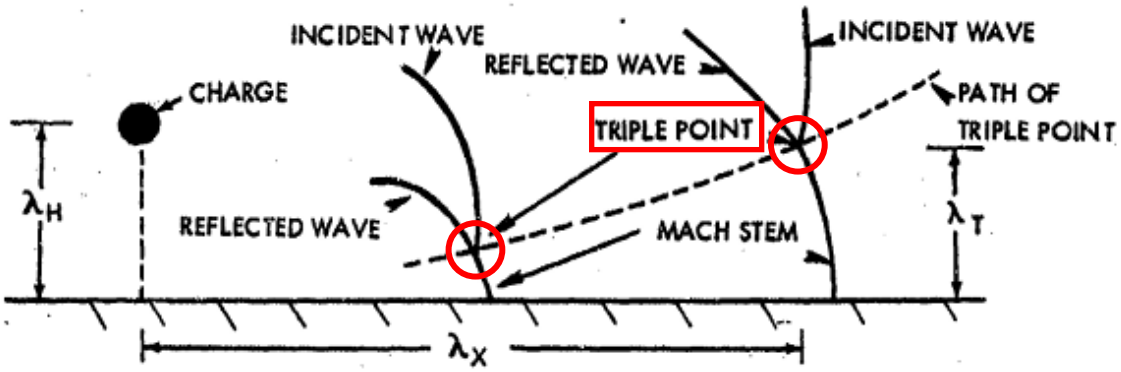

Figure 2.6. Propagation of a shockwave indicating the development of a Mach stem and triple point (Swisdak, 1975).

Theoretically, a given pressure will occur at a distance from an explosion that is proportional to the cube root of the charge weight (Michael M Swisdak, 1975). This is known as the scaled distance. When two charges differ in either the amount of explosive (charge weight) or distance to the point of interest the shockwaves produce similar

pressures at the same-scaled distance (Baird, Shockwaves, 2016). This holds true for explosives of the same material and geometry detonated in the same atmosphere.

The scaled distance is used to correlate a given charge weight and standoff distance to a 1 lb charge. For example: a 0.25 lb charge of C-4 with a 6 ft standoff will produce the same pressure as a 1 lb charge at a 9.5 ft standoff. The cube root scaling law has been shown to hold true over a wide range of explosive charge weights, from microtons to megatons, (Michael M Swisdak, 1975). Equation 3 details the scaled distance calculation.

$$Z_D = \frac{Distance}{Charge\ weight^{\frac{1}{3}}} \tag{3}$$

The scaled distance classification used in the research herein is as follows (S. J. Smith, D. M. McCann, M. E. Kamara, 2009):

- Close-in: $Z_D < 3$
- Near-Field: $3 < Z_D < 10$
- Far-Field: $Z_D > 10$

The distance between the charge and ground (λ_H) affects the time it takes the reflected wave to overtake the initial shockwave. Figure 2.7 uses the scaled charge height and the scaled distance (λ_X) to predict the scaled height of the triple point (λ_T). This author used Figure 2.7 to design the experiments of this research (see Appendix B) to insure that the initial pressure interacting with the pipe is the incident pressure and not the reflected ground pressure or the corresponding Mach stem.

Using Figure 2.7 to obtain the standoff distance (scaled horizontal distance) and charge height (charge height > scaled height of triple point) ensured that the pressure measured in this research was from the most basic shockwave interactions possible. Allowing the triple point to interact with the pressure sensors would significantly increase

the level of complexity of this research. The added complexity is beyond the scope of this project.

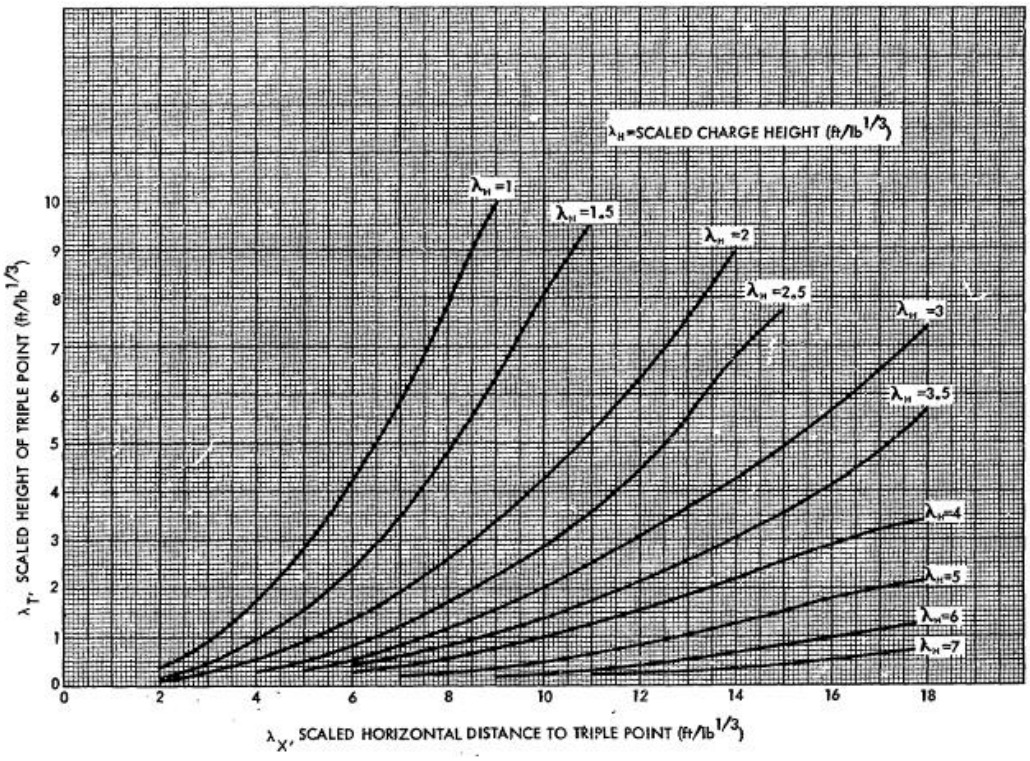

Figure 2.7. Height of triple point relative to height of burst (Michael M Swisdak, 1975).

The formation of a shockwave and its interaction with the surrounding media is an important aspect of this research. The blast pressure associated with a shockwave will be discussed further in Section 3.3 (How to Use the Peak Pressure Predictive Method). The following section explains the interaction of a shockwave with a cylindrical structure.

2.3. SHOCKWAVE INTERACTION WITH A CYLINDRICAL SURFACE

The angular interaction discussion thus far has pertained to a shockwave colliding with a flat surface at a given angle. The reflected pressure amplification (see Figure 2.5, Section 2.2) can be higher at an angle of interaction other than normal to the reflected surface. The shockwave interaction with a cylindrical surface differs from the interaction with a flat plate in that the reflected surface is continuously changing in the cylindrical case. The rate of change, relative to the angle Θ_w, is dependent upon the cylinder's radius. The angle Θ_w is measured from the plane parallel the x-axis and the line tangent to the cylinder surface at the point of interest (see Figure 2.8). For example in Figure 2.8 Θ_w at point "b" is measured from the horizontal plane b to the line b′. The line b′ is tangent to the cylinder surface, relative to the center of the cylinder. The rate of change for Θ_w relative to four points along a cylinder's radius is illustrated in Figure 2.8.

According to Ben-Dor's work (1950), the pressure decays as the shockwave traverses the cylindrical surface. The pressure decay is due to the decreasing angle Θ_w. The rate Θ_w decreases affects the rate at which the pressure decays. As with a flat reflective surface, the incident shockwave traverses the cylindrical surface and forms a reflected shockwave. As the shockwave interacts with the cylindrical surface, a Mach stem can be formed even though Θ_w is constantly changing. The angle at which a Mach stem is formed is an important part of the Peak Pressure Predictive Method described in Section 3.

The estimated angle at which the Mach stem begins to form (based on empirical testing) is 40-degrees (Needham, 2010). The Mach stem continues to grow and propagate about the cylinder's surface (Needham, 2010). However, Needham's (2010) work does not

detail the Mach stem's propagation beyond 90-degrees nor does it detail the shockwave's initial condition.

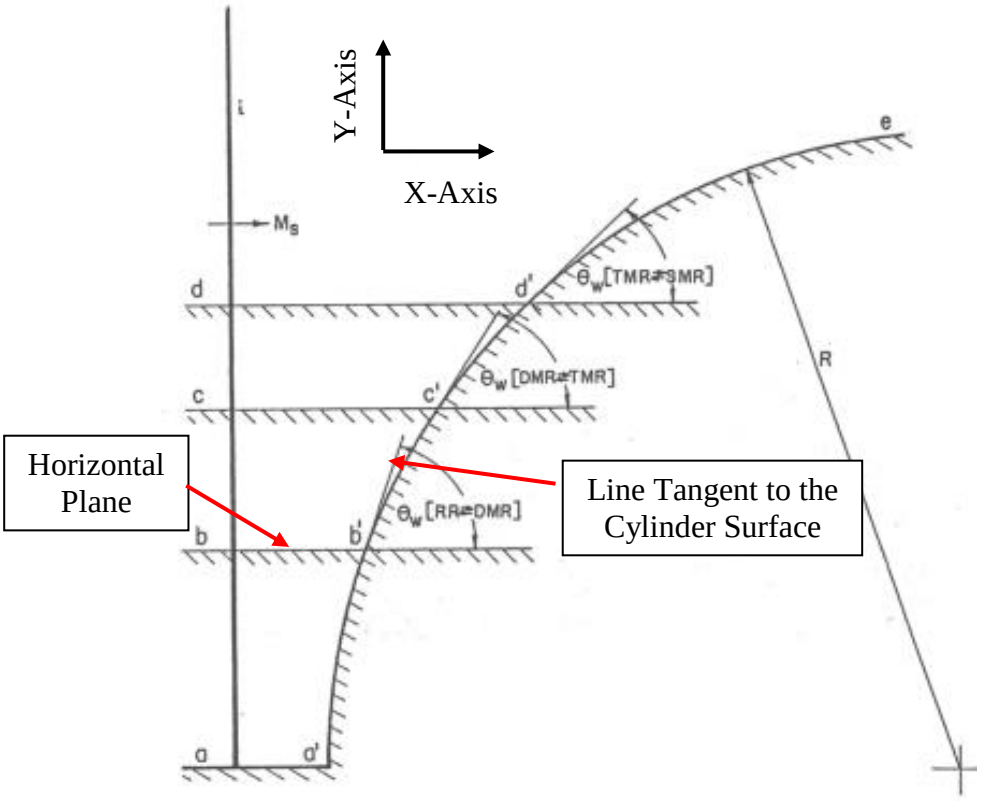

Figure 2.8. The changing angular reflection about a cylinder (Ben-Dor, 1950).

The shockwave velocity and cylinder diameter have a substantial influence on when or if a Mach stem is formed. Needham's work confirms that a Mach stem can be formed. However, the lack of setup information in Needham's (book) limits the applicability to the research described herein of the Mach stem forming when θ_w equals 40-degrees. The following section presents a study conducted by the Department of the Army, which examined the shockwave interaction with a cylindrical surface using shadowgraphs.

2.3.1. Department of Army Shadow Graph Analysis of a Shockwave Wrapping Around a Cylindrical Body. The Department of the Army produced a document (1974) detailing their work on explosions in air: "*Engineering Design Handbook: Explosions in Air, Part One."* One area of their study specific to this research concerned the interactions of a shockwave with a cylindrical surface using shadowgraphs (see Figure 2.9). The specific points of Figure 2.9 relevant to this research are the formation of a Mach stem, the time duration the shockwave remains in contact with the cylindrical surface, and the formation of vortices. "*Explosions in Air, Part One"* does not discuss the pressure associated with a shockwave wrapping around a cylindrical body.

Figure 2.9B (top right) highlights the formation of a Mach stem on each side (top and bottom) of the cylindrical body. The angle (θ in Section 2.3 and Figure 2.9) when a Mach stem forms is not discussed. However, this further illustrates that Mach stems can form on cylindrical surfaces. Figure 2.9C (bottom left) demonstrates that the shockwave remains in contact with all 360-degrees of the cylindrical surface. This differs from what will be discussed in the following section (Section 2.3.2). However, if the shockwave does remain in contact with the entire cylindrical surface it would explain the pressure spike this author observed on the back of the cylinder (see Section5).

The final point of interest in Figure 2.9 is the formation of vortices on the backside of the cylinder. The vortices are highlighted with red ovals in Figure 2.9D. The vortices will have an adverse effect on the impulse in the regions where the vortices exist (see Section 2.3.2). The following section correlates the formation of vortices to the shockwave velocity.

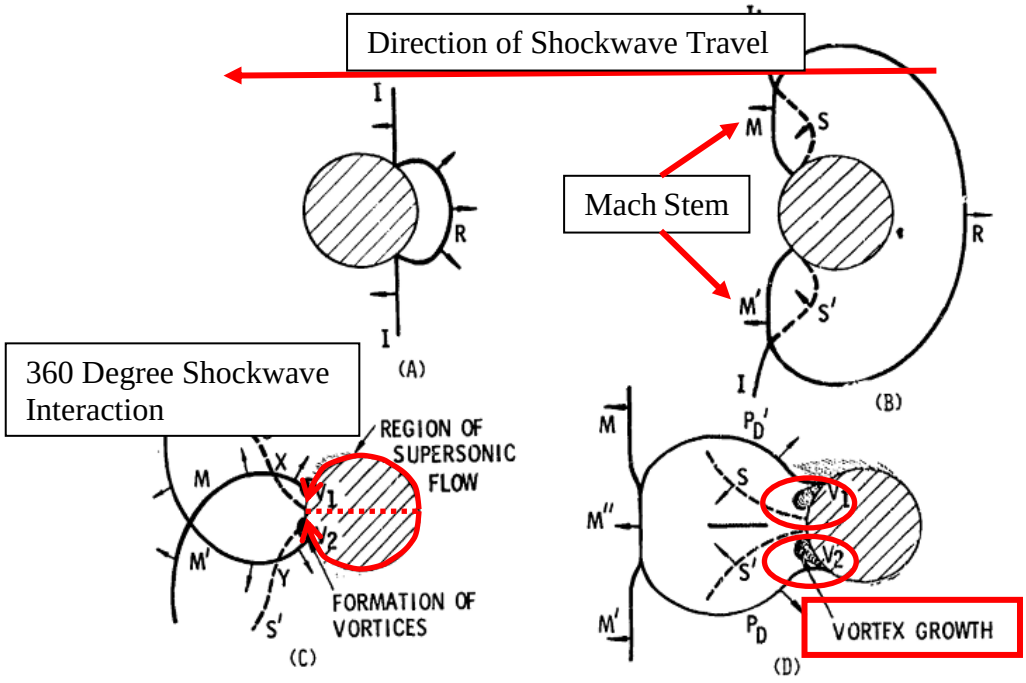

Figure 2.9. Traces of shadowgraphs that reveal the interaction of a shock front with a cylinder (Department of the Army, 1974).

2.3.2. Turbulent Flow Around a Cylindrical Body. The shockwave's interaction with a cylinder as it wraps around the cylinder is a fundamental aspect of this research. The formation of vortices and the approximate angular position (θ) where they form is needed to analyze the impulse information presented in Section 5. The works reviewed in this section addressed the vortices and wake generated by the shockwave-cylinder interaction at a high Reynolds number (Re). The Re is a dimensionless number that gives a measure of the ratio of inertial forces to viscous forces for given flow conditions (Anderson & Emeritus, 2012). The velocity of the shockwave, in this research, resulted in a high Re value. This is important to note, as the shockwave interaction with the cylindrical surface changes as the Re value increases.

If the shockwave is moving from left to right, meets a cylindrical body, and does not interact with the right side (back) of the cylinder, then a positive pressure exists on the left. The pressure decreases as the shockwave moves around the cylinder's surface. If the drag force is neglected a negative pressure exists on the right side of the cylinder. This condition exists for Re equal to or greater than 10e5 (see Figure 2.10). In Figure 2.10, the positive pressure is illustrated by an inward dip at the stagnation point, and negative pressure is illustrated by an outward expansion of the plot. Note that Figure 2.10 is of subsonic flow (i.e. no shockwave exists). Supersonic flow acts different from subsonic flow because of air compressibility and the presence of a shockwave (Shahriar, 2015). However, the pressure conditions highlighted also exist when a shockwave is present and understanding the pressure distribution around the cylinder is important to this research.

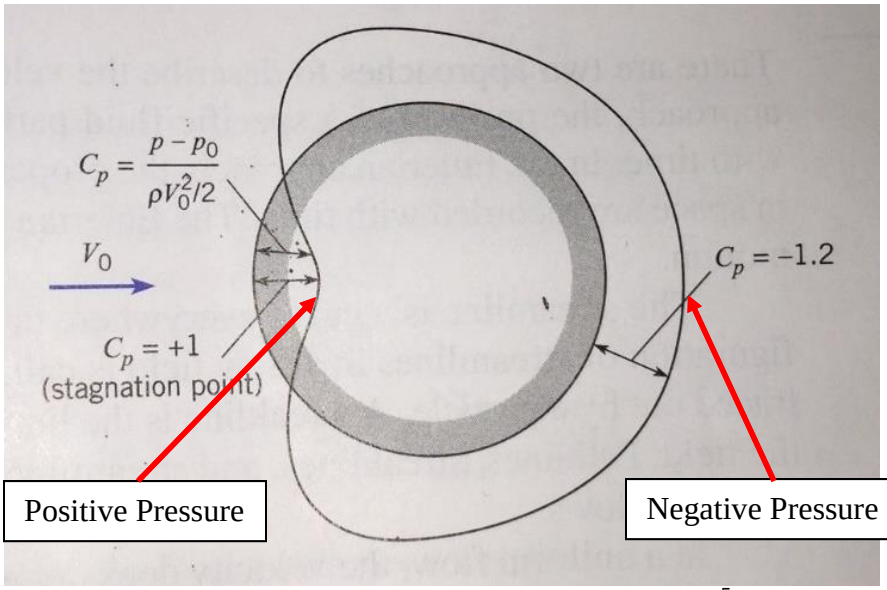

Figure 2.10. Pressure distribution on a circular cylinder, Re = 10^5 (C. T. Crowe, D. F. Elger, and J.A. Roberson, 2005).

The Re for a fluid flowing over a cylinder can be calculated using Equation 4 (Sunden, 2016). The calculated Re based on theoretical shockwave velocity for a 0.2 lb C-4 charge (U = 1,493 ft/sec) across a cylinder (D = 0.55 ft) in air, which has a kinematic viscosity of $1.46e^{-4}$ (υ) is 5.65e6. This Re classifies the fluid flow as turbulent flow, Re>4000 (Engineering Toolbox, 2015).

$$R_e = \frac{U*D}{\upsilon} \tag{4}$$

Anderson and Emeritus (2012) stated that the flow at the surface adheres to the surface because of friction between the gas and the solid material. The flow velocity is theoretically zero at the contact surface between the gas and solid, and as one moves away from that surface there is a thin region of retarded flow known as the boundary layer (Anderson & Emeritus, 2012). Therefore, the velocity changes from zero to the free-stream velocity across the boundary layer (C. T. Crowe, D. F. Elger, and J.A. Roberson, 2005). The boundary layer thickness grows as the flow moves over the body (i.e. the flow is more affected by friction between the gas and the solid the further the flow travels along the solid body (Anderson & Emeritus, 2012) see Figure 2.11).

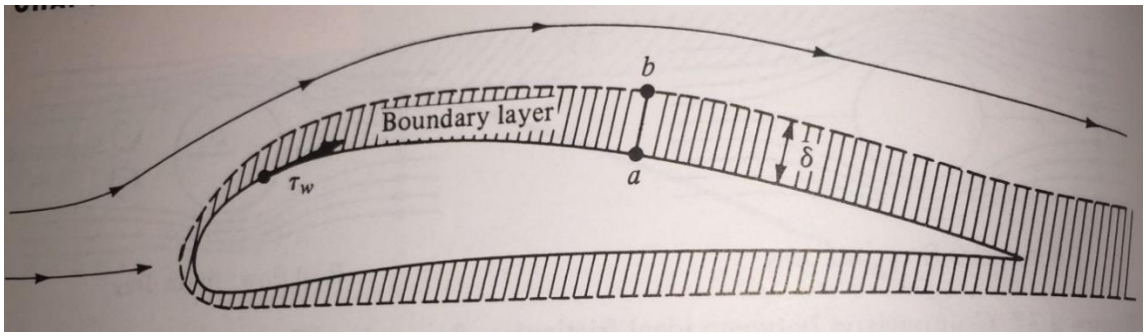

Figure 2.11. Boundary layer growth (Anderson & Emeritus, 2012).

With the low velocity in the boundary layer, the fluid particles can only travel so far against the adverse pressure gradient until they are forced to detour away from the surface (C. T. Crowe, D. F. Elger, and J.A. Roberson, 2005). This is known as the separation point. The separation point is dependent upon the fluid, its free-stream velocity, the diameter of the solid object, the Re number, and the object's surface roughness (C. T. Crowe, D. F. Elger, and J.A. Roberson, 2005). Figure 2.12 shows the fluid flow past a cylinder with the separation point and the wake.

Keeping the cylinder diameter and surface roughness constant and changing the free-stream velocity (shockwave velocity) causes the angular position of the separation point to change (C. T. Crowe, D. F. Elger, and J.A. Roberson, 2005). The wake zone leads to drag or flow resistance. Crowe (2005) stated that the process of vortex generation and decay is typical of all turbulent flows and is one of the most significant aspects of fluid mechanics.

As with subsonic flow (previously discussed), supersonic flow around a cylindrical body has flow seperation and wake turbulance similar to Figure 2.12. Additionally, supersonic flow generates a standing bow shockwave (see Figure 2.13). A standing bow shockwave is a curved stationary shockwave that forms at the front of a cylindrical body in supersonic flow (Shahriar, 2015). Note the separation points proximity similarity to the vortices presented in the Department of Army's work shown in Figure 2.9

From the fluid mechanics discussed in this section, the pressure associated with the backside of the cylinder appears to be the drag force acting on the cylinder. Based on the theories and literature discussed in this section, the shockwave does not remain in contact with the cylinder's surface, and the separation point is dependent upon the shock velocity.

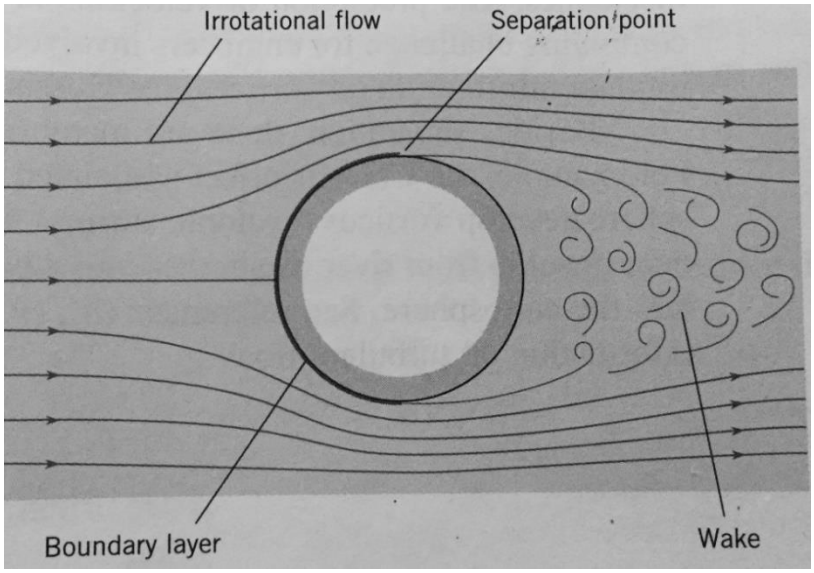

Figure 2.12. Fluid flow around a cylinder (C. T. Crowe, D. F. Elger, and J.A. Roberson, 2005).

Understanding how the shockwave wraps around the cylinder is only part of a shockwave interaction with a cylindrical body. The pressure associated with the shockwave is an important part of the Peak Pressure Predictive Method discussed in Section 3. The following section is one of the two discussions on the peak pressure associated with the shockwave interaction with a cylindrical body.

2.3.3. Haxton and Haywood Examination of a Shockwave Wrapping around a Cylindrical Body. Haxton and Haywood investigated the interaction of shockwaves with submerged cylindrical surfaces (Haxton & Haywood, 1986). Their research re-affirms that the pressure decays as it wraps around the pipe (Haxton & Haywood, 1986). The initial reflected pressure ($\theta=0$) is approximately that measured with a flat plate at an equal distance. The reflected pressure decays to the incident pressure as the shockwave traverses the cylindrical surface. The measured pressure on the cylindrical surface is equal to the

incident pressure when θ equals θ_t (Haxton & Haywood, 1986) see Figure 2.14. The angle θ_t exists when the line from the center for the initial charge location is tangent to the cylinder surface (R_t), see Figure 2.14.

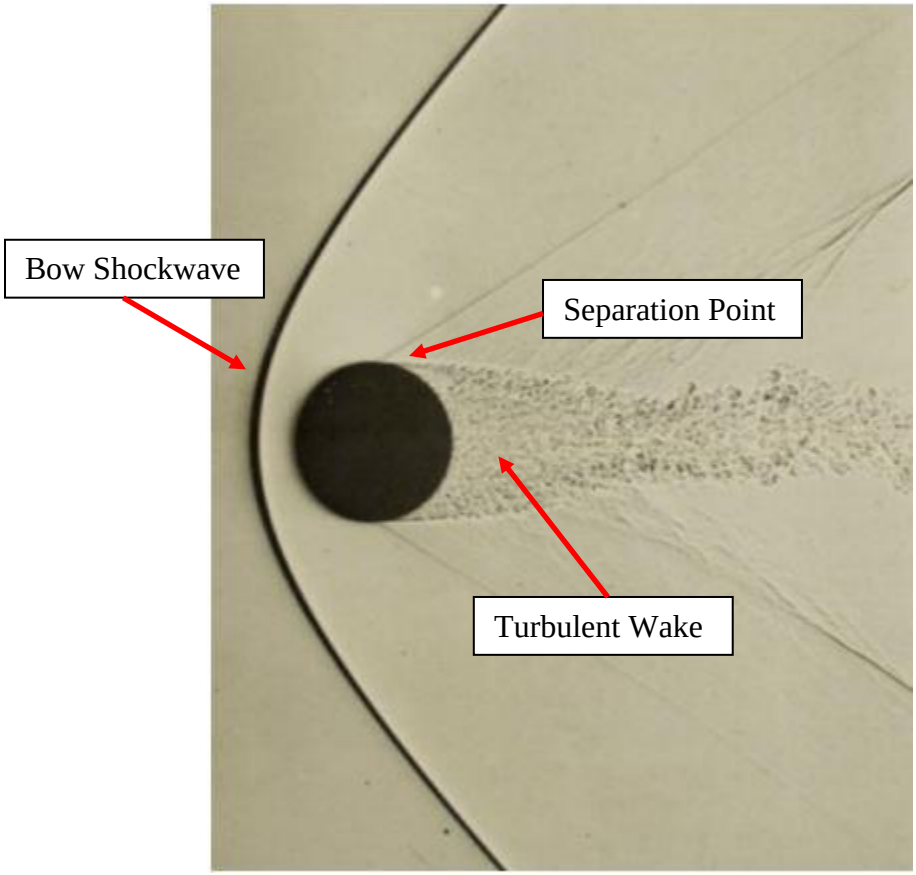

Figure 2.13. Shadowgraph image of a sphere where a bow shockwave, separation point, and a turbulent wake are present in the flow (Shahriar, 2015).

The wave continues to decay as the angular position increases from θ_t to $\theta = 90$ degrees (Haxton & Haywood, 1986). Any point beyond 90-degrees is considered to be in the shadow region of the cylinder (Haxton & Haywood, 1986). The shadow region is the area behind an object in which there is a significant pressure drop due to the deflection of

the shockwave by the object (Department of the Army, 1974). Haxton and Haywood's equations do not predict the pressure on the cylindrical surface beyond 90-degrees.

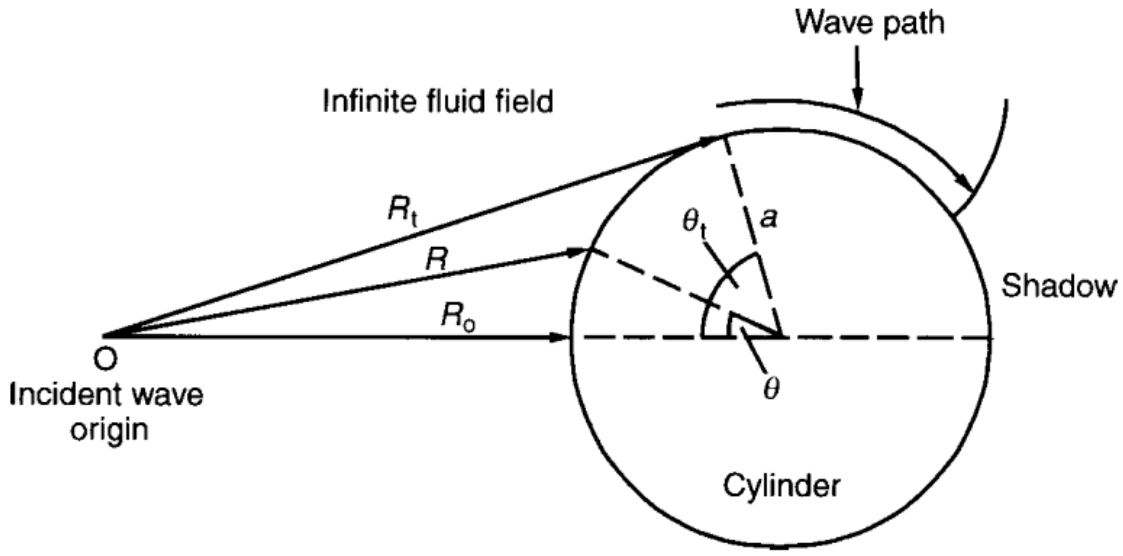

Figure 2.14. The underwater shockwave interaction with a cylinder (Haxton & Haywood, 1986).

The equations presented by Haxton and Haywood are also only applicable for charges within one cylinder diameter (Close-in scaled distance). The experiments detailed in Appendix B place the charge for this research in the near-field scaled distance. As a result, Haxton and Haywood's equations were not used in this research to predict the pressure associated with a shockwave wrapping around the cylindrical surface.

2.3.4. Glasstone's Examination of a Shockwave from a Nuclear Explosion Interacting with a Cylindrical Body. Glasstone's work (1962) *"The Effects of Nuclear Weapons"* includes the examination of a shockwave from a nuclear blast interacting with

a cylindrical body. Some examples of cylindrical bodies studied are telephone poles, smoke stacks, Quonset huts, and spherical huts (Glasstone, 1962). Glasstone's work, shown in Figure 2.15, is the result of charges in the "Near-Field" and "Far-Field." The peak pressure predictions from a shockwave wrapping around a cylindrical body presented in Glasstone's work were re-drawn, for the work presented herein, and are presented in Figure 2.15. The pressure is presented as a ratio of the reflected pressure (P_1) at θ divided by the initial reflected pressure at $\theta = 0$ degrees (P_r).

To predict the peak pressure at an angle on the cylindrical surface ($0<\theta\leq180$ degrees) using Figure 2.15, multiply the pressure at the apex of the cylinder by the ratio corresponding to the angle of interest. For example if the angles of interest are 40 and 180-degrees. Then the corresponding ratios are 0.8 and 0.3, respectively. If the peak pressure at the apex of the cylinder is 50 psi. Then the predicted peak pressures at the angles of interest are 40 and 15 psi, respectively.

Understanding the pressure associated with the shockwave traversing a cylindrical surface is only part of the problem. Using the ratio of P_1/P_r to represent the peak pressure associated with a shockwave wrapping around the cylindrical surface is a fundamental part of the Peak Pressure Predictive Method described in Section 3. The following section details two shockwave interactions with respect to angular influence and explosive lenses.

2.4. TWO SHOCKWAVE INTERACTIONS

This section discusses the angular influence on pressure amplification. This section also describes explosive lenses formed by multiple shockwaves. A shockwave generates a front-boundary condition with an increased density from the ambient media it is traversing. This increased density changes the impedance of the media at the shock front and creates

an impedance mismatch when two shockwaves collide. The shockwaves will interact with this impedance mismatch similar to how a shockwave interacts with a reflective surface, see Section 2.2.

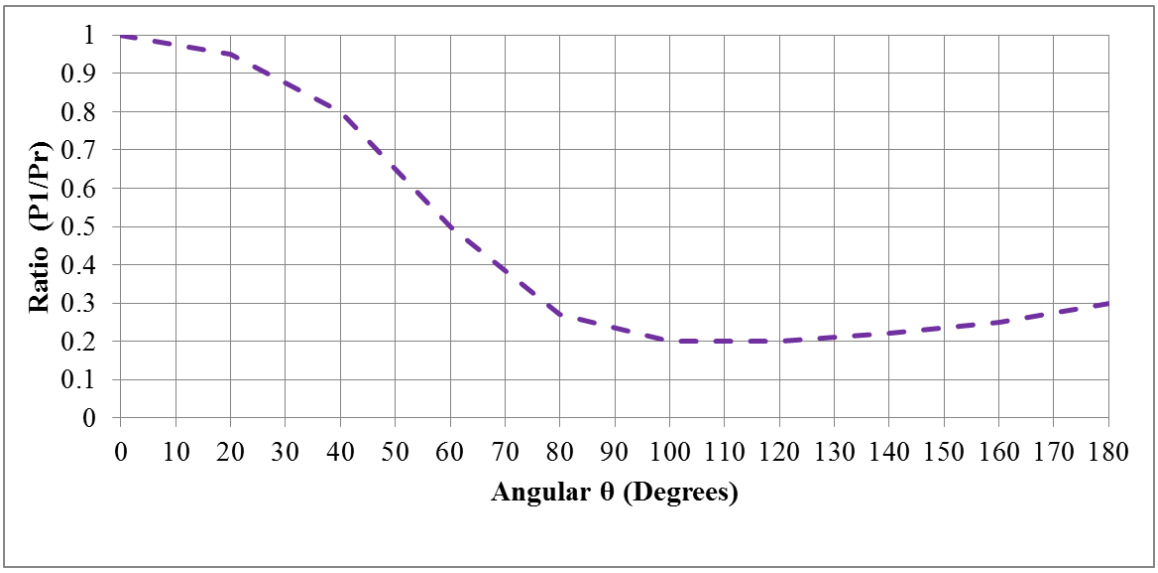

Figure 2.15. The ratio for P_1/P_r at angular positions from a shockwave traversing an arched structure (Glasstone, 1962).

The nature of the interactions is dependent on the number of shockwaves, the strength of the shockwaves, the direction of the shockwaves, and the angle of interaction. The measured pressure at the point of collision will be greater than the summation of the two incident shockwaves. A pressure amplification of two shockwaves of unequal amplitude colliding head on is illustrated in Figure 2.16. The strength of the shockwaves involved in the interaction determines the reflected pressure's amplification.

In Figure 2.16 U, u, rho, and P denote the shockwave velocity, particle velocity, density, and pressure, respectively. The subscript correlates to the shockwave. In Figure

2.16 the pressure from the right moving shockwave (P_1) is less than the pressure from the shockwave traveling to the right (P_2). When the two shockwaves collide the resultant pressure (P_3), is higher than the summation of P_1 and P_2.

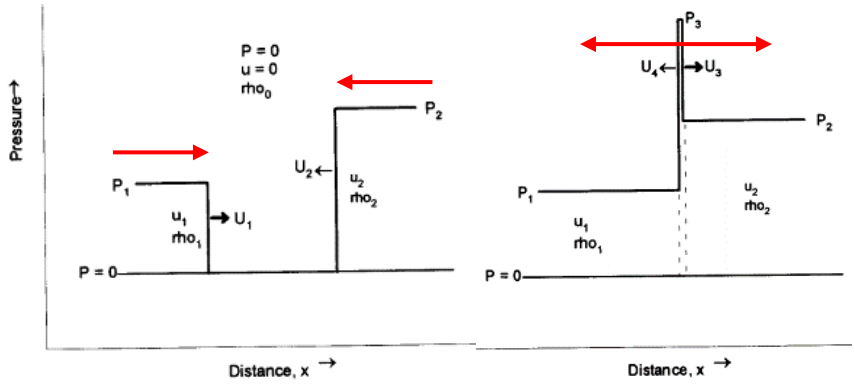

Figure 2.16. The pressure amplification of two shockwaves of unequal amplitude colliding (Cooper, 1996).

The shockwave in Figure 2.16 are colliding "head-on." Understanding this point is important when the shockwaves collide on the cylindrical surface. However, with multiple charges converging on a cylindrical body the shockwaves may interact prior to the cylindrical surface. Therefore, it is important to understand how the angle the shockwaves interact affects peak pressure. The following section examines how peak pressure can be influenced by two shockwaves colliding at different angles.

2.4.1. Angular Influence on Pressure Amplification of Two Shockwaves Interacting. The angle of interaction significantly affects the reflected pressure amplification. Figure 2.5 in Section 2.2 illustrates the angular influence on amplification from a single shockwave colliding with a flat surface. This same principle governs the

angle of interaction between two shockwaves. Shanes (1947) examined the effects of the angle of interaction between two shockwaves and the resulting peak pressure. He was particularly interested in the incident shockwaves generated from two charges underwater. Shanes (1947) examined two 3.75 lbs charges placed 4 ft from the sensor. The angle between the charge and the sensor varied with each test, see Figure 2.17.

The pressure measured from a single 3.75 lb charge was 8,360 psi. A single 7.5 lb charge was 11,000 psi. Two 3.75 lb charges that were separated by 12-degrees (84-degrees in Figure 2.18) generated a peak pressure of 11,700 psi. At 46-degree (66-degrees in Figure 2.18) spacing, the peak pressure increased to 2.9 times the pressure of a single 3.75 lb charge.

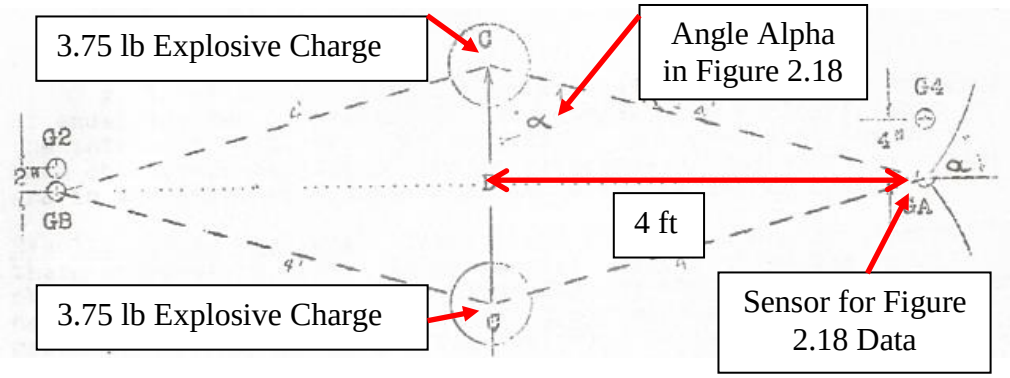

Figure 2.17. Set-up for Shane's (1947) underwater multiple shockwave tests.

The peak pressure amplification began to diminish once α exceeded 64-degree. He also noticed that the impulse increased to two times that of a single charge when α was 64-degree. Shanes' (1947) findings on angular influence on pressure amplification of two

shockwaves interacting are illustrated in Figure 2.18. Shanes (1947) did not measure the shockwave's interaction beyond 90-degrees.

From Shanes' work, it is clear that two 3.75 lb charges can impart a higher peak pressure and impulse on a flat surface than a charge of equal net weight (7.5 lbs). Shanes' work does not address more than two charges interacting on a centrally located sensor. In addition, Shanes' work does not address multiple shockwaves interacting on a cylindrical surface. However, using a charge configuration to improve a desired performance parallels the technique of explosive lensing. The following section details explosive lensing and the models of importance to this research.

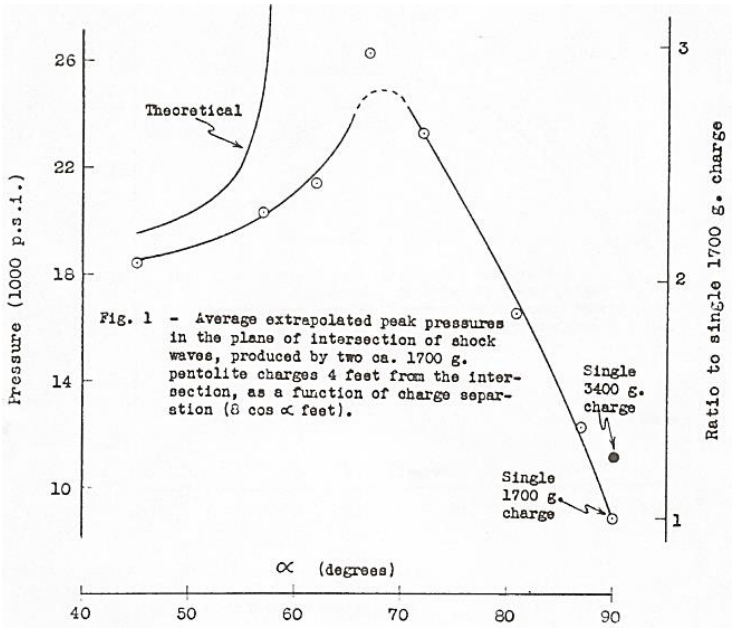

Figure 2.18. Results gathered from underwater multiple shockwave tests (Shanes, 1950).

2.4.2. Explosive Lenses Formed by Multiple Shockwaves. An explosive lens can be summarized as the use of charge geometry, additional explosives, inert material, and/or multiple initiations points to achieve a desired performance from shockwave interactions in a system. The use of explosive lenses allows researchers to obtain a detonation wave of virtually any shape by either changing the shape of the explosive or making the explosive non-homogeneous (D. B. Moore & T. C. Poulter, 1956). An explosive can be made non-homogeneous by inserting an additional explosive with a different detonation velocity and/or inserting an inert material of a specific shape and thickness (Busco, 1970). An example of a non-homogeneous explosive lens is shockwave refractive tape invented by Sir Sydney Alford (Kenward, 1986).

Modifying the geometric conditions of an explosive is a commonly practiced lensing technique. Melvin A. Cook (1958) demonstrated that a traditional conical shaped charges (CSCs) could be improved by modifying an explosive's geometric conditions. The modified geometric shape drastically reduced the amount of explosive used in the CSC. A CSC with a modified geometric shape then exhibited a similar performance to the initial design (see Figure 2.19). As a result, many explosive devices have since modified the explosive's geometric conditions as a means of reducing the amount of explosives required to accomplish a desired performance. In some cases, a detonation wave generator (DWG) has been utilized as an explosive lens to reduce the amount of explosive.

Busco (1970) examined the optical properties of detonation waves (i.e., optics of explosives) as they traveled through various explosive lenses. He determined that the optics of explosives could be modeled similarly to optics in other fields (e.g., in optics of light,

sound waves, microwaves). Busco also provided the classification for different explosive lenses.

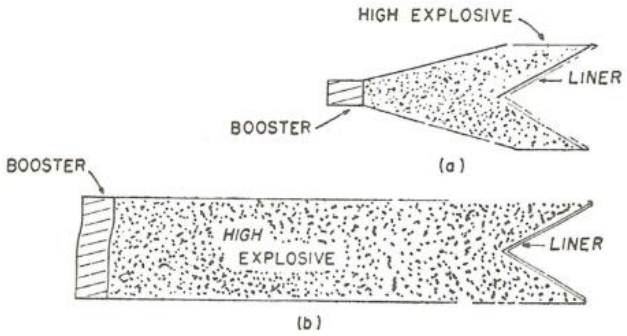

Figure 2.19. A CSC with modified geometric conditions (Cook, 1958).

Busco's (1970) two classifications for explosive lenses are pure DWGs and hybrid DWGs (Busco, 1970). Pure DWGs consist of only explosive media. Either the explosive's shape is modified or an additional explosive of a different detonation velocity is used to shape the detonation wave (Busco, 1970). Hybrid DWGs consist of both explosive media and inert material. In a hybrid DWG, an inert material is inserted into the explosive to modify the detonation wave (Busco, 1970). Figure 2.20 illustrates the explosive lenses listed in Busco's work. This research was focused on a circular implosive discontinuous DWG. The circular implosive discontinuous lens is highlighted in Figure 2.20.

A circular implosive discontinuous DWG consists of "n" charges with the same explosive weight that implode on a central point. An explosive lens can consist of different conditions. No general equation can calculate both a shockwave's pressure and shape at a given time. Rather, an analysis of the explosive detonation process is performed as it interacts with the lens to determine the geometric shape of the detonation. The density of

the explosive(s) and the media in which it transfers into are used to calculate the detonation pressure.

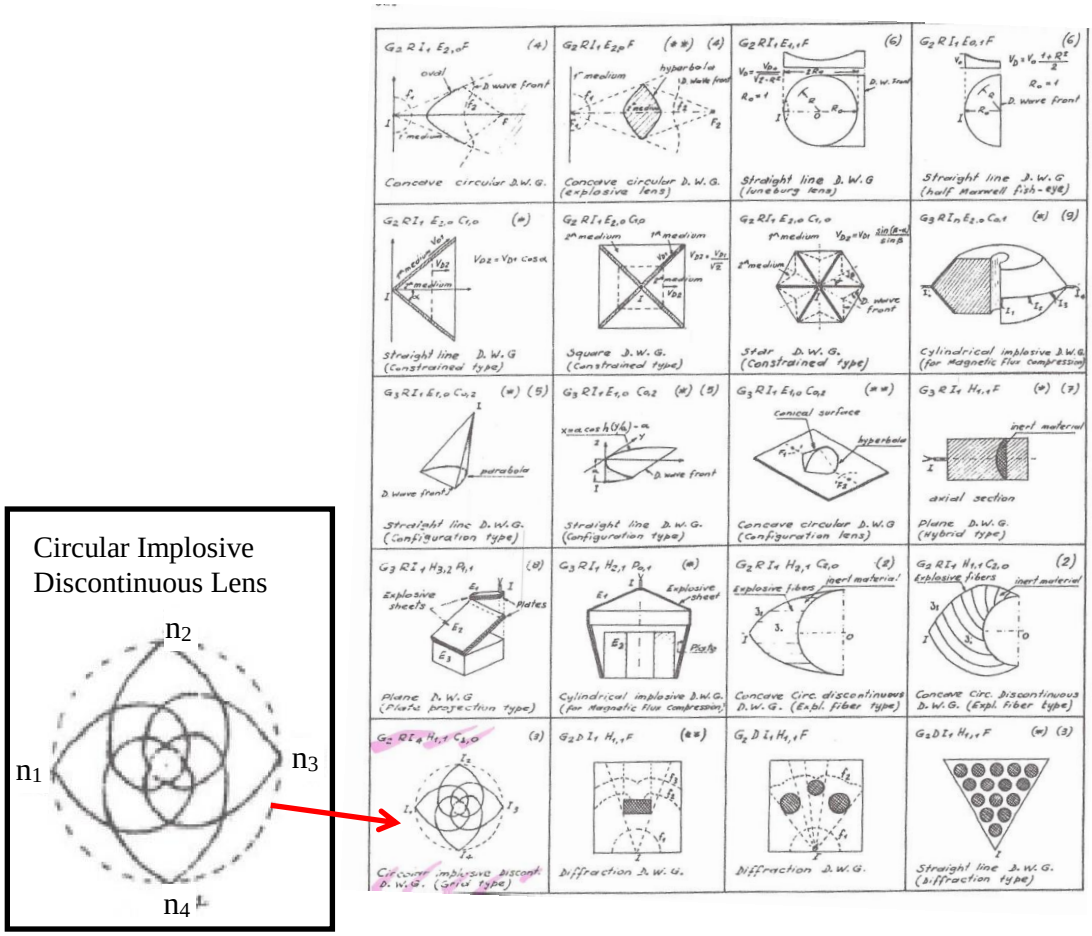

Figure 2.20. Optical properties of explosive lenses (Busco, 1970).

Explosive lenses can reduce the amount of explosives needed to achieve a desired performance. The Busco Model of a circular, implosive, discontinuous explosive lens predicts neither the peak pressure at the center point of the lens nor the effects of the lens interacting with a curved surface. This research focused on the resultant peak pressure and impulse from a circular, implosive, discontinuous explosive lens as it interacted with a

cylindrical surface. The objectives of this research will contribute to the modeling of explosive lenses.

Explosions have a number of phenomena that can make collecting empirical data challenging. These challenges can be a result of equipment limitations, test site, weather (e.g. rain, temperature, humidity, and air pressure), and charge configuration that induce pressure variances. The following section details how the charge configuration can contribute to variances in pressure.

2.5. BLAST PRESSURE MEASUREMENT VARIANCES

The charges used throughout this research were hand packed C-4 charges. Hand packed charges have an increased potential to induce variances when measuring peak pressure. For this research, variance in peak pressure refers to a difference in the recorded pressure, measured radially, from a centrally located charge. Figure 2.21 shows four pressure sensors that were used to measure the radially expanding peak pressure from a centrally located explosive charge. The methods used to suspend the charges and how the charge is confined can induce variances when measuring peak pressure. This section details how changes in the charge density and charge confinement can induce variances in peak pressure.

The charge's density directly affects its detonation velocity (Cooper, 1996). A series of hand-packed charges can vary in density from charge to charge. Thus, they also affect both the rate at which the explosive detonates and the rate at which the shockwave expands. The detonation velocity relationship between two charges of similar explosives with varying densities can be approximated with Equation 5, where D_1 and D_2 are the detonation velocities of the two explosives and ρ_1 and ρ_2 are the densities of the two

explosives (Cooper, 1996). When the density change is small, within a 10-15% range, β can be assumed to be β =3 (Cooper, 1996).

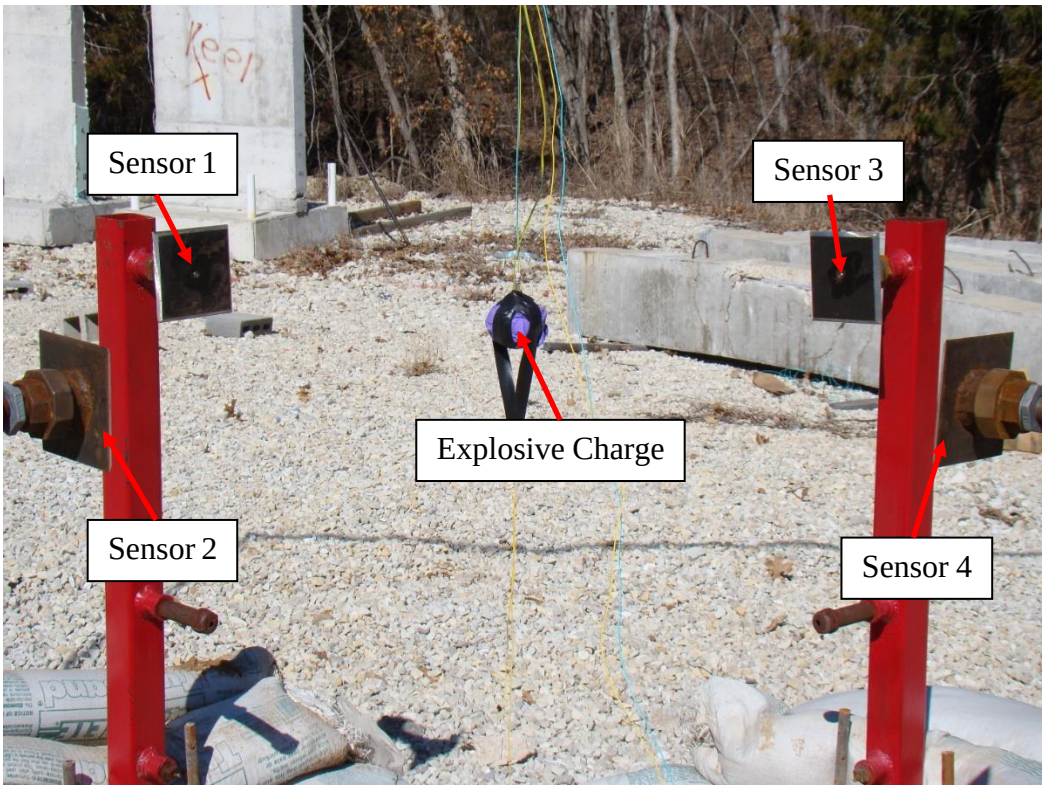

Figure 2.21. Radial pressure measurement from a centrally located explosive charge.

$$D_1 = D_2 + \beta(\rho_1 - \rho_2) \quad (5)$$

The charge density directly affects the velocity of the shockwave (Cooper, 1996). The pressure associated with a shockwave is affected by the shockwave's velocity. Therefore, variations in the charge density can induce variations in the pressure measurements. This principle is important to the empirical tests described in this research.

The tests conducted in Appendix C were confounded with pressure variances and consequently the test results were inconclusive. The tests in Appendix C lead to a second test series (Appendix A) that examined the charge geometry and pack ability on shockwave radial expansion.

The nature of how the hand packed spherical charge in Figure 2.21 was suspended resulted in a non-uniform radial expansion (see Appendix A). Needham (2010) discussed a similar suspension method for a spherical charge in which a 100 lb cast TNT charge was suspended by seatbelt straps. The straps impeded the shockwave expansion and resulted in a non-uniform radial expansion (see Figure 2.22).

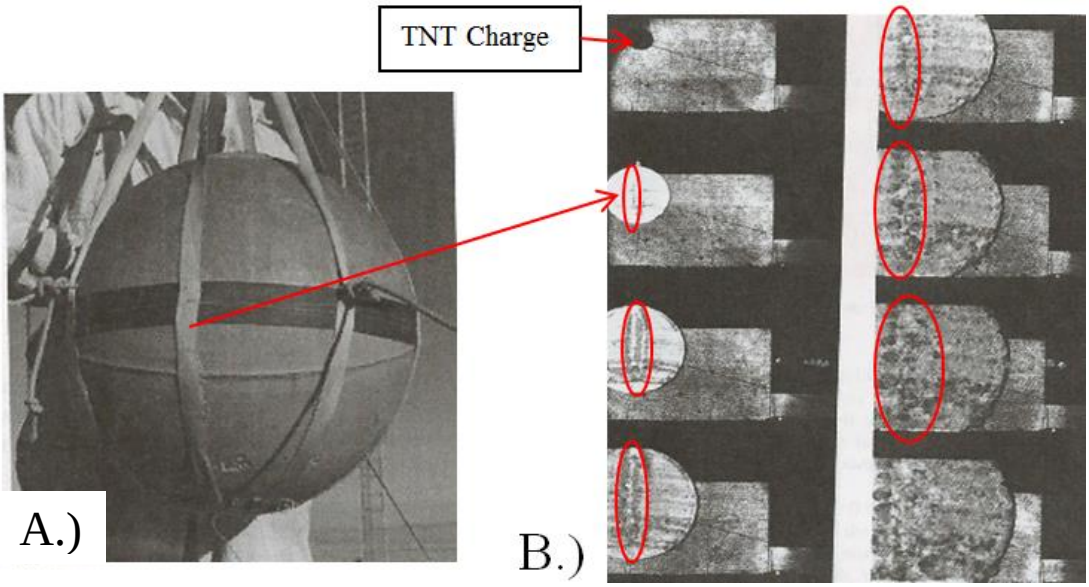

Figure 2.22. The initial charge prior to detonation (A) and the blast wave expansion to four times the initial diameter highlighting the impeded shockwave expansion (B) (Needham, 2010).

The work the shockwave is imparting on the seatbelt straps diminishes the available explosive energy for the shockwave. Cooper (1996) stated that the amount of energy available for the explosive might be partitioned between the air shock and other work that the explosive is doing at the same time. This explanation summarizes the point Needham is making with the seatbelt straps suspending the 100 lb TNT charge. The work the shockwave imparts on the straps reduces the potential near-field pressure measurements that align with the original seatbelt strap radial position. While Needham's work does not specify any pressure measurement variances, Dr. Grulke's work on blast pressure discusses the pressure variances from small charges with a near field scaled distance.

Dr. Grulke (2006) discusses blast pressure variances from small charges close to the pressure sensor. Dr. Grulke examined 10 gram charges positioned 17 inches from the sensor. The fireball expansion was not perfectly spherical, as one would expect from a spherical charge, see Figure 2.23.

The non-uniformity of the fireball correlates to asymmetrical radial pressure measurements. The four free field pressure sensors, in Figure 2.23, have an average pressure variance of 7.6 psi. The average pressure variance was obtained from the maximum and minimum pressure from each of the six repetitions. Dr. Grulke reaffirms Cooper and Needham's point that the work the shockwave imparts on the confining material directly affects the shockwave expansion. Dr. Grulke also states that the detonator orientation and charge shape can contribute to variances in pressure measurements.

The explosive charges used in this research were 1.5-inch diameter cylinders. The C-4 was hand packed in a cardboard shipping tube with uniform confinement. The uniform confinement reduced the likelihood of a non-uniform pressure distribution similar to what

has been shown in this section. The radial expansion of this charge configuration was compared to hand packed spheres and a 1-inch diameter cylinder in Appendix A. Understanding how confinement affects the shockwave expansion is an important part of the experimental design (Section 4).

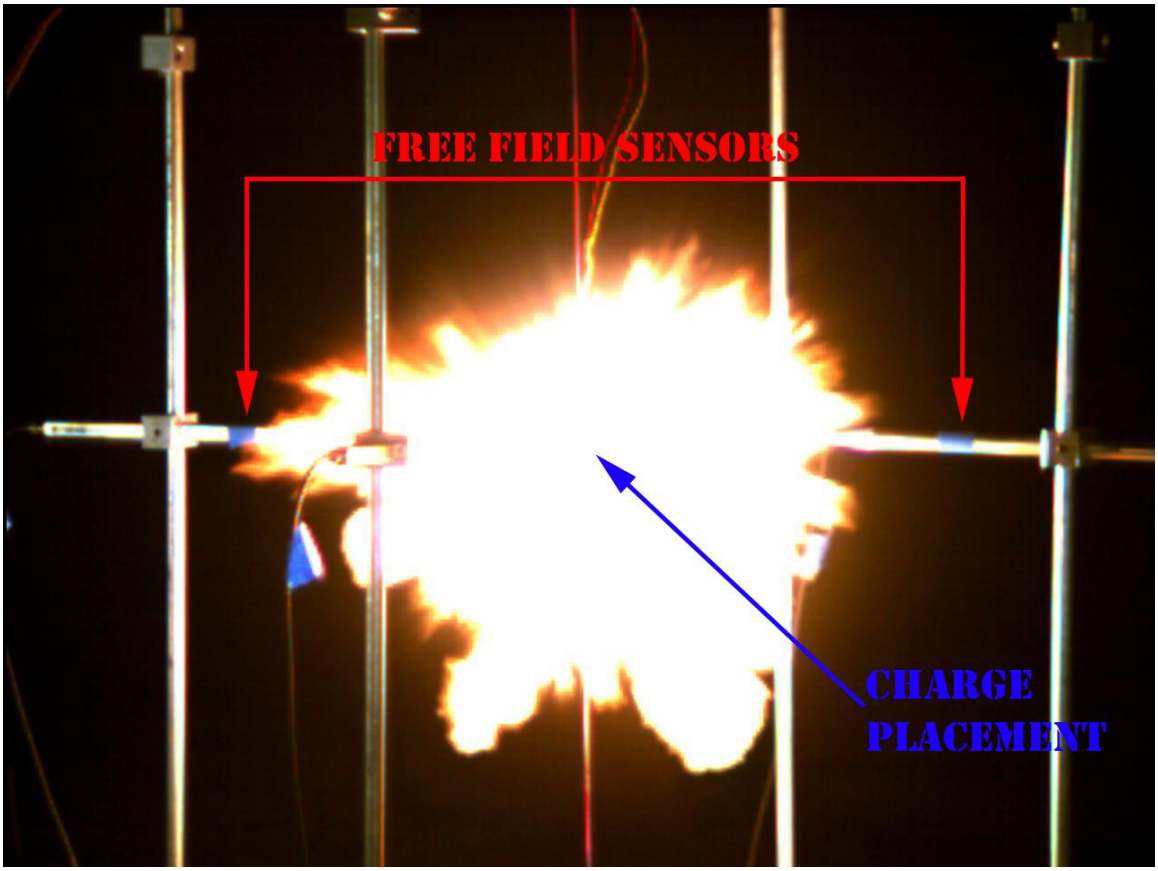

Figure 2.23. Asymmetrical 10 gram explosive event captured with high-speed camera (Grulke E. A., Lusk B. T., Perry K. A. Hoffman J. M., and Saito K., 2006).

2.6. SUMMARY

The concepts and theories discussed in this section examine a shockwave generated from a chemical explosion. How the pressures associated with a shockwave can be amplified and the shockwave interaction with a cylindrical surface and are important concepts to this research. The current research investigated shockwaves from multiple charges interacting with a centrally located cylinder, which had not been previously examined (to this author's knowledge). This research opens significant opportunities to advance the use of explosives lensing through a number of disciplines.

The following section will detail this authors Peak Pressure Predictive Method for multiple shockwaves converging on a centrally located cylinder. The sources of pressure measurement variances were considered during the experimental design process to minimize the pressure variances recorded during the empirical testing.

3. MULTIPLE SHOCKWAVE, CYLINDRICAL SURFACE PEAK PRESSURE PREDICTIVE METHOD FOR PRESSURE ALONG THE SYMMETRY PLANE (OBJECTIVE 1)

3.1. ROAD MAP TO THIS SECTION

The literature review in the previous section has laid the foundation to explain the Peak Pressure Predictive Method. This section guides the reader through the theory of the Peak Pressure Predictive Method (Section 3.2). Once the theory of the Peak Pressure Predictive Method is explained, Section 3.3 describes the process for predicting the pressure associated with shockwaves from multiple charges converging on a centrally located cylinder - at the symmetry plane. Section 3.3 provides the predicted pressures for the angular spacings of interest. These predicted pressures will be compared to the empirical results presented in Section 5.

3.2. THEORY OF THE MULTIPLE SHOCKWAVE, CYLINDRICAL SURFACE PEAK PRESSURE PREDICTIVE METHOD FOR PRESSURE ALONG THE SYMMETRY PLANE (OBJECTIVE 1)

To elaborate on the Peak Pressure Predictive Method, the inefficiency of a single charge acting on a centrally located cylinder needs to be discussed. Shanes' (1947) work reviewed in Section 2.4.1, indicates that multiple charges are more effective at imparting a higher peak pressure on a flat reflective surface than a single charge of equal net weight. This research presented herein clarifies the inefficiency of a single charge acting on a centrally located cylinder with respect to pressure amplification and total impulse.

The percentage of the explosive pressure acting on the pipe is relative to the cylinder size and the charge standoff (i.e. a bigger cylinder will result in a larger percentage of explosive pressure acting on the cylinder surface than a smaller cylinder each with the

same standoffs). Similarly, a smaller standoff will result in a larger percentage of explosive pressure acting on the cylinder surface than larger standoff (see Figure 3.1).

For a charge that is not in contact with the cylindrical surface the percentage of the explosive pressure, relative to the radial expansion, cannot be greater than fifty percent of the total available energy. The black dashed line in Figure 3.1 illustrates this. None of the gas expanding to the right of the dashed line will interact with the cylindrical surface. This is true regardless of the standoff distance, charge size and pipe diameter.

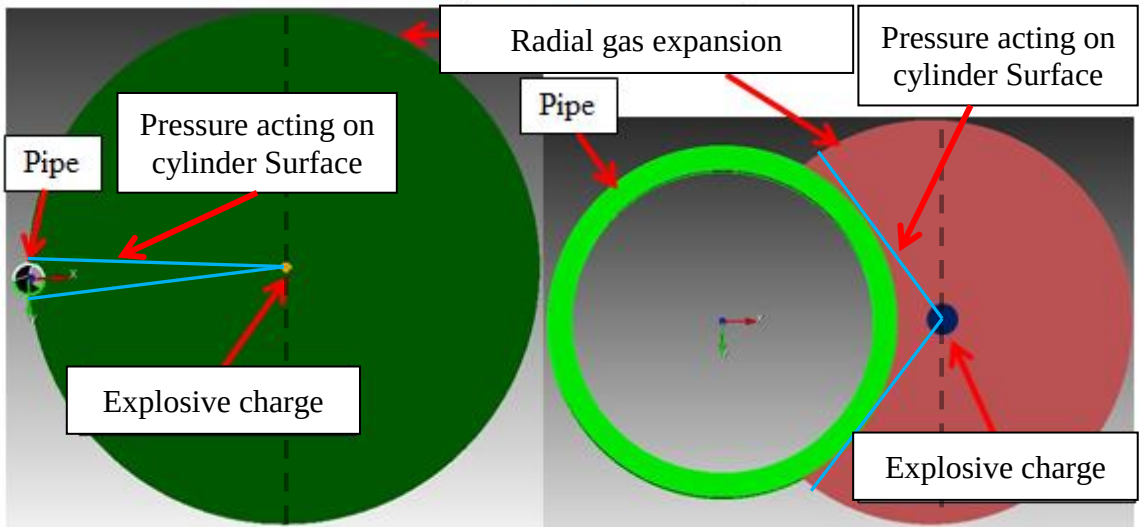

Figure 3.1. Comparison of explosive pressure acting on a cylinder for different standoffs.

The scaled distance of the scenario depicted in the left-hand schematic in Figure 3.1 puts the charge in the "far-field" range, whereas the right-hand schematic shows the charge in the "close-in" scaled distance range. The radial expansion between the blue lines depicts the difference in the explosive pressure acting on the pipe.

Only a fraction of the explosive gas from an individual charge is acting on the cylinder. There is no means of amplifying the pressure of a free airburst explosion beyond introducing boundary reflections or reducing the scaled distance. Once, the charge is fully detonated the peak pressure cannot be increased without a reflective boundary.

The use of multiple charges allows for an amplification of the pressure field over the cylindrical target surface. Therefore, to create the desired pressure amplification on the cylinder surface, interactions with reflective boundary conditions need to be generated. Multiple charges enable the shockwave expansion of a single charge to serve as a reflective boundary for each neighboring charge.

The shockwaves from the two charges interact along a plane that is equidistant from each charge and passes through the center of the cylinder. This plane serves as a symmetry plane and therefore it serves as a reflecting plane similar to a free airburst interacting with the ground (Baird, Symmetry Plane, 2012). Not only does the shockwave act as a reflecting boundary, increasing the associated pressure from each charge acting on the cylindrical surface. The increase in pressure can be attributed to the reflected shockwave from the symmetry plane and possibly the formation of a Mach stem. In Figure 3.2, I_X represents the incident shockwave and R_X represents the reflected shockwave from the symmetry plane, where "X" corresponds to the charge.

The symmetry planes essentially "focus" the explosive gasses for charges that have two or more neighbors (see Figure 3.3). The red segment, highlighted in Figure 3.3, represents the portion of Charge 1's radial expansion "trapped" between its neighboring charges. The green segment, highlighted in Figure 3.3, illustrates the path the "trapped" explosive gasses will follow as it is focused on the cylinders surface.

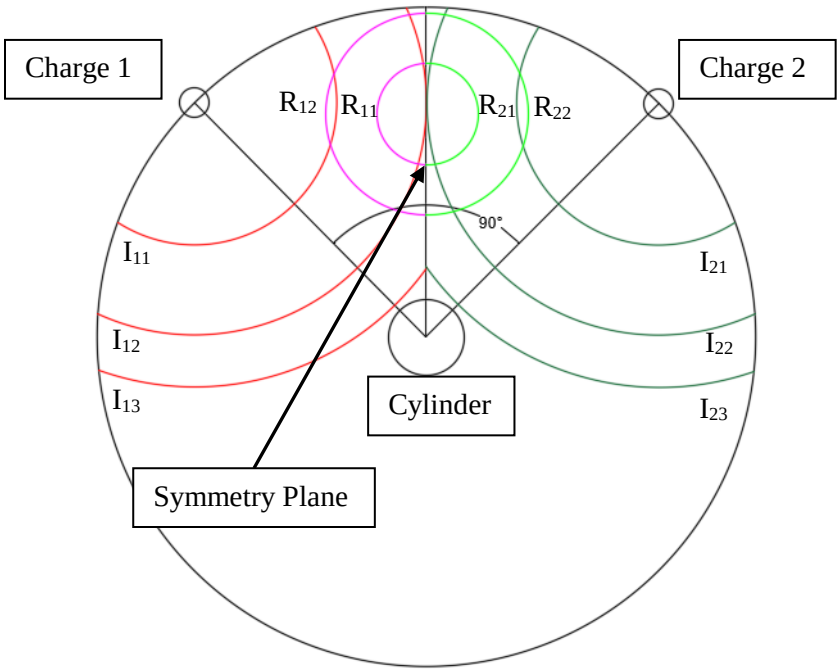

Figure 3.2. Shockwaves from two charges forming reflected shockwaves along the symmetry plane.

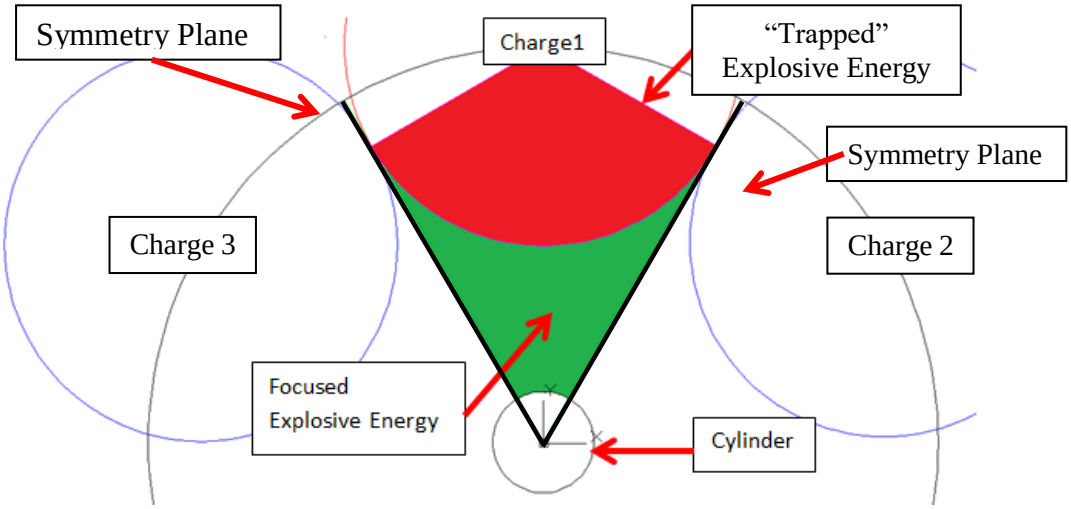

Figure 3.3. Focusing of explosive energy on cylinder surface.

The Peak Pressure Predictive Method assumes the shockwave interactions at the symmetry plane parallel how a shockwave interacts with a solid reflective surface (see Figure 3.4). This means the shockwave interaction will generate two reflected shockwaves traveling away from the line of interaction, see Figure 3.2. This also means the reflected shockwaves can form a Mach stem and a triple point.

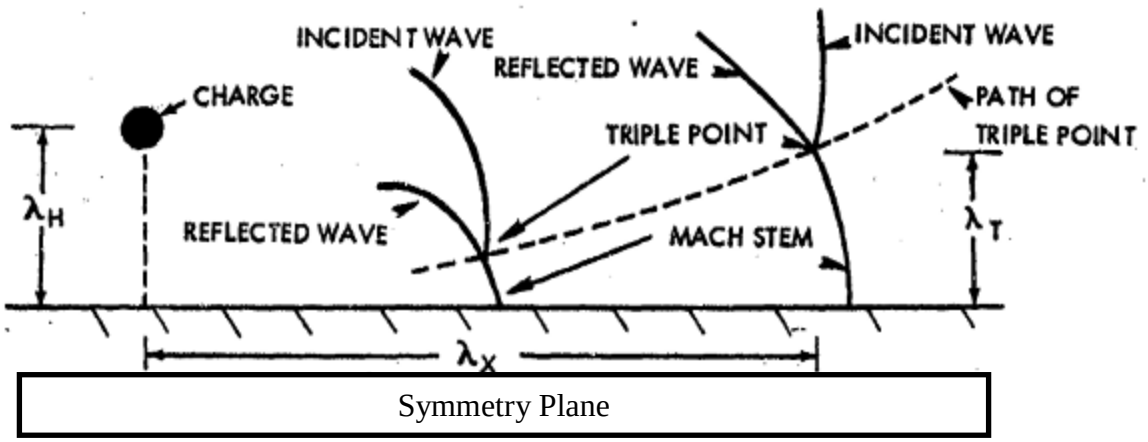

Figure 3.4. Figure 2.6 edited to illustrate the aspects of a shockwave interaction with a symmetry plane (Swisdak, 1975).

This assumption enables using conventional pressure predictive techniques for multiple shockwave interactions with a centrally located cylinder. The question then becomes, “does the shockwave interact with the cylinder surface before the Mach stem overtakes the incident shockwave?” If the incident shockwaves interact with the cylinder before the Mach stem overtakes it, then the multiple shockwaves will collide on the cylindrical surface at the symmetry plane.

This collision is assumed to be a head-on collision. The incident shockwave interacts with the cylindrical surface and generates a reflected shockwave prior to the head-

on collision. Therefore, the two shockwaves colliding head-on, on the cylinder surface, are the two reflected shockwaves from the initial incident shockwaves. For this case, the pressure (P_c) can be predicted using the amplification factors from a head on collision (Figure 3.5). In Figure 3.5, a ratio of P_i/P_0 was used to predict the amplification of P_i. However, the research presented herein uses the ratio of P_1/P_0 to predict the amplification of P_c. Where P_1 is the pressure associated with the shockwave reflecting off the cylindrical surface.

INCIDENT OVERPRESSURE RATIO / ANGLE (degrees)	P_1/P_0										
	0.05	0.10	0.20	0.30	0.50	1.00	2.00	3.00	5.00	10.0	20.0
Head-on Collisions	2.04	2.08	2.17	2.25	2.40	2.75	3.33	3.80	4.50	5.53	6.44

Figure 3.5. Figure 2.5 edited to illustrate pressure amplification associated with various P_1/P_o ratios (Swisdak, 1975), modified.

The reflected pressure (P_1) used in the P_1/P_0 ratio is the pressure associated with the angular position of the symmetry plane. For example if two charges have an angular spacing of 90-degrees, then P_1 is the pressure associated with 45-degrees. Glasstone's work reviewed in Section 2.3.4 presents P_1 as a ratio of the reflected pressure at the apex of the cylinder surface (P_r). This research uses the same technique for predicting the pressure of the colliding shockwaves along the symmetry plane, but the ratios are specific for a 6.65-inch diameter cylinder.

When the Mach stem overtakes the incident shockwave, the Mach stem imparts a pressure on the cylindrical surface, along the symmetry plane. The pressure along the

symmetry plane (P_c) is the reflected pressure from the Mach stem (P_M) and the Mach stem is the pressure reflection from the incident shockwave (P_i). The incident pressure is assumed to be the pressure at the cylinder apex, prior to generating a reflection. For example, if a cylinder is 52 inches from a charge, then Pi is the incident pressure 52 inches from the charge. The reflected pressure (P_M) from the incident shockwave can be calculated using the amplification factor in Figure 3.5 for the corresponding P_i/P_o ratio. The pressure along the symmetry plane (P_c) from the Mach stem reflection can be calculated using the amplification factor in Figure 3.5 for the corresponding P_M/P_o ratio.

By assuming the shockwave reflection along the symmetry plane is similar to the shockwave from a free airburst interacting with the ground, Figure 2.7 can be used to determine if a Mach stem is present for different angular spacings and standoff configurations. For example, consider two charges with an angular spacing of 40-degrees and each charge is 4.33 ft from the cylindrical surface. Then the distance between charges is 1.5 ft. and the distance from the charge plane to the cylindrical surface is 4 ft. Using a 0.2 lb charge λ_H and λ_X are 2.5 and 6.9, respectively. Knowing λ_H and λ_X the length of the Mach stem can be obtained using Figure 2.7. From Figure 2.7 λ_T is 1.2, which translates to a Mach stem length of 8.4 inches on one side of the symmetry plane.

The amplification of the reflected shockwave (R_x in Figure 3.2) is dependent upon the boundary conditions that generated the reflected shockwave (see Section 2.2). Therefore, the boundary conditions associated with a “solid” reflective surface will likely produce a higher amplification than two shockwaves of equal amplitude colliding head on. The pressure amplification used in the Peak Pressure Predictive Method uses the amplification from a shockwave colliding with a “solid” reflective surface (see Figure 3.5).

As a result, the Peak Pressure Predictive Method may need to be adjusted to account for this lower amplification.

Additionally, the length of the Mach stem predictions is for a shockwave interaction with a "solid" reflective surface. As a result, the length of the Mach stem may be over predicted. Without empirical testing, the extent of the potential Mach stem length over prediction is unknown. The Peak Pressure Predictive Method does not account for the Mach stem and assumes the shockwave interactions will occur on the cylindrical surface. The following section details how to use the Peak Pressure Predictive Method to estimate the pressure from two charges acting on a cylindrical surface along a symmetry plane.

3.3. HOW TO USE THE PEAK PRESSURE PREDICTIVE METHOD

This research identified the following steps to predict the peak pressure along the symmetry plane from two shockwaves colliding on a cylindrical surface. Each step is explained and calculated in this section for the angular spacings of interest. The angular spacings of interest are 40, 60, 90, 120, and 180-degrees. Section 4 discusses why these angular spacings were selected. The steps of the Peak Pressure Predictive Method are as follows:

Step 1: Calculate the TNT equivalent charge weight (if applicable).

Step 2: Estimate the peak overpressure using Figure 3.7.

Step 3: Calculate the Charge Geometry's Effect on Estimated Peak over Pressure (if applicable).

Step 4: Calculate the reflected pressure.

Step 5: Identify the angular position of symmetry plane.

Step 6: Calculate the pressure wrapping around the cylindrical surface (P_1) using Equations 7 and 8.

Step 7: Calculate the P_1/P_0 ratio.

Step 8: Use Equation 9 to calculate the pressure amplification (P_{Amp}).

Step 9: Calculate the pressure for the colliding shockwaves at the symmetry plane using Equation 10.

The following sections present the techniques for predicting the pressure from a 0.2 lb cylindrical charge acting on a cylindrical surface. The pressure acting on the cylindrical surface is then used to predict the pressure along the symmetry plane for two shockwaves colliding head-on.

3.3.1. Step 1: Calculate the TNT Equivalent Charge Weight. There are a number of explosive predictive calculators that can be used to estimate the pressure from a 0.2 lb spherical charge. These pressure calculators typically use curve fit equations developed from empirical tests. The tests used to produce the curve fit equations often used TNT as the explosive of interest. This section describes the process of predicting the pressure from a 0.2 lb C-4 spherical charge using Figure 3.6.

TNT has a lower detonation pressure than C-4 (Michael M Swisdak, 1975). Not accounting for this lower detonation pressure can result in an under prediction of the peak pressure. The TNT pressure equivalent of C-4, for a pressure range of 10-100 psi, is 1.37 (EW=1.37) (Michael M Swisdak, 1975). Calculating the equivalent TNT charge weight for a 0.2 lb C-4 charge is demonstrated in Equation 6 (Michael M Swisdak, 1975).

$$\text{TNT Equivalent} = \text{CW}_{\text{C4}} * \text{EW}_{\frac{\text{C4}}{\text{TNT}}} \quad (6)$$

3.3.2. Step 2: Estimate the Peak Overpressure. The TNT equivalent of the 0.2 lb C4 charge is 0.274 lbs. Using the equivalent charge weight and a standoff distance of 4.33 ft the scaled distance can be calculated using Equation 3 (Section 2.2). The calculated scaled distance is 6.67. This scaled distance can be used with Figure 3.6 to estimate the peak overpressure (Step 2).

The 6.67 scaled distance was plotted in Figure 3.7. Where the scaled distance plot and the peak pressure curve intersect (blue circle in Figure 3.7) is the estimated peak pressure (Right Y axis), so the estimated peak incident pressure for a 0.2 lb C4 sphere is 15 psi.

The charge's shape significantly affects the shockwave's propagation and can therefore generate a focusing effect of the associated pressure. A spherically-shaped charge has a different shockwave expansion than a cylindrically-shaped charge or a cubic charge (Swisdak, 1975). This research uses a cylindrically shaped charge to use smaller charges, yet have an amplified pressure along the plane of interest. This was important to accommodate Missouri University of Science and Technology's (Missouri S&T's) recently imposed air blast limits. Using a cylinder also helped reduce the pressure variance associated with hand packed charges.

3.3.3. Step 3: Calculate the Charge Geometry's Effect on Estimated Peak Over Pressure. Understanding how the charge's shape affects the shockwave expansion is an important aspect of this research. The discussion thus far has included the assumption

that the shockwave propagation is a spherical shockwave. The assumption includes the rate of expansion is equal in all directions for a spherical shockwave.

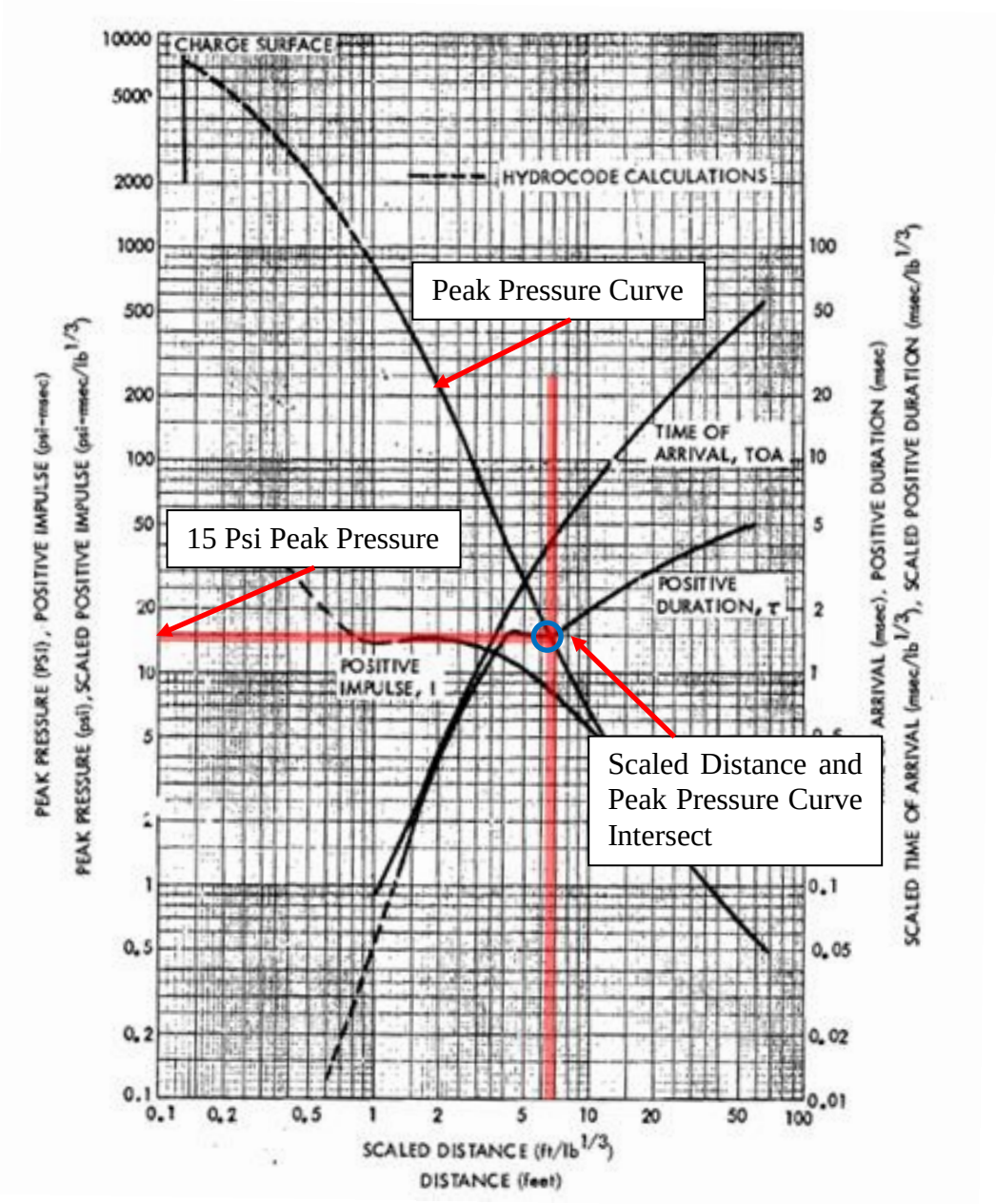

Figure 3.6. Shockwave parameters for a 1 lb. sphere of TNT (Michael M Swisdak, 1975)

Figure 3.7 shows the difference between the shockwave expansion of a spherical charge (left) and that of a cylindrical charge (right). Note the semi-uniformity of the spherical charge vs. the non-uniformity of the cylindrical charge. The non-uniformity of the cylindrical charge correlates to the center XY-plane of the cylinder (Blue dotted line) and the Z-axis (Green dashed line).

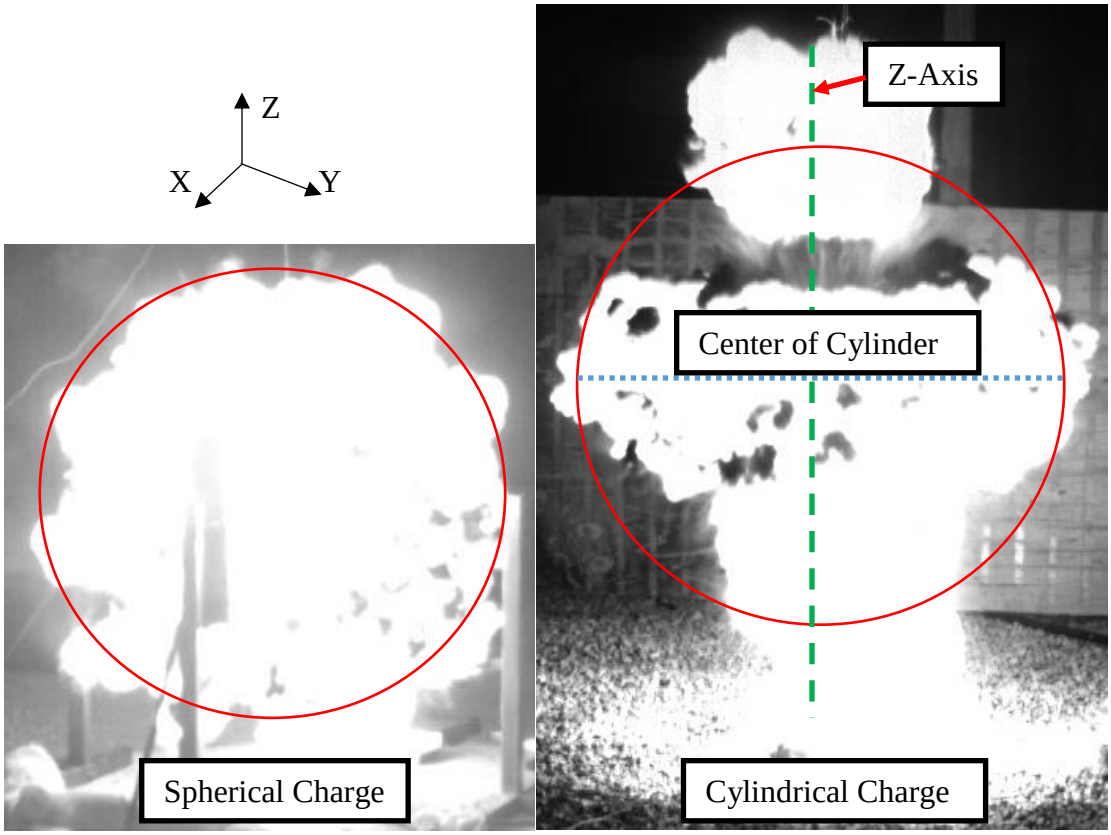

Figure 3.7. Shockwave expansion of a spherical charge compared to the shockwave expansion of a cylindrical charge.

An increase in peak pressure from a cylindrical charge, compared to a spherical charge, exists on the XY-plane in the center of the cylinder charge (Swisdak, 1975). The

increase in pressure can be attributed to the detonation propagating through the cylinder. A center-initiated spherical charge's detonation wave propagates radially with minimal effects from the geometry. However, with a cylindrical geometry detonated at one end, the detonation wave interacts with the edges of the cylinder and quickly generates a planar detonation wave. The charges used for these experiments were end initiated cylindrical shaped charges. Once the planar detonation wave has been established, the expansion of the shockwave is traveling faster along the X-Y axis of the charge (Walters W. P. & Zukas J. A., 1989).

Figure 3.8 illustrates using the cylinder length to diameter ratio with the scaled distance to obtain the estimated pressure amplification associated with the cylinder geometry (Step 3). When the charge length to diameter ratio is 1:1.16 at a scaled distance of 6.67, the resulting pressure is 1.1 times that of a spherical charge of equal charge weight.

3.3.4. Step 4: Calculate the Reflected Pressure. Multiplying the amplification factor times the peak incident pressure from a sphere (15 psi) results in a pressure of 16.5 psi. The 16.5-psi incident pressure (P_i) will impact the cylindrical surface of the target and the pressure sensors will theoretically record the reflected pressure at the apex of the target cylinder. Using Figure 3.9 and interpolation the predicted reflected pressure (P_r) is approximately 46.4 psi (Step 4).

The 46.4 psi represents the predicted reflected pressure at the apex of the cylinder. Knowing the pressure at the apex of the cylinder enables the prediction of the pressure associated with the shockwave wrapping around the cylindrical surface. The following section uses a technique similar to P_1/P_r ratios presented in Section 2.3.4.

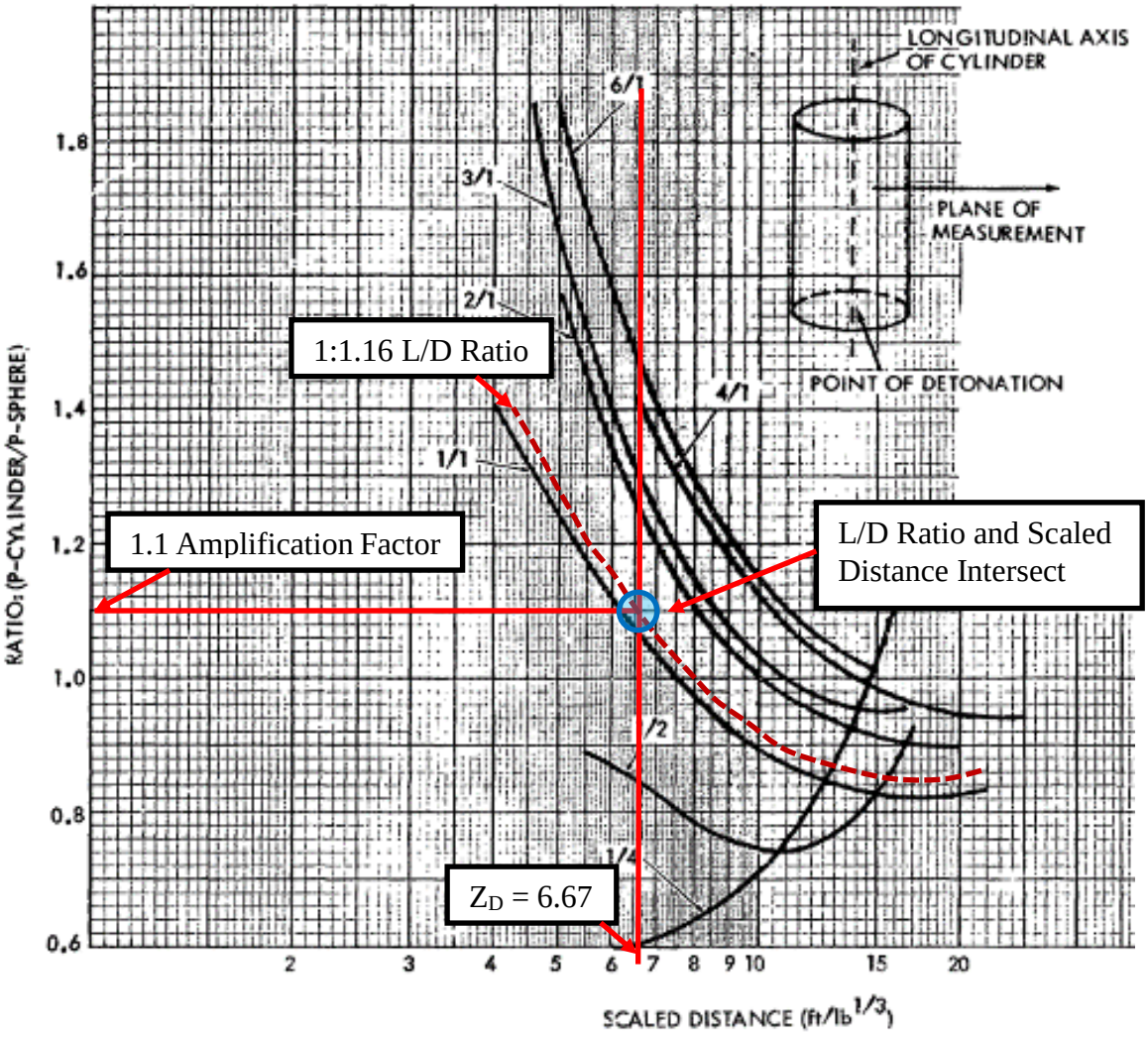

Figure 3.8. Pressure relationship between cylindrical charges and spherical charges of equal charge weight (Swisdak, 1975)

OVER PRESSURE (PSI)	SHOCK VELOCITY (FT/SEC)	PARTICLE VELOCITY (FT/SEC)	DENSITY RATIO	DYNAMIC PRESSURE (PSI)	REFLECTED PRESSURE (PSI)
10	1371.1	424.23	1.448	2.21	25.31
15	1493.1	584.53	1.643	4.77	41.45
20	1605.8	724.85	1.823	8.14	59.53

Figure 3.9. Figure 2.5 edited to view 15-20 psi overpressure in order to estimate the reflected pressure from 16.5 psi overpressure

3.3.5. Step 5: Identify the Angular Positions of Symmetry Plane. The symmetry planes of interest are dependent upon the angular spacing between charges. The angular spacings of interests to this research are 180, 120, 90, 60, and 40-degrees. Section 4.4.14 elaborates on how and why these angular spacings were selected. The angular position of the symmetry plane is the half angle of the angular spacing, so in this research the angular position of the symmetry planes are 90, 60, 45, 30, and 20-degrees (Step 5).

3.3.6. Step 6: Calculate the Pressure Wrapping Around the Cylindrical Surface. The work presented in Section 2.3.4 relates the peak pressure acting on the cylindrical surface as a percentage of P_r, where P_r is the pressure at the apex of the cylinder. The P_1/P_r ratios presented in Figure 2.15 can be used to estimate the pressure associated with a shockwave wrapping around the cylindrical surface. The cylinder diameter and charge weight (nuclear explosion) likely influence the rate the pressure decays as the shockwave traverses the cylindrical surface. Therefore, the P_1/P_r ratios ($P_{\%}$) for a 0.2 lb charge interacting with a 6.65 inch diameter are required for the Peak Pressure Predictive Method.

The data from a single 0.2 lb C-4 charge was used to generate two predictive equations for $P_{\%}$ associated with a shockwave traversing a cylindrical surface. The equation was broken into two parts to improve the accuracy of the predicted ratio. The two parts are divided into $0 \leq \theta \leq 90$ and $90 < \theta \leq 180$, Equations 7 and 8 respectively.

$$P_{\%} = (4e^{-7} * \theta^3) - (8.5e^{-5} * \theta^3) - (0.0028 * \theta) + 1 \quad \text{for } 0 \leq \theta \leq 90 \tag{7}$$

$$P_{\%} = (3e^{-7} * \theta^3) - (6.6e^{-5} * \theta^3) - (0.0013 * \theta) + 0.805 \quad \text{for } 90 < \theta \leq 180 \tag{8}$$

The predicted $P_{\%}$ is plotted for $0 \leq \theta \leq 180$ degrees in Figure 3.10 using Equations 7 and 8. The Predicted $P_{\%}$ is compared to the empirical $P_{\%}$ for a single 0.2 lb C-4 charge. Note that the empirical data has a spike in the $P_{\%}$ at 30-degrees. From the discussion in Section 2.3, this is likely a Mach Stem overtaking the incident shockwave.

When compared to the validation tests Equations 7 and 8 have an average error of 10.5%. Equation 1 (Section 1.5) was used to calculate the error for each test. The model error for each angular position on the cylinder surface is shown in Figure 3.11. The accepted error for CONWEP is 6 percent. However, the error can be up to 25 percent for small charges similar to the ones used in this research.

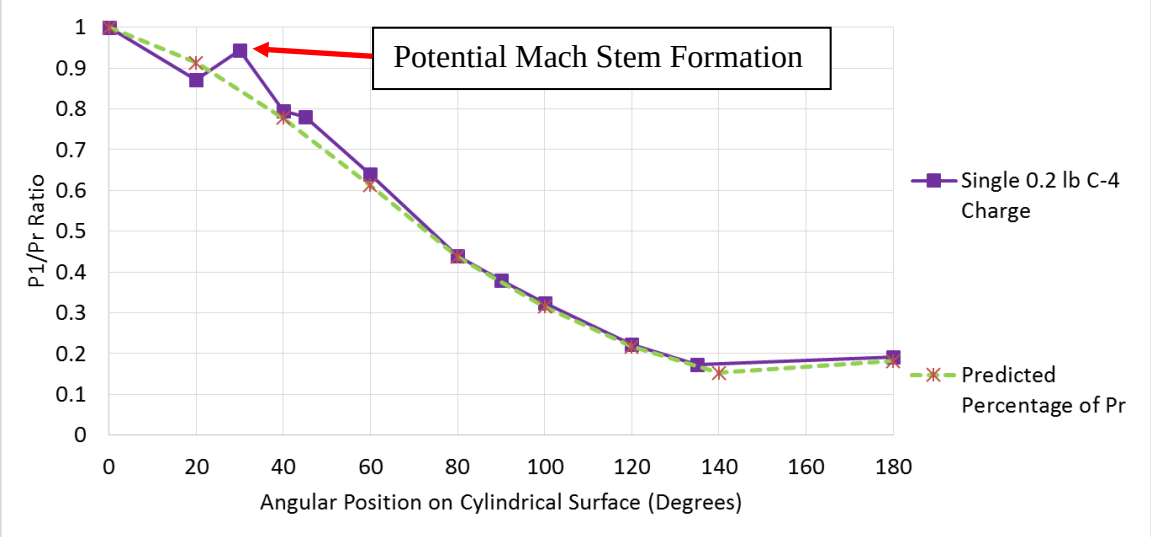

Figure 3.10. Predicted $P_{\%}$ compared to the empirical $P_{\%}$ for a single 0.2 lb c-4 charge illustrating the accuracy of the $P_{\%}$ equations.

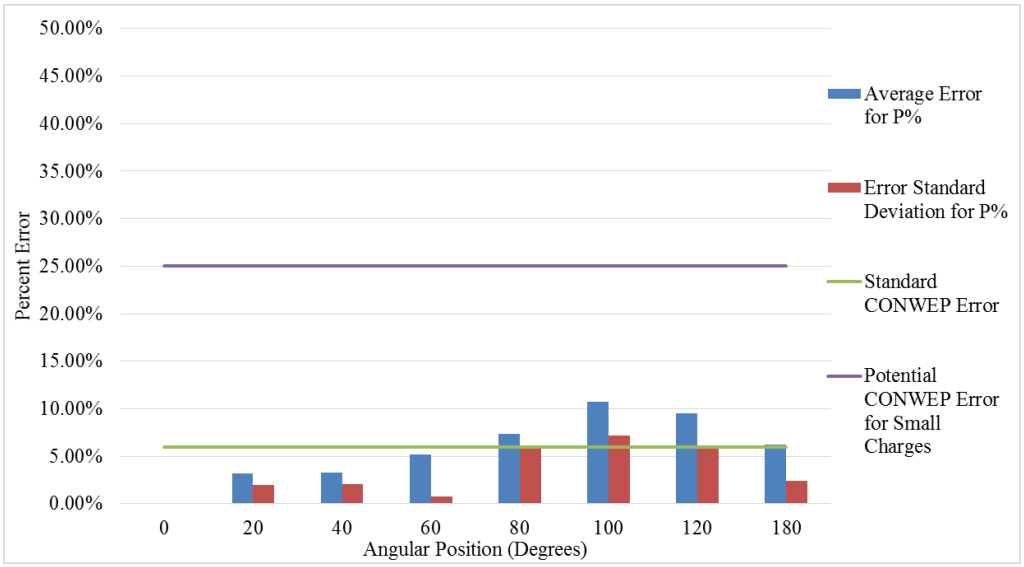

Figure 3.11. Average error and standard deviation for angular position θ compared to accepted CONWEP error.

The accuracy of Equations 7 and 8 for predicting $P_{\%}$, indicates these equations can be used in the Peak Pressure Predictive Method. The pressures at given angular spacings ($0 \leq \theta \leq 180$) are shown in Table 3.1, using ratios from Equations 7 and 8 (Step 6). However, $P_{\%}$ at 30-degrees was adjusted to account for the Mach stem overtaking the incident shockwave. In the previous section, the pressure acting on the apex of the cylinder was estimated to be 46.9 psi (P_r).

Having P_1 for different angular positions (θ) on the cylindrical surface is an essential part of the Peak Pressure Predictive Method. The estimated pressure acting on the cylindrical surface can now be used to identify the pressure associated with the two shockwaves that will collide along the symmetry plane on the cylindrical surface (P_c). The following section details the process for using P_1 to predict P_c.

Table 3.1. Predicted peak pressure at a specified angular spacings using ratios $P_{\%}$.

Angular Position (Degrees)	Percentage of P_r From ($P_{\%}$)	Predicted Peak Pressure (Psi)
0	100.00%	46.4
20	87.20%	40.5
30	94.41%	43.8
40	79.59%	36.9
45	77.96%	36.2
60	63.94%	29.7
80	43.90%	20.4
90	37.92%	17.6
100	32.30%	15.0
120	22.34%	10.4
135	17.29%	8.0
180	19.12%	8.9

3.3.7. Step 7: Calculate the P_1/P_0 Ratio. Knowing P_1, the P_1/P_0 Ratio can be calculated. The ambient over pressure (P0) in Rolla, Missouri at the time these tests were conducted was 14.75 psi. Using the P_1 values in Table 3.1, for the angular position of the symmetry planes of interest, the P_1/P_0 ratios were calculated and are listed in Table 3.2 (Step 7). The angular spacings tested are 40, 60, 90, 120, and 180-degrees. Section 4 discusses why these angular spacings were selected. The symmetry plane's angular position is half the angular spacing.

3.3.8. Step 8: Calculate the Pressure Amplification (P_{Amp}). The ratios and amplification factors from Figure 3.5 were plotted in excel. Equation 9 was obtained from a third-order polynomial curve fit of the data. Using the P_1/P_0 ratios from Table 3.2, Equation 9 can calculate the pressure amplification factor (P_{Amp}).

Table 3.2. P1/P0 ratios for the angular position of the symmetry planes of interest.

Angular Position (Degrees)	Predicted Peak Pressure (Psi)	P_1/Po Ratio
0	46.4	3.1
20	40.5	2.7
30	43.8	3.0
45	36.2	2.5
60	29.7	2.0
90	17.6	1.2

$$P_{Amp} = \left(0.0064 * \left|\frac{P_1}{P_0}\right|^3\right) - \left(0.1003 * \left|\frac{P_1}{P_0}\right|^2\right) + \left(0.8419 * \left|\frac{P_1}{P_0}\right|\right) + 2.0016 \qquad (9)$$

The pressure amplifications calculated using Equation 9 is listed in Table 3.3 (Step 8).

Table 3.3. Pressure amplification calculated using Equation 9 for the angular position of the symmetry planes of interest.

Angular Position (Degrees)	P_1/P_o Ratio	Pressure Amplification Factor (P_{Amp})
0	3.1	3.9
20	2.7	3.7
30	3.0	3.8
45	2.5	3.6
60	2.0	3.3
90	1.2	2.9

3.3.9. Step 9: Calculate the Pressure for the Colliding Shockwaves at the Symmetry Plane. The pressure along the symmetry plane (P_c) can be calculated by

multiplying the pressure of the symmetry plane of interests (P_1) by the pressure amplification factor (P_{Amp}). Equation 10 shows this calculation.

$$P_C = P_1 * P_{Amp} \tag{10}$$

The pressure for the angular positions of interests was calculated. The calculated pressure is plotted in Figure 3.12 (Step 9). The predicted pressures shown in Figure 3.12 are for two charges colliding on the cylindrical surface. The predicted reflected pressure from a single 0.4 lb charge (P_r) is also plotted in Figure 3.12. Note the predicted pressure from multiple charges using Peak Pressure Predictive Method generates an estimated peak pressure higher than then the single 0.4 lb charge when the angular spacing is reduced.

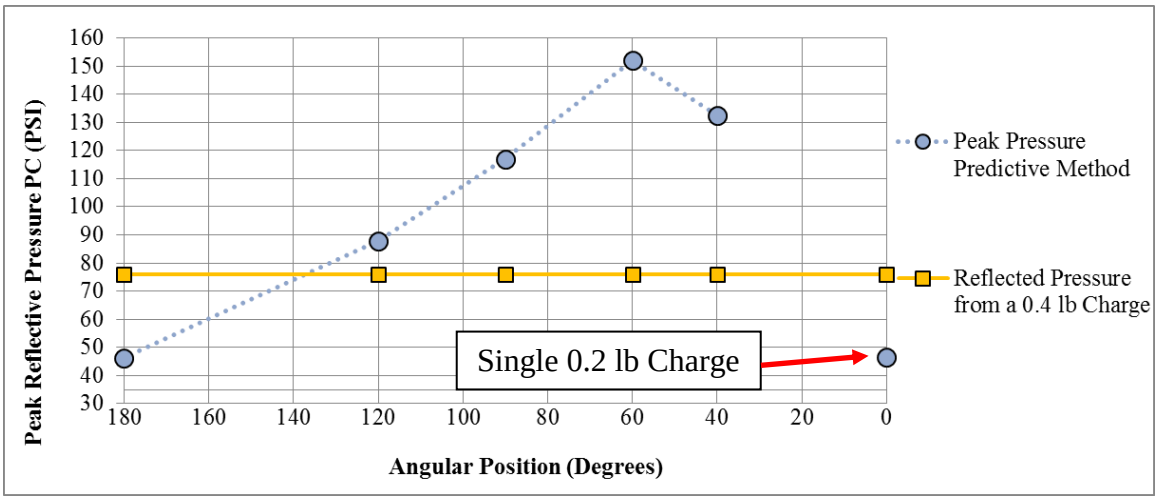

Figure 3.12. Pressure obtained using the peak pressure predictive method for the symmetry planes of interest.

3.4. SUMMARY

This section has presented the theory of the Peak Pressure Predictive Method (Section 3.2). The dynamics of shockwave interactions is the foundation of the Peak Pressure Predictive Method. The pressure amplification used in the Peak Pressure Predictive Method uses the amplification from a shockwave colliding with a solid reflective surface. As a result, the Peak Pressure Predictive Method may need to be adjusted to accommodate this lower amplification.

The predicted pressures calculated in this section need to be validated with empirical testing. The experiments outlined in Section 4 will be used to validate the pressures calculated in this section. The pressures calculated in Section 3.3 will be compared to the data presented in Section 5 to determine the validity of the Peak Pressure Predictive Method. If the data collected and presented in Section 5 matches the predicted pressures presented in this section, within ±6 percent, then the Peak Pressure Predictive Method has been validated.

4. EXPERIMENTAL DESIGN TO EVALUATE THE OBJECTIVES OF THIS RESEARCH

4.3. ROAD MAP TO THIS SECTION

This section provides the factors (variables) and levels (value) identified for the experimental design to test the objectives of this research (Section 4.4). The factors and levels were used to generate the five test series of this research (Section 4.3).

This section then discusses the test site and the physical orientation of the test site used to test these experiments (Section 4.6). The results from the experimental design discussed in this section will be compared to the predicted pressures shown in Figure 3.12 to determine the validity of the Peak Pressure Predictive Method in Section 5.

4.4. EXPERIMENTAL FACTORS TO TEST THE VALIDITY OF THE PEAK PRESSURE PREDICTIVE METHOD

The factors and levels used to test the validity of the Peak Pressure Predictive Method (Objective 1) are listed in Table 4.1. The factors and levels listed in Table 4.1 were used to design the four experiments listed in Section 4.3. The factors and levels were also used to design an experiment to examine the "Multiple Charges Focusing on a Cylindrical Surface Hypothesis" (Objective 2) in Section 4.3.

The factors that were varied to test the validity of the Peak Pressure Predictive Method are the number of charges and the angular spacing between charges. The "Multiple Charges Focusing on a Cylindrical Surface Hypothesis" compares the effects of multiple charges to a charge of equal net weight (e.g. two 0.2 lb charges compared to a 0.4 lb charge).

Table 4.1. Experimental factors to test the research objectives.

Experimental Factor	Type of Factor	Value
Standoff Distance	Controlled	52 inches
Charge Height	Controlled	39.5 inches
Sensor Height	Controlled	39.5 inches
Cylinder Dimensions	Controlled	6.65 inch diameter 0.63 inch thickness 4 ft in length
Charge Mount System	Controlled	2 inch diameter cardboard tube
Initiation System	Controlled	Detonation cord
Test Site	Controlled	Missouri S&T Blast Site
Charge Geometry	Controlled	1.5 inch diameter cylinder 1.65 inches in length Cardboard confinement
Weather	Noise	Go / No-Go on Testing
*Charge Weight	Variable	0.2, 0.4, 0.6 lbs
*Angular Spacing	Variable	180, 120, 90, 60, and 40 Degrees
**Number of Sensors per cylinder	Variable	8, 10 and 14
*Number of Charges	Variable	1,2,3,4,5

* Value specific to test series: Alpha, Bravo, Charlie, Delta, or Echo

** Value determined by cylinder required to test the angular spacing: Pipe 1, Pipe 2, or Pipe 3.

The angular spacing required for a test determined which cylinder was used to measure the pressure from the shockwave interacting with its surface. The remaining factors were held constant throughout this research. The techniques used to identify and justify the levels of each factor are discussed in the following sections. The factors that were held constant are discussed as well.

4.4.4. Standoff Distance. Section 2.5 highlighted some issues associated with measuring the pressure from an explosion. Therefore, an experiment was conducted (see Appendix B) that examined the effects standoff distance and charge size have on pressure

measurement variances. These experiments measured the pressure uniformity from a shockwave as it expands radially. This was done by measuring the pressure with four pressure sensors oriented in 90-degree intervals around a single charge (see Figure 4.1). Inadvertently, the experiments in Appendix B identified the limitations of the data acquisition system's max sample rate (2 MHz/sec) when measuring peak pressure. The sample rate is not fast enough to record the peak pressure for charges in the "close-in" scaled distance.

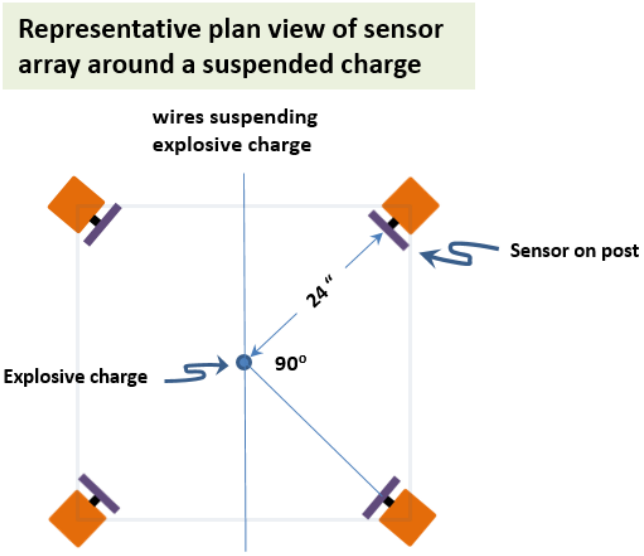

Figure 4.1. Test site orientation for measuring the pressure with four pressure sensors oriented in 90-degree intervals around a single charge.

The results from these experiments indicate the pressure variances reduce with charge weight and standoff. Two charge weights were tested (0.5 and 0.25 lbs) at three standoffs. Both charges were tested at a scaled distance of 2.5 (Close-in scaled distance). The second scaled distance was just beyond the initial fireball expansion. These scaled

distances were 6.3 and 5.9 for the 0.5 lb and 0.25 lb charges, respectively. The third scaled distance was greater than the second scaled distance, but randomly selected. These scaled distances were 9.2 and 15.6 for the 0.5 lb and 0.25 lb charges, respectively. The results from these tests are shown in Figure 4.2.

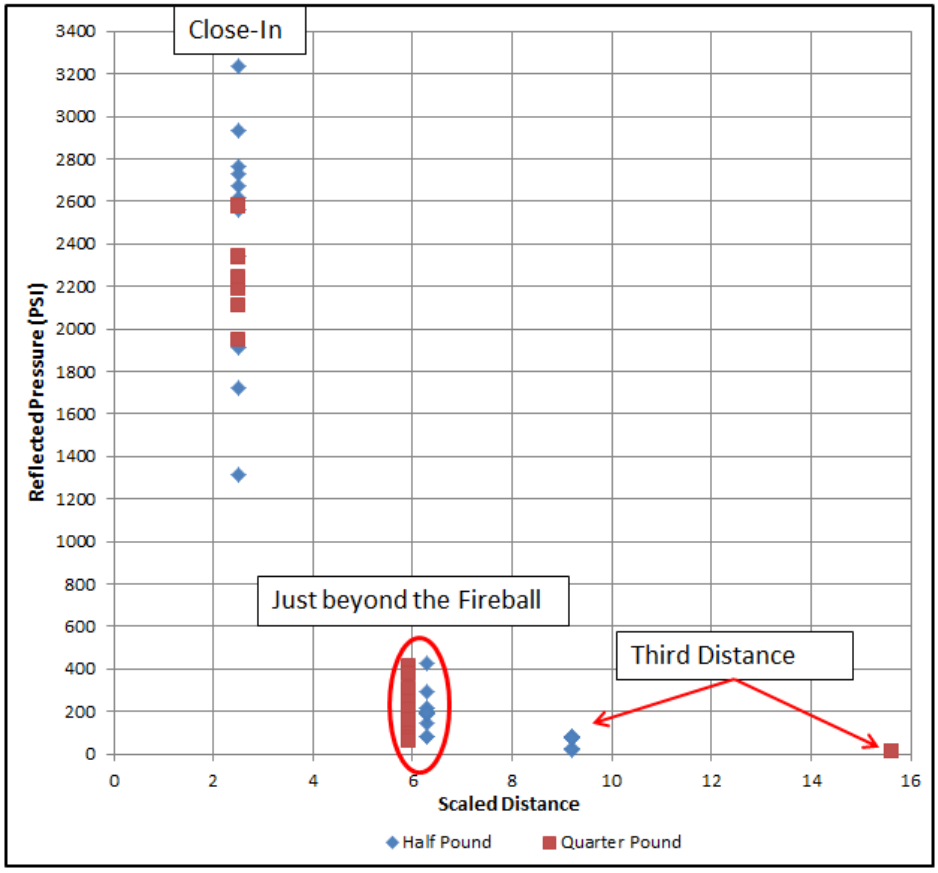

Figure 4.2. Pressure variance associated with 0.5 and 0.25 lb charges at different scaled distances.

From Figure 4.2 it is clear that the charge weight and standoff distance influence the pressure variances from an explosion. The 0.25 lb charge weight has a smaller pressure variance than the 0.5 lb charge at a scaled distance of 2.5. Additionally, as the scaled

distance increased the pressure variance decreased. With this understanding, a standoff distance between the charge and the cylindrical surface was 52 inches. This standoff distance places the cylindrical surface outside the fireball radius.

4.4.5. Charge Height. The Peak Pressure Predictive Method assumes the shockwaves interacting with the cylindrical surface (single charge) or along the symmetry plane (two or more charges) is the incident shockwave (i.e. has not reflected off any rigid bodies). In order to reduce the likelihood of measuring any reflected shockwaves from the ground. Ground conditions affect the shockwave's reflection. Each surface of each stone creates a non-normal reflection. This reflection can significantly complicate and confound the data collected should the reflected shockwave be relative to the analysis. Therefore, Figure 2.7 (Section 2.2) was used with the standoff distance for a 0.2 lb charge to determine the charge height. The charge height needed to be higher than the triple point in order to prevent measuring any reflected shockwaves from rigid bodies. The determined charge height to the center of the cylinder was 39.5 inches.

4.4.6. Sensor Height. In order to utilize the pressure amplification of the cylinder geometry, the sensors needed to be at the same height as the center of the explosive charge. Therefore, the sensor height was 39.5 inches. All three cylinders positioned the sensors on the same plane as the center of the charge.

4.4.7. Cylinder Dimensions. The cylinder's diameter significantly affects how the shockwave wraps around the cylinder (as referenced in Section 2.3; Ben-Dor, 1950). A smaller cylinder diameter, relative to the shockwave expansion, allows for a greater angular

displacement per distance the shockwave traverses. The angular displacement correlates to the reduction in pressure (also noted in Section 2.3).

Experiments were conducted to examine how the curvature of the cylinder affects the peak pressure at the apex of the cylinder. Three cylinder diameters were tested and the pressure was compared to the peak pressure from a flat reflective surface. The three cylinder diameters were 2, 4, and 6.63 inches. The results were inconclusive, due to large variances in the pressure reading from test to test. Therefore, this research used the same cylinder diameter as the cylinder in the Deepwater Horizon accident, to test the objectives of this research. The cylinder in the Deepwater Horizon accident had a diameter of 6.63 inches and a thickness 0.63 inches (LP, 2014). The results are given in Appendix C.

Note: If the cylinder's surface is not smooth, the shockwaves cannot maintain contact with the cylinder's surface. This can create irregularities in the data collected. Therefore, after the sensor mounts were secured in the cylinder wall. The cylinders were resurfaced to minimize any surface roughness.

4.4.8. Charge Mount System. The mount used to suspend the charge in the appropriate location could have an influence on the data (see Section 2.5). Therefore, suspending the charge with a wire does not work for this research. The wires impede the expansion of the shockwave and confound the data. In addition, the wire mount system allows the charges to swing making their exact positions at the time of detonation unknowable. The wire mount system also tilted the charge and evidence could be seen in the high-speed camera where the wires impeded the shockwave expansions (see Figure 2.23, Section 2.5).

A new charge mount system was developed to place the cylindrical charges in the appropriate location. This system consisted of a 1.75-inch outer diameter tube mounted to a 6-inch steel plate. A 2-inch shipping tube was used to obtain the correct charge height. This new system allowed the charges to be easily positioned radially. The new system also enabled a consistent vertical charge height for all of the charges in the test. The charge mounting system is pictured in Figure 4.3.

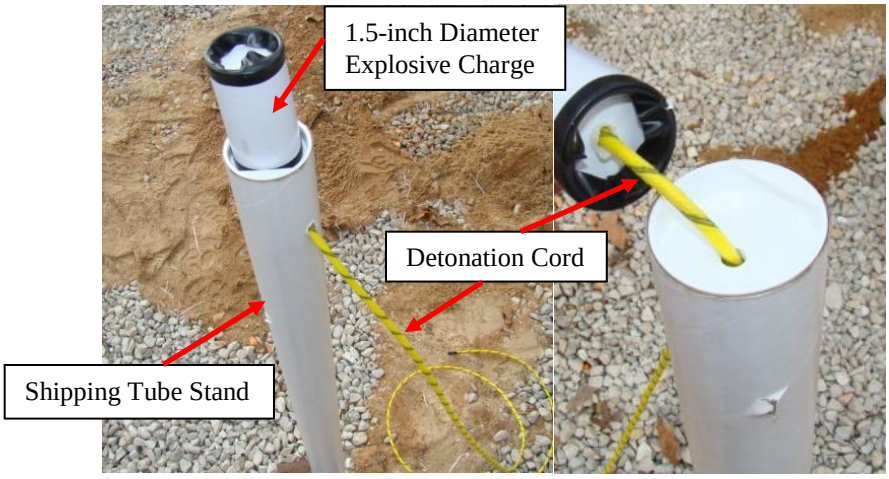

Figure 4.3. Charge mounting system developed for these tests.

4.4.9. Initiation System. The simultaneous initiation of the charges is important for the shockwave interactions to occur on the cylinder surface. Several initiation options exist that can detonate C-4. These options are listed in Table 4.2. The associated initiation scatter (cap scatter or low function time simultaneity standard deviation) is also listed in Table 4.2. Cap scatter is the timing deviation associated with a detonator (blasting cap). Some of the scatter associated with the initiation options was readily available from the manufacturer. For the initiation options that were the scatter associated with the initiation

option was not readily available, a series of experiments were conducted to determine the associated scatter. These experiments are discussed in Appendix D.

Table 4.2. Available initiation options and their associated initiation scatter

Initiation Option	Initiation Scatter	Source
Electric Blasting Cap	± 26 Percent of Delay Time	(Hoffman J., 2013)
Non-Electric Blasting Cap (NonEL)	± 26 Percent of Delay Time	(Hoffman J., 2013)
Electronic Blasting Cap	218.5 Microseconds (Zero delay)	Appendix D
Exploding Bridge Wire (EBW)	0.125 Microseconds	(Teledyne, 2015)
Non-El without delay fuse	6 Microseconds	(Farnfield et. al. 2009)
Detonation Cord	12 Microseconds	Appendix D

Based on the cap scatter presented in Table 4.2, Missouri S&T's initiation equipment and accessibility of the initiation options, detonation cord was the initiation option chosen for this research. Appendix D provides details the experiments conducted to identify the cap scatter and why detonation cord was chosen for this research.

4.4.10. Test Site. The test site used for the objectives of this research was Missouri S&T's outdoor test site. The site is equipped with a research bunker that allowed the equipment to be close to the tests. The open-air configuration reduced any reflections that might occur if the tests were done in the underground test facility at Missouri S&T.

4.4.11. Charge Geometry. The shape of an explosive has an effect on how the shockwave expands (see Section 3.3.3). A hand packed C-4 sphere, unless perfectly spherical and symmetrically initiated at its exact center will produce asymmetric radial shock waves and pressure contours. Therefore, this author conducted experiments to determine the appropriate charge geometry for this research.

The experiments used three charge shapes and examined the uniformity of the shockwave expansion from each:

1. 0.2 lb sphere: neoprene glove confinement
2. 0.2 lb cylinder with a 1.5 inch diameter: cardboard confinement
3. 0.2 lb cylinder with 1 inch diameter: cardboard confinement

From these experiments, detailed in Appendix B, it was determined that the cylindrical charges had the more uniform shockwave expansion along the sensor plane. Of the two cylinder designs, the 1.5-inch cylinder better accommodated the detonation cord triple role knot selected for charge initiation. Therefore, a 1.5-inch diameter cylinder with a 1.1 length-to-diameter ratio and 0.125-inch thick cardboard confinement was selected for testing the validity of the Peak Pressure Method.

4.4.12. Weather. Weather conditions can significantly influence the outcome of this research. These factors were identified in an attempt to either control them evenly within the data or avoid them entirely throughout the study.

- Rain
- Wind
- Temperature
- Frontal system/low ceilings

The weather factors could not be controlled. Tests could not be performed in the rain because to the rain reduced the high-speed video clarity. High wind can blow the charge either toward or away from the sensors when the original charge mounting technique was used. The mounting technique removed the possibility that wind could move the charge. Temperature affects the density of C-4 and, therefore, both detonation velocity and pressure. All of the tests were conducted within a four-week period (December 2013) in consistent weather in an effort to control the effect of temperature on the data.

A weather front directly affects the ceiling height. The ceiling height is the measure of cloud base height relative to the Earth's surface. A low ceiling traps the explosive energy and reflects it down creating a higher reflected pressure at greater distances away from the charge than the pressure from an identical charge detonated with a higher ceiling. A low ceiling means the charge weights have to be lowered to accommodate the amplified air blast. Unfortunately, this author had no choice other than to conduct many of the tests under low ceilings.

4.4.13. Charge Weight. The charge weight was highly influenced by the test site's charge weight restrictions. At the time this experimental design was created, the total charge weight could not exceed two pounds. Due to the simultaneous detonation of the charges, the total charge weight encompasses the weight of each individual charge and the explosive weight of the detonation cord used to initiate it.

The combination of charge weight restrictions and the finding that smaller charges at larger standoff distances have low pressure variances from test to test and sensor and sensor, led to the decision to use 0.2 lb charges detonated simultaneously to test the objectives of this research. A single 0.2 lb charge was also used to examine how the

shockwave wraps around a 6.63-inch diameter cylinder, simulating the pipe in the Deepwater Horizon accident.

Objective 2 of this research is to prove the hypothesis that multiple charges can impart a higher peak pressure or impulse on a cylindrical surface than a charge of equal net weight. Therefore, two charges at the angular spacings of interest will be compared to a single 0.4 lb charge. Additionally, three charges will be compared to a 0.6 lb charge.

4.4.14. Angular Spacing. Of course, this factor was only considered when two or more charges were required in the experimental design (Bravo, Charlie, Delta tests). Angular spacing refers to the angle between charges, measured from the center of the cylinder. The angular spacing between the multiple-charge configurations used in this research was based on both of the following:

- Total number of charges that can be evenly spaced within a 360-degree domain.
- The minimum allowable spacing between sensors in the cylinder body.

The green highlighted cells in Table 4.3 represent the angular spacings selected to examine how multiple shockwaves from multiple explosions interact and affect a centrally located cylinder. If the angular spacing were less than 40-degrees, there would not be enough material to secure the sensor mounts in the wall of the cylinder. Closer positioning also prevented the cables from being connected to the sensors due to the lack of spacing; therefore, the minimum angular spacing between charges was limited to 40-degrees and sensors are needed in 20-degree increments. The process for developing and securing the sensor mounts is detailed in Appendix E.

Table 4.3. Integer number of charges with angular spacing

Angle	Number of Charges
40	9
45	8
60	6
72	5
90	4
120	3
180	2
360 (Zero)	1

To examine how multiple shockwaves converge on a cylindrical surface, the sensors are positioned at the half angle of the charges' angular spacing. This positioning should capture the pressure amplification along the symmetry plane. Figure 4.4 shows the five charge angular positions (Blue) that are highlighted in Table 4.3 and the corresponding half angles (Black).

The number of cylinders with sensor mounts was limited to three due to the complexity of mounting the sensors in the cylinder wall. The cylinders, the angular position of the sensors, and the charge angular spacing tested on the cylinder are as follows:

- Pipe 1 - 45 degrees – 180 and 90 degree angular spacings
- Pipe 2 - 30 degrees - 120 and 60 degree angular spacings
- Pipe 3 - 20 degrees - 40 degree angular spacing

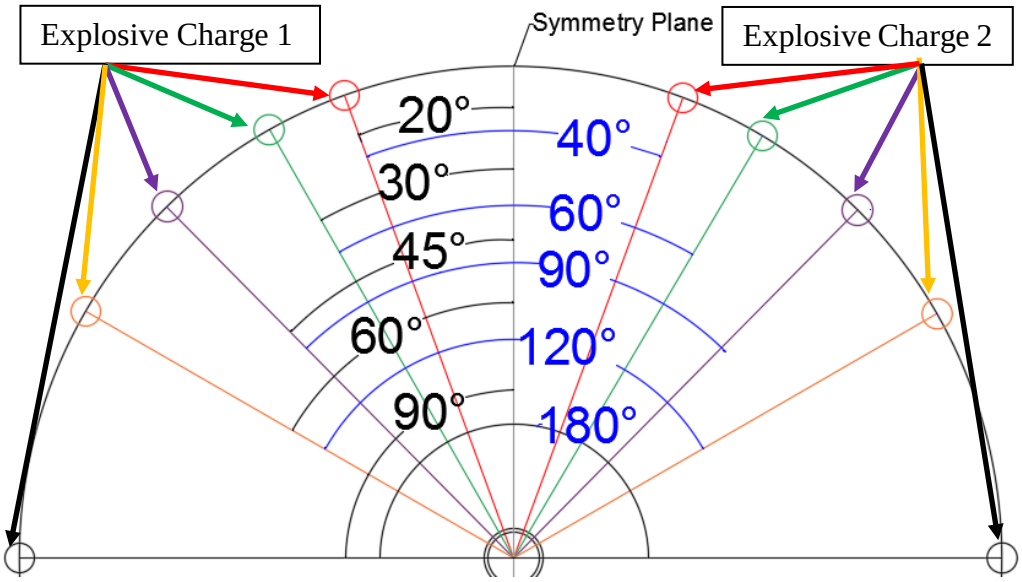

Figure 4.4. Demonstration of angular spacing with respect to the charge positioning and the symmetry plane for the two charge tests.

4.4.15. Number of Sensors per Cylinder. The number of sensors per cylinder was determined by the following and discussed below:

- The required angular position of the sensors.
- Number of sensors to cover 240-degrees of the cylinder surface (± 120 degrees from signature sensor).
- A sensor was always positioned at 180 degrees (opposite the signature sensor).

The signature sensor was the sensor in line with the single charge in the Alpha and Echo tests. The position of this sensor never changed throughout the testing, regardless of the cylinder or number of charges used. The two-charge tests (Bravo) were oriented so the signature sensor would record the two shockwave colliding along the symmetry plane. For example, the two charges with 40 degree angular spacing were positioned at +20 degrees and -20 degrees from the signature sensor. The three-charge tests (Charlie) were oriented

so the center charge was in line with the signature sensor. For example, the three charges with 40 degree angular spacing were positioned at +20, 0 (signature sensor), and -20 degrees.

The decision was made to only cover ± 120 degrees of the cylindrical surface, measured from the signature sensor, with sensors. This was due to how the experimental design oriented the shockwave interactions; all of the shockwave interactions from 1-5 charges would occur in this region or at 180-degrees. Thus, the last sensor was positioned at 180-degrees.

The number of sensors per cylinder is as follows:

- Pipe 1 – 8 sensors
- Pipe 2 – 10 sensors
- Pipe 3 – 14 sensors

The sensors used varied depending on the predicted pressure for a given angular position. This reduced the likelihood of damaging the sensors. The pressure sensors used throughout this research were PCB Piezotronic's 102B, 102B06, and 102B15. These sensors have a measurement range of 5,000, 500, and 100 psi, respectively. The Data sheets are listed in Appendix F.

4.4.16. Number of Charges. The Peak Pressure Predictive Method is for predicting the pressure along a symmetry plane, which exists when two or more charges are positioned around the cylinder surface. Therefore, in order to examine the validity of the Peak Pressure Predictive Method, multiple charges were used. Table 4.4 shows the number of charges used in each test series and the individual charge weights.

Table 4.4. Number of charges in each test series and the individual charge weight per test

Test Series	Number of Charges	Individual Charge Weight (lbs)
Alpha 1	1	0.2
Alpha 2	1	0.2
Alpha 3	1	0.2
Bravo 1	2	0.2
Bravo 2	2	0.2
Bravo 3	2	0.2
Bravo 4	2	0.2
Bravo 5	2	0.2
Charlie 1	3	0.2
Charlie 2	3	0.2
Charlie 3	3	0.2
Charlie 4	3	0.2
Delta 1	4	0.2
Delta 2	5	0.2
Echo 1	1	0.4
Echo 2	1	0.6

The first test series (Alpha) used a single 0.2 lb charge. This test examined how the shockwave from a 0.2 lb charge interacted with a cylinder that has a diameter of 6.63 inches. The results from this test were used as a baseline for the pressure amplification calculations and to generate Equations 7 and 8 (see Section 3.3.6).

The second test series (Bravo) examined the validity of the Peak Pressure Predictive Method for two charges (0.2 lbs each) at different angular spacings. The results from this test were compared to the predicted pressures shown in Figure 3.13. If the predicted pressure was within ± 6 percent of the empirical data, then the Peak Pressure Predictive Method was validated for the angular spacings tested in this research.

Assuming the shockwaves interact on the cylinder surface, then the number of charges should not influence the peak pressure along the symmetry plane. However,

depending on the angular spacing it is possible that the shockwaves will form a Mach stem that will overtake the incident wave and interact with the cylindrical surface. To determine if the number of charges influences the peak pressure along the symmetry plane, the third test series (Charlie) has three charges (0.2 lbs each) at specified angular spacings.

The fourth test series (Delta) maintains the assumption that the number of charges should not influence the peak pressure along the symmetry plane, so long as the Mach stem has not overtaken the incident shockwave. Keeping the charge weight restrictions in mind the Delta tests were designed to cover the front half of the cylindrical surface (θ>180 degrees) with charges at a given angular spacing. When the angular spacing was 180-degrees, two charges (in the Bravo test series) covered the entire cylindrical surface so the 180-degree angular spacing with two charges was not repeated for this test series. Additionally, when the angular spacing was 120-degrees, three charges (in the Charlie test series) covered the entire cylindrical surface, so the 120-degree angular spacing with three charges was not repeated for this test series. The number of charges required to cover the front half of the cylindrical surface, when the angular spacing was 40-degrees, exceeded the charge weight limit when the Detonation cord was added to the total charge weight. Therefore, the 40-degree angular spacing was not tested in this series. Subsequently, only 90- and 60-degree spacings were tested during the Delta test series. The number of charges for each test were four and five (0.2 lbs each), respectively.

The final test series (Echo) was used to examine the "Multiple Charges Focusing on a Cylindrical Surface Hypothesis" (Objective 2). This test series uses a single, but larger charge in each test. Test 1 uses a 0.4 lb charge, and the results from this test were compared to the results from the Bravo tests. Test 2 uses a 0.6 lb charge, the results from which were

compared to the results from the Charlie tests. Larger charge weights (0.8 and 1.0 lbs) were not tested due to time constraints. The following section provides the test matrices for each test series (Alpha, Bravo, Charlie, Delta, and Echo) using the factors and levels presented in this section.

4.3. TEST MATRICES TO TEST THE VALIDITY OF THE PEAK PRESSURE PREDICTIVE METHOD

The factors previously discussed were used to design the test matrices to examine the objectives of this research. The experiments were broken into five test series. These test series are Alpha, Bravo, Charlie, Delta and Echo. These experiments examined single charges in line with the signature sensor with various charge weights (0.2, 0.4, and 0.6 lb). These experiments also examined multiple 0.2 lb charges varying the number of charges (1-5) and the angular spacing between charges (180, 120, 90, 60, and 40-degrees).

A "one-factor at a time" approach was used to evaluate the factors of this research. This approach has a baseline and only changes one factor-level at a time (Montgomery, 2009). A single charge 0.2 lb charge was used as the baseline in the study reported herein. The data collected from the experiments detailed in this section is presented in Section 5.

4.3.1. Alpha Experimental Design: Single 0.2 lb Charge Positioned in Line With the Signature Sensor.

The Alpha test examined the pressure associated with a shockwave, from a single 0.2 lb charge, traversing a cylinder with a diameter of 6.63 inches. The recorded pressure was used to generate Equations 7 and 8. The peak pressure at the signature sensor and the impulse were used to examine "Multiple Charges Focusing on a Cylindrical Surface Hypothesis." The Alpha test series was composed of three experiments (Alpha 1, 2, and 3) with three test repetitions (A, B, and C) per experiment,

and each repetition used a 0.2 lb charge. For Alpha 1, there was a 45 degree angle between the sensors; for 2, there was a 30 degree angle, and for 3 there was a 20 degree angle.

4.3.2. Bravo Experimental Design: Two 0.2 lb Charges Tested at Specified Angular Spacings. The Bravo test series examines the peak pressure from two 0.2 lb charges interacting with a cylindrical surface. The peak pressure from the Bravo test series will be compared to the predicted peak pressures shown in Figure 3.12. If the predicted pressure is within ± 6 percent of the empirical data, then the Peak Pressure Predictive Method has been validated for the angular spacings tested in this research. The Bravo test series was composed of five experiments (Bravo 1, 2, 3, 4, and 5) with three test repetitions (A, B, and C) per experiment, and each repetition used a 0.2 lb charge. For Bravo 1 and 3, there was a 45 degree angle between the sensors; for 2 and 4, there was a 30 degree angle, and for 5 there was a 20 degree angle.

4.3.3. Charlie Experimental Design: Three 0.2 lb Charges Tested at Specified Angular Spacings. The Charlie test series is designed to identify if the Peak Pressure Predictive Method is applicable when the shockwave from more than two charges are converging on a centrally located cylindrical surface. Assuming the shockwaves interact on the cylinder surface, before the Mach stem overtakes the incident shockwave, then the number of charges should not influence the peak pressure along the symmetry plane. Therefore, the Charlie test series examined the effects three charges (0.2 lbs each) have on the peak pressure along the symmetry plane. The Charlie test series was composed of four experiments (Charlie 1, 2, 3, and 4) with three test repetitions (A, B, and C) per experiment, and each repetition used a 0.2 lb charge. For Charlie 1 and 3, there was a 30 degree angle

between the sensors; for 2, there was a 45 degree angle, and for 4 there was a 20 degree angle.

4.3.4. Delta Experimental Design: Charges Positioned at Specified Angular Spacings to Cover 180-Degrees of the Cylindrical Surface. The Delta test series expands on the experiments in the Charlie test series and examines the peak pressure when charges are positioned to cover front half of the cylindrical surface (θ>180 degrees) at a given angular spacing. Only 90 and 60 degrees were tested during the Delta test series due to explosive charge weight limitations. The number of charges for each test were four and five (0.2 lbs each), respectively. The Delta test series was composed of two experiments (Delta 1 and 2) with three test repetitions (A, B, and C) per experiment, and each repetition used a 0.2 lb charge. For Delta 1, there was a 45 degree angle between the sensors and for 2 there was a 30 degree angle.

4.5.8. Echo Experimental Design: Baseline for the "Multiple Charges Focusing on a Cylindrical Surface Hypothesis" (Objective 2). The Echo test series served as the baseline for the analysis of the "Multiple Charges Focusing on a Cylindrical Surface Hypothesis" (Objective 2). This test series uses a single charge. The Delta test series was composed of two experiments (Echo 1 and 2) with three test repetitions (A, B, and C) per experiment. Test 1 used a 0.4 lb charge. The results from this test were compared to the results from the Bravo tests. Test 2 uses a 0.6 lb charge. The results from this test were compared to the results from the Charlie tests.

4.6. TEST SITE PHYSICAL ORIENTATION

A majority of the test materials, stands, and mounting systems were designed and constructed specifically for the tests described in this research. Some of the techniques developed for this research are detailed in Appendices D-J. The techniques discussed in these appendices are as follows:

- Appendix D: Cylinder sensor mount construction
- Appendix E: Explosive charge construction
- Appendix F: Charge stand construction
- Appendix G: Explosive charge positioning technique
- Appendix H: Charge stand construction required to tests the objectives of this research
- Appendix I: Explosive charge positioning technique used to position the charges throughout this research
- Appendix J: Triggering system

Per the mine supervisor's recent enacted procedures, all of the tests were monitored via a blast seismograph's microphone. The permanent seismograph, located at the Missouri S&T test facility, monitored each blast. If the air blast became too high (in excess of 134 Db, per the new procedure), the tests were shut down for the day. Several weather fronts interrupted the tests, forcing them to be postponed due to the air blast.

The pipe stand was positioned such that the signature sensor either pointed away from the test bunker or was parallel to the bunker's front surface. The signature sensor was pointing parallel to the bunker's surface for the single charge tests. When multiple charges were used, the stands were turned so the signature sensor was pointed away from the

bunker. These different positions oriented the setup so the Phantom camera was in the best position to observe the shockwave interactions with a cylinder. The pipe stand's orientations relative to the camera view are pictured in Figure 4.5 and 4.6.

Figure 4.5. Single charge (Pipe 2) pipe stand setup for phantom side view, signature sensor pointed parallel to the bunker.

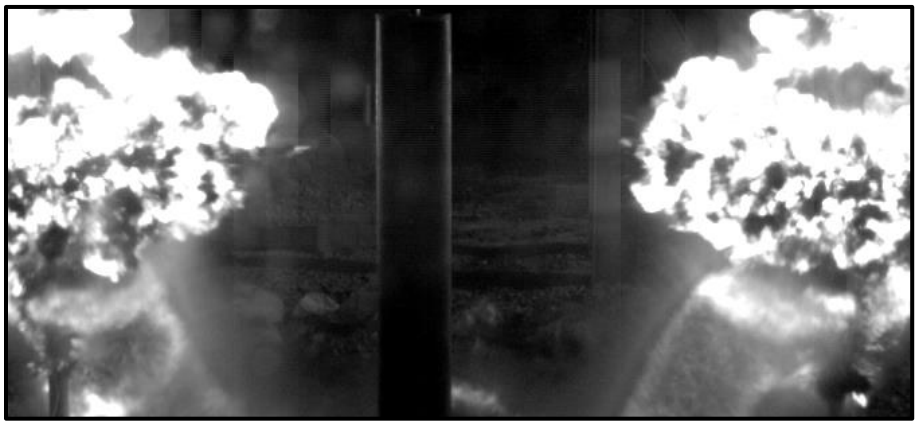

Figure 4.6. Pipe stand setup of phantom view with the signature sensor pointing away from the bunker.

In order to trigger the data acquisition system at the proper time to capture the relevant data from each test, the author used a so-called make trigger. A make trigger works by using plasma generated from the explosion to bridge two contacts, thereby causing current to flow through the contacts' circuit. The number of make triggers depended on the number of charges per test and the cylinder used. The data acquisition system has 16 channels. When possible all 16 channels were used to record data from the pressure sensors and trigger timing (See Appendix J).

Di-electric grease was placed on each sensor to minimize the effects of thermal shock on the pressure readings. Thermal shock is when the heat associated with the shockwave causes the piezo crystal to expand and generate a false pressure reading (PCB Piezotronics, 2011). Pre and post-test pictures were taken for each test. These pictures were used to document any damage or test-to-test variances. An overview of Delta 2 prior to initiation is in Figure 4.7.

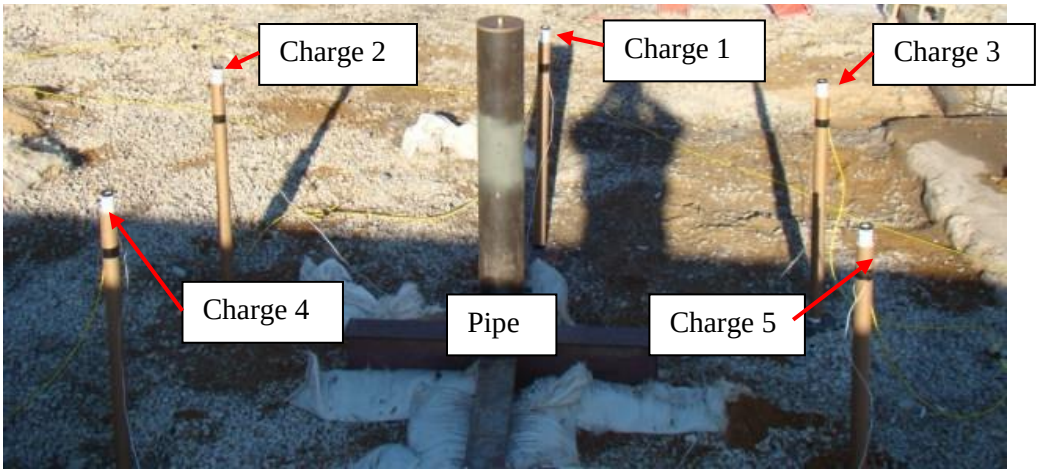

Figure 4.7. Overview of the final setup for test 17, immediately prior to initiation.

4.7. SUMMARY

The experiments discussed in this section were used to achieve the objectives of this research. The Alpha test series was used to generate Equations 7 and 8, in addition to serving as a baseline for examining the "Multiple Charges Focusing on a Cylindrical Surface Hypothesis." The Bravo tests were used to validate the Peak Pressure Predictive Method for two charges interacting with a cylindrical surface. The Charlie and Delta test continued the validation of the Peak Pressure Predictive Method by examining the peak pressure from three charges, and when half the cylinder is surround by charges. The final test series (Echo) was used, in addition to the Alpha tests, as a baseline for the "Multiple Charges Focusing on a Cylindrical Surface Hypothesis." The following section discusses the data extraction and results from these tests.

5. RESULTS

5.3. ROAD MAP TO THIS SECTION

This section presents how the data from the experiments discussed in Section 4 were analyzed to extract the peak pressure and impulse (Section 5.2) for comparison to the two objectives of this research. The peak pressure results from Alpha, Bravo, Charlie, and Delta tests were used to assess the validity of the Peak Pressure Predictive Method (Section 5.3), which was the first objective. The second objective of this research was to examine if multiple charges can generate a higher peak pressure or impulse on the cylindrical surface than a charge of equal net weight. Therefore, Section 5.4 compares the results from Bravo and Charlie tests to the Echo 1 and Echo 2 tests. Section 5.4 also examines the total impulse acting on the cylindrical surface from all five test series. This information will serve as a first step towards understanding how to seal an underwater oil pipeline using explosives.

5.4. DATA ANALYSIS OF ALPHA, BRAVO, CHARLIE, DELTA AND ECHO TESTS

The data from the experiments detailed in Section 4 were collected using a Hi-Techniques Synergy P data acquisition system with PCB Piezotronic sensors. The data were analyzed for the following information:

- Peak Pressure (psi)
- Arrival Time of the Shockwave (microseconds)
- Positive Pressure Duration (microseconds)
- Impulse (psi*microseconds)

This section briefly describes how the data was extracted. Additionally, this section details the process of generating the polar plots that were used to illustrate the peak pressure and impulse acting on the cylindrical surface.

5.4.4. Data Extraction Data Acquisition System Files. The five test series each had 16 tests. Each test was repeated three times, so a total of 48 tests were used to examine the objectives of this research. The 48 tests produced data from 525 sensors that needed to be analyzed for the peak pressure, arrival time of the shockwave, positive pressure duration, and impulse. Each sensor recorded at a sample rate of 2 MHz/sec for a total of two seconds. This resulted in a large number of data points that were analyzed to extract the necessary information.

The sensor this section will use to demonstrate how the data was extracted was located in the flat plate reflective surface in Alpha test 1. The flat plate reflective surface was placed in the Alpha and Echo tests to compare the peak pressure at the apex of the cylindrical surface to a flat reflective surface. Figure 5.1 shows the location of the flat plate reflective surface relative to the charge and pipe locations.

Using the data from the flat plate reflective surface, the data of interest was narrowed to 1,001 independent discrete data points collected every 0.5 microseconds. This data has been plotted in Figure 5.2. The peak pressure, arrival time of the shockwave, positive pressure duration, and impulse are also highlighted in Figure 5.2.

The extraction of the peak pressure, arrival time of the shockwave, positive pressure duration, and impulse was broken down into five steps. These five steps are:

1. Establish when the data acquisition system was triggered
2. Ascertain the peak pressure (47.8 psi)

3. Identify when the shockwave arrived at the sensor (1,448 microseconds)
4. Determine the positive pressure duration (351.5 microseconds)
5. Calculate the positive impulse for sensor (7.07 psi*microseconds)

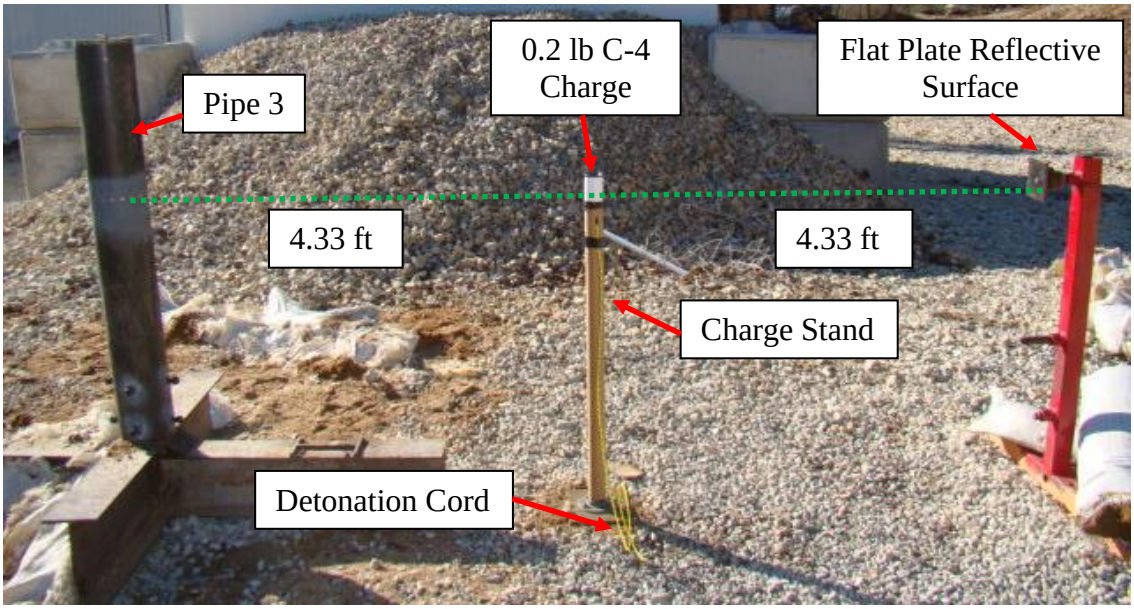

Figure 5.1. The test site setup illustrating the location of the flat plate reflecitve surface relative to the explosive charge and pipe locations.

The arrival time is determined to be when the pressure on the sensor rose above 5% of the peak pressure. The data in Figure 5.2 was examined for when the pressure rose above 2.39 psi. The arrival time of the shockwave for Figure 5.2 is 1,448 microseconds.

For this research the positive pressure duration is defined as the duration of time between the arrival time and the point in time when the pressure drops below “zero” psi. The standard technique for identifying the positive pressure duration states that the pressure returns to “zero” when the pressure returns to within 1% of the peak pressure (Kinney & Graham, 1985). This technique was not used to analyze this data due to the uncertainty that

the lingering pressure was not associated with the multiple shockwave interactions rather than the sensor's sensitivity. It is understood that there is potentially an error associated with how this author identified the arrival time and duration of pressure for each sensor. Although it is small, this technique does have an impact on the recorded impulse data.

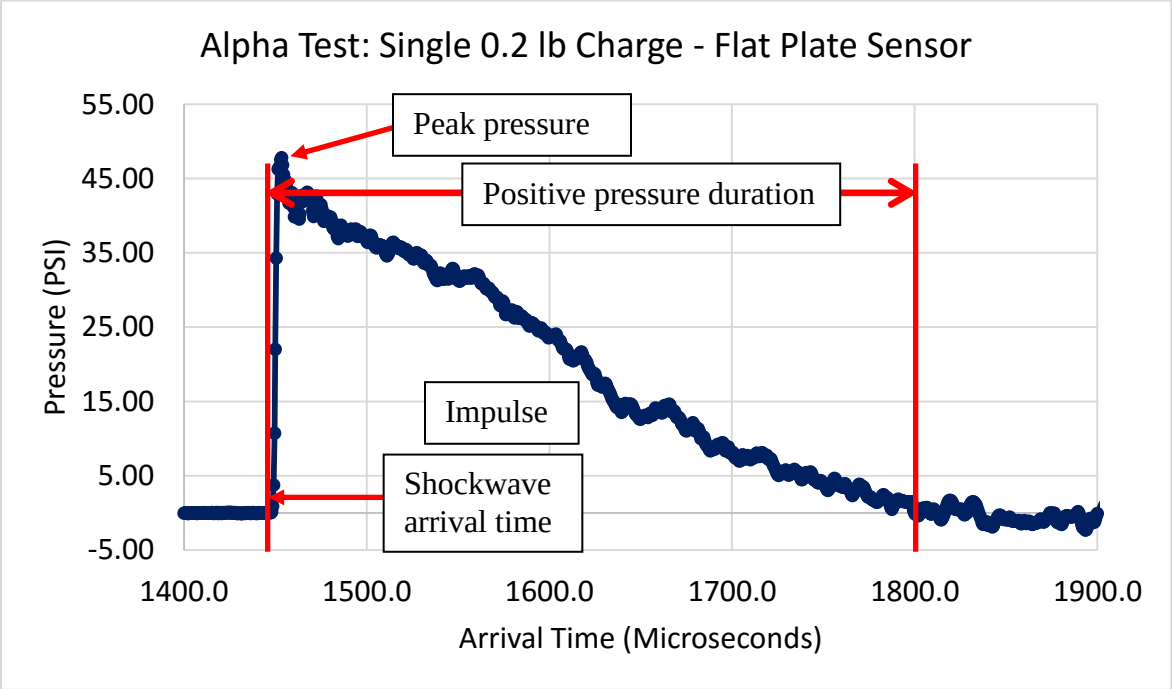

Figure 5.2. Alpha tests Run 1 of 3, sensor data from flat plate.

The impulse calculations in this research used the Midpoint Riemann Sum (MRS) technique. The MRS technique divides the area under a curve into columns of equal width, where the center of the column intersects the curve of interest. Figure 5.3 shows the first 190 half microsecond samples, of the 1,001 samples shown in Figure 5.2. These half microseconds samples shown in Figure 5.3 illustrate how the pressure curve was divided into columns for the MRS technique.

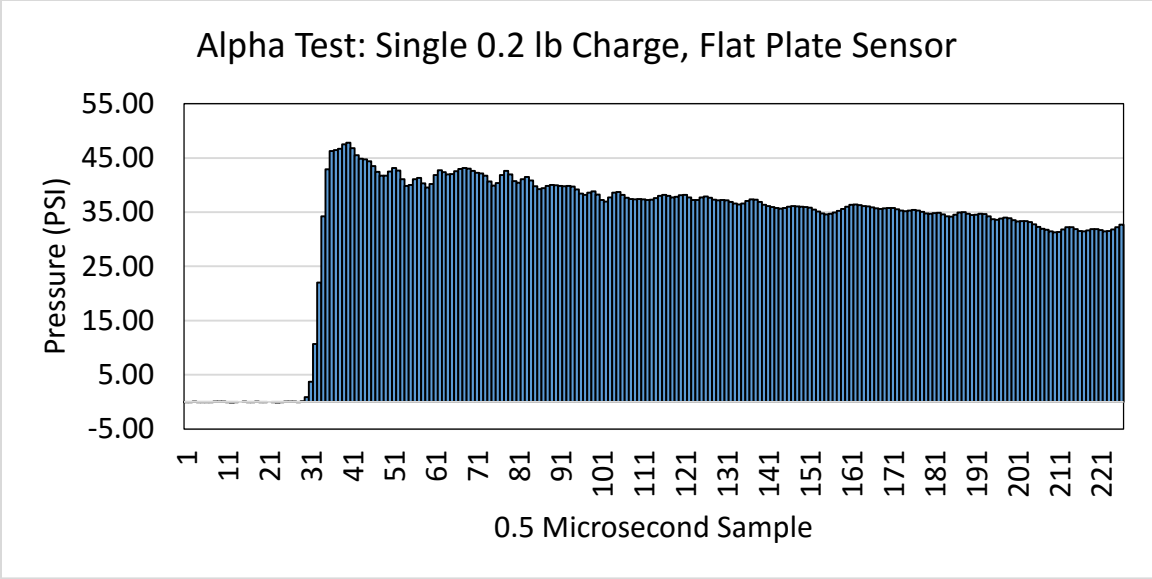

Figure 5.3. MRS technique showing the pressure of the first 190 half -microsecond samples for Figure 5.2.

Using the MRS technique, the impulse for the data plotted in Figure 5.2 is 7.07 psi*microseconds. These five steps were repeated for each of the 525-pressure sensor. A data summary from each test is listed in Appendices K-O.

The data presented in Sections 5.5 focuses on the peak pressure. The data presented in Section 5.4 examines both peak pressure and the impulse associated with single and multiple charges focusing on the cylindrical surface. The shockwave arrival time and positive pressure duration were required to calculate the positive impulse for each sensor. The data for each sensor has been summarized according to the corresponding tests.

5.4.5. Population of Polar Plots. The traditional technique for plotting the peak pressure associated with a shockwave wrapping around a cylindrical surface has been to use an XY plot of the data, where the X-axis represents the angular position of the sensor and Y represents either peak pressure or a percentage of the peak pressure, see Figure 5.4.

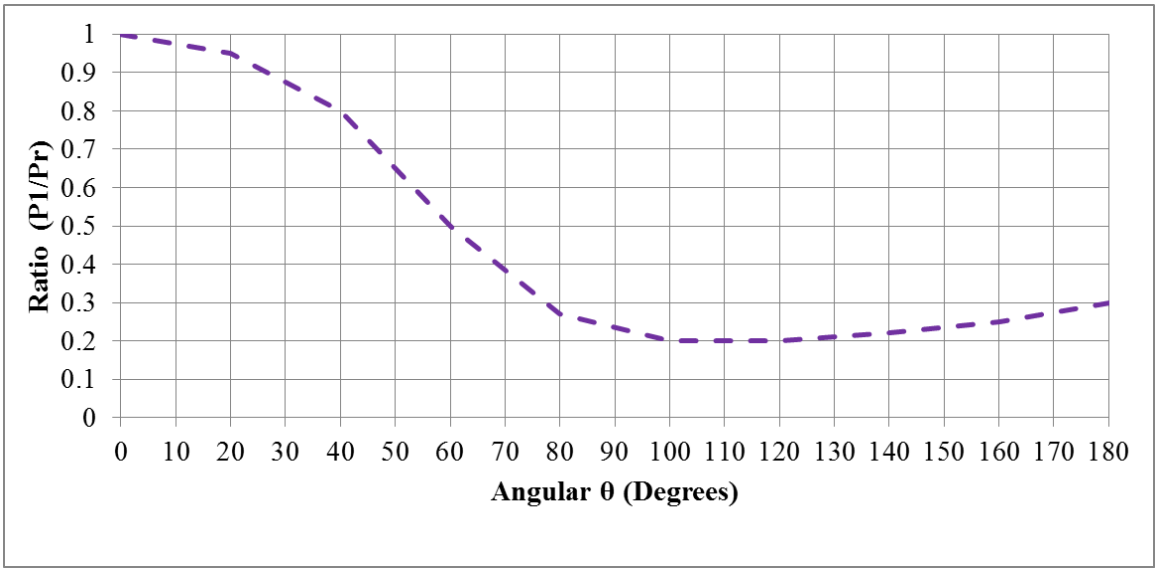

Figure 5.4. Traditional method for plotting pressure interactions with a cylinder, replotted from Figure 2.16 (Glasstone, 1962).

Plots similar to Figure 5.4 suffice to represent the pressure acting on the cylindrical surface for a single charge. However, when multiple charges interact with the cylindrical surface, plots similar to Figure 5.4 quickly become confusing. Therefore, polar plots are used herein to illustrate the peak pressure and impulse acting on the cylindrical surfaces during testing.

Polar plots represent the data as a radius at a given angular coordinate. For this research, the radius represents the pressure recorded on the cylindrical surface. The angular coordinate corresponds to the angular position of the sensor. An example of the data used to generate a peak pressure polar plot is listed in Table 5.1. The data corresponding to Sensor 1 was repeated at 360 degrees to close the pressure contour for plotting.

The macro used in this research was constructed specifically to generate these polar plots and is not standard in Excel (Pope, 2013). The polar plot generated using the

tabularized data from Table 5.1 is shown in Figure 5.5. The blue “Xs” are not part of the polar plot, but rather were added to illustrate the data points in Table 5.1.

Table 5.1. Tabularized peak pressure data and corresponding angular position for peak pressure polar plot.

Corresponding Sensor	Angular Position (Degrees)	Peak Pressure - Radius (PSI)
Sensor 1	0	46.9
Sensor 2	30	42.2
Sensor 3	60	22.5
Sensor 4	90	9.4
Sensor 5	120	9.4
Sensor 6	150	11.7
Sensor 7	180	14.1
Sensor 8	210	11.7
Sensor 9	240	9.4
Sensor 10	270	9.4
Sensor 11	300	22.5
Sensor 12	330	42.2
Sensor 1	360	46.9

In Figure 5.5, the green line represents the pressure acting on the cylinder’s surface (over 360-degrees) from a single 0.2 lb charge located along the 0-degree angular spoke. The pressure is plotted in 10-psi increments along the 0-degree angular spoke starting at zero psi in the center of the plot. The pressure increments are represented by rings expanding from the center of the plot (Origin). The 40-psi increment has been called out in Figure 5.5 with a dashed red line. Note the cylinder’s position is not present in the polar plots.

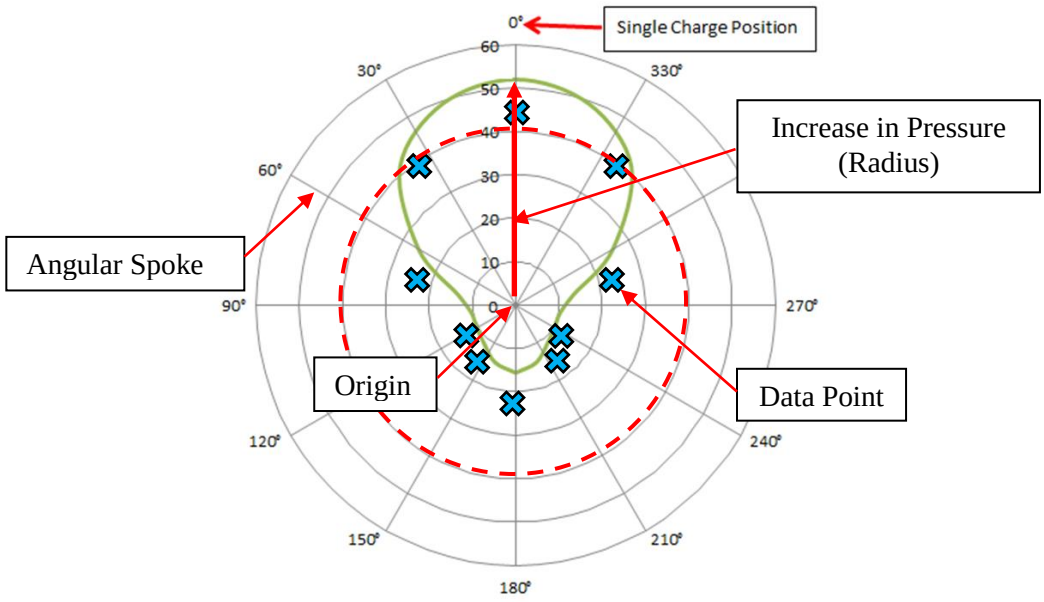

Figure 5.5. Peak pressure polar plot of predicted pressure (psi) from a single 0.2 lb charge.

The number of data points used to make each polar plot was dependent on the number of sensors in each pipe. When the polar plots required data from multiple pipes, a plot was generated for each pipe and the plots were laid over one-another. The process of generating a polar plot was repeated for the impulse acting on the cylindrical surface. Polar plots are used in addition to XY plots to present the peak pressure and impulse in the following sections.

5.5. PEAK PRESSURE PREDICTIVE METHOD VERIFICATION RESULTS (OBJECTIVE 1)

The results presented in this section are from the Alpha, Bravo, Charlie, and Delta tests specifically analyzing the validity of the Peak Pressure Predictive Method. The results from the Alpha tests were used to generate Equations 7 and 8 (Section 3.3), and to analyze the peak pressure at the apex of the pipe compared to the peak pressure on flat reflective

surface. The Alpha tests were also used to find the pressure wrapping around the cylindrical surface for all three pipes.

The Bravo test results will be used to explore the validity of the Peak Pressure Predictive Method for estimating the peak pressure along the symmetry plane for two charges. If the error from the predicted pressure using Equation 1 is ± 6 percent, the Peak Pressure Predictive Method has been validated for the angular spacings tested in this research. The Charlie and Delta tests results will be used to examine how well the Peak Pressure Predictive Method works for predicting the pressure along the symmetry plane, when more than two charges are used.

5.5.4. Alpha Test Results with Respect to Multiple Shockwave Pressure Predictive Method. How the curvature affects the reflected pressure at the signature sensor significantly affects this research. How the curvature impacts the reflected pressure is important, because the data used to estimate Pr in Steps 1-4 in Section 3.3 was obtained from a flat reflective surface. If the curvature does not affect Pr, than Steps 1-4 are an acceptable means of predicting the peak pressure at the apex of the cylindrical surface.

The recorded pressure at the signature sensor in the pipe was compared to the recorded pressure for a sensor mounted in a flat plate. The two sensors were an equal distance (4.33 ft) from the center of the charge. The recorded peak pressure at the apex of the cylindrical surface and the flat reflective surface were 42.68 and 43.94 psi, respectively. The two surfaces differ in the peak pressure by three percent. This small difference indicates the pipe's curvature does not appear to impact the reflect pressure at the apex of the cylinder for this charge weight. As the charge weight increases, the curvature's effect

on the peak pressure may become more predominant. Further testing is needed to examine if the curvature has an effect on the peak pressure from larger charges.

The pressure associated with the shockwave wrapping around the three pipes was compared to determine if the pipe surfaces induced any anomalies in the data. The recorded reflected pressure, for each pipe is shown in Figure 5.6. The three pipes have similar pressure traces associated with the shockwave traversing the cylindrical surface. There is a rise in pressure when the angular position is 30-degrees. As discussed in Section 2.3, this rise in pressure can be attributed to the Mach stem forming on the cylindrical surface.

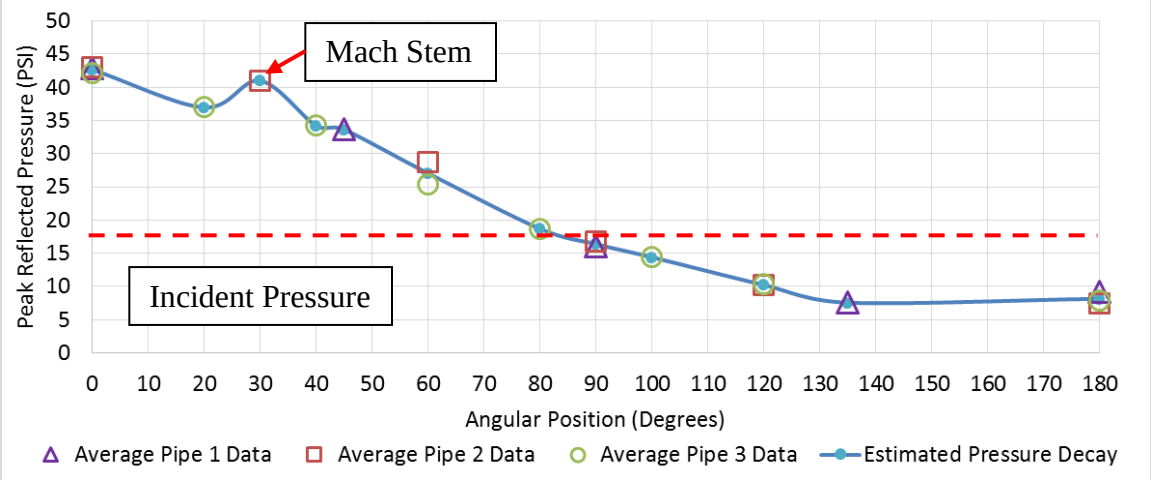

Figure 5.6. Estimated pressure decay from a shockwave wrapping around the pipe's surface.

The incident pressure shown in Figure 5.6 (red dashed line) is the estimated incident pressure required to generate the reflected pressure at the apex of the pipe (42.68 psi) using Figure 2.5 (see Section 2.2). As expected, the reflected pressure decayed as the shockwave traversed the cylindrical surface, in a manner similar to Glasstone's work (1962) presented

in Section 2.3.4. The initial estimate of 46.4 psi at the apex of the pipe's surface was higher than the recorded reflected pressure of 42.7 psi. As the pressure decayed around the pipe's surface, the pressure reduced to the predicted incident pressure of 18-psi at approximately 90-degrees.

No anomalies were identified that would indicate one of the pipe's surfaces needed further resurfacing. Therefore, the data collected on each pipe could be compared to one another. This is important, as each pipe was used to test specific angular spacings. Knowing the pipes are comparable, the results from the Bravo test can be used to validate the Peak Pressure Predictive Method.

5.3.2. Bravo Test Results with Respect to Multiple Shockwave Pressure Predictive Method. The Bravo tests were designed to examine the shockwaves from two charges converging on a cylindrical surface. The point of convergence was designed to be at the signature sensor. The results from the Bravo tests were compared to the estimated pressures from the Peak Pressure Predictive Method to identify the model error.

The first step in examining the validity of the Peak Pressure Predictive Method was to examine if the shockwaves are colliding on the cylindrical surface or if the Mach stem has over taken the incident shockwave. To do this the data acquisition system's data viewer was used to determine the shockwave's path, from each charge, along the cylindrical surface. Figure 5.7 demonstrates how the data acquisition system's data viewer was used to analyze how the two shockwaves interact with the cylindrical surface. The shockwaves from two charges with 180-degree angular spacing are illustrated in Figure 5.7.

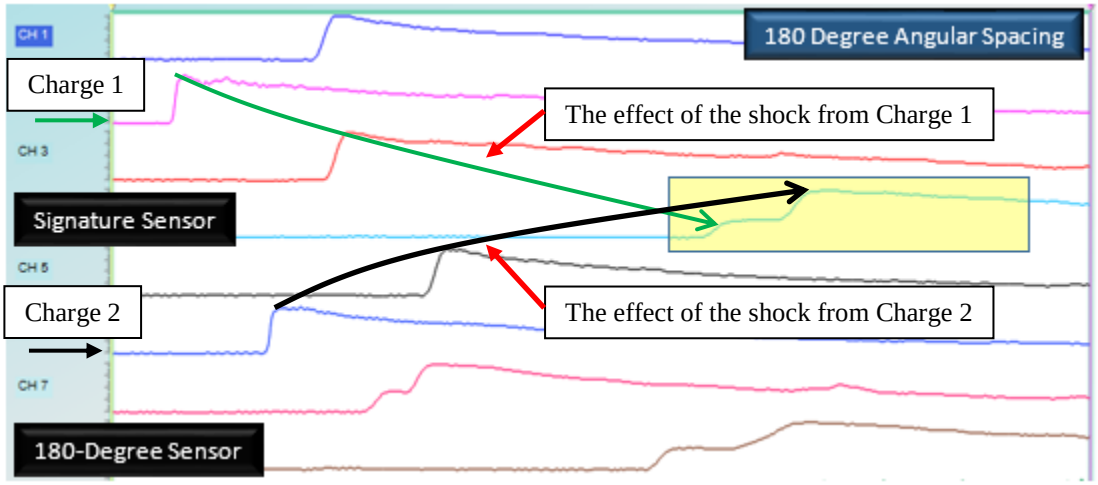

Figure 5.7. Shockwave propagation on a cylindrical surface from two charges with 180-degree angular spacing.

The channel (sensor) in which the two charges are in line with are highlighted on the left (Channels 2 and 6). There are two distinct shockwaves wrapping around the cylindrical surface and colliding at the signature sensor. Interestingly, as the angular spacing reduces to 40-degrees there are no longer two distinct shockwaves interacting with the cylindrical surface (see Figure 5.8). The pressure traces indicate that only one shockwave is interacting with the cylindrical surface. This indicates that the Mach stem has over taken the incident shockwave prior to the incident shockwaves interacting with the cylindrical surface.

Understanding that when the angular spacing is 40-degrees the two shockwaves have formed a Mach stem is important to the Peak Pressure Predictive Method. In this case, the Mach stem is formed from two shockwaves colliding, rather than a shockwave interacting with a rigid reflecting surface. Therefore, the Mach stem pressure amplifications may be different from predicted.

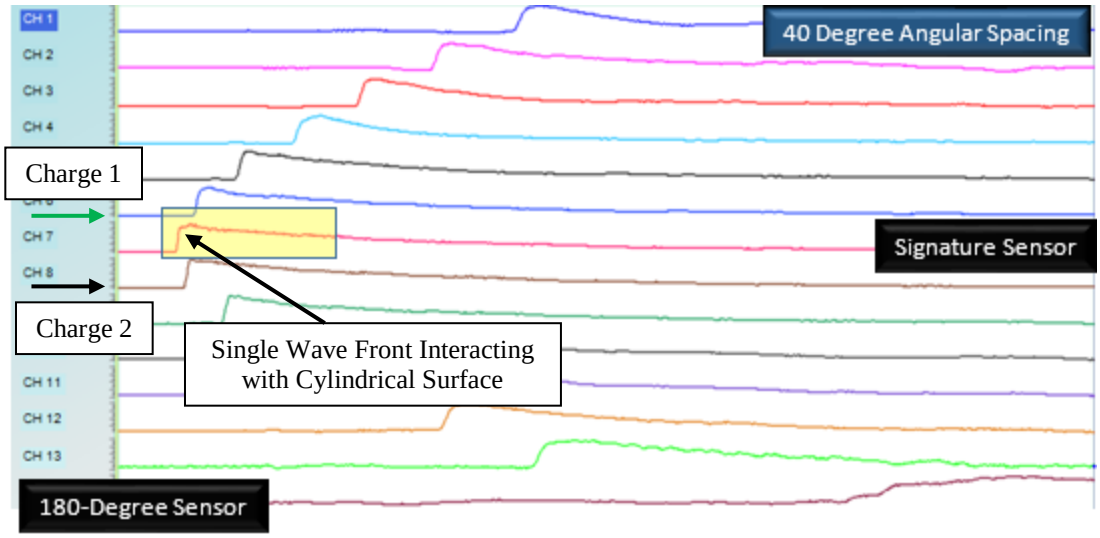

Figure 5.8. Shockwave propagation on a cylindrical surface from two charges with 40-degree angular spacing.

When comparing the estimated pressure from the Peak Pressure Predictive Method to the empirical data, note that Mach stem amplification for a 40-degree angular spacing is 80 percent of the estimated pressure, see Figure 5.9. This can be attributed to the lower Mach stem amplification produced from two shockwaves colliding rather than a shockwave interacting with a rigid reflecting surface. Figure 5.9 compares the estimated pressure for the angular spacings of interest to the pressure amplification recorded in this testing along the symmetry plane.

. The empirical (test) data is consistently 80 percent of the estimated peak pressure. Again, this can be attributed to the lower amplification of two shockwaves colliding, rather than a shockwave colliding with a rigid reflecting surface. Therefore, the Peak Pressure Predicted Method was adjusted to account for the lower pressure amplification. Figure 5.10 compares the adjusted estimated pressure using the Peak Pressure Predictive Method to the empirical pressure amplification along the symmetry plane.

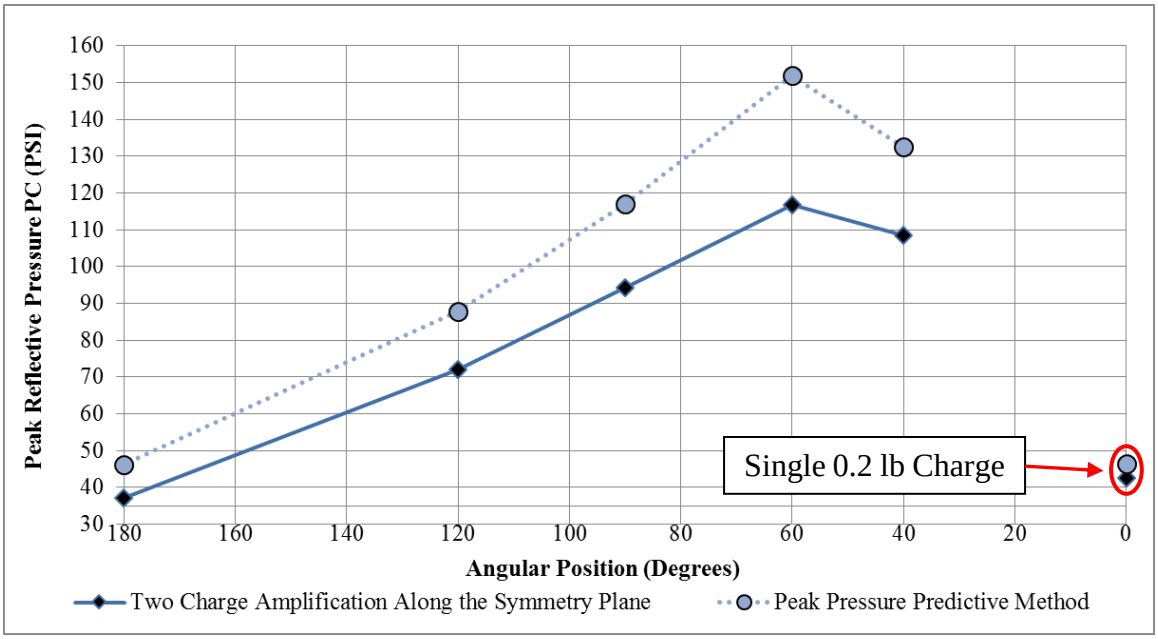

Figure 5.9. Estimated pressure from the peak pressure predictive method to test data.

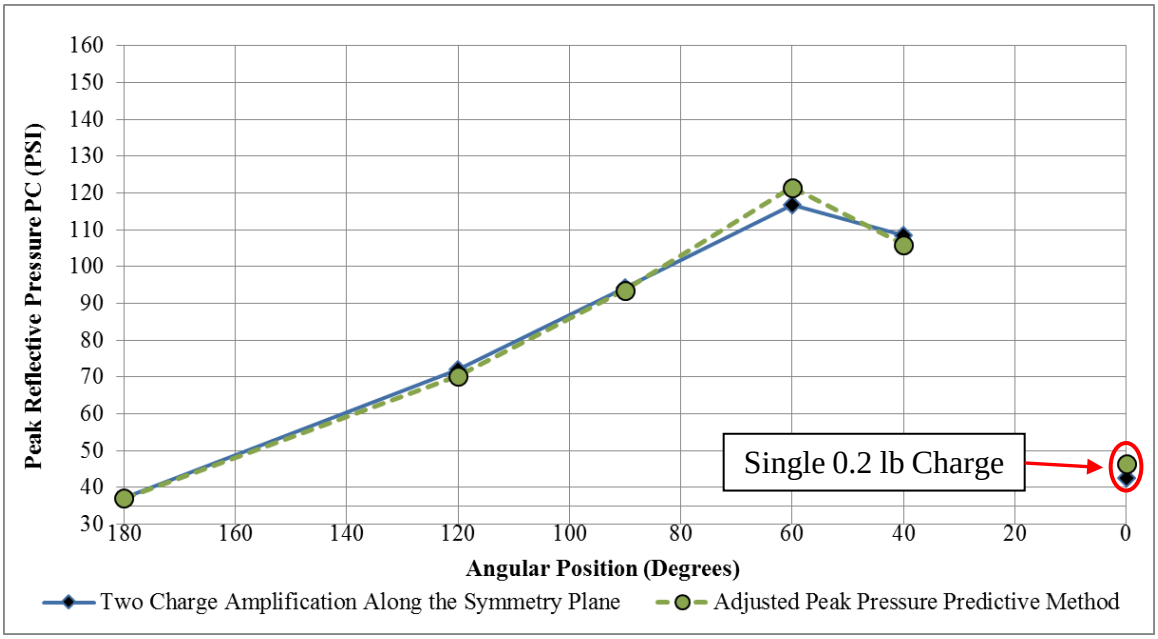

Figure 5.10. Adjusted pressure from the peak pressure predictive method compare to the emperical data.

The adjusted estimated pressure and the empirical pressure amplification along the symmetry plane appear to validate the Peak Pressure Predictive Method. However, the model error needs to be calculated using Equation 1 (see Section 1.5) for the predicted pressure. The calculated percent error for each angular spacing is compared to the accepted CONWEP error (see Section 1.5) in Figure 5.11.

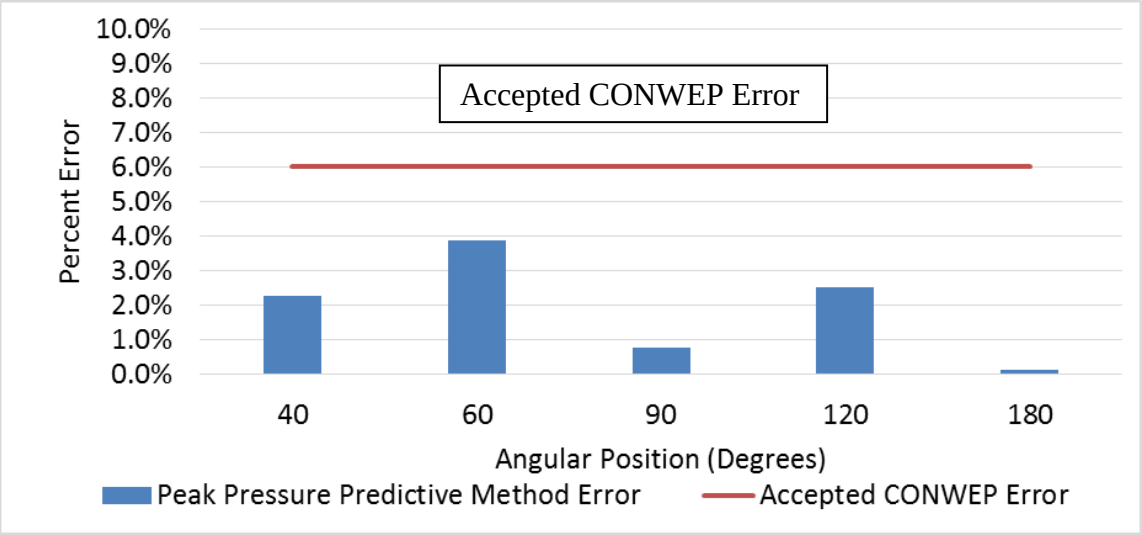

Figure 5.11. Peak pressure predictive method error compared to the accepted CONWEP error.

The model errors calculated using Equation 1 validate the Peak Pressure Predictive Method. Further research is needed to account for the reduced amplification from two shockwaves colliding head on. However, for this research the amplification was 80 percent of that for a shockwave colliding with a rigid reflecting surface. The following section examines how three charges influence the peak pressure on the cylindrical surface.

5.3.3. Charlie Test Results with Respect to Multiple Shockwave Pressure Predictive Method. For the Charlie tests, this author examined the effects three charges (0.2 lbs each) have on the peak pressure along the symmetry plane. With three charges, the center charge was always positioned in line with the signature sensor. The two remaining charges were positioned in accordance with the angular spacing from the center charge. Ideally, by setting up the tests this way, the signature sensor would represent and collect the peak pressure associated with the focused explosive pressure discussed in Section 3.2.

As with the Bravo test, the first step in examining the peak pressure from three charges interacting with the cylindrical surface was to examine how the shockwaves propagate around the pipe. The technique for examining three shockwave was the same as described for the Bravo tests. The shockwaves from three charges with 120-degree angular spacing are illustrated in Figure 5.12.

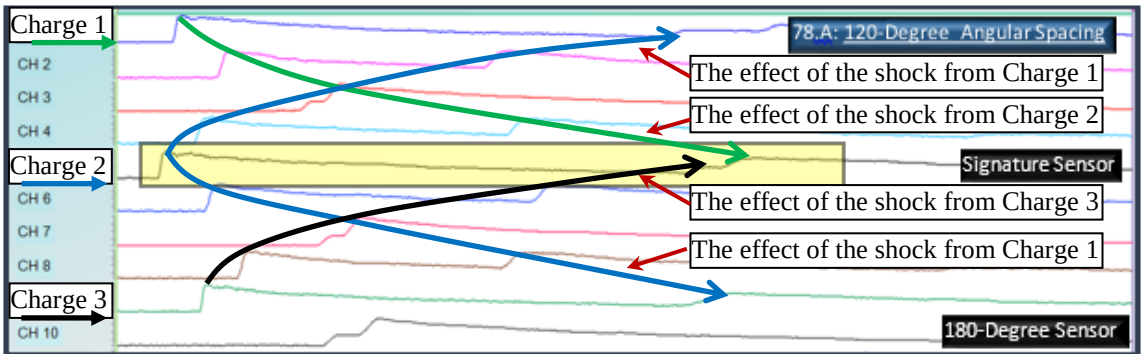

Figure 5.12. Shockwave propagation on a cylindrical surface from three charges with 120-degree angular spacing.

The channel (sensor) in which the three charges are in line with are highlighted on the left (Channel 1, 5 and 9). As with the Bravo tests, the shockwave from each charge can

be seen traversing the pipe's surface. Additionally, as the angular spacing reduced to 40-degree there is again one distinct shockwave interacting with the cylindrical surface; Figure 5.13 illustrates the single shockwave, from three charges with 40-degree angular spacing, interacting with the cylindrical surface.

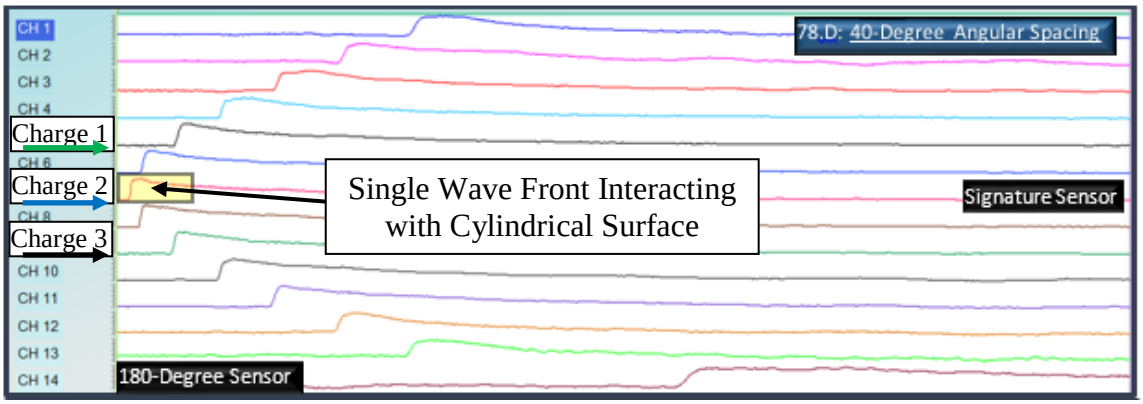

Figure 5.13. Shockwave propagation on a cylindrical surface from three charges with 40-degree angular spacing.

The signature sensor no longer represents the symmetry plane. With three charges two symmetry planes exist and the signature sensor will represent the pressure associated with any trapped pressure or the formation of a Mach stem. Therefore, to grasp the full impact of three charges acting on a cylindrical surface, polar plots were used to represent the peak reflected pressure of each angular spacing; see Figure 5.14.

In Figure 5.14, the ⊗ represents the center charge position for all of the angular spacings. The circles represent the remaining two charge positions, for the respective angular spacing. The circles are colored to match the data plotted in Figure 5.14. For example, the two red circles represent the remaining two charges for the 90-degree angular

spacing test (Charlie 2). The stars represent spikes in the peak pressure. Again, the stars are color coded to correspond to the pressure data. The dashed lines represent the symmetry plane. The dashed lines are also color coded to match the pressure data. Note the 120 and 90-degree angular spacings have a higher reflected pressure along the symmetry plane than at the signature sensor.

In the Bravo tests, the 60-degree angular spacing had the highest peak reflected pressure at the symmetry plane. In the Charlie tests, the 40-degree angular spacing had the highest peak pressure at the signature sensor (not the symmetry plane). This indicates that, for three charges, there was an increased pressure amplification for angular spacings less than 60-degrees.

Figure 5.15 illustrates the pressure amplification for the angular spacings tested for three charges at the signature sensor, along the symmetry plane, and two charges along the symmetry plane. The signature sensor data shows an increase in the peak pressure as the angular spacing decreases. However, when the angular spacing is greater than 60-degrees the peak pressure is lower at the signature sensor than along the symmetry plane. This lower pressure is highlighted in Figure 5.15 with a red oval.

The peak pressure is the same when the angular spacing is greater than 60-degrees for two and three charges along the symmetry plane. This indicates the Peak Pressure Predictive Method can be used to estimate the peak pressure for three charges acting on a cylindrical surface, when $\theta \geq 60$ degrees. The three charges with 40-degree angular spacings deviated from this predictive technique. This is due to the generation of a Mach stem prior to the pipe surface.

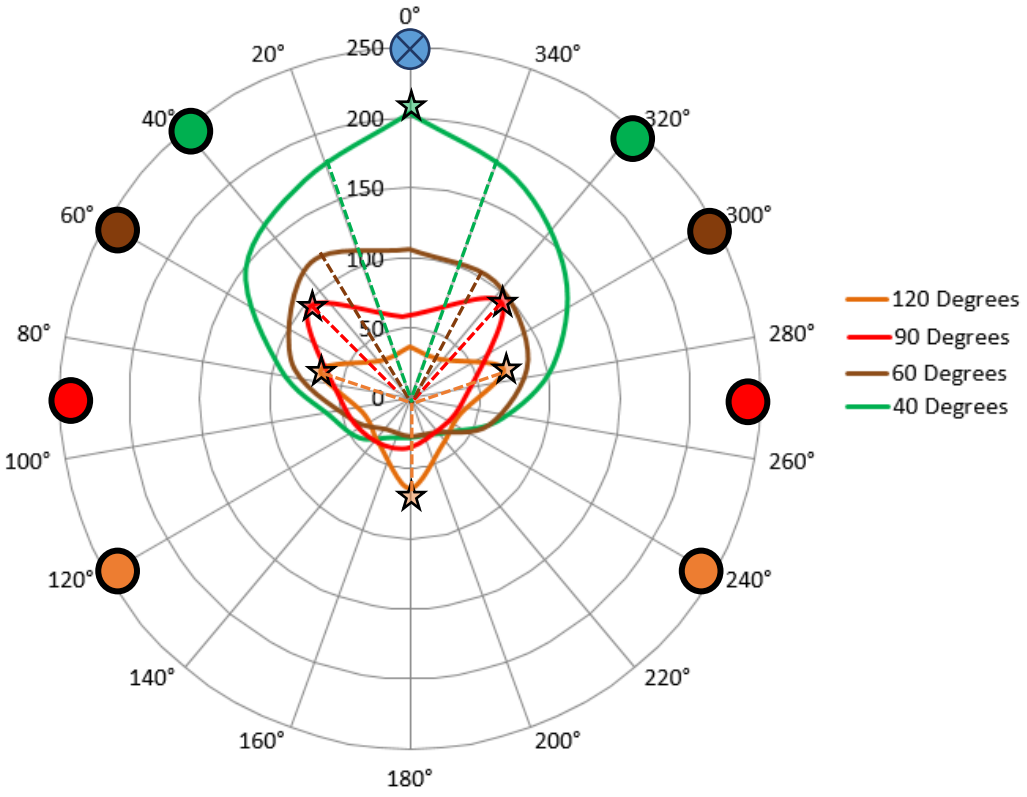

Figure 5.14. Pressure polar plot of three shockwave interactions with pipe surface (psi).

If the incident pressure from the shockwaves interacts prior to reaching the pipe's surface and generates a Mach stem, assuming an 18-psi incident pressure, then the pressure associated with the Mach stem is 52-psi. The reflection associated with the Mach stem interacting with the pipe would be approximately 209-psi. The measured peak reflected pressure at the signature sensor was 203-psi. The model error associated with this technique is 3 percent. By accounting for the Mach stem's reflected pressure the shockwave interaction from three charges on a cylinder's surface can be reasonably predicted.

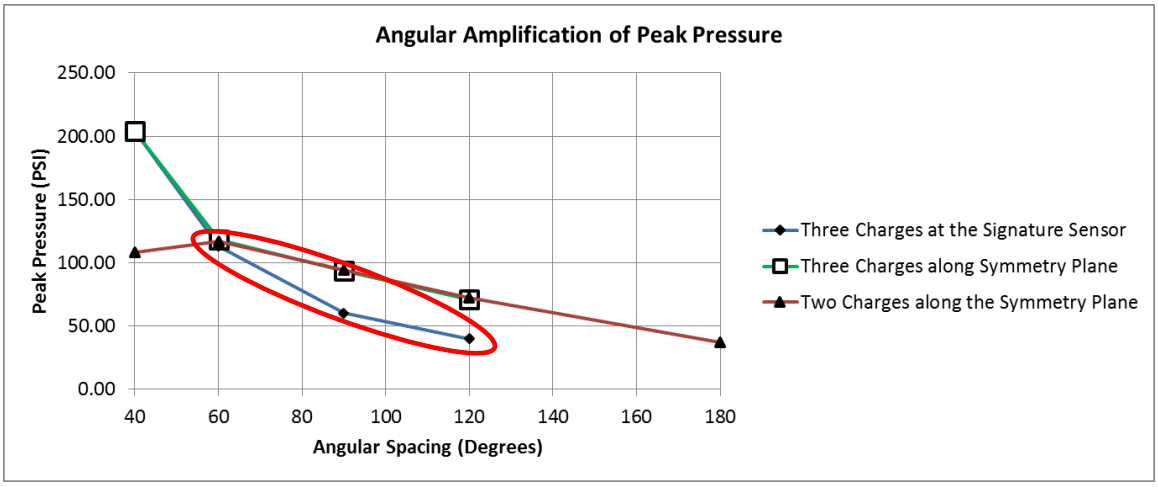

Figure 5.15. Peak pressure amplification associated with one, two, and three charges. Red oval highlights lower pressure at the signature sensor vs the symmetry plane.

5.3.4. Delta Test Results with Respect to Multiple Shockwave Pressure Predictive Method. The Delta tests were designed to examine the peak pressure when charges, at a given angular spacing, are positioned to cover the front half of the cylindrical surface (θ_T>180 degrees). The 180-degree angular spacing with two charges was not repeated for this test series (see Bravo tests, Section 5.3.2). Additionally, the 120-degree angular spacing with three charges was not repeated for this test series (see Charlie tests, Section 5.3.4).

As represented before in Figure 5.14, in Figure 5.16 and each following polar plot, the circles are color coded to correspond to the pressure data. The stars represent a spike in the peak pressure. Again, the stars are color coded to correspond to the pressure data. The dashed lines represent the symmetry plane. The dashed lines are also color coded to match the pressure data. The following circles represent the positions where single charges from two tests occupy the same angular spacings in Figure 5.16:

A 90 degree and 60 degree charge (red and brown)

A 180 degree and 90 degree charge (blue and red)

A 120 degree and 60 degree charge (yellow and brown)

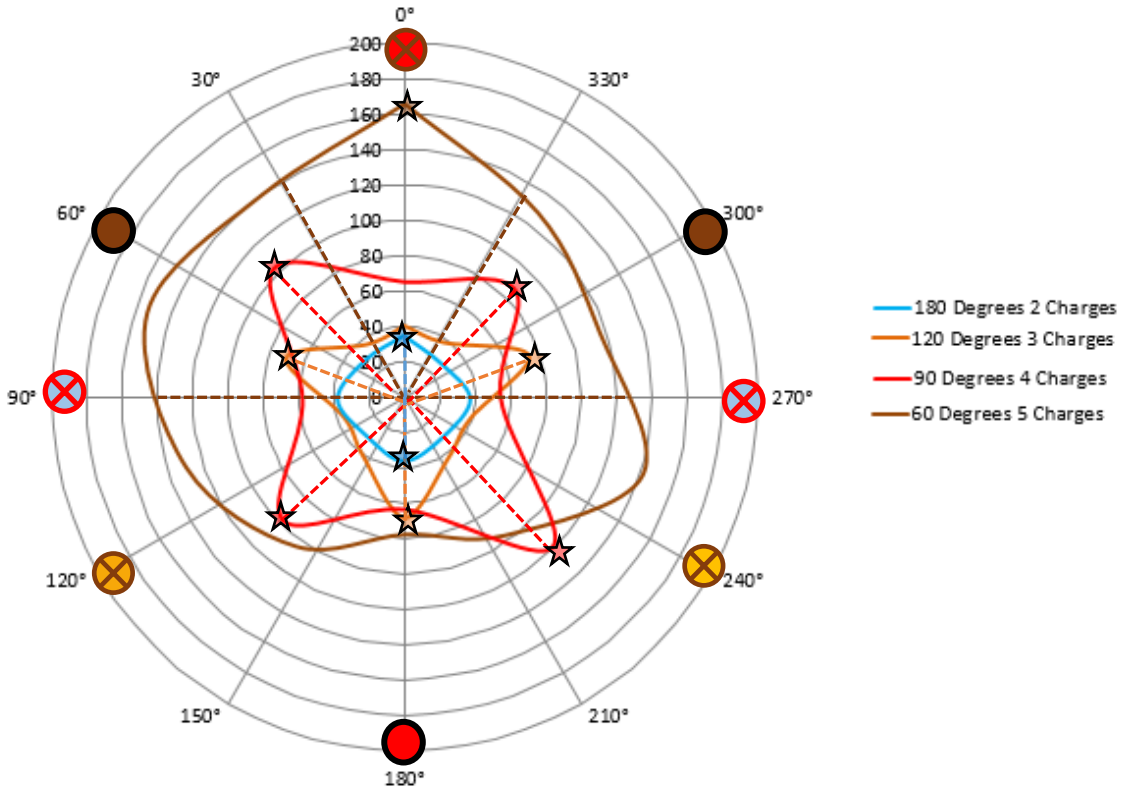

Figure 5.16. Peak pressure associated with the 180-degree tests (psi).

From Figure 5.16 it is clear that the pressure acting on the cylindrical surface also becomes uniform as the number of charges increases to cover more of the cylindrical surface. As with the Charlie tests the pressure along the symmetry plane is higher than the pressure in line with the charge, when the angular spacing is greater than 60-degrees. The pressure acting on the pipe's surface is more uniform for five charges with 60-degree angular spacing than three charges with 120-degree angular spacing. This is an important

aspect to understand when trying to seal a leaking oil pipe, as a uniform loading may not be the ideal configuration to seal the pipe. Future testing will need to examine the appropriate loading conditions required to seal a leaking oil pipe.

When comparing the peak pressure along the symmetry plane, the Charlie tests do not show an increase over the Bravo tests when θ≥ 60-degrees. When the front half of the pipe was covered with charges the peak pressure acting on the cylindrical surface begins to rise exponentially as the angular spacing decreased and the number of charges increased. This indicates the increase in the number of charges confines and focuses the pressure from each individual charge (see Figure 5.17).

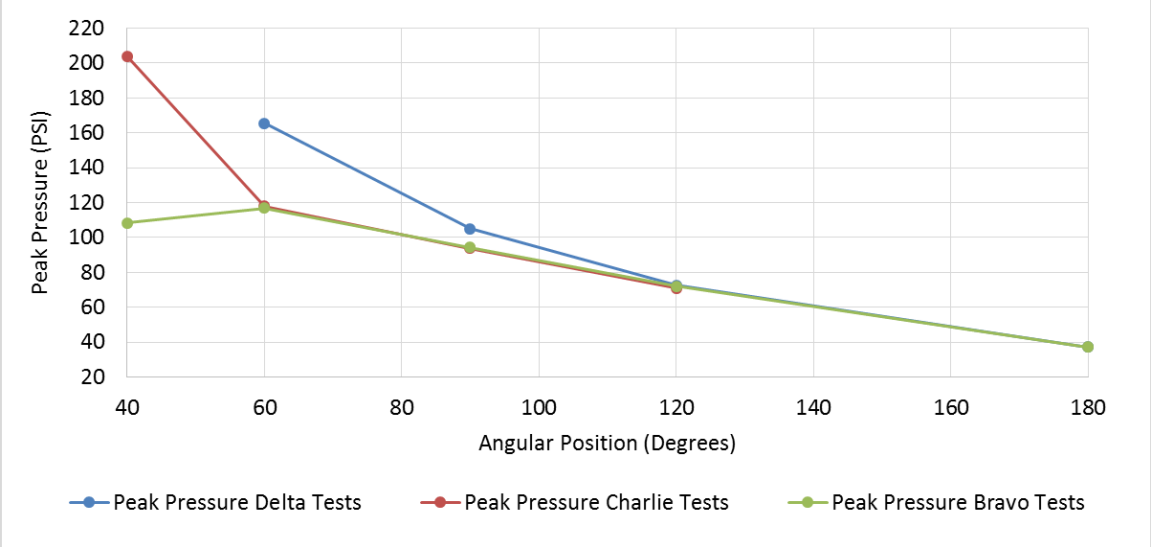

Figure 5.17. Peak pressure amplification from Bravo, Charlie, and Delta test.

The 90 and 60-degree angular spacings in the Delta test have higher peak pressures than the estimated peak pressure using the Peak Pressure Predictive Method. From the data plotted in Figure 5.17 it is clear that the Peak Pressure Predictive Method will need to be

adjusted in order to account for the increased number of charges. Further research is needed to identify the modifications that will be needed to expand the Peak Pressure Predictive Method to include multiple (more than three) charges converging on the cylindrical surface.

5.3.5. Summary of Multiple Shockwave Peak Pressure Predictive Method Verification Results. Several key conclusions were identified through the Peak Pressure Predictive Method verification results. The first and most significant was the Bravo tests (two 0.2 lb charges) validate the Peak Pressure Predictive Method for estimating the peak pressure along the symmetry plane for two charges. The peak pressure in the Bravo test was consistently 80 percent of the estimated value. When this was accounted for, the maximum model error was ± 4 percent. The Peak Pressure Predictive Method could, therefore, be used as a first step towards sealing an underwater offshore oil spill.

The Alpha tests (single 0.2 lb charge) indicated the pipe's curvature did not affect the reflected pressure at the apex of the cylinder for a 0.2 lb charge. In addition, no anomalies were identified that indicated one of the pipe surfaces needed further resurfacing. This is important, as surface anomalies could have significantly affected the peak pressure data.

The three charge interactions (Charlie tests: three 0.2 lb charges) for angular spacings greater than 60-degrees can also be predicted with Peak Pressure Predictive Method. The three charges with 40-degree angular spacings deviated from the estimated pressure. When the Mach stem was accounted for, the model error for three charges with 40-degree angular spacing dropped to three percent.

The Delta tests (four and five 0.2 lb charges) highlighted the limitation of the current Peak Pressure Predictive Method. Further testing is needed to expand the method to include a higher number of charges with lower angular spacings. This will likely include examining the pressure from two Mach stems forming a new Mach stem along the plane of shockwave interaction.

5.4. MULTIPLE CHARGES FOCUSING ON A CYLINDRICAL SURFACE HYPOTHESIS (OBJECTIVE 2)

The results presented in this section compare the pressure and impulse acting on the cylindrical surface data from Bravo and Charlie tests to the results from the Echo tests. Understanding how multiple charges compare to a single charge is important for development of a rapid response system to seal a leaking oil pipe. Determining the appropriate charge weight and the number of charges at a given angular spacing to generate the appropriate Pressure-Impulse response is a fundamental part of developing a rapid response system to seal a leaking oil pipe. The analysis presented in this section is intended to aid in the understanding of how the pressure and impulse will act on the cylindrical surface, for different charge configurations. This section will also look at the total impulse acting on the cylindrical surface, in addition to the impulse recorded at each sensor (Section 5.4.3).

5.4.1. Two Charges Compared To Echo 1. The following sections will compare the results to determine if two charges can impart a higher peak pressure or impulse on the cylindrical surface than a 0.4 lb charge. The two charge data was obtained from the Bravo tests. The Echo 1 tests provided the data for the 0.4 lb charge.

5.4.1.1. Peak pressure comparison. The peak pressure from two charges with 90, 60, and 40-degree angular spacing can produce a higher peak pressure along the symmetry plane than a single charge of equal net weight. The 120 and 90-degree angular spacings generated a spike at the signature sensor. However, the 60 and 40-degree angular spacings produced a pressure trace similar to a single 0.4 lb charge, but of greater magnitude. Figure 5.18 is a polar plot of the Alpha, Bravo, and Echo 1 tests. It is clear that two 0.2 lb charges with angular spacings of 60 or 40-degrees can produce a pressure on the cylindrical surface greater than a single 0.4 lb charge.

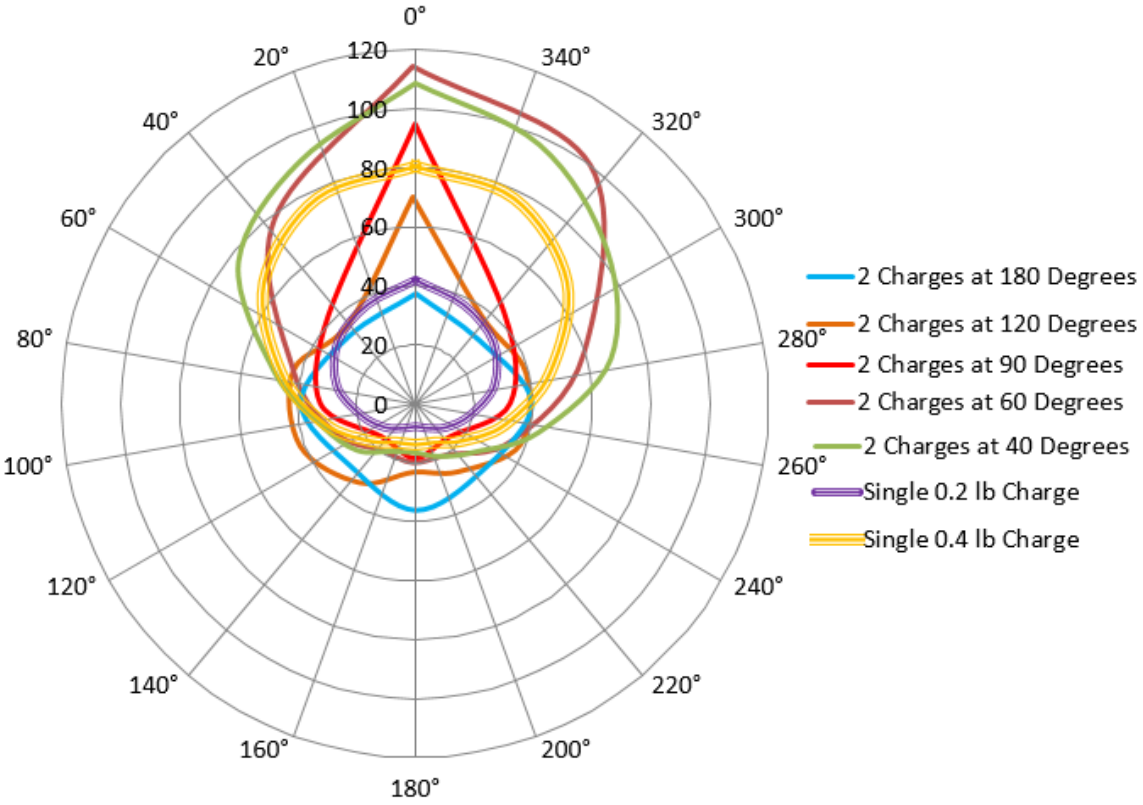

Figure 5.18. Comparison of pressure acting on a cylindrical surface from two 0.2 lb charges, a single 0.2 lb charge, and a single 0.4 lb charge.

5.4.1.2. Impulse comparison. The impulse associated with an angular spacing of less than 90-degrees generates an impulse at the signature sensor that is greater than the impulse from a single 0.4 lb charge. As with the peak pressure, the 180-degree angular spacing had a uniform impulse around the pipe surface than the other angular spacings or the single charges. The impulse associated with each sensor at the various angular spacings is presented in Figure 5.19.

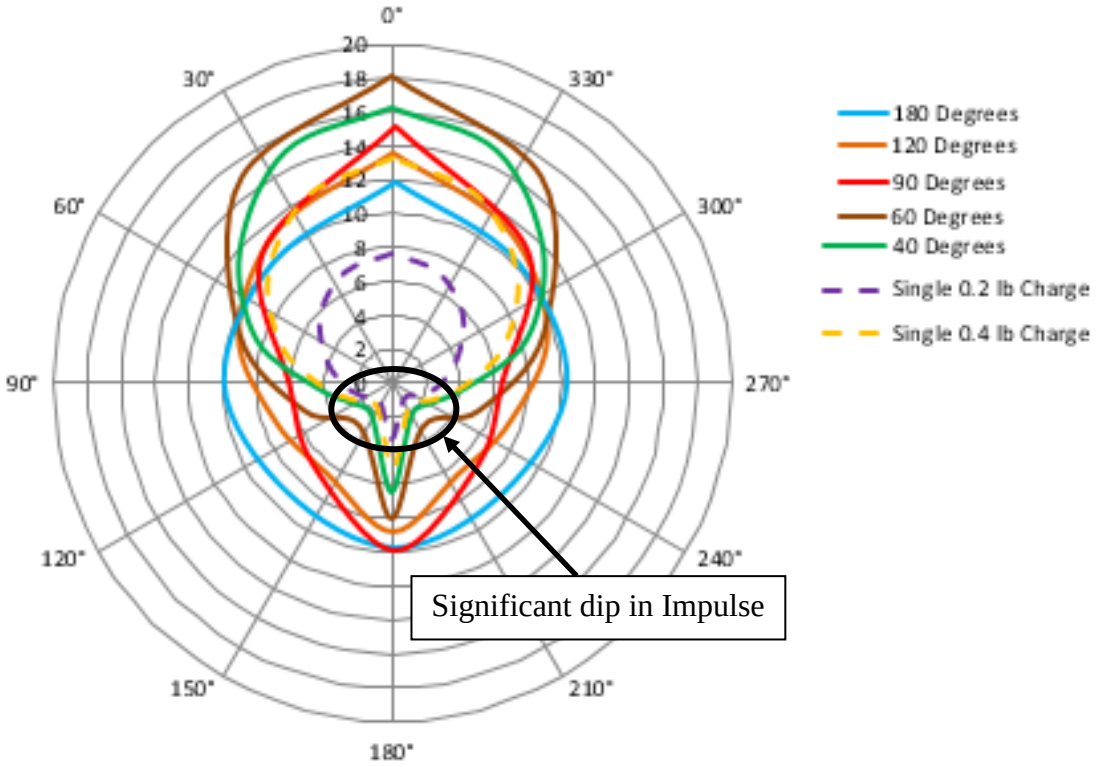

Figure 5.19. Polar plot of the impulse analysis of the shockwaves from two 0.2 lb charges, a single 0.2 lb charge, and a single 0.4 lb charge wrapping around the pipe's surface (units are psi-microseconds).

In the document, "*Engineering Design Handbook: Explosions in Air, Part One*" (Department of the Army, 1974), the authors discussed the shockwave interaction with a

cylindrical surface and the vortices generated beyond 90-degrees. Figure 2.9 (Section 2.3.1) illustrates the vortices associated with cylinder-shockwave interaction as a shadowgraph. Figure 5.20 shows Figure 2.9 compared to the impulse data from Figure 5.19. The locations of vortices 1 and 2 in Figure 5.20 correlate with the region where the impulse shows a significant dip.

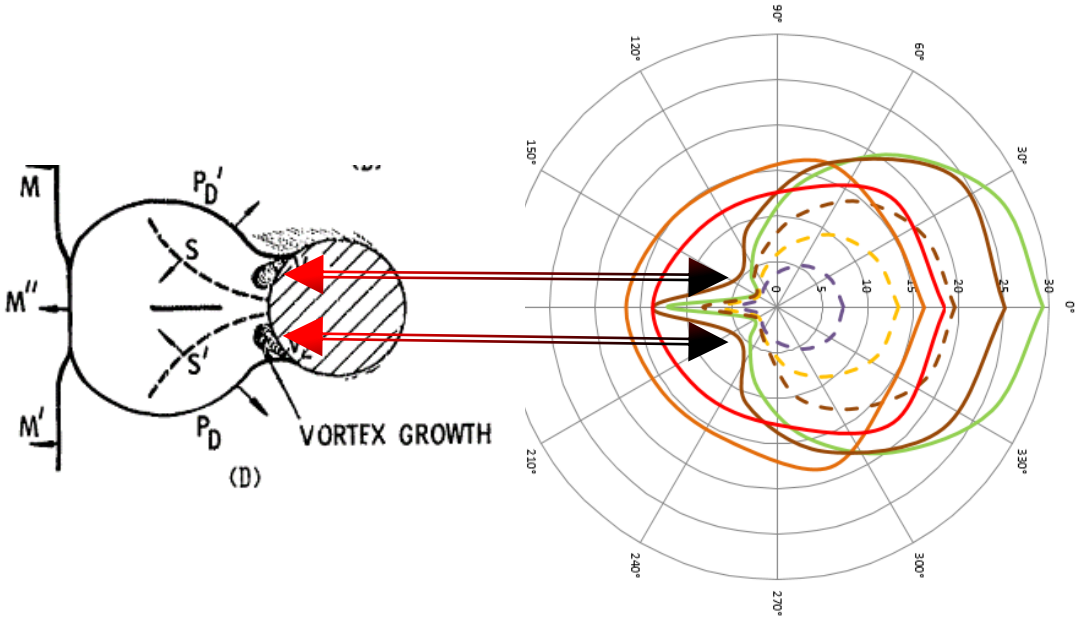

Figure 5.20. Department of the Army's shadowgraph research (1974) compared to the impulse data from multiple charges simultaneously detonated.

The discussion of turbulent flow around a cylindrical body (Section 2.3.2) illustrated that the shockwave separates from the cylinder's surface. The velocity of the shockwave and the cylinder surface roughness determines the angular position where the shockwave separates from the cylinder surface. This separation results in a drop in the pressure acting on the cylinder and, consequently, the impulse. Although the in "*Engineering Design Handbook: Explosions in Air, Part One"* (Department of the Army,

1974) the authors did not discuss the impulse associated with the shockwave wrapping around a cylinder, it is clear from Figure 5.20 that the vortices correlate well with the 150 and 210-degree angular positions.

Based on the information presented in this section, the impulse from the three single charge weights and from the 40-degree angular spacing tests are similar at 150 and 210-degrees because the shockwave has separated from the pipe surface at these points. The shockwave's interaction with the cylinder creates a drag force that acts on the backside of the cylinder (see Section 2.3.2). This drag force is the reason for the pressure and impulse changes on the back of the cylinder ($150<\theta<210$-degrees) as compared to the remainder of the cylinder.

5.4.2. Three Charges Compared To Echo 2. The following sections will present the results that led to determination if three charges can impart a higher peak pressure or impulse on the cylindrical surface than a 0.6 lb charge. The three charge (0.2 lb each) data was obtained from the Charlie tests. Echo 2 tests provided the data for the 0.6 lb charge.

5.4.2.1. Peak pressure comparison. As discussed in the Charlie tests (Section 5.3.3), the larger angular spacings (120 and 90-degrees) produce an amplification of the peak pressure along the symmetry plane. The 60- and 40-degree angular spacings generated a uniform pressure acting on the cylindrical surface at the apex of the pipe. Figure 5.21 is a polar plot of the Charlie and Echo 2 tests.

Unlike the two-charge comparison, only three charges with 40-degree angular spacing can produce a higher peak pressure on the cylindrical surface greater than a single charge of equal net weight. This indicates that as the net charge weight increases the pressure amplification from multiple charges might no longer produce a higher peak

pressure, even though the peak pressure from a single charge decays as the shockwave traverses the cylindrical surface. Therefore, because of this pressure decay, multiple charges can provide a uniform pressure of greater magnitude, relative to the angular positions, than a charge of equal net weight. Further testing with additional charges is needed to confirm this result.

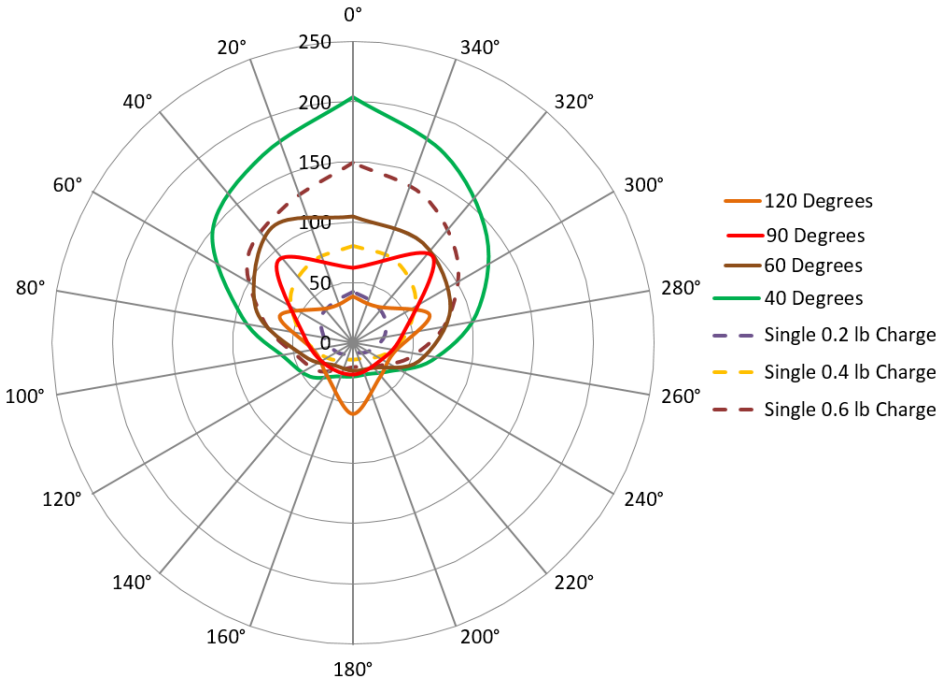

Figure 5.21. Comparison of pressure acting on a cylindrical surface from three 0.2 lb charges, a single 0.2 lb charge, a single 0.4 lb charge, and a single 0.6 lb charge.

5.4.2.2. Impulse comparison. The impulse amplification associated with the Charlie tests resulted in less of a "spike" at the signature sensor and a uniform distribution between the reflecting planes, than Bravo tests. Three charges at 120-degree angular spacings cover the 360-degree domain around the pipe's surface, as a result the impulse imparted on the pipe was relatively uniform. The 60 and 40-degree angular spacings

resulted in an impulse at the signature sensor greater than from a single 0.6 lb charge. Figure 5.22 is a polar plot of the impulse data collected during the three-charge tests.

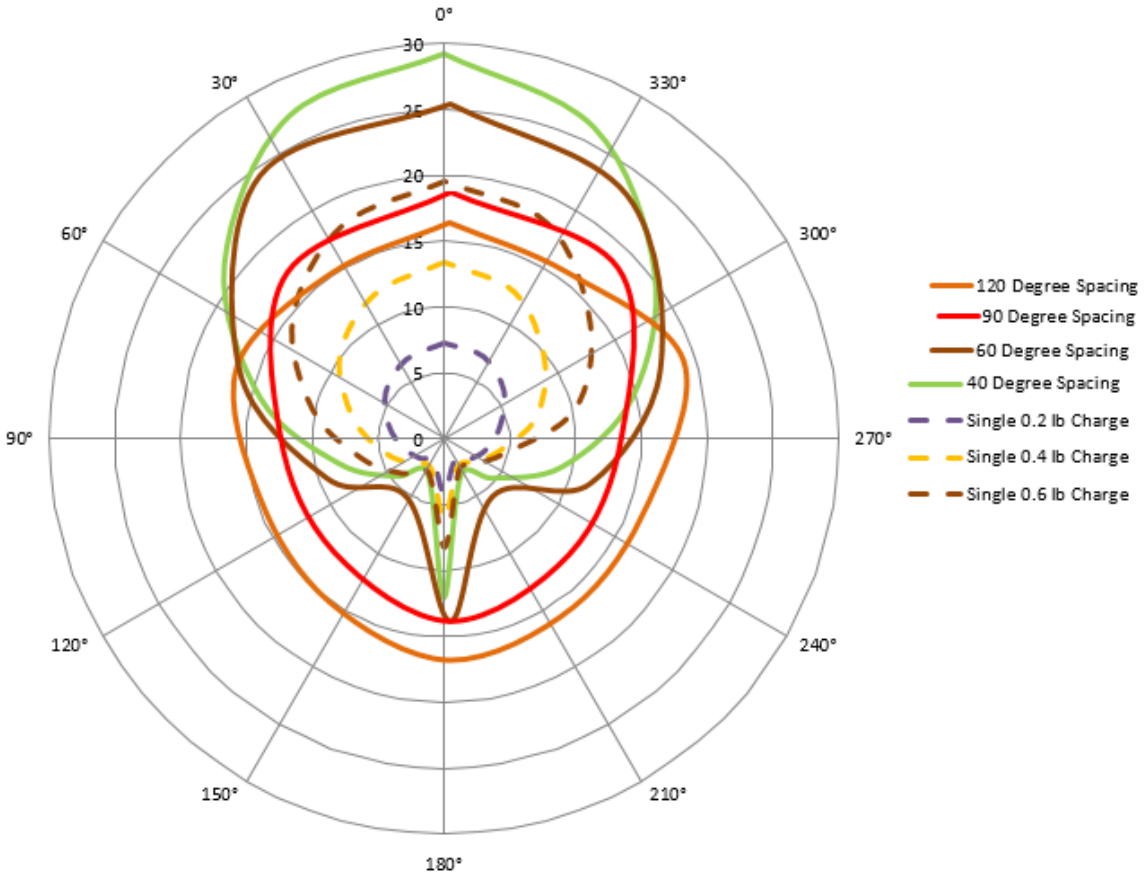

Figure 5.22. Polar plot of the impulse analysis of the shockwaves from three 0.2 lb charges wrapping around the pipe, compared to single 0.2, 0.4, and 0.6 lb charges (units are psi-microseconds).

The smaller angular spacings (60 and 40-degrees) and single charges exhibited a substantial dip in the impulse at the 120 and 240-degree angular position. All of the tests showed an increase in the impulse at 180-degrees; the impulse on the back of the pipe showed a spike that appeared to increase as the angular spacing was reduced. When compared to the impulse from a single charge, the multi-charge impulse amplification was

higher at 180-degrees. An interesting point to note is the impulse from the 40-degree angular spacing (green line) of 0.2 lb charges was equal to the impulse associated with a 0.6 lb charge at 150 and 210-degree angular positions. The similarity in impulse can be attributed to the single-charge shockwave separation from the cylindrical surface, as discussed in Section 5.4.1.2, above. Figure 5.23 is a zoomed view of Figure 5.22 for the impulse opposite the signature sensor.

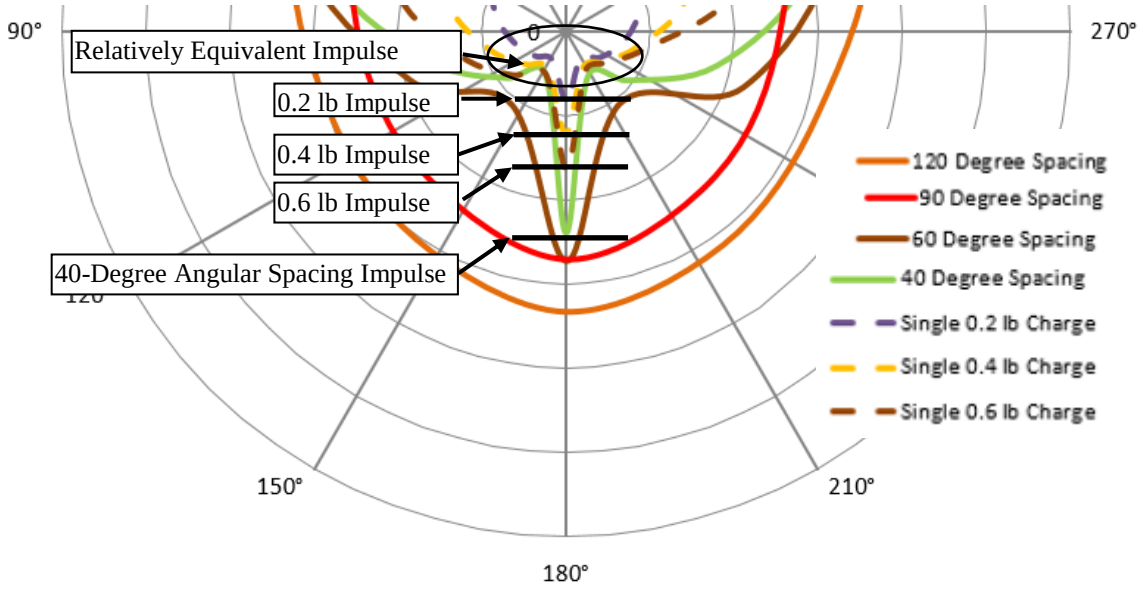

Figure 5.23. Zoomed view of Figure 5.22 at 180-degree angular position.

The impulse amplification associated with 40-degree angular spacing of three 0.2 lb charges can be seen in Figure 5.23. At the 180-degrees, the 40-degree angular spacing had an impulse that was 1.5 times greater than the 0.6 lb charge. The impulse traces for three charges with 40-degree angular spacing and the single charges are similar. This

indicated that the three 0.2 lb charges with 40-degree angular spacing were able to act as a single charge larger than 0.6 lb, with respect to impulse.

5.4.3. Total Impulse Analysis. The analysis of impulse at each sensor does not provide a full picture of how much impulse is imparted on the cylindrical surface. Therefore, the total impulse was calculated using the MRS. By analyzing the total impulse with the MRS technique using the measured impulse and the angular spacing between sensors, a bigger picture of the impulse imparted on the cylindrical surface begins to emerge.

The MRS technique was chosen over simply summing the impulse calculated on each pipe, because the pipes had a different number of sensors. For example, Pipe 3 would measure a higher "total impulse" than Pipe 1, for the same charge weight. Figure 5.24 shows the total impulse calculated for each of the tests.

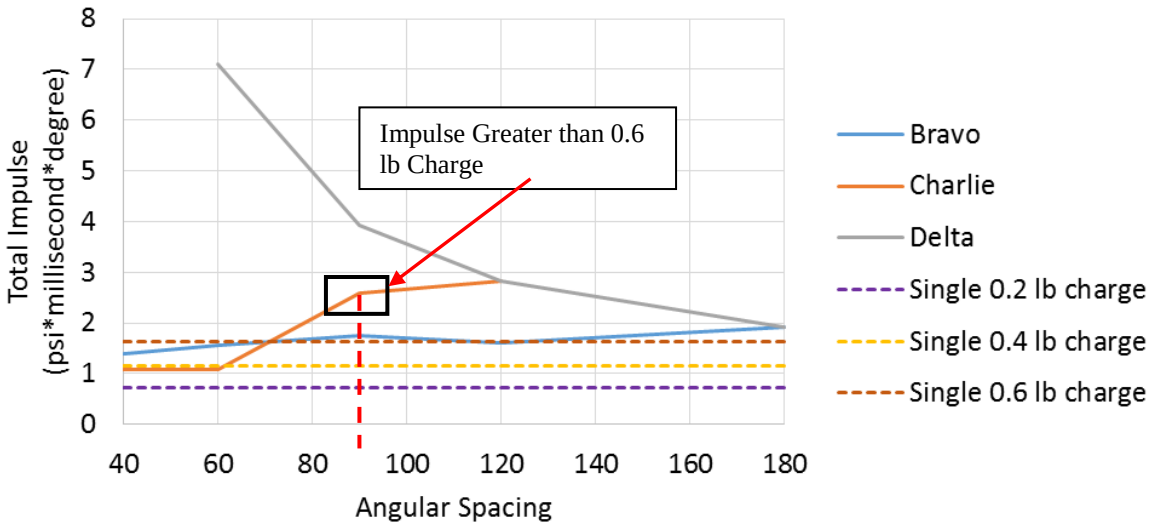

Figure 5.24. Total impulse associated with all of the tests.

In Figure 5.24, it is clear that multiple charges can generate a total impulse greater than a single charge of equal net weight. All of the angular positions in the Bravo tests generated a total impulse greater than a single 0.4 lb charge. However, the Charlie tests did not generate a total impulse greater than a single 0.6 lb charge until the angular spacing was greater than 90-degrees. Determining the exact angular spacing between 60 and 90-degrees required to exceed the total impulse from a 0.6 lb requires further testing.

For the Bravo and Charlie tests, as the angular spacing was reduced, the total impulse amplification was reduced. As the angular spacing decreases, the shockwaves begin to act as one shockwave and the total impulse decreases. For the Charlie tests the total impulse acting on the pipe from three charges decreases with the angular spacing to less than the impulse from a single charge of equal net weight; an angular spacing below 70-degrees results in a lower total impulse, see Figure 5.25.

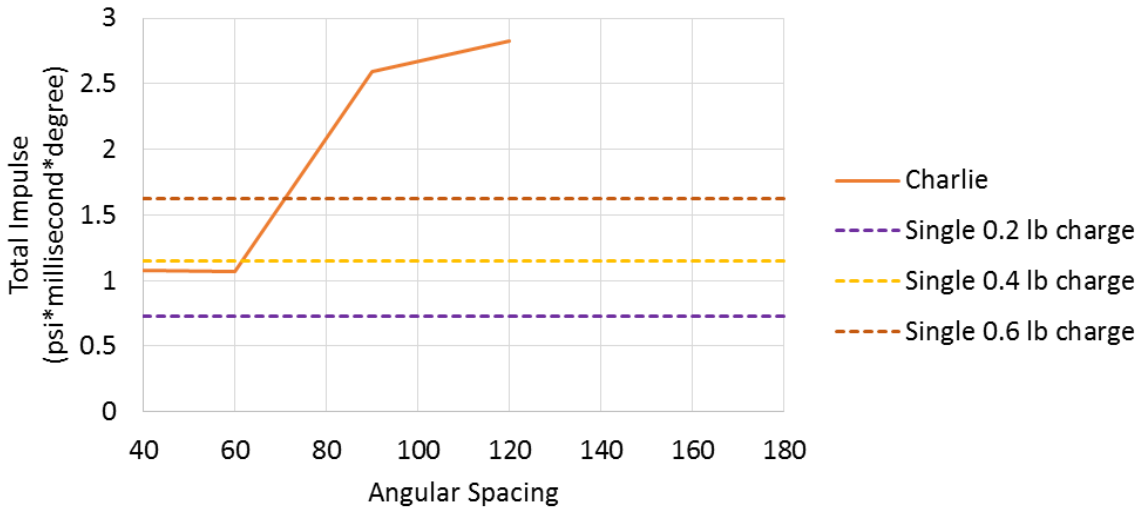

Figure 5.25. Total impulse associated with the three charge tests.

The Bravo and Charlie tests (recall that the Bravo tests had two, 0.2 lb charges each while the Charlie tests had three, 0.2 lb charges) indicate that as the angular spacing decreases the total impulse decreases. However, the Delta tests (4 x 0.2 lb and 5 x 0.2 lb charges) show that as the angular spacing decreases and more of the cylinder is surrounded with charges, the total impulse increases significantly. For example, the total impulse from the five 0.2 lb charges at a 60-degree angular spacing is 9.75 times greater than a single 0.2 lb charge.

When examining the total impulse amplification response associated with the increasing charge weight the response was linear, see Figure 5.26. Figure 5.26 is a plot of the total impulse amplification associated with the 0.2, 0.4, and 0.6-lb charge weights. The charge weights are listed as the multiplier of a 0.2 lb charge weight. For example, the 0.4 lb charge is listed as 2 because it is two times the 0.2 lb charge.

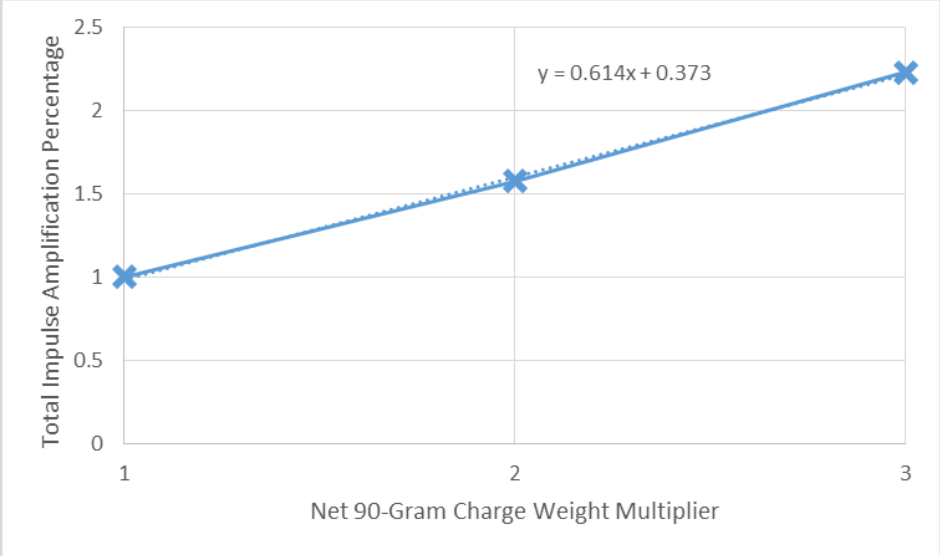

Figure 5.26. Total impulse amplification associated with the single charge weights tested.

Equation 11 was generated from the data plotted in Figure 5.26. From Equation 11, a charge fifteen times the 0.2 lb charge would be required to equal the total impulse imparted on a cylinder surface from five 0.2 lb charges spaced at 60 degrees (7.1 psi*millisecond*degree).

$$\text{Total Impulse Amplification Percentage} = 0.614\,(\text{Net Charge Weight Multiplier}) + 0.373 \quad (11)$$

The three charge weights tested (0.2, 0.4, and 0.6 lbs) indicated that, as the charge weight increases, the peak pressure diminishment rate increases and subsequently, so does the impulse. If this prediction is validated with further testing, then five 0.2 lb charges with 60-degree angular spacings can impart more energy on a centrally located cylinder than a 3 lb charge (15 times a 0.2 lb charge). It should be noted that the pressure response from a charge fifteen times greater than the 0.2 lb charge acting on a cylinder would need to be tested to confirm this prediction.

This amplification demonstrates how the energy from the surrounding charges interact to amplify the effect of each charge. The impulse from each individual charge acts on the cylinder, and each shockwave collision further amplifies the total impulse. This illustrates that surrounding the cylinder with a circular implosive discontinuous explosive lens would result in the highest impulse amplification on the cylinder. The results in this section (Section 5.4), present strong evidence to support the hypothesis that *"Multiple charges focusing on a cylindrical surface <u>can</u> produce a higher peak pressure or impulse than does a single charge of equal net charge weight."*

5.4.4. Summary of Multiple Charges Focusing on a Cylindrical Surface Hypothesis. Comparing the pressure and impulse from multiple charges acting on a cylindrical surface to a single charge of equal net weight provided an understanding of possible methods of sealing an underwater offshore oil spill using explosive charges. The tests results presented in Section 5.4 demonstrate multiple charges can produce a higher peak pressure and impulse on a cylindrical surface than a charge of equal net weight.

Multiple charges with a 40-degree angular spacing around a pipe can produce a higher peak pressure and impulse than a single charge of equal net weight. As the angular spacing of the charges increases (Delta and Charlie tests), the peak pressure amplification decreases. In addition to the peak pressure amplification decreasing, as the angular spacing increases the total impulse acting on the cylindrical surface increases. The Delta tests indicate the total impulse acting on the cylindrical surface increases significantly, when the number of charges around the cylinder increases. This indicates a more of the explosive energy is acting on the cylinder surface when multiple charges are used.

The three charge weights tested (0.2, 0.4, and 0.6 lbs) indicated that, as the charge weight increases, the peak pressure diminishment rate increases and subsequently, so does the impulse. If this prediction is validated with further testing, then five 0.2 lb charges with 60-degree angular spacings can impart more energy on a centrally located cylinder than a 3 lb charge (15 times a 0.2 lb charge). As the number of charges increase to surround the cylinder and the angular spacing decreases, the number of shockwave interactions increase. Each shockwave interaction creates a reflected shockwave and subsequently a higher peak pressure and impulse.

6. CONCLUSIONS

This research was intended to serve as first step towards finding a method of sealing an underwater offshore oil pipe using explosive charges. Two objectives were identified to achieve this goal. The first objective was to identify the validity of a technique for determining the cylindrical surface peak pressure from multiple shockwave colliding along a symmetry plane; this author calls the Peak Pressure Predictive Method. The second objective was to examine the theory that multiple charges distributed around a cylinder or pipe can impart a higher peak pressure or impulse on a cylindrical surface than a single charge of equal net weight. Five experimental test series were developed to achieve these objectives, and the test results allowed for the identification of several key conclusions. The following sections summarize these conclusions.

6.1. PEAK PRESSURE PREDICTIVE METHOD VALIDATION

The primary objective (Objective 1) of this research is to identify applicability and accuracy of the Peak Pressure Predictive Method. The applicability and accuracy of the Peak Pressure Predictive Method have been identified for the tests presented throughout this research. The following conclusions were drawn from the test results presented in Section 5.3.

1. The Bravo tests (two 0.2 lb charges) identified that the Peak Pressure Predictive Method is accurate to ± 4 percent, when the angular position is $180 \geq \theta \geq 40$ degrees (see Section 5.3.2).
2. The Charlie tests (three 0.2 lb charges) indicate when the angular position is $\theta<60$ degrees a Mach stem forms prior to the shockwave interacting with the cylinder surface (see Section 5.3.3).

3. The Charlie tests (three single 0.2 lb charges) indicate that accounting for the Mach stem enables the Peak Pressure Predictive Method to predict the pressure at the signature sensor, when $\theta = 40$ (see Section 5.3.3).
4. The Delta tests demonstrated further testing is needed to expand the method to include a higher number of charges with lower angular spacings (see Section 5.3.4).

Therefore, this author has concluded the Peak Pressure Predicted Method can used to predict the pressure along the symmetry plane when $180 \geq \theta \geq 60$ degrees for two and three charges in a circular implosive discontinuous lens orientation. The present Peak Pressure Predictive Method needs further testing to expand its applicability beyond the experimental setups tested in this research.

6.2. MULTIPLE CHARGES FOCUSING ON A CYLINDRICAL SURFACE HYPOTHESIS

Objective 2 of this research was to determine if "*Multiple charges focusing on a cylindrical surface do produce a higher peak pressure or impulse, than does a single charge of equal net charge weight."* This objective was examined by comparing the experimental results from the Bravo and Charlie tests (two and three 0.2 lb charges) to the peak pressure and impulse from the Echo tests (0.4 and 0.6 lb charges). The following conclusions were drawn from the test results presented in Section 5.4.

1. Multiple charges can produce a higher peak pressure and impulse on a cylindrical surface than a charge of equal net weight (0.4 and 0.6 lbs) (see Sections 5.4.1 and 5.4.2).
2. Increasing charge weight results in a lower attenuation of peak pressure as the shock wave traverses around the cylinder (see Section 5.4.1 and 5.4.2).

3. As the charge weight increases, the velocity of the shockwave traversing the cylinder surface increases; assuming a constant standoff distance (see Section 5.4.1 and 5.4.2).
4. The duration of time the shockwave is acting on the cylinder surface is inversely proportional to the velocity of the shockwave (see Section 5.4.3).
5. A reduction in the duration of time the shockwave is acting on the cylinder surface results in a lower total impulse acting on the cylinder surface. (see Section 5.4.3).
6. As the number of charges increase to surround the cylinder and the angular spacing decreases, the number of shockwave interactions increase (see Section 5.4.3).
7. Each shockwave interaction creates a reflected shockwave and subsequently a higher peak pressure and impulse (see Section 5.4.3).

Therefore, this author has concluded that multiple charges in a circular implosive discontinuous lens can impart a higher peak pressure and impulse on a centrally located cylinder. Comparing the pressure and impulse from multiple charges acting on a cylindrical surface to a single charge of equal net weight provided an understanding of possible methods of sealing an underwater offshore oil spill using explosive charges. Further testing is needed to examine this principle beyond what was presented in this research.

6.3. OVERALL RESULT

Achieving these two objectives advances the state of the art in the possible use of distributed explosive charges to seal leaking underwater pipes. This may prove to be an aid

in generating a rapid response system to help prevent underwater disasters similar to the Deepwater Horizon event.

6.4. CLOSING REMARKS

Recall the accident of the Deepwater Horizon oil spill, detailed in Section 1, which motivated this research. The research presented herein is paving the way to possible solutions that may prevent ecological devastation of the same magnitude. As the knowledge of Explosive Engineering and explosive lensing continues to expand, the Peak Pressure Predictive Method can be used in a number of applications to generate a higher peak pressure or impulse than a single charge of equal net weight, on a centrally located target.

The Peak Pressure Predictive Method presented here provides an effective means of estimating the peak pressure on a centrally located target. As implied by the future work section, there still several steps required to generate a rapid response system to seal an underwater offshore oil spill. However, the results presented in this research have shown a multiple charge configuration can impart a higher impulse and peak pressure when acting on a centrally located cylinder than a single charge of equal net weight.

7. FUTURE WORK

Further research is needed to develop a readily available explosively generated solution for future events similar to the Deepwater Horizon accident. The research presented in this section is the first step towards technology that may be useful for sealing an offshore underwater oil spill. This research focused on Steps 1 and 2 in Table 1.1, reproduced for convenience here as Table 7.1. The remaining eight steps need to be addressed before a solution can developed. These steps will need to include examining the objectives of this research underwater.

Table 7.1. Required research to seal an underwater cylinder via explosive lensing.

Step	Specific Focus of Each Step	Explosive Media
1	Single Shockwave interaction with a cylindrical surface.	Air
2	Multiple shockwave interactions with a cylindrical surface.	Air
3	Cylinder diameter's effect on peak pressure from the shockwave traversing the cylindrical surface.	Air
4	Dynamic loading required to collapse a centrally located cylinder.	Air
5	Single Shockwave interaction with a cylindrical surface.	Water
6	Multiple shockwave interactions with a cylindrical surface.	Water
7	Cylinder diameter's effect on peak pressure from the shockwave traversing the cylindrical surface.	Water
8	Bubble dynamics from multiple charges detonated simultaneously.	Water
9	Bjerknes force from multiple charges acting on a centrally located cylinder.	Water
10	Dynamic loading required to collapse a centrally located cylinder.	Water

Additional future research should examine the reflection amplification associated with colliding shockwaves of equal amplitude. This research should aim at making a

correlation between the amplitude of the initial shockwave and the measured reflected pressure. This correlation can be compared to the predicted pressures shown in Figure 2.4 to determine how colliding shockwaves of equal amplitude differ from a single shockwave colliding with a reflective surface.

An additional aspect identified that requires further research, is the total impulse amplification from multiple charges when compared to the total impulse from a single charge of equal net weight. The total impulse amplification response associated with the increasing charge weight was linear, see Figure 5.26. The three charge weights tested (0.2, 0.4, and 0.6 lbs) indicated that, as the charge weight increases, the peak pressure diminishment rate increases and subsequently, so does the impulse. More single charges of a larger charge weights need to be examined to validate the prediction. If this prediction is validated with further testing, then five 0.2 lb charges with 60-degree angular spacings can impart more energy on a centrally located cylinder than a 3 lb charge (15 times a 0.2 lb charge).

APPENDIX A

CHARGE GEOMETRY EXPERIMENT TO IDENTIFY THE GEOMETRY REQUIRED TO TESTS THE OBJECTIVES OF THIS RESEARCH

Both the explosive material used and the geometry applied significantly affect how the shockwave expands (as discussed in Section 2). This appendix presents the small-scale experiment conducted to determine the charge geometry design. The results from the tests presented in this appendix are summarized in Section 4.2.8.

The experiment presented in this section examined three explosive charge shapes. The configurations listed below were based on the available materials and "common-practice" techniques used at Missouri S&T. Each configuration was tested three times. The shape and confinement configurations tested were as follows:

1. 0.2 lb sphere: neoprene glove confinement
2. 0.2 lb cylinder with a 1.5 inch diameter: cardboard confinement
3. 0.2 lb cylinder with 1 inch diameter: cardboard confinement

The half-pound sphere in the neoprene glove were often used to suspend explosive charges at Missouri S&T. The explosive charge used in this technique were weighed out and placed in a neoprene glove. The detonator was placed inside the charge. The detonator's wires were then wrapped around the glove to prevent the detonator from pulling out. An effort was made to ensure the charge had a spherical shape. It was then suspended from a stand and raised to the appropriate height. A wire suspended beneath the charge was attached to an anchor to minimize how much the charge swung.

The two remaining designs (1" and 1.5" cylinders) were used in an attempt to utilize the cylindrical shape's ability to amplify the radial incident pressure. Using a standard casing ensures a uniform and repeatable shape. The two diameters used were based on available cardboard shipping tube cylinder diameters. Shipping tubes were chosen due to their low confining strength and material density. Each diameter provided a different

charge to diameter length ratio, which translates into different amplification factors. The 1-inch diameter had a 1:4.6 ratio, and the 1.5-inch diameter charge had a 1:1.36 ratio. The diameter to length ratios translate to a 1.35 and a 1.1 reflective factor, respectively.

The cylinders were cut slightly longer than needed to accommodate the volume of explosive. This length also allowed holes to be drilled into the cylinder for mounting purposes. A wire was run to the top mounting holes and a second wire was run though the bottom mounting holes. These wires were used to suspend the charge and minimize how much the charge swung. C-4 was the only explosive used throughout this research. It is easy to pack and handle, easily accessible to this author, and has a high explosive energy.

Two high-speed CASIO EX-FH25 HD cameras were placed 30 ft. from the center of the charge. These cameras were positioned 90 degrees from each other (see Figure A.1). The images collected were used to analyze how the shockwaves and fireballs expand as a result of the charge's geometry. A third high-speed camera (Phantom v10) was also used to observe the shockwave expansion at a higher frame rate.

The CASIO high-speed cameras' images revealed a uniform radial expansion of the fireballs. The Phantom high-speed camera, however, provided the clearest insight into the shockwaves early in time. The camera setup cannot capture the front of the shockwave, but rather the distortion of the images of objects behind the shockwave due to its passing. This distortion and the fireball were used to analyze the performance of the geometry.

The Phantom video analysis revealed that the cylindrical charges had a more uniform radial expansion than the sphere in the neoprene glove. Examples of the Phantom high-speed video of the three designs at the same point in time, relative to detonation are presented in Figure A.2.

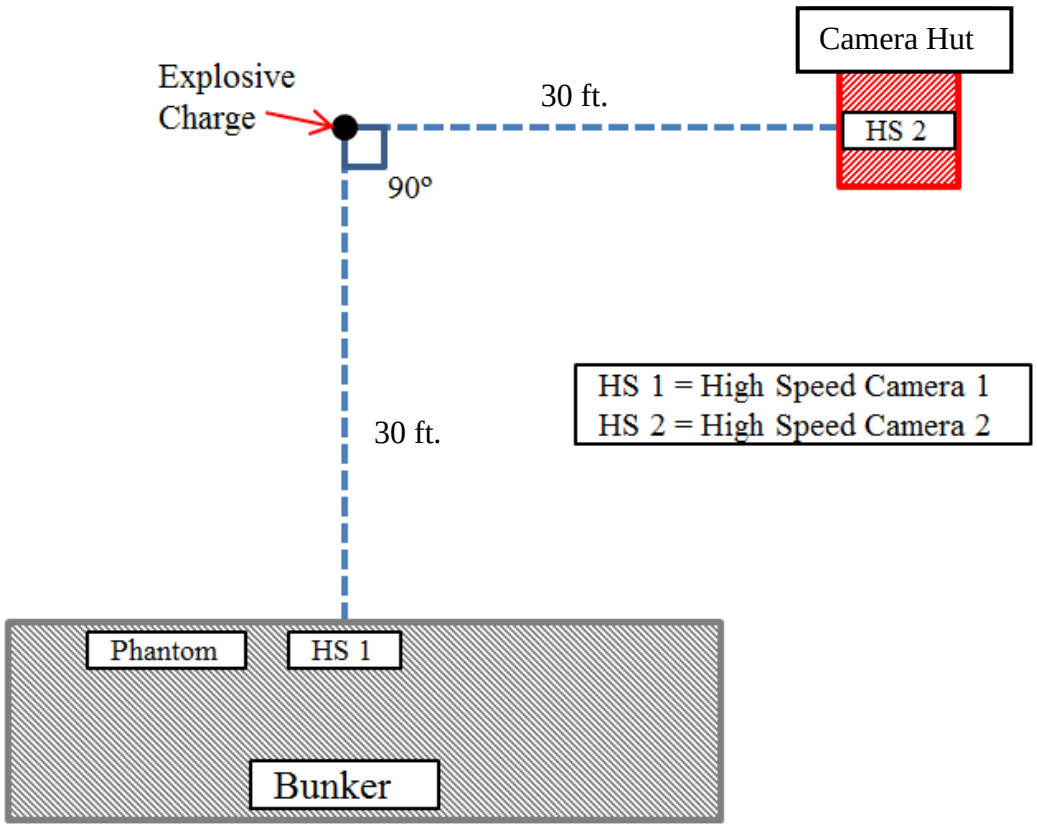

Figure A.1. Fireball and shockwave expansion experiment setup.

Using the Phantom Viewer software each video was analyzed to determine the uniformity of the shockwave expansion. This was done by measuring distance the shockwave travels between frames along the X and Y-axis from the origin. The cylinder designs had a more uniform shockwave expansion than the hand packed sphere. The 1.5-inch cylinder was used to examine the effects of single and multiple shockwaves converging on a cylindrical surface. The decision to use the 1.5-inch cylinder over the 1-inch cylinder was due to the ease of construction. Appendix G details the construction of the explosive charges.

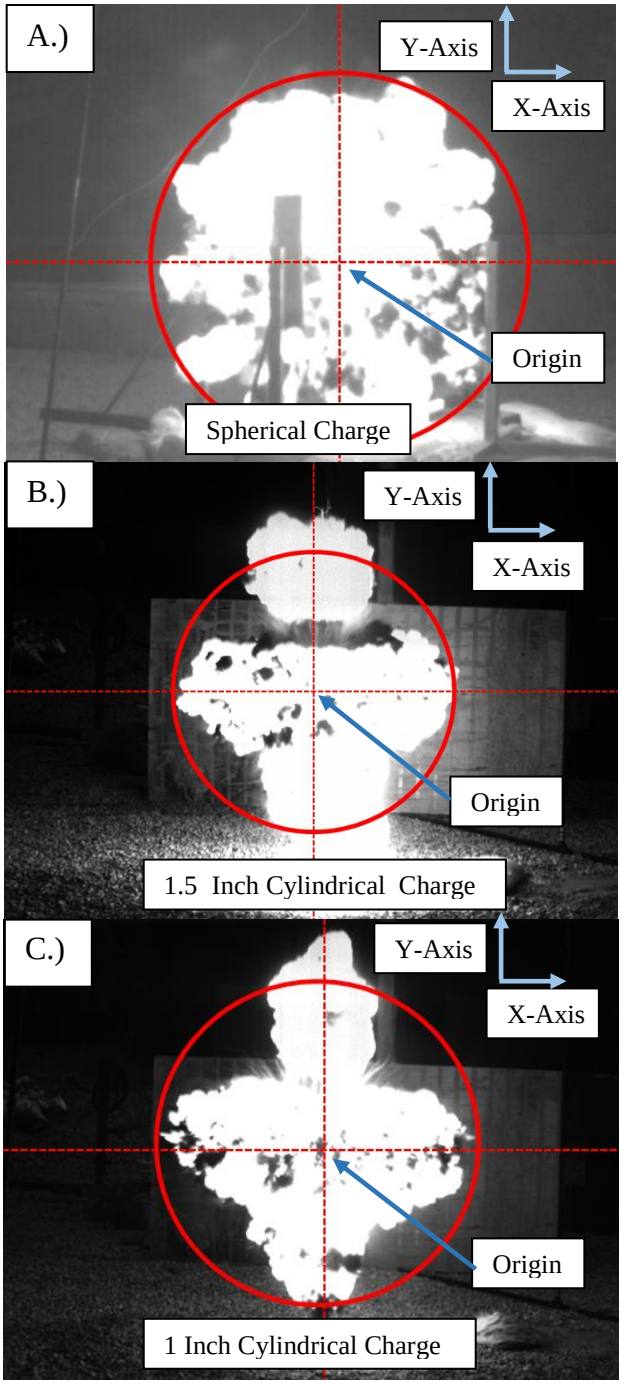

Figure A. 2. Radial expansion of spherical charge, 1.5” cylinder, and 1” cylinder.

APPENDIX B

STANDOFF DISTANCE EXPERIMENT TO IDENTIFY THE DISTANCE REQUIRED TO TESTS THE OBJECTIVES OF THIS RESEARCH

The information presented in this appendix is a small-scale experiment designed to identify the scaled distance range that the data acquisition system can consistently record the peak reflected pressure. The initial experimental design required the charges to have a scaled distance in the "close-in" range. However, the inconsistency in the peak reflected pressure measured with the four curved surfaces detailed in Appendix C and the literature presented in Section 2.5 a small-scale experiment was conducted to identify the scaled distance presented in Section 4.2.1.

Three distances were used to analyze the shockwave expansion. These distances included the original point of interest, the outer edge of the fireball, and a point beyond the fireball. Understanding the shockwave expansion assisted in selecting the appropriate standoff distance of the charge to the cylinder surface.

The initial distance of interest was a 0.5 lb charge 2 ft from the cylinder surface. This charge weight and distance combination had a scaled distance of 2.51. This scaled distance was used to identify a standoff distance for a 0.25 lb charge. The resultant standoff distance was 1.59 ft. The smaller charge was tested to examine how the shockwave expansion rate, relative to the fireball, differed between the two charges.

The C-4 detonation produced two fireball stages. The first was a result of the C-4 detonation. The second was the ignition ("afterburn") of the unburned fuels, generated during the detonation, once they reached the right fuel-air mixture (Cooper, 1996). Therefore, the diameters of the initial fireballs for both the 0.25 and 0.5 lb charges were obtained from the high-speed video. The resulting standoff distances were 5 ft. for the 0.5 lb charge and 3.75 ft for the 0.25 lb. charge.

Walter (2012) stated that a researcher measuring pressure from a free airburst should not expect equal pressure at sensors equal distant from the charge until the pressure sensors are below the triple point. The assumption is that the shockwave will be more radially stable because of the Mach stem. Placing the cylinder so the sensors will measure the Mach stem adds additional complexity to this research. The additional complexity is due to the environmental factors that can interact with the shockwave as the triple point reaches the sensor height. Additionally, distances required for the triple point to be 39.5 inches high for single 0.5 and 0.25 lb charges are 15.59 ft. and 20 ft respectively. Due to the large distance and added complexity the third distance was placed beyond the fireball separation and before the triple point interacting with the sensor height. The third distance was 7.3 and 9.9 ft. for the 0.5 and 0.25 lb charges.

Four pressure sensor stands were positioned at 0, 90, 180, and 270-degree angular intervals when observed from above similar to Figure B.1; the 0-degree reference was consistent in all tests. The charge-to-sensor standoff distance was from the center of the charge to the front of the reflective surface.

The Blast Effects Computer (BEC) predicts a reflected pressure of 1,483.6 psi. The BEC used was developed by the Department of Defense's Explosive Safety Board from curve fit equations of data collected from explosive tests. The data used to generate these equations was obtained from tests conducted in both the far and near field. It was extrapolated for the close-in range.

Each distance and charge weight combination was repeated three times. Sensor selection was based on the predicted pressure associated with each distance, as calculated with the BEC, so that the best performance could be achieved from each sensor without

damaging it. The sensors selected were 102B, 102B06, and 102B15. These sensors have a measurement range of 5,000, 500, and 100 psi respectively. The Data sheets are listed in Appendix F. The distances are listed in Table B.1 with the predicted BEC pressure and scaled distance.

Table B.1. Test distances, predicted pressures, and associated sensors.

	Half Pound charge			Quarter Pound charge		
	Distance	BEC Pressure	Scaled Distance	Distance	BEC Pressure	Scaled Distance
	Feet	PSI		Feet	PSI	
Initial Distance	2.00	1,424.4	2.51	1.59	1,477.4	2.51
Fireball	5.00	101.9	6.29	3.75	120.6	5.93
Third Distance	7.31	36.1	9.19	9.88	12.5	15.62

The peak pressures from each sensor were recorded for each experiment. Table B.2 is a compilation of the recorded pressures. The average pressure from each test was substantially higher than that calculated by the BEC (shown in Table B.2); the BEC did not account for either the HOB or the shape of the charge, both of which affected the pressure.

The variance in the measurements taken beyond the initial fireball were significantly better than those taken within the initial fireball. The charge weight also appears to have affected the variance. The initial fireball distances for both the 0.5 lb and 0.25 lb charges had the same scaled distance (2.51). Although the scaled distance is the

same for both charge weights, the variance for the 0.25 lb charge is less than the 0.5 lb charge.

Table B.2. Data collected from pressure variance tests.

Half Pound Charge				
	Distance	Scaled Distance	Reflected Pressure	Average Pressure
	ft		psi	psi
Initial Interest	2.0	2.5	1,424.4	2,416.1
Flame Ball	5.0	6.3	101.9	201.0
Triple Point	7.3	9.2	36.1	64.5
Quarter Pound Charge				
	Distance	Scaled Distance	Reflected Pressure	Average Pressure
	ft		psi	psi
Initial Interest	1.6	2.5	1,477.4	2,242.8
Flame Ball	3.8	5.9	120.6	215.1
Triple Point	9.9	15.6	12.5	8.1

The results indicate that with the instrumentation and set-up used, there is a significant reduction in pressure variance associated with measurements taken from beyond the initial fireball. The proximity of the charge to the sensor significantly influenced the variance of the reflected pressure measurement at a sample rate of 2MHz. The shockwave's rise time becomes slower over time (Cooper, 1996). Therefore, sensors placed at a greater scaled distance from the charge have a better chance to catch the peak pressure pulse than do those placed closer to the charge.

The significant increase in variance for the pressures measured within the initial fireball could have been produced by thermal shock. Di-electric grease was placed on each sensor to minimize the effects of thermal shock on the pressure readings. Additional causes of the pressure variance could be unreacted particulates and pieces of the cardboard shipping tubes hitting the sensor. The peak pressures vs scaled distance are plotted in Figure B.2.

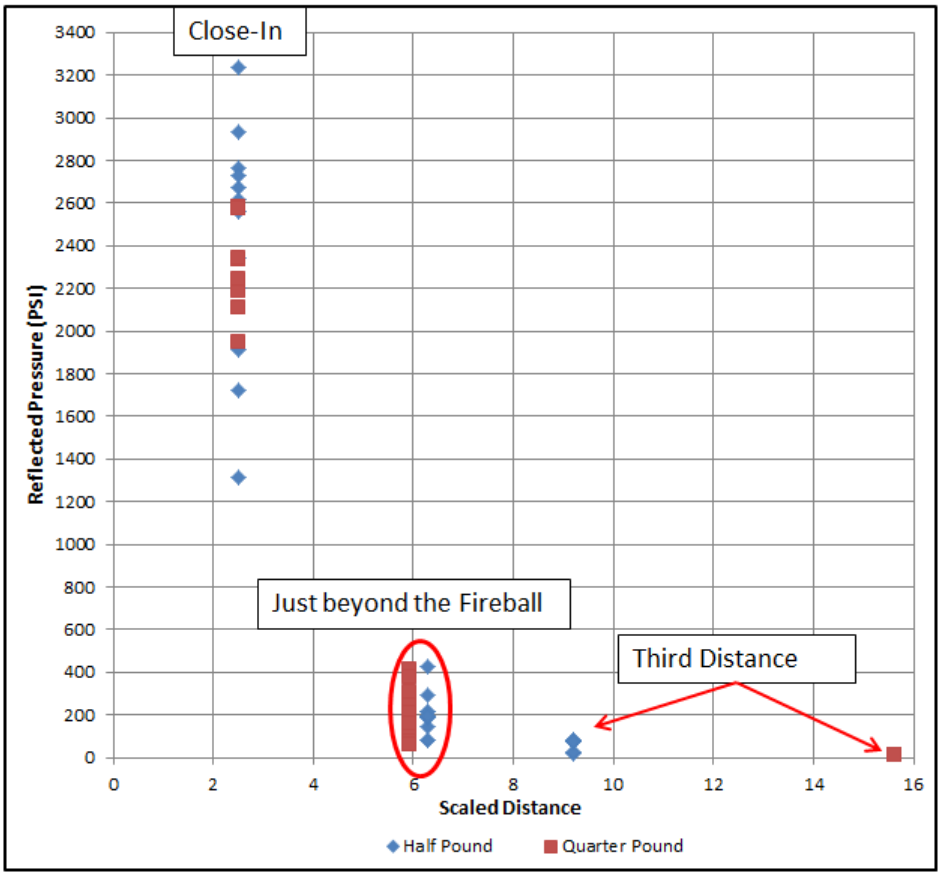

Figure B.1. Plot of the pressure data vs distance.

Based on the data plotted in Figure B.2, a charge weight of 0.2 lbs. at a scaled distance of 7.4 will have a reduced pressure variance when measured radially. Having a

uniform pressure distribution is necessary to reduce the possibility of generating highly skewed data. The 0.2 lb charge weight was used rather than either the 0.25 or the 0.5 lb charges tested to allow more charges to be simultaneously detonated while remaining under the charge weight restrictions. A scaled distance of 7.4 for a 0.2 lb charge produced a 52-inch standoff. This scaled distance will position the sensors beyond the fireball and before a Mach stem is formed.

APPENDIX C

CYLINDER DIAMETER EXPERIMENT TO IDENTIFY THE PIPE DIAMETER TO TEST THE OBJECTIVES OF THIS RESEARCH

The cylinder's diameter significantly affects how the shockwave wraps around the cylinder (as referenced in Section 2.3; Ben-Dor, 1950). A smaller cylinder diameter pipe, relative to the shockwave expansion, allows for a greater angular displacement per distance the shockwave traverses. The angular displacement correlates to the reduction in pressure (also noted in Section 2.3). As a result, a small-scale experiment was conducted to examine the effects of the cylinder's diameter relative to a 0.5 lb charge with a 2ft standoff. Note the experiments presented in this appendix were conducted prior (chronologically) to the experiments in Appendix B.

The three cylinder diameters tested to examine the reflected pressure variance at the cylinder apex were 2, 4, and 6.63 inches. Each cylinder had a PCB Piezotronics sensor placed at the pipe's apex. The three cylinders and a flat plate were placed with 90 degree angular spacing similar to Figure 4.1. The sensors were oriented inward toward a single charge (see Figure C.1). Placing the charge at the center of the four sensors allowed each surface to be compared without a shot-to-shot bias (assuming the explosive charges were packed uniformly). This placement also reduced the number of charges needed to run the tests. A laser level was used to ensure each sensor was at the center height of the explosive charge.

Two different blast pressure prediction sources were used to estimate the flat plate's reflected pressure. The blast pressure prediction sources were the BEC and BlastCalc. BlastCalc is an app used on smartphones and tablets. It uses the methods described in UFC3-340-02, Structures to Resist the Effects of Accidental Explosions as published by the US Department of Defense. Here, the curve fit equations are based on a different series of tests than those used by the BEC (CMV Technologies, 2011). The predicted BEC

reflected pressure was 1,483.6 psi (10.22 Mpa). The BlastCalc predicted reflected pressure was 1,804.5 psi (12.4 Mpa). Both predicted pressures are charted in Figure C.2.

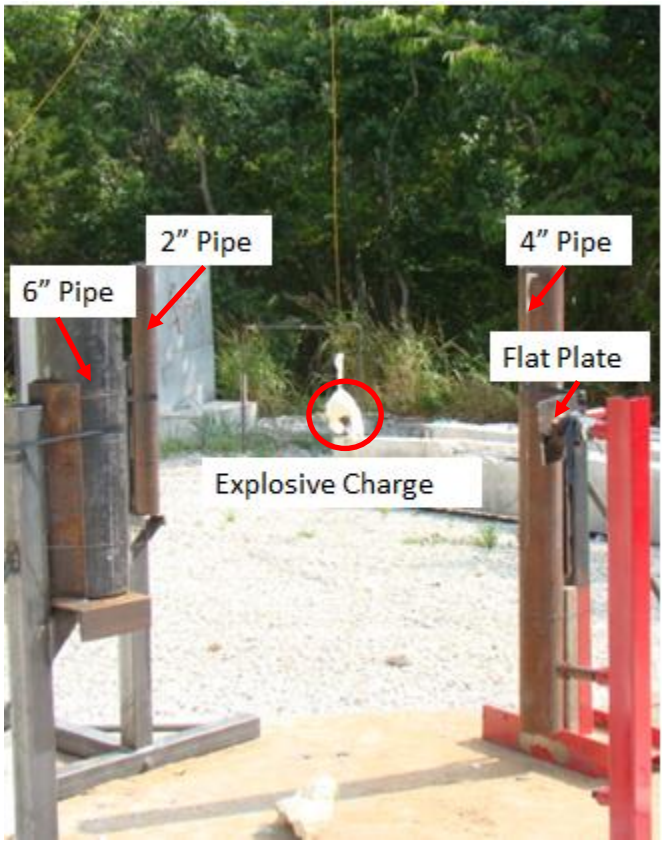

Figure C.1. Cylinder diameter test setup illustrating the three cylinder diameters pointed inward at a centrally located charge.

The recorded peak reflected pressure was highly inconsistent; it had an average spread in the data of 750 psi for each sensor. The total range for the reflected pressure data was over 1,000 psi for the four sensors over all of the tests. Sensors, cables, and data acquisition system channels were rotated and replaced. Tests were conducted both underground and above ground at sample rates ranging from 200,000 and 2,000,000

samples per second. The adjustments in the setup did not improve the data variance. It was concluded, through a series of discussions with Dr. Patrick Walters, that samples per second were not high enough to accurately capture the reflected pressure wave's peak pressure (Walters, 2012). The results were inconclusive.

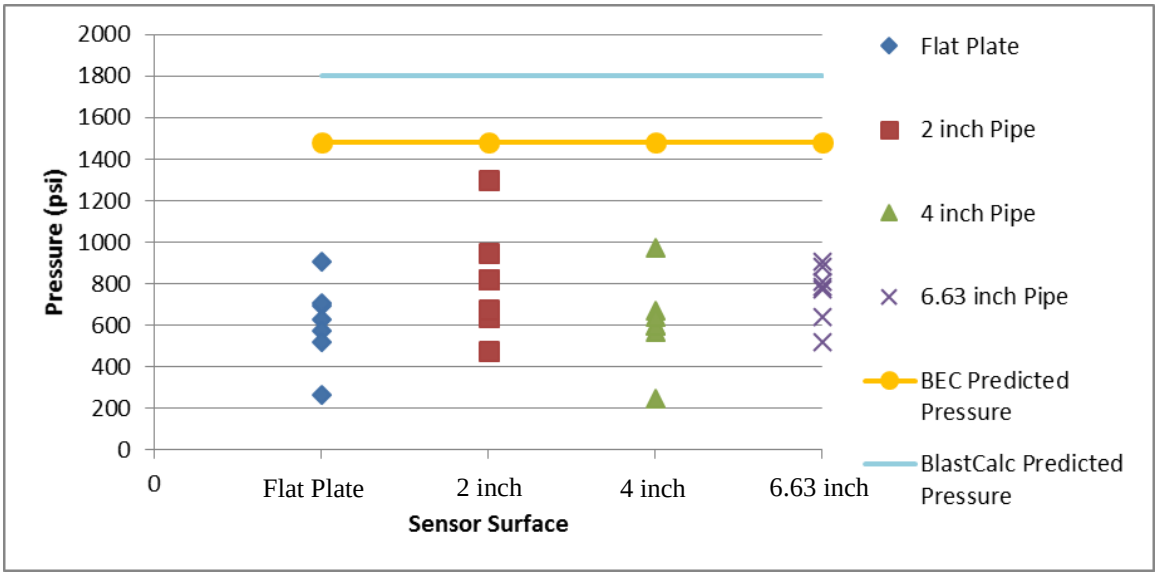

Figure C.2. Test results taken from cylinder reflections tests illustrating the high pressure vairances.

Further testing will however, be needed; testing multiple cylinder diameters was beyond the scope of this research. Only the 6-inch diameter pipe was used for the remainder of this research due to the inconclusiveness of the experiments and the setup limitations of both the 2-inch and the 4-inch diameter pipes

APPENDIX D

TIMING EXPERIMENT TO IDENTIFY THE TIMING VARIANCE ASSOCIATED WITH DETONATION CORD INITIATION OF SEVEN CHARGES

Understanding the timing variance of the available initiation options is imperative to ensuring the shockwaves interact on a mid-plane (a half angle off the angular spacing). Therefore, this appendix presents the small-scale experiment designed to examine the timing variances associated with several available initiation devices. The following, however, were the only methods examined. Not all of the following options required testing as the cap scatter data is readily available from the manufacturer.

- Blasting Caps
  - Electric
  - Non-Electric (NonEL)
  - Electronic
- Exploding Bridge Wire (EBW)
- Non-El without delay fuse
- Detonation Cord

The sensor's diameter was 5/16 inches. The shock velocity of an 18 psi overpressure can be estimated using Figure 2.4. The estimated shock velocity is 0.0187 inch/microsecond. Therefore with the sensor diameter, a cap scatter greater than 16 microseconds will likely result in the shockwaves interacting on a point other than the sensor's surface. Cap scatter is the timing deviation associated with a detonator (blasting cap). Variance in the shockwave interaction either along or not along the mid-plane was likely due to the charge's packing density at a cap scatter less than 16 microseconds.

Both electric and NonEL blasting caps have well-documented cap scatter. The measured cap scatter for a 9 millisecond, for new caps, NonEL is ± 26 percent (Hoffman J., 2013). The percentage of the delay produces a cap scatter of ±2,340 microseconds. Electric blasting caps exhibit similar cap scatter. This cap scatter was unacceptable to use for the research herein. Therefore, these blasting caps were not used.

The EBW detonators have a very low function time simultaneity standard deviation; for example, an RP-80 EBW has a 0.125-microsecond simultaneity standard deviation (Teledyne, 2015). Missouri S&T is not equipped to simultaneously initiate seven EBW detonators. As a result, these detonators were not used.

Farnfield et al. (2009) explored the accuracy of NonEL initiators without a fuse delay. Their findings are summarized in Figure D.1. The NonEL detonators without the delay fuse had a cap scatter of 6 microseconds. Therefore, this technique had promise, as it would not add to the total charge weight. It also had the lowest cap scatter. Detonators without a fuse delay, however, are not readily available. Therefore, this technique was not used either.

	Mean Delay (millisec)	Maximum Delay (millisec)	Minimum Delay (millisec)	Delay Range (millisec)	Standard Deviation (millisec)
Plain detonator with Shock Tube	0.059	0.071	0.050	0.021	0.006
Commercial 'Zero' delay detonator	22.2	23.4	20.9	2.5	0.9

Figure D.1. NonEL cap scatter comparison with and without a fuse delay (R. Farnfield, W. J. Birch and G.D Rangel-Sharp, 2009).

The remaining two detonator options (electronic blasting caps and Detonation Cord) were tested to measure the corresponding cap scatter. A make trigger was placed around each detonator. The electronic detonators were programmed to a zero millisecond delay. Five repetitions of four detonators per test were recorded. The total cap scatter was

218.5 microseconds. The measured cap scatter for the electronic detonators was above the acceptable range and, therefore, electronic detonators were not used.

The Detonation Cord was the last initiation option examined. Detonation Cord can initiate C-4 when tied in a "Triple Roll Knot," see Figure D.2. Timing is relative to the length of Detonation Cord, and the scatter is linked to a variance in the Detonation Cord length, explosive quality, and explosive packing density consistency through the length of cord used. Detonation Cord has a typical detonation velocity of 26,000 ft/sec. The distance the shockwave can travel at this detonation velocity can vary by ± 2.4 inches and meet the minimum timing requirements. Theoretically, at the maximum Detonation Cord velocity variation one blasting cap can initiate seven charges without exceeding the minimum timing variation requirements for this set of experiments, as long as the detonation wave traverses the same distance from the blasting cap to the charge.

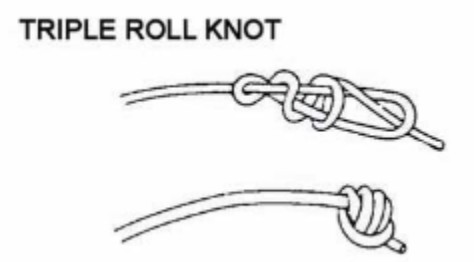

Figure D.2. Triple roll knot (Stiehr, 2011).

A single blasting cap set off seven Triple Roll Knots. However, the Detonation Cord has to be the same length in order for the seven charges to simultaneously detonate. With the charge positioning around the cylinder, seven strands of equal length Detonation Cord could not be positioned so they would not cross each other, move in front of the

charge and generate fall positive pressures, or cross over themselves. As a result a “tree” layout was developed that used short strands of Detonation Cord tied together to ensure the detonation of the seven Triple Roll Knots was simultaneous. The required layout for the Detonation Cord technique is depicted in Figure D.3.

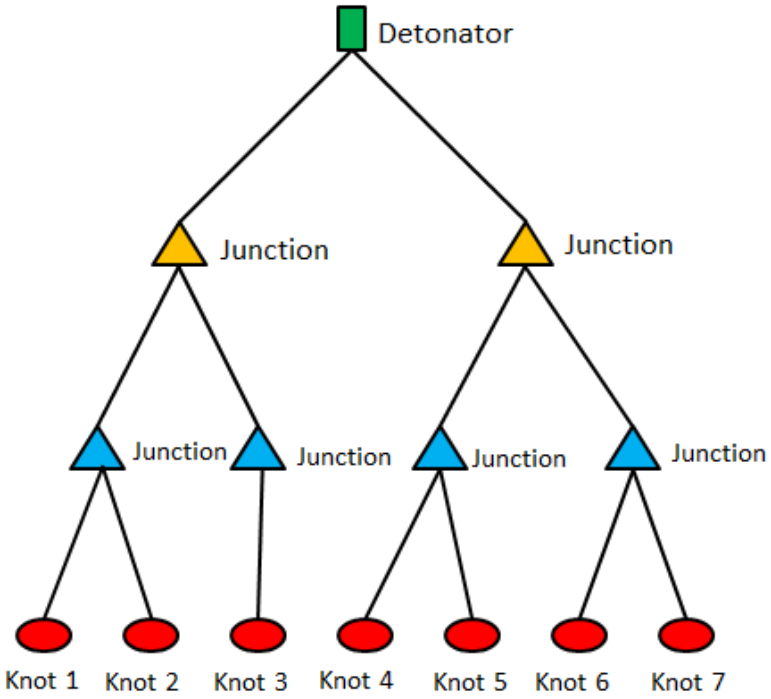

Figure D.3. Simultaneous initiation achieved by using identical detonating cord path length to each charge which were commonly initiated using a single detonator.

Each color represents a different level in time. The green rectangle represents the detonator. The red ovals represent the Triple Roll Knots. The triangles represent junction points where a single strand of Detonation Cord splits into two strands. This was done with a ½-inch diameter tube that was cut to 3-inches. The branch-off lines were run through the tube (similar to that shown in Figure D.4), and the main line was run through the subsequent loop. This technique allowed the branch lines to be placed 6-inches from the end of the

main line. These lines were placed on opposite sides of the mark. The 6-inch spacing from the end of the line was done to ensure that the branch lines were not blown off. Placing the branch lines on opposite sides of the mark kept the initiation timing as close as possible.

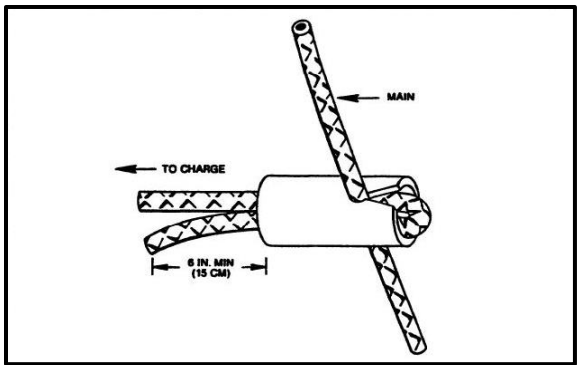

Figure D.4. Detonation Cord tie in technique (Stiehr, 2011)

These tests were conducted to examine the scatter of the Detonation Cord technique. A make trigger attached to the initial blasting cap triggered the data acquisition system. A break trigger was placed at each junction of the Detonation Cord and on each Triple Roll Knot. The total scatter among the 21 knots was 12 microseconds, plenty accurate for the proposed research herein.

Although the Detonation Cord technique is the most complicated to setup, it also has the least amount of scatter. Unfortunately, it also adds to the total charge weight detonated for each test limiting the amount of C-4 that can be used. The accuracy of the detonation timing is more critical than the size of the charge given that a distance can be adjusted to accommodate a desired reflected pressure. Therefore, the Detonation Cord technique was used for the duration of this research.

APPENDIX E

CYLINDER SENSOR MOUNT CONSTRUCTION REQUIRED TO OBTAIN A FLUSH MOUNT SENSOR CONFIGURATION

The information presented in this appendix details how the PCB sensors were mounted in the 6.63-inch diameter cylinder. The 6.63-inch diameter cylinder used in this study had a wall thickness of 0.43 inches. The PCB 102B series piezoelectric pressure sensors used in these tests had a thread length of 0.34 inches (see Figure E.1). Consequently, the sensor would not thread all the way through the cylinder wall. The sensors used in a study such as this need to be flush with the cylinder's surface.

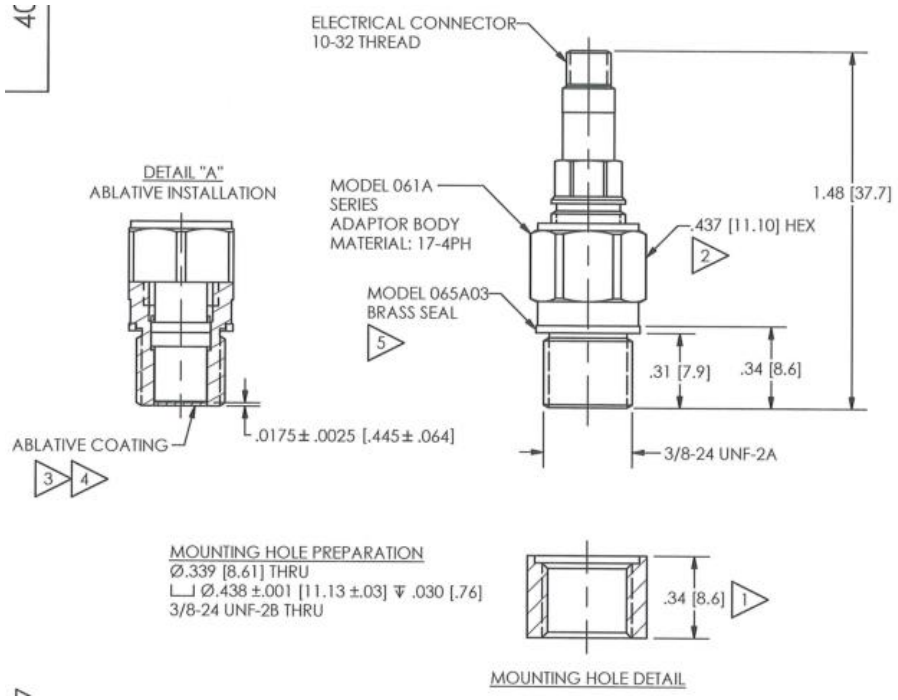

Figure E.1. The PCB piezotronic's 102b pressure sensor design (PCB Piezotronics, 2011).

A system was developed to accommodate the cylinder's wall thickness and the sensor's thread length. A hex nut 0.34 inches thick was placed in the cylinder wall to address this issue. The Missouri S&T water-jet system was used to cut out the through-

dimensions. This technique was also used for the larger mounting hex nuts that secured the pipe to the pipe stand. The nuts were inserted and positioned flush with the outer cylinder's surface after the hex nut hole had been cut.

The angular position for each nut was marked on the cylinder's surface before the hex nuts were inserted in the cylinder wall. A series of CAD drawings were taped together on the cylinder's surface, at the appropriate position to mark the hex nut's position. These drawings were printed at a 1:1 scale. The sensor's paper was positioned on the pipe so that the sensor's height would be 39.5 inches off the ground. This distance translates into 29.5 inches from the bottom of the pipe, as the stand the pipe sat on was 10 inches high. The drawings had intersections positioned at the appropriate arc lengths necessary for the desired angular position. This technique is illustrated in Figure E.2.

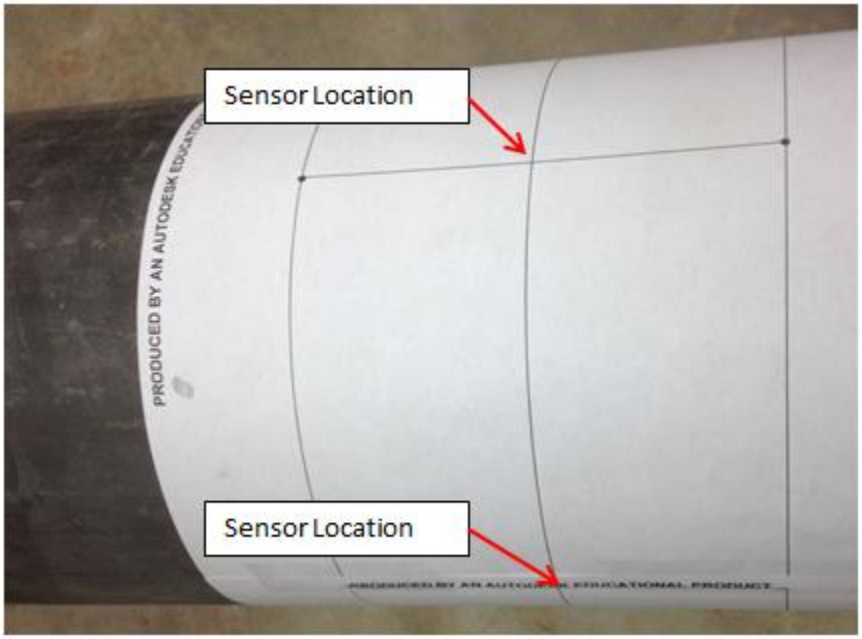

Figure E.2 CAD drawing positioned on the cylinder surface to mark the center of each sensor location.

Three pipes were used, each with a different sensor angular position. Angular position refers to the angle between sensors measured from the center of the cylinder. The hex nuts in place immediately after water jetting in Pipe 1 can be seen in Figure E.3.

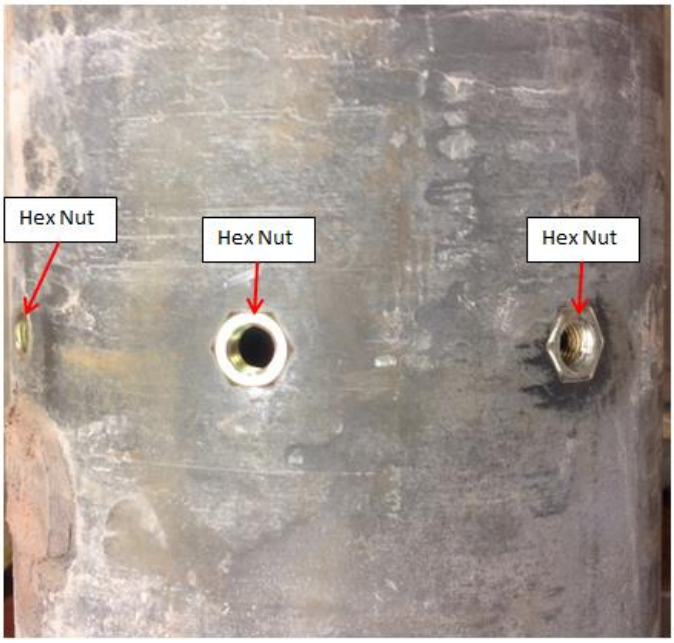

Figure E.3. The hex nuts inserted into the cylinder wall of Pipe 1 to serve as the sensor mounts.

Welding the nuts from inside the cylinder, however, was not possible with the available equipment. The hex nuts were, instead, welded in place from the outside. The welds had to be ground down flush with the original cylinder's outer diameter. However, simply grinding down the welds can still leave irregularities on the cylinder surface. As a result, the surfaces were polished and resurfaced after grinding. Pipe 1 after resurfacing is pictured in Figure E.4.

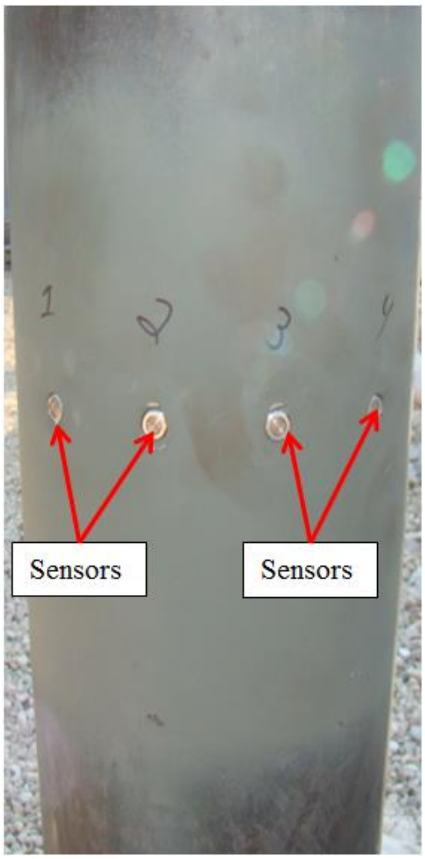

Figure E.4. Pipe 1 with the pressure sensors inserted after resurfacing was complete.

Eight hex nuts were welded into the bottom of the pipe, similar to the nuts inserted for the sensors. They were grouped in sets of two with 8-inches of spacing between the nuts in a group. Each group was positioned at 90 degree intervals. These hex nuts hosted 5/8-inch bolts that were used to secure the pipe to the mounting posts.

A stand was built to support the pipes. This stand consisted of two steel I-beams welded in an "X" shape that laid flush with the ground. Two steel tubes were welded to the center of the "X." These tubes served as mounting posts for each pipe (see Figure E.5). The mounting posts were welded in the center of the I-beam "X." This mounting technique

allowed the pipes to be fastened securely to the stand while also allowing them to be positioned easily as needed. This maneuverability was found to be vital to the pipe's setup.

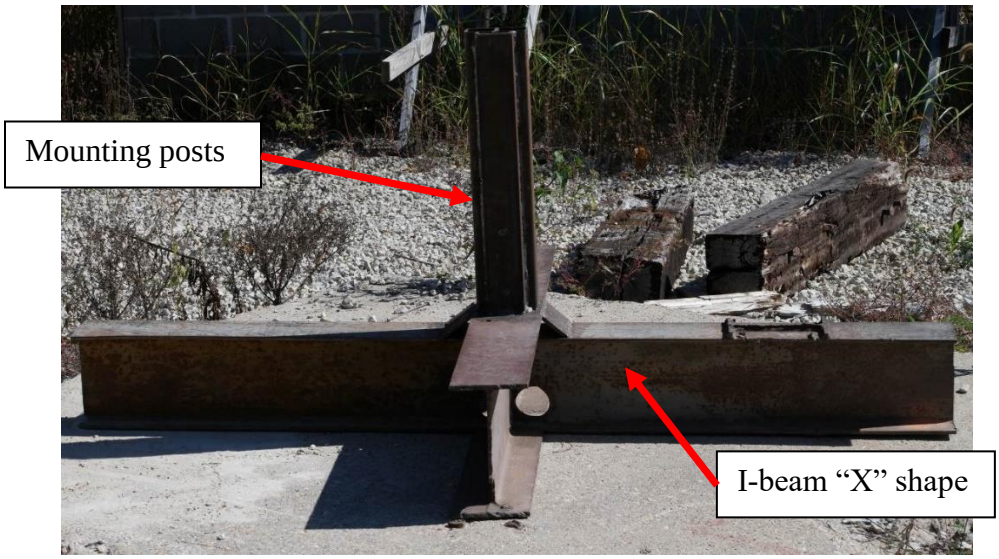

Figure E.5. Pipe stand required to support and secure the pipes during testing.

APPENDIX F

PCB PIEZOTRONIC PRESSURE SENSOR SPECIFICATION FOR THE SENSORS USED (102B, 102B06, 102B15)

The three sensors used in this research were PCB's 102B, 102B06 and 102B15. The data presented in this section details the pressure sensor specifications provided on PCB Piezotronic's website. This information includes the sensors measurement range, max pressure, sensitivity, resonant frequency, and rise time of each sensor. This information was used to determine the appropriate sensor for the test setup detailed in Section 4.

102B

	ENGLISH	SI	
Performance			
Measurement Range	5000 psi	34500 kPa	
Useful Overrange	10000 psi	69000 kPa	[2]
Sensitivity (±10 %)	1.0 mV/psi	0.15 mV/kPa	
Maximum Pressure	15000 psi	103000 kPa	
Resolution	20 mpsi	0.14 kPa	[3]
Resonant Frequency	≥500 kHz	≥500 kHz	
Rise Time	≤1.0 µ sec	≤1.0 µ sec	
Low Frequency Response (-5 %)	0.001 Hz	0.001 Hz	
Non-Linearity	≤1.0 % FS	≤1.0 % FS	[1]
Environmental			
Acceleration Sensitivity	≤0.002 psi/g	≤0.0014 kPa/(m/s²)	
Temperature Range (Operating)	-100 to +275 °F	-73 to +135 °C	
Temperature Coefficient of Sensitivity	≤0.03 %/°F	≤0.054 %/°C	[3]
Maximum Flash Temperature	3000 °F	1650 °C	
Maximum Shock	20000 g pk	196000 m/s² pk	
Electrical			
Output Polarity	Positive	Positive	
Discharge Time Constant	≥500 sec	≥500 sec	
Excitation Voltage	20 to 30 VDC	20 to 30 VDC	
Constant Current Excitation	2 to 20 mA	2 to 20 mA	
Output Impedance	≤100 Ohm	≤100 Ohm	
Output Bias Voltage	8 to 14 VDC	8 to 14 VDC	
Electrical Isolation	100000000 Ohm	100000000 Ohm	
Physical			
Sensing Geometry	Compression	Compression	
Sensing Element	Quartz	Quartz	
Housing Material	Stainless Steel	Stainless Steel	
Diaphragm	Invar	Invar	
Sealing	Welded Hermetic	Welded Hermetic	
Electrical Connector	10-32 Coaxial Jack	10-32 Coaxial Jack	
Weight	0.44 oz	12.5 gm	

(PCB Piezotronics, 2011)

102B06

	ENGLISH	SI	
Performance			
Measurement Range	500 psi	3450 kPa	
Useful Overrange	1000 psi	6895 kPa	[2]
Sensitivity (±10 %)	10 mV/psi	1.45 mV/kPa	
Maximum Pressure	10000 psi	68950 kPa	
Resolution	2 mpsi	0.014 kPa	[3]
Resonant Frequency	≥500 kHz	≥500 kHz	
Rise Time	≤1.0 µ sec	≤1.0 µ sec	
Low Frequency Response (-5 %)	0.01 Hz	0.01 Hz	
Non-Linearity	≤1.0 % FS	≤1.0 % FS	[1]
Environmental			
Acceleration Sensitivity	≤0.002 psi/g	≤0.0014 kPa/(m/s²)	
Temperature Range (Operating)	-100 to +275 °F	-73 to +135 °C	
Temperature Coefficient of Sensitivity	≤0.03 %/°F	≤0.054 %/°C	[3]
Maximum Flash Temperature	3000 °F	1650 °C	
Maximum Shock	20000 g pk	196000 m/s² pk	
Electrical			
Output Polarity	Positive	Positive	
Discharge Time Constant	≥50 sec	≥50 sec	
Excitation Voltage	20 to 30 VDC	20 to 30 VDC	
Constant Current Excitation	2 to 20 mA	2 to 20 mA	
Output Impedance	<100 Ohm	<100 Ohm	
Output Bias Voltage	8 to 14 VDC	8 to 14 VDC	
Electrical Isolation	100000000 Ohm	100000000 Ohm	
Physical			
Sensing Geometry	Compression	Compression	
Sensing Element	Quartz	Quartz	
Housing Material	Stainless Steel	Stainless Steel	
Diaphragm	Invar	Invar	
Sealing	Welded Hermetic	Welded Hermetic	
Electrical Connector	10-32 Coaxial Jack	10-32 Coaxial Jack	
Weight	0.41 oz	11.6 gm	

(PCB Piezotronics, 2011)

102B15

	ENGLISH	SI	
Performance			
Measurement Range	200 psi	1379 kPa	
Useful Overrange	400 psi	2758 kPa	[2]
Sensitivity (±5 mV/psi)	25 mV/psi	3.6 mV/kPa	
Maximum Pressure	1000 psi	6895 kPa	
Resolution	0.001 psi	0.007 kPa	[3]
Resonant Frequency	≥500 kHz	≥500 kHz	
Rise Time	≤1.0 µ sec	≤1.0 µ sec	
Low Frequency Response (-5 %)	0.5 Hz	0.5 Hz	
Non-Linearity	≤1.0 % FS	≤1.0 % FS	[1]
Environmental			
Acceleration Sensitivity	≤0.002 psi/g	≤0.0014 kPa/(m/s²)	
Temperature Range (Operating)	-100 to +275 °F	-73 to +135 °C	
Temperature Coefficient of Sensitivity	≤0.03 %/°F	≤0.054 %/°C	[3]
Maximum Flash Temperature	3000 °F	1650 °C	
Maximum Shock	20000 g pk	196000 m/s² pk	
Electrical			
Output Polarity	Positive	Positive	
Discharge Time Constant	≥1.0 sec	≥1.0 sec	
Excitation Voltage	20 to 30 VDC	20 to 30 VDC	
Constant Current Excitation	2 to 20 mA	2 to 20 mA	
Output Impedance	<100 Ohm	<100 Ohm	
Output Bias Voltage	8 to 14 VDC	8 to 14 VDC	
Electrical Isolation	100000000 Ohm	100000000 Ohm	
Physical			
Sensing Geometry	Compression	Compression	
Sensing Element	Quartz	Quartz	
Housing Material	Stainless Steel	Stainless Steel	
Diaphragm	Invar	Invar	
Sealing	Welded Hermetic	Welded Hermetic	
Electrical Connector	10-32 Coaxial Jack	10-32 Coaxial Jack	
Weight	0.41 oz	11.6 gm	

(PCB Piezotronics, 2011)

APPENDIX G

EXPLOSIVE CHARGE CONSTRUCTION REQUIRED TO TEST THE OBJECTIVES OF THIS RESEARCH

The explosive charges used throughout this research were detonated with detonation cord tied in a Triple Roll Knot. As a result, the cylinders needed to be constructed and packed in a specific format. This appendix presents how the cylinders were constructed and packed for the 0.2, 0.4 and 0.6 lb charges.

It is important to keep the amplification factor similar for each charge weight, as a change in the amplification factor could inadvertently lead to evidence that would support the false hypothesis. The length to diameter ratio of the 0.2 lb charge (1:1.1) was used in conjunction with available shipping tube diameters to obtain the geometry of the larger charges (0.4 and 0.6 lb).

The Triple Roll Knot presented a difficult packing requirement. The cylinder's diameter made it difficult to pack C-4 around the Triple Roll Knot. As a result, a 5/16-inch diameter hole was drilled into one of the cylinder's end caps. Detonation Cord was run through the hole such that the knot was inside the tube when the end cap was placed on the cylinder. The knot was positioned at the end of the Detonation Cord with as little Detonation Cord extruding beyond the knot as possible. The cylinder was secured to this end cap and the knot pulled all the way through the cylinder. This process allowed the bottom of the cylinder to be packed with approximately ¼-inch of explosives.

Approximately 0.011 lbs of C-4 was packed around the knot filling any external voids present. The knot was pulled back down into the cylinder "squishing" the explosives around the sides of the knot. The remaining explosives were packed around the knot, filling the remainder of the cylinder. This technique positioned the knot in the diametric center at the bottom of the cylinder (see Figure G.1). Each cylinder end cap was secured with approximately three complete wraps of electrical tape. Special care was taken to ensure the

electrical tape was applied within a minimal, uniform surface area of the cylinder to minimize the effects the tape had on the shockwave's expansion.

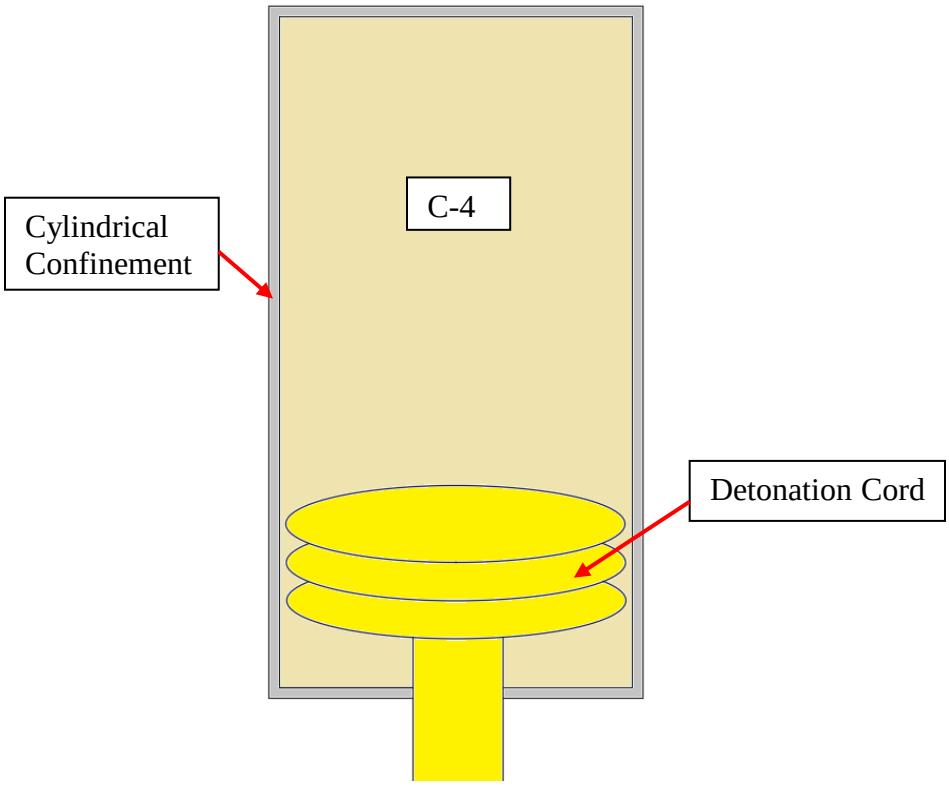

Figure G.1. Detonation cord position within the cylinder.

The cylinders were marked at the centers of their respective lengths. These markings allowed for easier inspection of the charge's vertical positioning relative to the sensor heights with the laser level. They also provided a reference plane, sensor position to the center of the charges, for the standoff measurements.

APPENDIX H

CHARGE STAND CONSTRUCTION REQUIRED TO TEST THE OBJECTIVES OF THIS RESEARCH

Suspending the charge did not provide a consistent, reliable mounting system. The suspension system proved difficult when attempting to ensure consistency in charge height; the wind consistently blew the charge out of position. The suspension mounting system also proved difficult when attempting to keep the charge oriented vertically. Therefore, a new support mounting system was designed and used to position the charges. This appendix presents the new support mounting system.

The charge stand consisted of a 2-inch diameter shipping tube 3 ft in height. The shipping tube was placed over a 1.75-inch outer diameter pipe mounted to a 6-inch steel plate. A series of cardboard wedges were used to raise the tubes and position the charges at the desired height. These wedges were placed between the inner diameter of the shipping tube and the outer diameter of the mounting pipe. A 0.4 lb charge on the shipping tube stands prior to final inspection and hookup is pictured in Figure H.1. Each charge was positioned such that the center of the charge was 39.5-inches from the ground and aligned vertically relative to the sensor. A laser level was used to confirm the charges were level with the sensors.

Two holes were drilled into the shipping tubes stands approximately 1-inch from the top of the tube. One hole was used to run the Detonation Cord. The second hole enabled the make triggers to be away from the charge without placing any rotational forces on the charge. The Detonation Cord was pulled taunt, and electrical tape was used to tape it into position. The charge tended to tilt away from the side on which the Detonation Cord was run if the tape was not used. The Detonation Cord mounting technique for a 0.4 lb charge is illustrated in Figure H.2. This technique was used for all of the charge weights.

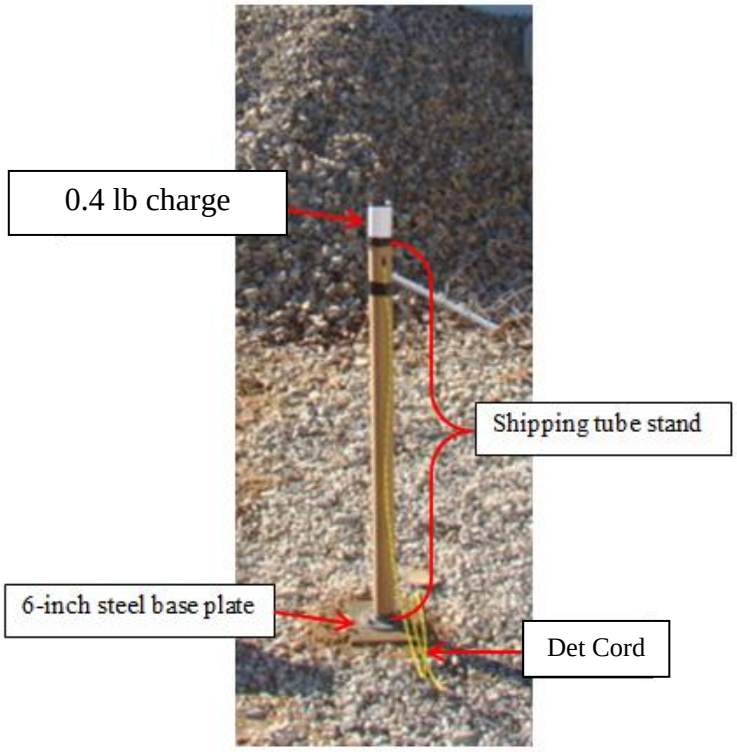

Figure H.1. Shipping tube stand with 0.4 lb charge mounted to the top.

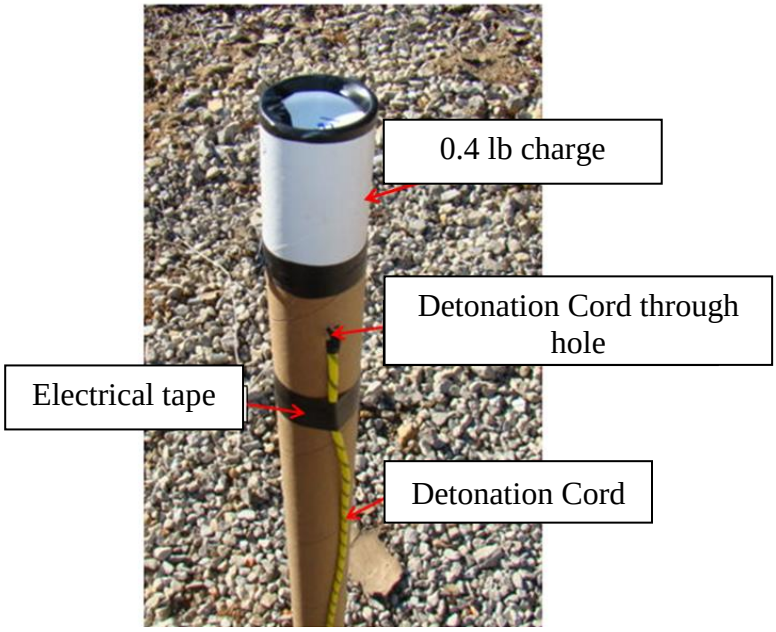

Figure H.2. Charge mounting system illustrating how the Detonation Cord runs through the mounting system and the charge is positioned on top.

The center of the charge cylinder was aligned with the sensor height. The high-speed video did not indicate that this mounting technique inhibited the shockwave formation. While the shipping tube and cap provide impedance barriers, the Detonation Cord will destroy the shipping tube and cap and thereby eliminating any strength/resistance that this technique would generate for the primary C-4 charge. Also, the direction of potential impedance is below the charge. This would impede the shockwaves ground interaction and the formation of the Mach stem on the ground. The repeatability and standardization associated with this technique outweigh the potential impedance of the shockwave formation.

APPENDIX I

EXPLOSIVE CHARGE POSITIONING TECHNIQUE USED TO POSITION THE CHARGES THROUGHOUT THIS RESEARCH

The information presented in this appendix details how each charge was positioned to improve the accuracy of the charge placement. The success or failure of this research was highly dependent on charge placement accuracy. Therefore, a series of checks was followed each time a charge was placed. The steps for this process were as follows:

1. Place the pipe stand on a flat, level surface.
2. Level the charge stand.
3. Insert the custom laser in the appropriate sensor location.
4. Check the mock charge's height.
5. Check the charge-to-pipe distance.
6. Check the charge-to-charge distance.
7. Obtain the charge stand's coordinates relative to the pipe stand.
8. Re-setup the pipe stand at the blast site.
9. Ensure the stand is level and stable.
10. Use the charge stand's coordinates to place the base.
11. Level the charge stand's base.
12. Place the shipping tube (with the charge) on the charge stand's base.
13. Tie in the Detonation Cord and make triggers.

14. Position the charge to the correct height.
15. Check the distance from the charge to the pipe.
16. Check the distance between charges.
17. Double-check the charge stand base's coordinates.

The pipe stand was setup on a level surface to obtain the coordinates was imperative; an un-level site would have created an inaccurate coordinate location for the charge stand base. The level surface used was inside, allowing the setup to be conducted in all types of weather.

A custom laser mount was threaded into the sensor mount locations at the desired charge's angular spacing in order to position the charges at the correct angular spacing. For example, the setup for Delta 2 required the laser to be placed in the 0, 60, 120, 240, and 300-degree sensor locations on Pipe 2 to accommodate the 5 charges with 60-degree angular spacing. The laser mount and laser combination was accurate to ± 0.181-inches at 52-inches.

A shipping tube with a mock charge was placed on the charge stand's base to represent the actual charges. The base was examined to ensure the shipping tubes were perpendicular to the stands base without any radial deviations. The charge stands were moved away from the pipe until the center was at 52-inches, and the laser was pointing at the charge's center. The charge's position was re-examined once the charge stands were positioned at the appropriate distance relative to the pipe.

Points were selected on the pipe stand to represent the reference points for the charge stand's coordinates (see Figure I.1). These points were identified as the corners of the I-beams. The distances to the closest two reference points on the pipe stand were used to determine the charge stands coordinates. A third distance was obtained as a "check-distance" for the final setup. This "check-distance" was used as a backup measurement in the event that a reference point on the pipe stand became damaged during testing. The coordinate system ensured the charge stands were setup in the correct locations. The coordinate system also allowed the charge stands to be examined and repositioned (when needed) after each test.

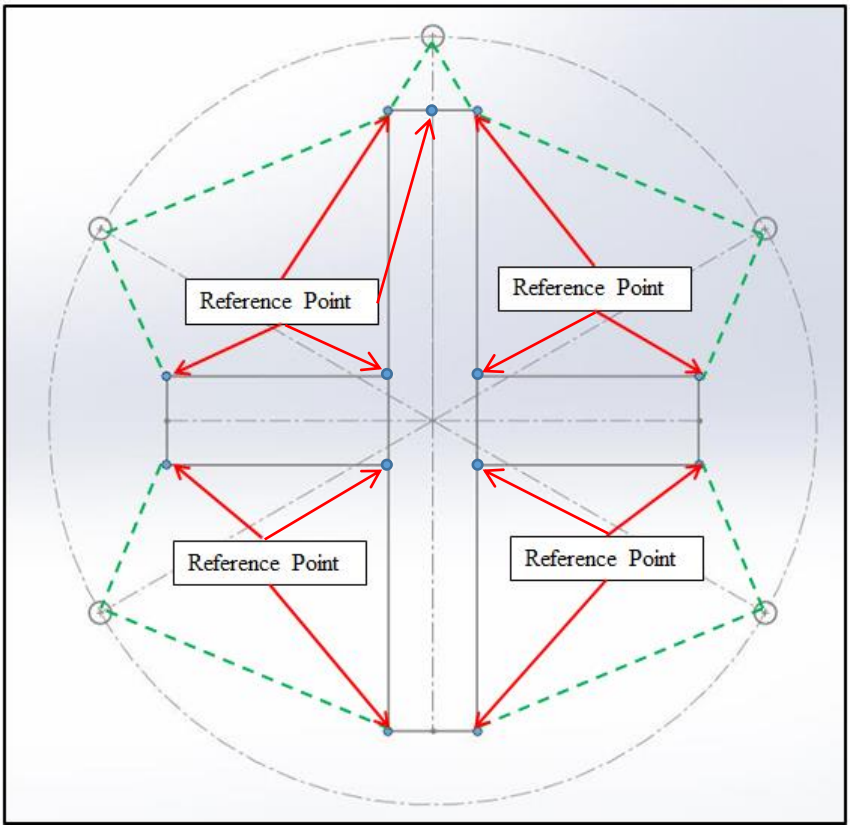

Figure I.1. Charge stands reference points for generating the charge positioning coordinate system.

The pipe stand was moved to the test site after the charge stand's coordinates had been obtained. The pipe stand was leveled and weighted down. The pipe was aligned relative to the positioning marks on the pipe and pipe stand. It was secured via the mounting bolts previously discussed. The appropriate sensors and cabling were hooked up after the pipe was secured.

The charge stands required for the desired test were setup with their previously obtained coordinates. The shipping tube and charge assembly were placed on the charge stand's base. The charges were positioned for their height relative to the sensor's height, the distance from the center of the charges to the pipe, levelness, and the distances from the center of one charge to the center of the next charge. The Detonation Cord and make triggers were connected prior to the charge's final positioning to prevent the potential for incidental (deviation of the charges) during the setup process.

Finally, the charge stand's coordinates relative to the pipe stand were re-examined, via the charge stand coordinates and the third "check-distance." If either the charge stand or charge was off in any of the distance checks, this process was repeated until the charges were in the appropriate positions. All three repetitions of the test number were conducted once the charge stands were in place.

APPENDIX J

TRIGGERING SYSTEM USED TO INITIATE THE DATA ACQUISITION SYSTEM TO RECORD THE DATA FOR EACH TEST

This appendix presents the make trigger used to record the initiation time for the multiple charges used throughout this research. In order to trigger the data acquisition system at the proper time to capture the relevant data from each test, the author used a so-called make trigger. A make trigger works by using plasma generated from the explosion to bridge two contacts, thereby causing current to flow through the contacts' circuit. The make trigger that was used to trigger the data acquisition system was set to record at a 2 MHz sample rate.

A make trigger was placed on every charge when the data acquisition system had the available channels (16 total channels). For example, Pipe 3 had 14 channels and therefore not every charge could be monitored when more than two charges were used. The make trigger used to analyze when the charges detonated consisted of piano wire tied around the Detonation Cord 1-inch from the bottom of the charge. The piano wire was too fragile to run the 25 ft to the trigger box. As a result, 14-gauge wire was run 10-ft away from the charge. The 14-gauge wire was then connected into a cat5 cable, which connected into a custom tiger box. The piano wire passing through the through hole and connecting into the 14-gauge wire is pictured in Figure J.3.

All of the make triggers were run back into the custom trigger box. This box was vital to ensuring no data was lost during the duration of this research. If the data acquisition system did not trigger or the triggers shorted out prior to detonation, no pressure data was recorded. A trigger check was done prior to initiation of the blasting cap. LED lights were built into the box, which indicated whether or not the circuit was made or broken. If the trigger test failed (LED was not lit up), the lines were diagnosed to determine the source of the trigger failure. The make trigger box and its connections are illustrated in Figure J.2.

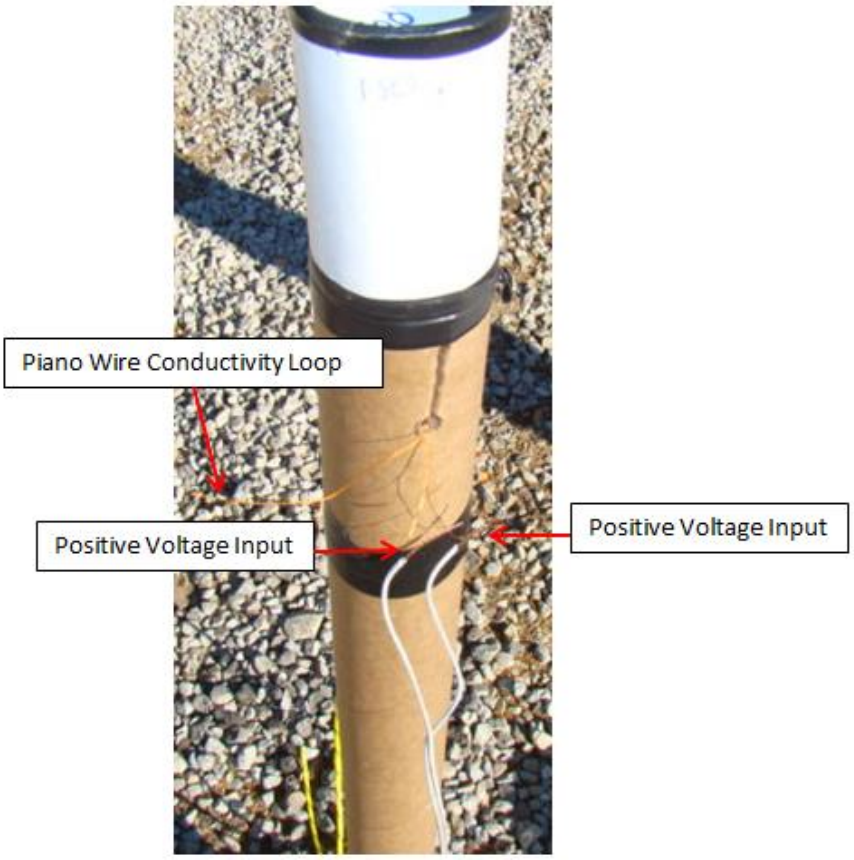

Figure J.1. Make wire connection between the piano wire and the 14-gauge wire.

The make trigger box consisted of four CAT5 inputs. Each CAT5 input could carry the signal from four make triggers. Thus, the trigger box had 16 BNC output connections. Each output had an indicator signal that illuminated when a closed circuit is present (make trigger) and is not illuminated when an open circuit was present (break trigger). Both the inputs and the outputs were broken into the four groups generated by the CAT5 inputs. Each group had an on/off switch to conserve battery life.

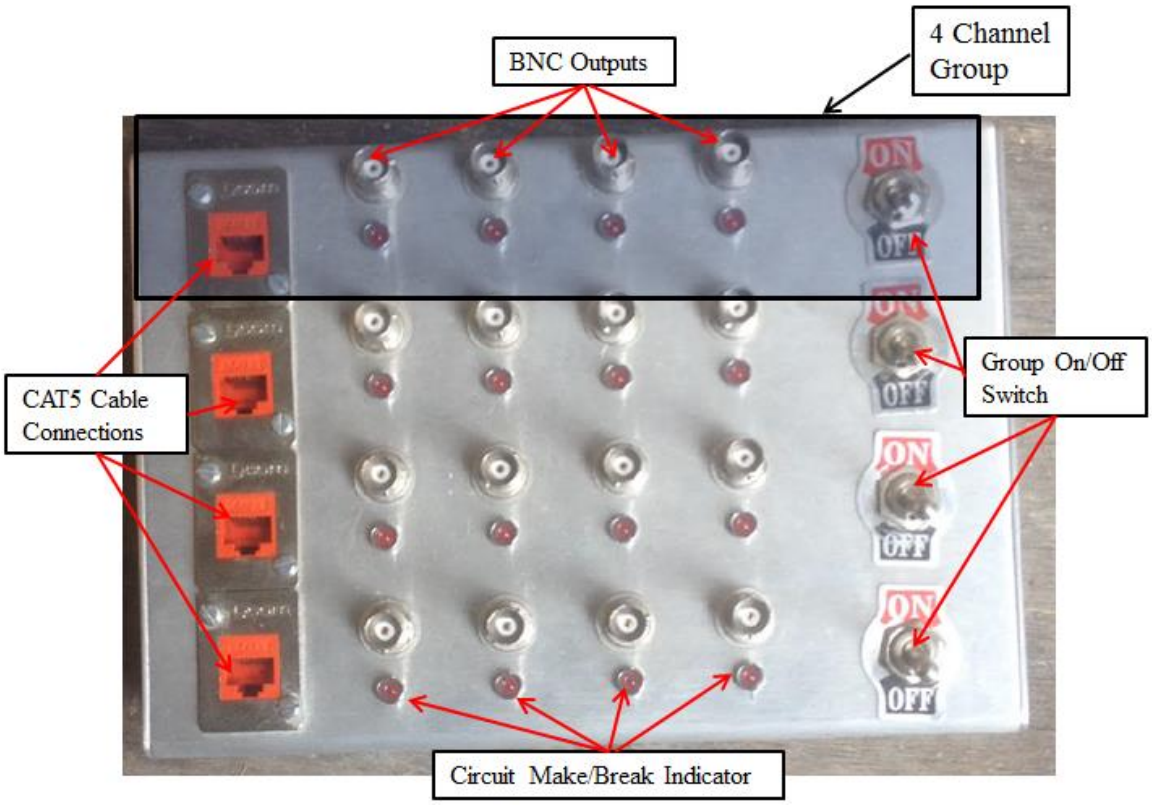

Figure J.2. Make trigger box used to trigger the data acquisition system.

A backup pressure-based trigger was set for the signature sensor as a precaution to the make trigger failing. The sensor at the apex of the cylinder, relative to a single charge position, has been identified as the signature sensor. The pressure trigger triggered the data acquisition system if the pressure rose above a set threshold (20 percent of the sensors measurement range). The data acquisition system was set to trigger if either the make trigger or the pressure trigger were recognized.

APPENDIX K

ALPHA TEST DATA SUMMARY

The data presented in this appendix is the summarized data from Alpha tests detailed in Section 5.3.1. Each file highlights the signature sensor with the cells filled blue. The data presented in this appendix was extracted in accordance with the technique described in Section 5.2. The max pressure, arrival time, positive pressure duration, and impulse data was extracted from each test.

Alpha 1 - Repetition A - Pipe 1: Single 90-Gram Charge

	CH 1 [PSI]	CH 2 [PSI]	CH 3 [PSI]	CH 4 [PSI]	CH 5 [PSI]	CH 6 [PSI]	CH 7 [PSI]	CH 8 [PSI]	CH 9 [PSI]	CH 12 [V]		
	7.32634	16.0383	30.7256	38.6502	29.639	15.8185	7.68605	8.98478	47.8113	5.00		
Initial Pressure Arival	0.0018825	0.00172	0.001594	0.0015395	0.001598	0.001729	0.0018875	0.0020665	0.001448			
Time in microsec	1882.5	1720	1594	1539.5	1598	1729	1887.5	2066.5	1448			
Min time	1448											
Max time	2066.5											
arival spread	618.5											
max time duration	843.00	841.00	1,109.00	1,060.00	1,056.00	832.00	820.00	1,736.00	704.00			
	0.0023035	0.00214	0.002148	0.002069	0.0021255	0.0021445	0.002297	0.002934	0.0017995			
Time in microsec	2303.5	2140	2148	2069	2125.5	2144.5	2297	2934	1799.5			
Duration	421	420	554	529.5	527.5	415.5	409.5	867.5	351.5			
Impulse (sec*psi)	1.61E-03	2.66E-03	5.39E-03	7.12E-03	5.05E-03	2.55E-03	1.57E-03	3.74E-03	7.07E-03			
Impulse (millisec*psi)	1.61	2.66	5.39	7.12	5.05	2.55	1.57	3.74	7.07			
Time							Pressure					
Signature Sensor		1539.5	Microseconds				Signature Sensor		38.6502			
	Dif	Average	Dif					Dif	Average	Dif		
Channel 3	54.5	174	58.5				Channel 3	79.50%	78.09%	76.69%	Channel 5	
Channel 2	180.5	185	189.5	Channel 6			Channel 2	41.50%	41.21%	40.93%	Channel 6	
Channel 1	343	345.5	348	Channel 7			Channel 1	18.96%	19.42%	19.89%	Channel 7	
Channel 8		527	Microseconds				Channel 8		23.25%			
Flat Plate		-91.5	Microseconds				Flat Plate		123.70%			

Alpha 1 - Repetition B - Pipe 1: Single 90-Gram Charge

	CH 1 [PSI]	CH 2 [PSI]	CH 3 [PSI]	CH 4 [PSI]	CH 5 [PSI]	CH 6 [PSI]	CH 7 [PSI]	CH 8 [PSI]	CH 9 [PSI]	CH 12 [V]	
	6.97915	17.0484	35.9997	46.7767	35.9963	16.1014	7.69234	8.34695	41.018	5.00	
Initial Pressure Arival	0.001793	0.001635	0.001508	0.001455	0.0015145	0.0016385	0.001746	0.0019765	0.001505		
Time in microsec	1793	1635	1508	1455	1514.5	1638.5	1746	1976.5	1505		
Min time	1455										
Max time	1976.5										
arival spread	521.5										
max time duration	1,964.00	1,023.00	1,259.00	1,210.00	1,316.00	1,036.00	2,402.00	1,733.00	853.00		
	0.0027745	0.002146	0.002137	0.0020595	0.002172	0.002156	0.0029465	0.0028425	0.001931		
Time in microsec	2774.5	2146	2137	2059.5	2172	2156	2946.5	2842.5	1931		
Duration	981.5	511	629	604.5	657.5	517.5	1200.5	866	426		
Impulse (sec*psi)	2.83E-03	2.76E-03	5.54E-03	7.77E-03	5.67E-03	2.85E-03	3.08E-03	3.91E-03	6.59E-03		
Impulse (millisec*psi)	2.83	2.76	5.54	7.77	5.67	2.85	3.08	3.91	6.59		
Time							Pressure				
Signature Sensor		1455	Microseconds				Signature Sensor		46.7767		
	Dif	Average	Dif					Dif	Average	Dif	
Channel 3	53	145.5	59.5				Channel 3	76.96%	76.96%	76.95%	Channel 5
Channel 2	180	181.75	183.5	Channel 6			Channel 2	36.45%	35.43%	34.42%	Channel 6
Channel 1	338	314.5	291	Channel 7			Channel 1	14.92%	15.68%	16.44%	Channel 7
Channel 8		521.5	Microseconds				Channel 8		17.84%		
Flat Plate		50	Microseconds				Flat Plate		87.69%		

Alpha 1 – Repetition C - Pipe 1: Single 90-Gram Charge

	CH 1 [PSI]	CH 2 [PSI]	CH 3 [PSI]	CH 4 [PSI]	CH 5 [PSI]	CH 6 [PSI]	CH 7 [PSI]	CH 8 [PSI]	CH 9 [PSI]	CH 12 [V]	
	7.23218	15.3149	32.0274	43.3619	35.2764	16.0952	7.3713	10.0458	47.7191	4.99725	
Initial Pressure Arival	0.001839	0.001676	0.001551	0.0014945	0.0015435	0.001671	0.0018065	0.0020165	0.001516		
Time in microsec	1839	1676	1551	1494.5	1543.5	1671	1806.5	2016.5	1516		
Min time	1494.5										
Max time	2016.5										
arival spread	522										
max time duration	1,888.00	863.00	1,064.00	991.00	1,054.00	1,029.00	1,991.00	1,603.00	781.00		
	0.0027825	0.002107	0.0020825	0.0019895	0.00207	0.002185	0.0028015	0.0028175	0.001906		
Time in microsec	2782.5	2107	2082.5	1989.5	2070	2185	2801.5	2817.5	1906		
Duration	943.5	431	531.5	495	526.5	514	995	801	390		
Impulse (sec*psi)	2.77E-03	2.55E-03	5.14E-03	7.11E-03	5.29E-03	2.77E-03	2.86E-03	3.66E-03	6.80E-03		
Impulse (millisec*psi)	2.77	2.55	5.14	7.11	5.29	2.77	2.86	3.66	6.80		
Time							Pressure				
Signature Sensor		1494.5	Microseconds				Signature Sensor		43.3619		
	Dif	Average	Dif					Dif	Average	Dif	
Channel 3	56.5	156	49				Channel 3	73.86%	77.61%	81.35%	Channel 5
Channel 2	181.5	179	176.5	Channel 6			Channel 2	35.32%	36.22%	37.12%	Channel 6
Channel 1	344.5	328.25	312	Channel 7			Channel 1	16.68%	16.84%	17.00%	Channel 7
Channel 8	522						Channel 8	23.17%			
Flat Plate	21.5		0.01				Flat Plate	110.05%		0.03	

Alpha 2 - Repetition A - Pipe 2: Single 90-Gram Charge

	CH 1 [PSI]	CH 2 [PSI]	CH 3 [PSI]	CH 4 [PSI]	CH 5 [PSI]	CH 6 [PSI]	CH 7 [PSI]	CH 8 [PSI]	CH 9 [PSI]	CH 10 [PSI]	CH 11 [PSI]	CH 13 [V]
	8.97403	16.1817	27.3907	38.6132	42.494	41.1514	27.2442	15.9334	10.2115	7.46464	44.3047	5.00
Initial Pressure Arival	0.0016955	0.001553	0.0015145	0.0014755	0.0014555	0.001483	0.0015245	0.001629	0.0017345	0.001961	0.001516	
Time in microsec	1695.5	1553	1514.5	1475.5	1455.5	1483	1524.5	1629	1734.5	1961	1516	
Min time	1455.5											
Max time	1961											
arival spread	505.5											
max time duration	1,193.00	1,087.00	1,164.00	1,454.00	1,221.00	1,253.00	1,296.00	984.00	933.00	2,697.00	861.00	
	0.0022915	0.002096	0.002096	0.002202	0.0020655	0.002109	0.002172	0.0021205	0.0022005	0.003309	0.001946	
Time in microsec	2291.5	2096	2096	2202	2065.5	2109	2172	2120.5	2200.5	3309	1946	
Duration	596	543	581.5	726.5	610	626	647.5	491.5	466	1348	430	
Impulse (sec*psi)	2.06E-03	2.90E-03	4.38E-03	6.31E-03	7.18E-03	6.37E-03	4.35E-03	2.71E-03	1.91E-03	4.32E-03	6.61E-03	
Impulse (millisec*psi)	2.06	2.90	4.38	6.31	7.18	6.37	4.35	2.71	1.91	4.32	6.61	
Time							Pressure					
Signature Sensor		1455.5	Microseconds				Signature Sensor		42.494			
	Dif	Average	Dif					Dif	Average	Dif		
Channel 4	20	86.75	27.5	Channel 6			Channel 4	90.87%	93.85%	96.84%	Channel 6	
Channel 3	59	64	69	Channel 7			Channel 3	64.46%	64.29%	64.11%	Channel 7	
Channel 2	97.5	135.5	173.5	Channel 8			Channel 2	38.08%	37.79%	37.50%	Channel 8	
Channel 1	240	259.5	279	Channel 9			Channel 1	21.12%	22.57%	24.03%	Channel 9	

Alpha 2 - Repetition B - Pipe 2: Single 90-Gram Charge

	CH 1 [PSI]	CH 2 [PSI]	CH 3 [PSI]	CH 4 [PSI]	CH 5 [PSI]	CH 6 [PSI]	CH 7 [PSI]	CH 8 [PSI]	CH 9 [PSI]	CH 10 [PSI]	CH 11 [PSI]
	8.17961	15.3835	26.6056	39.4036	41.2616	39.6384	27.9996	16.4915	9.87948	7.48999	42.8331
Initial Pressure Arival	0.001808	0.001701	0.001586	0.0015515	0.0015225	0.0015405	0.0015795	0.001683	0.001789	0.002026	0.001497
Time in microsec	1808	1701	1586	1551.5	1522.5	1540.5	1579.5	1683	1789	2026	1497
Min time	1497										
Max time	2026										
arival spread	529										
max time duration	1,099.00	919.00	1,195.00	1,141.00	1,134.00	1,189.00	1,203.00	986.00	720.00	4,492.00	901.00
	0.002357	0.00216	0.002183	0.0021215	0.002089	0.0021345	0.0021805	0.0021755	0.0021485	0.0042715	0.001947
Time in microsec	2357	2160	2183	2121.5	2089	2134.5	2180.5	2175.5	2148.5	4271.5	1947
Duration	549	459	597	570	566.5	594	601	492.5	359.5	2245.5	450
Impulse (sec*psi)	2.04E-03	2.71E-03	4.21E-03	6.20E-03	7.16E-03	6.38E-03	4.48E-03	2.84E-03	1.88E-03	5.49E-03	6.44E-03
Impulse (millisec*psi)	2.04	2.71	4.21	6.20	7.16	6.38	4.48	2.84	1.88	5.49	6.44
Time							Pressure				
Signature Sensor		1522.5	Microseconds			Signature Sensor			41.2616		
	Dif	Average	Dif					Dif	Average	Dif	
Channel 4	29	23.5	18	Channel 6			Channel 4	95.50%	95.78%	96.07%	Channel 6
Channel 3	63.5	60.25	57	Channel 7			Channel 3	64.48%	66.17%	67.86%	Channel 7
Channel 2	178.5	169.5	160.5	Channel 8			Channel 2	37.28%	38.63%	39.97%	Channel 8
Channel 1	285.5	276	266.5	Channel 9			Channel 1	19.82%	21.88%	23.94%	Channel 9

Alpha 2 - Repetition C - Pipe 2: Single 90-Gram Charge

	CH 1 [PSI]	CH 2 [PSI]	CH 3 [PSI]	CH 4 [PSI]	CH 5 [PSI]	CH 6 [PSI]	CH 7 [PSI]	CH 8 [PSI]	CH 9 [PSI]	CH 10 [PSI	CH 11 [PSI]	CH 13 [V]
	7.64999	15.8574	28.9608	40.756	45.1175	42.2277	30.9142	17.945	10.5004	7.34	45.36	1.16
Initial Pressure Arival	0.001779	0.001613	0.001565	0.00153	0.001502	0.001521	0.001557	0.00166	0.001764	0.002004	0.001536	
Time in microsec	1779	1612.5	1565	1529.5	1501.5	1520.5	1557	1660	1764	2003.5	1536	
Min time	1501.5											
Max time	2003.5											
arival spread	502											
max time duration	1,104.00	1,036.00	1,211.00	1,276.00	1,225.00	1,379.00	1,232.00	974.00	945.00	7.34	859.00	
	0.002331	0.00213	0.00217	0.002167	0.002114	0.00221	0.002173	0.002147	0.002236	0.002853	0.0019645	
Time in microsec	2330.5	2130	2170	2167	2113.5	2209.5	2172.5	2146.5	2236	2852.5	1964.5	
Duration	551.5	517.5	605	637.5	612	689	615.5	486.5	472	849	428.5	
Impulse (sec*psi)	2.00E-03	2.75E-03	4.29E-03	6.40E-03	7.44E-03	6.64E-03	4.49E-03	2.78E-03	1.93E-03	3.70E-03	6.87E-03	
Impulse (millisec*psi)	2.00	2.75	4.29	6.40	7.44	6.64	4.49	2.78	1.93	3.70	6.87	
Time							Pressure					
Signature Sensor		1501.5	Microseconds				Signature Sensor		45.1175			
	Dif	Average	Dif					Dif	Average	Dif		
Channel 4	28	79.25	19	Channel 6			Channel 4	90.33%	91.96%	93.59%	Channel 6	
Channel 3	63.5	59.5	55.5	Channel 7			Channel 3	64.19%	66.35%	68.52%	Channel 7	
Channel 2	111	134.75	158.5	Channel 8			Channel 2	35.15%	37.46%	39.77%	Channel 8	
Channel 1	277.5	270	262.5	Channel 9			Channel 1	16.96%	20.11%	23.27%	Channel 9	

Alpha 3 - Repetition A - Pipe 3: Single 90-Gram Charge

	CH 1 [PSI]	CH 2 [PSI]	CH 3 [PSI]	CH 4 [PSI]	CH 5 [PSI]	CH 6 [PSI]	CH 7 [PSI]	CH 8 [PSI]	CH 9 [PSI]	CH 10 [PSI	CH 11 [PSI	CH 12 [PSI	CH 13 [PSI	CH 14 [PSI	CH 15 [PSI]
	9.22118	12.8393	19.6204	28.2822	36.4478	38.4131	44.6693	37.3617	34.7493	25.979	18.2417	13.9862	9.2538	7.68009	38.31
Initial Pressure Arival	0.001835	0.001801	0.001732	0.001673	0.001626	0.001579	0.001583	0.001596	0.001631	0.001681	0.00174	0.001802	0.001879	0.002112	0.002054
Time in microsec	1835	1801	1731.5	1673	1626	1578.5	1583	1596	1630.5	1681	1739.5	1802	1879	2111.5	2054
Min time	1578.5														
Max time	2111.5														
arival spread	533														
max time duration	1,187.00	1,207.00	1,117.00	1,199.00	1,305.00	1,483.00	1,301.00	1,196.00	1,129.00	1,058.00	976	1,043.00	1,001.00	2,996.00	1,799.00
	0.002428	0.002404	0.00229	0.002272	0.002278	0.00232	0.002233	0.002194	0.002195	0.00221	0.002227	0.002323	0.002379	0.003609	0.002418
Time in microsec	2428	2404	2289.5	2272	2278	2319.5	2233	2193.5	2194.5	2209.5	2227	2323	2379	3609	2418
Duration	593	603	558	599	652	741	650	597.5	564	528.5	487.5	521	500	1497.5	364
Impulse (sec*psi)	2.09E-03	2.70E-03	3.56E-03	4.83E-03	6.10E-03	7.33E-03	7.52E-03	6.93E-03	5.86E-03	4.48E-03	3.28E-03	2.53E-03	2.09E-03	4.59E-03	6.66E-03
Impulse (millisec*psi)	2.09	2.7	3.56	4.83	6.1	7.33	7.52	6.93	5.86	4.48	3.28	2.53	2.09	4.59	6.66
Time						Pressure						Impulse			
Signature Sensor		1583	Microseconds			Signature Sensor		44.6693				Signature Sensor		7.52	
	Dif	Average	Dif				Dif	1	Dif				Dif	Average	Dif	
Channel 6	-4.5	4.25	13	Channel 8		Channel 6	85.99%	84.82%	83.64%	Channel 8		Channel 6	97.48%	94.79%	92.10%	Channel 8
Channel 5	43	45.25	47.5	Channel 9		Channel 5	81.59%	79.69%	77.79%	Channel 9		Channel 5	81.14%	79.54%	77.95%	Channel 9
Channel 4	90	94	98	Channel 10		Channel 4	63.31%	60.74%	58.16%	Channel 10		Channel 4	64.19%	61.87%	59.55%	Channel 10
Channel 3	148.5	152.5	156.5	Channel 11		Channel 3	43.92%	42.38%	40.84%	Channel 11		Channel 3	47.31%	45.43%	43.54%	Channel 11
Channel 2	218	218.5	219	Channel 12		Channel 2	28.74%	30.03%	31.31%	Channel 12		Channel 2	35.86%	34.75%	33.65%	Channel 12
Channel 1	252	274	296	Channel 13		Channel 1	20.64%	20.68%	20.72%	Channel 13		Channel 1	27.74%	27.74%	27.73%	Channel 13
Channel 14		528.5	Microseconds			Channel 14		17.19%				Channel 14		61.00%		
Flat Plate		471	Microseconds			Flat Plate		85.76%				Flat Plate		88.52%		

Alpha 3 - Repetition B - Pipe 3: Single 90-Gram Charge

	CH 1 [PSI]	CH 2 [PSI]	CH 3 [PSI]	CH 4 [PSI]	CH 5 [PSI]	CH 6 [PSI]	CH 7 [PSI]	CH 8 [PSI]	CH 9 [PSI]	CH 10 [PSI]	CH 11 [PSI]	CH 12 [PSI]	CH 13 [PSI]	CH 14 [PSI]	CH 15 [PSI]	CH 16 [V]
	8.05014	12.4402	17.5	25.4231	31.8964	35.9495	40.8405	35.4174	32.658	24.8774	17.6697	12.8857	9.00437	7.61672	43.0541	5.00626
Initial Pressure Arival	0.001853	0.001784	0.0017125	0.0016505	0.001598	0.001564	0.0015525	0.0015645	0.0015985	0.0016485	0.0017075	0.001719	0.001847	0.0020815	0.00157	
Time in microsec	1853	1784	1712.5	1650.5	1597.5	1564	1552.5	1564.5	1598.5	1648.5	1707.5	1719	1847	2081.5	1570	
Min time	1552.5															
Max time	2081.5															
arival spread	529															
max time duration	1,127.00	1,245.00	1,071.00	1,310.00	1,416.00	1,452.00	1,456.00	1,224.00	1,142.00	1,054.00	989.00	1,168.00	1,099.00	2,934.00	965.00	
	0.002416	0.002406	0.0022475	0.002305	0.002305	0.00229	0.00228	0.002176	0.002169	0.002175	0.0022015	0.0023025	0.002396	0.003548	0.002052	
Time in microsec	2416	2406	2247.5	2305	2305	2289.5	2280	2176	2169	2175	2201.5	2302.5	2396	3548	2052	
Duration	563	622	535	654.5	707.5	725.5	727.5	611.5	570.5	526.5	494	583.5	549	1466.5	482	
Impulse (sec*psi)	2.03E-03	2.73E-03	3.45E-03	4.74E-03	5.97E-03	7.19E-03	7.55E-03	6.90E-03	5.92E-03	4.52E-03	3.30E-03	2.59E-03	2.16E-03	4.55E-03	6.95E-03	
Impulse (millisec*psi)	2.03	2.73	3.45	4.74	5.97	7.19	7.55	6.90	5.92	4.52	3.30	2.59	2.16	4.55	6.95	
Time						Pressure						Impulse				
Signature Sensor		1552.5	Microseconds			Signature Sensor		40.8405				Signature Sensor		7.55		
	Dif	Average	Dif			Dif		1 Dif				Dif	Average	Dif		
Channel 6	11.5	11.75	12	Channel 8		Channel 6	88.02%	87.37%	86.72%	Channel 8		Channel 6	95.22%	93.33%	91.44%	Channel 8
Channel 5	45	45.5	46	Channel 9		Channel 5	78.10%	79.03%	79.96%	Channel 9		Channel 5	79.12%	78.80%	78.47%	Channel 9
Channel 4	98	97	96	Channel 10		Channel 4	62.25%	61.58%	60.91%	Channel 10		Channel 4	62.85%	61.39%	59.92%	Channel 10
Channel 3	160	157.5	155	Channel 11		Channel 3	42.85%	43.06%	43.27%	Channel 11		Channel 3	45.70%	44.71%	43.73%	Channel 11
Channel 2	231.5	199	166.5	Channel 12		Channel 2	30.46%	31.01%	31.55%	Channel 12		Channel 2	36.19%	35.28%	34.36%	Channel 12
Channel 1	300.5	297.5	294.5	Channel 13		Channel 1	19.71%	20.88%	22.05%	Channel 13		Channel 1	26.96%	27.76%	28.56%	Channel 13

Alpha 3 - Repetition C - Pipe 3: Single 90-Gram Charge

	CH 1 [PSI]	CH 2 [PSI]	CH 3 [PSI]	CH 4 [PSI]	CH 5 [PSI]	CH 6 [PSI]	CH 7 [PSI]	CH 8 [PSI]	CH 9 [PSI]	CH 10 [PSI]	CH 11 [PSI]	CH 12 [PSI]	CH 13 [PSI]	CH 14 [PSI]	CH 15 [PSI]	CH 16 [V]
	10.8748	14.1738	19.1507	28.4242	32.8177	38.0177	40.9889	38.1694	35.2645	25.4187	20.2405	16.4084	12.6273	8.4595	45.0751	5.00626
Initial Pressure Arrival	0.001868	0.001799	0.001731	0.001669	0.001621	0.001587	0.001576	0.001586	0.001625	0.0016745	0.0017335	0.0018005	0.001876	0.002124	0.001516	
Time in microsec	1868	1799	1730.5	1668.5	1621	1587	1576	1586	1624.5	1674.5	1733.5	1800.5	1876	2124	1516	
Min time	1516															
Max time	2124															
arival spread	608															
max time duration	511.00	638.00	829.00	572.00	978.00	1,039.00	1,030.00	924.00	882.00	713.00	740.00	613.00	488.00	1,638.00	954.00	
	0.002145	0.002106	0.002145	0.001954	0.00211	0.002106	0.002091	0.0020475	0.002065	0.0020305	0.002103	0.0021065	0.0021195	0.0029425	0.0019925	
Time in microsec	2144.5	2106	2144.5	1954	2109.5	2106	2090.5	2047.5	2065	2030.5	2103	2106.5	2119.5	2942.5	1992.5	
Duration	276.5	307	414	285.5	488.5	519	514.5	461.5	440.5	356	369.5	306	243.5	818.5	476.5	
Impulse (sec*psi)	1.46E-03	2.18E-03	3.13E-03	3.59E-03	5.45E-03	6.36E-03	6.86E-03	6.30E-03	5.34E-03	3.97E-03	3.01E-03	2.07E-03	1.53E-03	3.56E-03	6.79E-03	
Impulse (millisec*psi)	1.46	2.18	3.13	3.59	5.45	6.36	6.86	6.30	5.34	3.97	3.01	2.07	1.53	3.56	6.79	
Time						Pressure					Impulse					
Signature Sensor		1576 Microseconds				Signature Sensor		40.9889				Signature Sensor		6.86		
	Dif	Average	Dif				Dif	Average	Dif				Dif	Average	Dif	
Channel 6	11	10.5	10	Channel 8		Channel 6	92.75%	92.94%	93.12%	Channel 8		Channel 6	92.66%	92.21%	91.76%	Channel 8
Channel 5	45	46.75	48.5	Channel 9		Channel 5	80.06%	83.05%	86.03%	Channel 9		Channel 5	79.36%	78.57%	77.78%	Channel 9
Channel 4	92.5	95.5	98.5	Channel 10		Channel 4	69.35%	65.68%	62.01%	Channel 10		Channel 4	52.38%	55.12%	57.85%	Channel 10
Channel 3	154.5	156	157.5	Channel 11		Channel 3	46.72%	48.05%	49.38%	Channel 11		Channel 3	45.67%	44.77%	43.87%	Channel 11
Channel 2	223	223.75	224.5	Channel 12		Channel 2	34.58%	37.31%	40.03%	Channel 12		Channel 2	31.70%	30.95%	30.20%	Channel 12
Channel 1	292	296	300	Channel 13		Channel 1	26.53%	28.67%	30.81%	Channel 13		Channel 1	21.30%	21.81%	22.32%	Channel 13
		548 Microseconds				Channel 14		20.64%				Channel 14		51.93%		
		-60 Microseconds				Flat Plate		109.97%				Flat Plate		98.96%		

APPENDIX L

BRAVO TEST DATA SUMMARY

The data presented in this appendix is the summarized data from Bravo tests detailed in Section 5.3.2. Each file highlights the signature sensor with the cells filled blue. The data presented in this appendix was extracted in accordance with the technique described in Section 5.2. The max pressure, arrival time, positive pressure duration, and impulse data was extracted from each test.

Bravo 1 - Repetition A - Pipe 1: Two 90-Gram Charges at 180-Degrees

	CH 1 [PSI]	CH 2 [PSI]	CH 3 [PSI]	CH 4 [PSI]	CH 5 [PSI]	CH 6 [PSI]	CH 7 [PSI]	CH 8 [PSI]	CH 14 [V]		
	30.4352	40.4635	34.5436	35.9826	30.9141	36.9876	31.0463	33.167	5.00015		
Initial Pressure Arival	0.0015305	0.001486	0.001534	0.0016745	0.0015635	0.0015155	0.0015605	0.0016515			
Time in microsec	1530.5	1486	1534	1674.5	1563.5	1515.5	1560.5	1651.5			
Min time	1486										
Max time	1674.5										
arival spread	188.5										
max time duration	3,019.00	3,076.00	3,061.00	2,956.00	3,450.00	3,643.00	3,685.00	1,791.00			
	0.0030395	0.0030235	0.003064	0.003152	0.003288	0.0033365	0.0034025	0.0025465			
Time in microsec	3039.5	3023.5	3064	3152	3288	3336.5	3402.5	2546.5			
Duration	1509	1537.5	1530	1477.5	1724.5	1821	1842	895			
Impulse (sec*psi)	1.03E-02	1.22E-02	1.14E-02	1.28E-02	1.07E-02	1.14E-02	1.03E-02	1.01E-02			
Impulse (millisec*psi)	10.32	12.22	11.44	12.78	10.71	11.44	10.33	10.12			
Time							Pressure				
Signature Sensor		1674.5	Microseconds				Signature Sensor		35.9826		
	Dif	Average	Dif					Dif	Average	Dif	
Channel 3	-140.5	-125.75	-111				Channel 3	96.00%	90.96%	85.91%	Channel 5
Channel 2	-188.5	-173.75	-159	Channel 6			Channel 2	112.45%	107.62%	102.79%	Channel 6
Channel 1	-144	-129	-114	Channel 7			Channel 1	84.58%	85.43%	86.28%	Channel 7

Bravo 1 - Repetition B - Pipe 1: Two 90-Gram Charges at 180-Degrees

	CH 1 [PSI]	CH 2 [PSI]	CH 3 [PSI]	CH 4 [PSI]	CH 5 [PSI]	CH 6 [PSI]	CH 7 [PSI]	CH 8 [PSI]	CH 14 [V]		
	32.2594	38.6864	27.4376	36.5939	33.562	40.5179	26.0356	33.4185	5		
Initial Pressure Arival	0.0015255	0.001472	0.0015195	0.00167	0.0015665	0.0015065	0.0015405	0.00165			
Time in microsec	1525.5	1472	1519.5	1670	1566.5	1506.5	1540.5	1650			
Min time	1472										
Max time	1670										
arival spread	198										
max time duration	2,366.00	1,255.00	3,365.00	3,314.00	3,623.00	3,575.00	2,204.00	1,570.00			
	0.002708	0.002099	0.0032015	0.0033265	0.0033775	0.0032935	0.002642	0.0024345			
Time in microsec	2708	2099	3201.5	3326.5	3377.5	3293.5	2642	2434.5			
Duration	1182.5	627	1682	1656.5	1811	1787	1101.5	784.5			
Impulse (sec*psi)	9.12E-03	7.56E-03	1.14E-02	1.33E-02	1.12E-02	1.15E-02	8.76E-03	9.99E-03			
Impulse (millisec*psi)	9.12	7.56	11.38	13.30	11.20	11.49	8.76	9.99			
Time							Pressure				
Signature Sensor		1670	Microseconds				Signature Sensor		36.5939		
	Dif	Average	Dif					Dif	Average	Dif	
Channel 3	-150.5	-64.75	-103.5				Channel 3	74.98%	83.35%	91.71%	Channel 5
Channel 2	-198	-180.75	-163.5	Channel 6			Channel 2	105.72%	108.22%	110.72%	Channel 6
Channel 1	-144.5	-137	-129.5	Channel 7			Channel 1	88.16%	79.65%	71.15%	Channel 7

Bravo 1 - Repetition C - Pipe 1: Two 90-Gram Charges at 180-Degrees

	CH 1 [PSI]	CH 2 [PSI]	CH 3 [PSI]	CH 4 [PSI]	CH 5 [PSI]	CH 6 [PSI]	CH 7 [PSI]	CH 8 [PSI]	CH 13 [V]	CH 14 [V]	
	33.3187	38.3683	28.6186	38.6255	31.6097	39.2263	34.754	41.9739	4.99969	4.99969	
Initial Pressure Arival	0.0015635	0.0015125	0.0015655	0.0016835	0.0015535	0.0015035	0.0015575	0.001686			
Time in microsec	1563.5	1512.5	1565.5	1683.5	1553.5	1503.5	1557.5	1686			
Min time	1503.5										
Max time	1686										
arival spread	182.5										
max time duration	2,736.00	2,796.00	2,894.00	2,286.00	2,476.00	2,310.00	2,121.00	1,634.00			
	0.002931	0.00291	0.003012	0.002826	0.002791	0.002658	0.0026175	0.0025025			
Time in microsec	2931	2910	3012	2826	2791	2658	2617.5	2502.5			
Duration	1367.5	1397.5	1446.5	1142.5	1237.5	1154.5	1060	816.5			
Impulse (sec*psi)	9.78E-03	1.12E-02	1.05E-02	1.19E-02	9.64E-03	1.08E-02	9.54E-03	1.09E-02			
Impulse (millisec*psi)	9.78	11.18	10.48	11.88	9.64	10.75	9.54	10.88			
Time							Pressure				
Signature Sensor		1683.5	Microseconds				Signature Sensor		38.6255		
	Dif	Average	Dif					Dif	Average	Dif	
Channel 3	-118	-63	-130				Channel 3	74.09%	77.96%	81.84%	Channel 5
Channel 2	-171	-175.5	-180	Channel 6			Channel 2	99.33%	100.44%	101.56%	Channel 6
Channel 1	-120	-123	-126	Channel 7			Channel 1	86.26%	88.12%	89.98%	Channel 7

Bravo 2 - Repetition A - Pipe 1: Two 90-Gram Charges at 90-Degrees

	CH 1 [PSI]	CH 2 [PSI]	CH 3 [PSI]	CH 4 [PSI]	CH 5 [PSI]	CH 6 [PSI]	CH 7 [PSI]	CH 8 [PSI]	CH 14 [V]		
	16.7594	32.6502	43.099	89.7558	45.5262	36.3542	16.7696	19.374	5.00137		
Initial Pressure Arival	0.001696	0.001576	0.0015285	0.0015455	0.00149	0.001541	0.001665	0.001823			
Time in microsec	1696	1576	1528.5	1545.5	1490	1541	1665	1823			
Min time	1490										
Max time	1823										
arival spread	333										
max time duration	3,207.00	1,120.00	1,518.00	1,420.00	1,506.00	1,203.00	2,971.00	3,020.00			
	0.003299	0.0021355	0.002287	0.002255	0.0022425	0.002142	0.00315	0.0033325			
Time in microsec	3299	2135.5	2287	2255	2242.5	2142	3150	3332.5			
Duration	1603	559.5	758.5	709.5	752.5	601	1485	1509.5			
Impulse (sec*psi)	7.29E-03	6.59E-03	1.17E-02	1.53E-02	1.09E-02	6.51E-03	7.67E-03	1.12E-02			
Impulse (millisec*psi)	7.29	6.59	11.70	15.27	10.94	6.51	7.67	11.20			
Time							Pressure				
Signature Sensor		1545.5	Microseconds				Signature Sensor		89.7558		
	Dif	Average	Dif				Dif	Average	Dif		
Channel 3	-17	59.75	-55.5				Channel 3	48.02%	49.37%	50.72%	Channel 5
Channel 2	30.5	13	-4.5	Channel 6			Channel 2	36.38%	38.44%	40.50%	Channel 6
Channel 1	150.5	135	119.5	Channel 7			Channel 1	18.67%	18.68%	18.68%	Channel 7

Bravo 2 - Repetition B - Pipe 1: Two 90-Gram Charges at 90-Degrees

	CH 1 [PSI]	CH 2 [PSI]	CH 3 [PSI]	CH 4 [PSI]	CH 5 [PSI]	CH 6 [PSI]	CH 7 [PSI]	CH 8 [PSI]	CH 14 [V]	
	15.5942	32.1576	41.9113	98.2713	36.8993	28.937	15.4602	18.2149	5.00137	
Initial Pressure Arival	0.001729	0.001606	0.0015555	0.001606	0.001543	0.0015845	0.00172	0.001875		
Time in microsec	1729	1606	1555.5	1606	1543	1584.5	1720	1875		
Min time	1543									
Max time	1875									
arival spread	332									
max time duration	3,373.00	1,135.00	1,474.00	1,347.00	1,430.00	1,237.00	2,827.00	2,543.00		
	0.003415	0.002173	0.002292	0.002279	0.0022575	0.0022025	0.003133	0.003146		
Time in microsec	3415	2173	2292	2279	2257.5	2202.5	3133	3146		
Duration	1686	567	736.5	673	714.5	618	1413	1271		
Impulse (sec*psi)	7.95E-03	6.88E-03	1.24E-02	1.67E-02	1.13E-02	6.59E-03	8.07E-03	1.07E-02		
Impulse (millisec*psi)	7.95	6.88	12.42	16.68	11.28	6.59	8.07	10.69		
Time							Pressure			
Signature Sensor		1606	Microseconds				Signature Sensor		98.2713	
	Dif	Average	Dif				Dif	Average	Dif	
Channel 3	-50.5	57	-63				Channel 3	42.65%	40.10%	37.55% Channel 5
Channel 2	0	-10.75	-21.5	Channel 6			Channel 2	32.72%	31.08%	29.45% Channel 6
Channel 1	123	118.5	114	Channel 7			Channel 1	15.87%	15.80%	15.73% Channel 7

Bravo 2 - Repetition C - Pipe 1: Two 90-Gram Charges at 90-Degrees

	CH 1 [PSI]	CH 2 [PSI]	CH 3 [PSI]	CH 4 [PSI]	CH 5 [PSI]	CH 6 [PSI]	CH 7 [PSI]	CH 8 [PSI]	CH 13 [V]	CH 14 [V]
	16.5946	32.1638	43.4949	94.7515	42.5489	31.3356	15.9575	18.313	4.99969	5.00015
Initial Pressure Arival	0.0017015	0.001579	0.0015275	0.0015535	0.001491	0.001538	0.001665	0.001824		
Time in microsec	1701.5	1579	1527.5	1553.5	1491	1538	1665	1824		
Min time	1491									
Max time	1824									
arival spread	333									
max time duration	2,343.00	1,294.00	1,498.00	1,560.00	1,831.00	1,294.00	2,679.00	2,561.00		
	0.0028725	0.0022255	0.002276	0.002333	0.002406	0.0021845	0.003004	0.003104		
Time in microsec	2872.5	2225.5	2276	2333	2406	2184.5	3004	3104		
Duration	1171	646.5	748.5	779.5	915	646.5	1339	1280		
Impulse (sec*psi)	6.14E-03	7.07E-03	1.27E-02	1.65E-02	1.16E-02	6.60E-03	6.72E-03	9.67E-03		
Impulse (millisec*psi)	6.14	7.07	12.67	16.52	11.59	6.60	6.72	9.67		
Time							Pressure			
Signature Sensor		1553.5	Microseconds				Signature Sensor		94.7515	
	Dif	Average	Dif				Dif	Average	Dif	
Channel 3	-26	55.75	-62.5				Channel 3	45.90%	45.40%	44.91% Channel 5
Channel 2	25.5	5	-15.5	Channel 6			Channel 2	33.95%	33.51%	33.07% Channel 6
Channel 1	148	129.75	111.5	Channel 7			Channel 1	17.51%	17.18%	16.84% Channel 7

Bravo 3 - Repetition A - Pipe 2: Two 90-Gram Charges at 60-Degrees

	CH 1 [PSI]	CH 2 [PSI]	CH 3 [PSI]	CH 4 [PSI]	CH 5 [PSI]	CH 6 [PSI]	CH 7 [PSI]	CH 8 [PSI]	CH 9 [PSI]	CH 10 [PSI	CH 14 [V]
	20.3902	36.7533	65.5376	99.9324	112.656	80.224	40.4257	26.2245	17.2814	17.2929	4.99802
Initial Pressure Arival	0.001783	0.001664	0.001619	0.001582	0.001562	0.001573	0.001603	0.001671	0.00172	0.00198	
Time in microsec	1783	1664	1619	1581.5	1561.5	1573	1602.5	1671	1719.5	1979.5	
Min time	1561.5										
Max time	1979.5										
arival spread	418										
max time duration	613.00	968.00	1,067.00	1,262.00	1,245.00	1,224.00	1,263.00	969.00	849.00	2,004.00	
	0.002089	0.002148	0.002152	0.002212	0.002184	0.002185	0.002234	0.002155	0.002144	0.002981	
Time in microsec	2089	2147.5	2152	2212	2183.5	2184.5	2233.5	2155	2143.5	2981	
Duration	306	483.5	533	630.5	622	611.5	631	484	424	1001.5	
Impulse (sec*psi)	2.76E-03	5.45E-03	9.20E-03	1.50E-02	1.77E-02	1.41E-02	9.11E-03	5.19E-03	3.30E-03	8.09E-03	
Impulse (millisec*psi)	2.76	5.45	9.20	14.98	17.69	14.12	9.11	5.19	3.30	8.09	
Time							Pressure				
Signature Sensor		1561.5	Microseconds				Signature Sensor		112.656		
	Dif	Average	Dif					Dif	Average	Dif	
Channel 4	20	54.75	11.5	Channel 6			Channel 4	88.71%	79.96%	71.21%	Channel 6
Channel 3	57.5	49.25	41	Channel 7			Channel 3	58.17%	47.03%	35.88%	Channel 7
Channel 2	102.5	106	109.5	Channel 8			Channel 2	32.62%	27.95%	23.28%	Channel 8
Channel 1	221.5	189.75	158	Channel 9			Channel 1	18.10%	16.72%	15.34%	Channel 9

Bravo 3 - Repetition B - Pipe 2: Two 90-Gram Charges at 60-Degrees

	CH 1 [PSI]	CH 2 [PSI]	CH 3 [PSI]	CH 4 [PSI]	CH 5 [PSI]	CH 6 [PSI]	CH 7 [PSI]	CH 8 [PSI]	CH 9 [PSI]	CH 10 [PSI	CH 14 [V]
	15.8002	29.8878	49.326	102.31	118.495	90.2489	44.0642	25.8565	17.3921	19.1178	4.99771
Initial Pressure Arival	0.001785	0.001675	0.00163	0.0016	0.001587	0.0016	0.001618	0.001684	0.001741	0.002001	
Time in microsec	1784.5	1674.5	1629.5	1599.5	1586.5	1599.5	1618	1684	1741	2000.5	
Min time	1586.5										
Max time	2000.5										
arival spread	414										
max time duration	877.00	984.00	1,111.00	1,402.00	1,236.00	1,255.00	1,141.00	994.00	868.00	1,647.00	
	0.002223	0.002166	0.002185	0.0023	0.002204	0.002227	0.002188	0.002181	0.002175	0.002824	
Time in microsec	2222.5	2166	2184.5	2300	2204	2226.5	2188	2180.5	2174.5	2823.5	
Duration	438	491.5	555	700.5	617.5	627	570	496.5	433.5	823	
Impulse (sec*psi)	3.16E-03	5.71E-03	9.45E-03	1.52E-02	1.81E-02	1.45E-02	9.29E-03	5.47E-03	3.56E-03	7.79E-03	
Impulse (millisec*psi)	3.16	5.71	9.45	15.21	18.07	14.49	9.29	5.47	3.56	7.79	
Time						Pressure					
Signature Sensor		1586.5	Microseconds			Signature Sensor		118.495			
	Dif	Average	Dif				Dif	Average	Dif		
Channel 4	13	48.75	13	Channel 6			Channel 4	86.34%	81.25%	76.16%	Channel 6
Channel 3	43	37.25	31.5	Channel 7			Channel 3	41.63%	39.41%	37.19%	Channel 7
Channel 2	88	92.75	97.5	Channel 8			Channel 2	25.22%	23.52%	21.82%	Channel 8
Channel 1	198	176.25	154.5	Channel 9			Channel 1	13.33%	14.01%	14.68%	Channel 9

Bravo 3 - Repetition C - Pipe 2: Two 90-Gram Charges at 60-Degrees

	CH 1 [PSI]	CH 2 [PSI]	CH 3 [PSI]	CH 4 [PSI]	CH 5 [PSI]	CH 6 [PSI]	CH 7 [PSI]	CH 8 [PSI]	CH 9 [PSI]	CH 10 [PSI	CH 13 [V]
	22.1144	39.4035	68.6444	105.953	119.325	69.7439	43.9446	29.8675	18.0683	18.5095	4.99985
Initial Pressure Arival	0.001621	0.001646	0.001602	0.001563	0.001544	0.00153	0.001561	0.001626	0.001699	0.001944	
Time in microsec	1620.5	1645.5	1601.5	1563	1543.5	1529.5	1560.5	1626	1699	1944	
Min time	1529.5										
Max time	1944										
arival spread	414.5										
max time duration	993.00	965.00	1,077.00	1,377.00	1,397.00	1,491.00	1,355.00	876.00	876.00	2,242.00	
	0.002117	0.002128	0.00214	0.002251	0.002242	0.002275	0.002238	0.002064	0.002137	0.003065	
Time in microsec	2116.5	2127.5	2139.5	2251	2241.5	2274.5	2237.5	2063.5	2136.5	3064.5	
Duration	496	482	538	688	698	745	677	437.5	437.5	1120.5	
Impulse (sec*psi)	2.98E-03	5.24E-03	9.91E-03	1.64E-02	1.86E-02	1.51E-02	9.86E-03	5.38E-03	3.43E-03	8.27E-03	
Impulse (millisec*psi)	2.98	5.24	9.91	16.39	18.65	15.10	9.86	5.38	3.43	8.27	
Time							Pressure				
Signature Sensor		1543.5	Microseconds				Signature Sensor		119.325		
	Dif	Average	Dif				Dif		Average	Dif	
Channel 4	19.5	41.25	-14	Channel 6			Channel 4	88.79%	73.62%	58.45%	Channel 6
Channel 3	58	37.5	17	Channel 7			Channel 3	57.53%	47.18%	36.83%	Channel 7
Channel 2	102	92.25	82.5	Channel 8			Channel 2	33.02%	29.03%	25.03%	Channel 8
Channel 1	77	116.25	155.5	Channel 9			Channel 1	18.53%	16.84%	15.14%	Channel 9

Bravo 4 - Repetition A - Pipe 2: Two 90-Gram Charges at 120-Degrees

	CH 1 [PSI]	CH 2 [PSI]	CH 3 [PSI]	CH 4 [PSI]	CH 5 [PSI]	CH 6 [PSI]	CH 7 [PSI]	CH 8 [PSI]	CH 9 [PSI]	CH 10 [PSI]	CH 13 [V]
	24.0563	35.3565	33.8861	36.2358	66.1357	36.9077	40.1991	36.4543	27.1486	20.1571	5.00
Initial Pressure Arival	0.0020235	0.0019535	0.0019155	0.0019395	0.0020055	0.001955	0.001933	0.0019575	0.0019925	0.0022145	
Time in microsec	2023.5	1953.5	1915.5	1939.5	2005.5	1955	1933	1957.5	1992.5	2214.5	
Min time	1915.5										
Max time	2214.5										
arival spread	299										
max time duration	2,529.00	1,500.00	1,576.00	1,605.00	1,479.00	1,566.00	1,563.00	1,457.00	2,614.00	2,635.00	
	0.0032875	0.002703	0.002703	0.0027415	0.0027445	0.0027375	0.002714	0.0026855	0.003299	0.0035315	
Time in microsec	3287.5	2703	2703	2741.5	2744.5	2737.5	2714	2685.5	3299	3531.5	
Duration	1264	749.5	787.5	802	739	782.5	781	728	1306.5	1317	
Impulse (sec*psi)	6.69E-03	7.15E-03	1.01E-02	1.12E-02	1.32E-02	1.11E-02	9.15E-03	6.98E-03	6.66E-03	8.78E-03	
Impulse (millisec*psi)	6.69	7.15	10.12	11.15	13.24	11.13	9.15	6.98	6.66	8.78	
Time							Pressure				
Signature Sensor		2005.5	Microseconds				Signature Sensor		66.1357		
	Dif	Average	Dif					Dif	Average	Dif	
Channel 4	-66	-24	-50.5	Channel 6			Channel 4	54.79%	55.30%	55.81%	Channel 6
Channel 3	-90	-81.25	-72.5	Channel 7			Channel 3	51.24%	56.01%	60.78%	Channel 7
Channel 2	-52	-50	-48	Channel 8			Channel 2	53.46%	54.29%	55.12%	Channel 8
Channel 1	18	2.5	-13	Channel 9			Channel 1	36.37%	38.71%	41.05%	Channel 9

Bravo 4 - Repetition B - Pipe 2: Two 90-Gram Charges at 120-Degrees

	CH 1 [PSI]	CH 2 [PSI]	CH 3 [PSI]	CH 4 [PSI]	CH 5 [PSI]	CH 6 [PSI]	CH 7 [PSI]	CH 8 [PSI]	CH 9 [PSI]	CH 10 [PSI	CH 14 [V]
	25.6392	39.8275	43.401	38.5453	85.0551	38.8143	44.5552	41.3177	32.0791	21.0759	4.9971
Initial Pressure Arival	0.001615	0.001549	0.001524	0.001546	0.001609	0.001545	0.001516	0.00154	0.001577	0.001785	
Time in microsec	1615	1549	1523.5	1545.5	1609	1545	1516	1540	1576.5	1785	
Min time	1516										
Max time	1785										
arival spread	269										
max time duration	2,530.00	1,390.00	1,483.00	1,461.00	1,363.00	1,417.00	1,509.00	1,453.00	2,929.00	2,804.00	
	0.00288	0.002244	0.002265	0.002276	0.00229	0.002253	0.00227	0.002266	0.003041	0.003187	
Time in microsec	2879.5	2243.5	2264.5	2275.5	2290	2253	2270	2266	3040.5	3186.5	
Duration	1264.5	694.5	741	730	681	708	754	726	1464	1401.5	
Impulse (sec*psi)	7.08E-03	7.39E-03	9.59E-03	1.15E-02	1.44E-02	1.15E-02	9.60E-03	7.38E-03	7.14E-03	8.97E-03	
Impulse (millisec*psi)	7.08	7.39	9.59	11.51	14.37	11.55	9.60	7.38	7.14	8.97	
Time							Pressure				
Signature Sensor		1609	Microseconds				Signature Sensor		85.0551		
	Dif	Average	Dif					Dif	Average	Dif	
Channel 4	-63.5	-34.5	-64	Channel 6			Channel 4	45.32%	45.48%	45.63%	Channel 6
Channel 3	-85.5	-89.25	-93	Channel 7			Channel 3	51.03%	51.71%	52.38%	Channel 7
Channel 2	-60	-64.5	-69	Channel 8			Channel 2	46.83%	47.70%	48.58%	Channel 8
Channel 1	6	-13.25	-32.5	Channel 9			Channel 1	30.14%	33.93%	37.72%	Channel 9

Bravo 4 - Repetition C - Pipe 2: Two 90-Gram Charges at 120-Degrees

	CH 1 [PSI]	CH 2 [PSI]	CH 3 [PSI]	CH 4 [PSI]	CH 5 [PSI]	CH 6 [PSI]	CH 7 [PSI]	CH 8 [PSI]	CH 9 [PSI]	CH 10 [PSI	CH 13 [V]
	28.9287	40.4885	43.9512	43.8065	65.2144	33.7465	43.3591	43.2005	33.2472	22.9896	5.00015
Initial Pressure Arival	0.0016285	0.001566	0.001537	0.001562	0.00157	0.0015	0.001491	0.00152	0.001549	0.001772	
Time in microsec	1628.5	1565.5	1536.5	1562	1570	1500	1490.5	1520	1548.5	1771.5	
Min time	1490.5										
Max time	1771.5										
arival spread	281										
max time duration	2,462.00	1,317.00	1,362.00	1,316.00	1,355.00	1,463.00	1,384.00	1,290.00	1,171.00	2,179.00	
	0.002859	0.002224	0.002217	0.00222	0.002247	0.002231	0.002182	0.002165	0.002134	0.002861	
Time in microsec	2859	2223.5	2217	2219.5	2247	2231	2182	2164.5	2133.5	2860.5	
Duration	1230.5	658	680.5	657.5	677	731	691.5	644.5	585	1089	
Impulse (sec*psi)	7.05E-03	7.40E-03	9.75E-03	1.18E-02	1.32E-02	1.12E-02	9.35E-03	7.31E-03	4.80E-03	8.43E-03	
Impulse (millisec*psi)	7.05	7.40	9.75	11.83	13.25	11.19	9.35	7.31	4.80	8.43	
Time							Pressure				
Signature Sensor		1570	Microseconds				Signature Sensor		65.2144		
	Dif	Average	Dif					Dif	Average	Dif	
Channel 4	-8	-25	-70	Channel 6			Channel 4	67.17%	59.46%	51.75%	Channel 6
Channel 3	-33.5	-56.5	-79.5	Channel 7			Channel 3	67.39%	66.94%	66.49%	Channel 7
Channel 2	-4.5	-27.25	-50	Channel 8			Channel 2	62.09%	64.16%	66.24%	Channel 8
Channel 1	58.5	18.5	-21.5	Channel 9			Channel 1	44.36%	47.67%	50.98%	Channel 9

Bravo 5 - Repetition A - Pipe 3: Two 90-Gram Charges at 40-Degrees

	CH 1 [PSI]	CH 2 [PSI]	CH 3 [PSI]	CH 4 [PSI]	CH 5 [PSI]	CH 6 [PSI]	CH 7 [PSI]	CH 8 [PSI]	CH 9 [PSI]	CH 10 [PSI]	CH 11 [PSI]	CH 12 [PSI]	CH 13 [PSI]	CH 14 [PSI]	CH 15 [V]	CH 16 [V]
	18.3776	23.8329	37.5296	58.7812	78.4232	92.9153	108.067	84.8043	68.3886	43.9886	29.0477	23.3185	17.3789	16.5388	5.00122	5.00641
Initial Pressure Arival	0.001666	0.0016175	0.001524	0.0015125	0.001473	0.001444	0.001435	0.001422	0.0014735	0.0015165	0.001566	0.0016055	0.0016895	0.001908		
Time in microsec	1666	1617.5	1524	1512.5	1473	1444	1434.5	1422	1473.5	1516.5	1566	1605.5	1689.5	1908		
Min time	1422															
Max time	1908															
arival spread	486															
max time duration	807.00	627.00	952.00	1,203.00	1,324.00	1,336.00	1,284.00	1,450.00	1,175.00	1,041.00	941.00	836.00	743.00	1,748.00		
	0.002069	0.0019305	0.0019995	0.0021135	0.0021345	0.002112	0.002076	0.0021465	0.0020605	0.0020365	0.002036	0.002023	0.0020605	0.0027815		
Time in microsec	2069	1930.5	1999.5	2113.5	2134.5	2111.5	2076	2146.5	2060.5	2036.5	2036	2023	2060.5	2781.5		
Duration	403	313	475.5	601	661.5	667.5	641.5	724.5	587	520	470	417.5	371	873.5		
Impulse (sec*psi)	2.54E-03	2.54E-03	3.44E-03	8.73E-03	1.20E-02	1.50E-02	1.60E-02	1.45E-02	1.17E-02	8.24E-03	5.27E-03	3.53E-03	2.66E-03	7.48E-03		
Impulse (millisec*psi)	2.54	2.54	3.44	8.73	11.99	15.01	15.96	14.48	11.72	8.24	5.27	3.53	2.66	7.48		
	Time					Pressure					Impulse					
	Signature Sensor		1434.5 Microseconds			Signature Sensor		108.067			Signature Sensor			15.96		
	Dif	Average	Dif			Dif		Average	Dif			Dif		Average	Dif	
Channel 6	9.5	-1.5	-12.5	Channel 8		Channel 6	85.98%	82.23%	78.47%	Channel 8		Channel 6	94.04%	92.36%	90.68%	Channel 8
Channel 5	38.5	38.75	39	Channel 9		Channel 5	72.57%	67.93%	63.28%	Channel 9		Channel 5	75.11%	74.28%	73.44%	Channel 9
Channel 4	78	80	82	Channel 10		Channel 4	54.39%	47.55%	40.70%	Channel 10		Channel 4	54.69%	53.16%	51.62%	Channel 10
Channel 3	89.5	110.5	131.5	Channel 11		Channel 3	34.73%	30.80%	26.88%	Channel 11		Channel 3	21.54%	27.28%	33.02%	Channel 11
Channel 2	183	177	171	Channel 12		Channel 2	22.05%	21.82%	21.58%	Channel 12		Channel 2	15.93%	19.01%	22.08%	Channel 12
Channel 1	231.5	243.25	255	Channel 13		Channel 1	17.01%	16.54%	16.08%	Channel 13		Channel 1	15.93%	16.29%	16.65%	Channel 13
Channel 14		473.5 Microseconds				Channel 14		15.30%				Channel 14		46.88%		

Bravo 5 - Repetition B - Pipe 3: Two 90-Gram Charges at 40-Degrees

	CH 1 [PSI]	CH 2 [PSI]	CH 3 [PSI]	CH 4 [PSI]	CH 5 [PSI]	CH 6 [PSI]	CH 7 [PSI]	CH 8 [PSI]	CH 9 [PSI]	CH 10 [PSI]	CH 11 [PSI]	CH 12 [PSI]	CH 13 [PSI]	CH 14 [PSI]	CH 15 [V]	CH 16 [V]
	23.3207	32.0765	54.7478	87.4833	89.515	101.827	101.478	86.6589	78.6551	51.3473	34.1462	25.8084	17.7655	16.6148	5.00031	5.0061
Initial Pressure Arival	0.001597	0.001544	0.001464	0.0014515	0.001414	0.001386	0.001373	0.0013795	0.001405	0.0014445	0.0014915	0.001508	0.0016095	0.0017815		
Time in microsec	1597	1544	1463.5	1451.5	1414	1385.5	1373	1379.5	1405	1444.5	1491.5	1508	1609.5	1781.5		
Min time	1373															
Max time	1781.5															
arival spread	408.5															
max time duration	786.00	694.00	954.00	1,071.00	1,128.00	1,369.00	1,386.00	1,504.00	1,136.00	1,062.00	929.00	892.00	625.00	1,876.00		
	0.0019895	0.0018905	0.00194	0.0019865	0.0019775	0.00207	0.002066	0.002131	0.0019725	0.001975	0.0019555	0.0019535	0.0019215	0.002719		
Time in microsec	1989.5	1890.5	1940	1986.5	1977.5	2069.5	2065.5	2131	1972.5	1975	1955.5	1953.5	1921.5	2719		
Duration	392.5	346.5	476.5	535	563.5	684	692.5	751.5	567.5	530.5	464	445.5	312	937.5		
Impulse (sec*psi)	2.60E-03	2.60E-03	3.71E-03	9.27E-03	1.27E-02	1.59E-02	1.69E-02	1.57E-02	1.25E-02	8.78E-03	5.45E-03	3.54E-03	2.58E-03	7.71E-03		
Impulse (millisec*psi)	2.60	2.60	3.71	9.27	12.65	15.91	16.94	15.71	12.55	8.78	5.45	3.54	2.58	7.71		
Time					Pressure						Impulse					
Signature Sensor	1373	Microseconds			Signature Sensor		101.478				Signature Sensor			16.94		
Dif	Average	Dif			Dif		Average	Dif			Dif			Average	Dif	
Channel 6	12.5	9.5	6.5	Channel 8	Channel 6	100.34%	92.87%	85.40%	Channel 8		Channel 6	93.94%		93.33%	92.73%	Channel 8
Channel 5	41	36.5	32	Channel 9	Channel 5	88.21%	82.86%	77.51%	Channel 9		Channel 5	74.70%		74.38%	74.06%	Channel 9
Channel 4	78.5	75	71.5	Channel 10	Channel 4	86.21%	68.40%	50.60%	Channel 10		Channel 4	54.74%		53.29%	51.84%	Channel 10
Channel 3	90.5	104.5	118.5	Channel 11	Channel 3	53.95%	43.80%	33.65%	Channel 11		Channel 3	21.91%		27.05%	32.20%	Channel 11
Channel 2	171	153	135	Channel 12	Channel 2	31.61%	28.52%	25.43%	Channel 12		Channel 2	15.32%		18.11%	20.90%	Channel 12
Channel 1	224	230.25	236.5	Channel 13	Channel 1	22.98%	20.24%	17.51%	Channel 13		Channel 1	15.32%		15.27%	15.23%	Channel 13
Channel 14		408.5	Microseconds		Channel 14		16.37%				Channel 14			45.53%		

Bravo 5 - Repetition C - Pipe 3: Two 90-Gram Charges at 40-Degrees

	CH 1 [PSI]	CH 2 [PSI]	CH 3 [PSI]	CH 4 [PSI]	CH 5 [PSI]	CH 6 [PSI]	CH 7 [PSI]	CH 8 [PSI]	CH 9 [PSI]	CH 10 [PSI]	CH 11 [PSI]	CH 12 [PSI]	CH 13 [PSI]	CH 14 [PSI]	CH 16 [V]
	17.8598	22.7292	37.4223	58.2008	81.9435	96.8387	115.665	100.987	83.6719	52.5937	35.5423	27.0564	18.6635	16.8683	5.0061
Initial Pressure Arival	0.0016155	0.0015725	0.001514	0.001466	0.0014265	0.0013975	0.001387	0.0013935	0.0014185	0.001458	0.0015045	0.001505	0.001622	0.0018455	
Time in microsec	1615.5	1572.5	1514	1466	1426.5	1397.5	1387	1393.5	1418.5	1458	1504.5	1505	1622	1845.5	
Min time	1387														
Max time	1845.5														
arival spread	458.5														
max time duration	611.00	619.00	967.00	1,063.00	1,177.00	1,322.00	1,343.00	1,257.00	1,163.00	1,063.00	930.00	929.00	580.00	1,779.00	
	0.0019205	0.0018815	0.001997	0.001997	0.0020145	0.002058	0.002058	0.0020215	0.0019995	0.001989	0.001969	0.001969	0.0019115	0.0027345	
Time in microsec	1920.5	1881.5	1997	1997	2014.5	2058	2058	2021.5	1999.5	1989	1969	1969	1911.5	2734.5	
Duration	305	309	483	531	588	660.5	671	628	581	531	464.5	464	289.5	889	
Impulse (sec*psi)	2.39E-03	3.41E-03	5.44E-03	8.70E-03	1.21E-02	1.55E-02	1.66E-02	1.54E-02	1.23E-02	8.49E-03	5.27E-03	3.48E-03	5.07E-03	7.48E-03	
Impulse (millisec*psi)	2.39	3.41	5.44	8.70	12.12	15.49	16.62	15.36	12.32	8.49	5.27	3.48	5.07	7.48	
Time						Pressure						Impulse			
Signature Sensor		1387	Microseconds			Signature Sensor		115.665				Signature Sensor		16.62	
	Dif	Average	Dif			Dif	Average	Dif				Dif	Average	Dif	
Channel 6	10.5	8.5	6.5	Channel 8		Channel 6	83.72%	85.52%	87.31%	Channel 8		Channel 6	93.22%	92.83%	92.44% Channel 8
Channel 5	39.5	35.5	31.5	Channel 9		Channel 5	70.85%	71.59%	72.34%	Channel 9		Channel 5	72.91%	73.51%	74.10% Channel 9
Channel 4	79	75	71	Channel 10		Channel 4	50.32%	47.89%	45.47%	Channel 10		Channel 4	52.36%	51.71%	51.07% Channel 10
Channel 3	127	122.25	117.5	Channel 11		Channel 3	32.35%	31.54%	30.73%	Channel 11		Channel 3	32.75%	32.23%	31.71% Channel 11
Channel 2	185.5	151.75	118	Channel 12		Channel 2	19.65%	21.52%	23.39%	Channel 12		Channel 2	20.53%	20.74%	20.94% Channel 12
Channel 1	228.5	231.75	235	Channel 13		Channel 1	15.44%	15.79%	16.14%	Channel 13		Channel 1	14.39%	22.45%	30.50% Channel 13
Channel 14		458.5	Microseconds			Channel 14		14.58%				Channel 14		45.01%	

APPENDIX M

CHARLIE TEST DATA SUMMARY

The data presented in this appendix is the summarized data from Charlie tests detailed in Section 5.3.2. Each file highlights the signature sensor with the cells filled blue. The data presented in this appendix was extracted in accordance with the technique described in Section 5.2. The max pressure, arrival time, positive pressure duration, and impulse data was extracted from each test. However, the data for three charges at 40 degree angular spacing files were corrupted and the summary data is no longer available.

Charlie 1 - Repetition A - Pipe 1: Three 90-Gram Charges at 90-Degrees

	CH 1 [PSI]	CH 2 [PSI]	CH 3 [PSI]	CH 4 [PSI]	CH 5 [PSI]	CH 6 [PSI]	CH 7 [PSI]	CH 8 [PSI]	CH 14 [V]	CH 15 [V]	
	35.3488	42.7084	97.0215	60.5658	84.8171	42.3015	33.4384	35.1786	4.99908	5.00259	
Initial Pressure Arival	0.0015175	0.001473	0.001529	0.001481	0.0015395	0.001526	0.0015745	0.00164			
Time in microsec	1517.5	1473	1529	1481	1539.5	1526	1574.5	1640			
Min time	1473										
Max time	1640										
arival spread	167										
max time duration	2,754.00	1,495.00	1,605.00	1,681.00	1,533.00	2,542.00	2,566.00	2,138.00			
	0.002894	0.00222	0.002331	0.002321	0.0023055	0.0027965	0.002857	0.0027085			
Time in microsec	2894	2220	2331	2321	2305.5	2796.5	2857	2708.5			
Duration	1376.5	747	802	840	766	1270.5	1282.5	1068.5			
Impulse (sec*psi)	1.20E-02	1.16E-02	1.75E-02	1.76E-02	1.69E-02	1.34E-02	1.25E-02	1.34E-02			
Impulse (millisec*psi)	12.00	11.56	17.54	17.60	16.85	13.42	12.51	13.37			
Time						Pressure					
Signature Sensor		1481	Microseconds				Signature Sensor		60.5658		
	Dif	Average	Dif					Dif	Average	Dif	
Channel 3	48	46.75	58.5				Channel 3	160.19%	150.12%	140.04%	Channel 5
Channel 2	-8	18.5	45	Channel 6			Channel 2	70.52%	70.18%	69.84%	Channel 6
Channel 1	36.5	65	93.5	Channel 7			Channel 1	58.36%	56.79%	55.21%	Channel 7

Charlie 1 - Repetition B - Pipe 1: Three 90-Gram Charges at 90-Degrees

	CH 1 [PSI]	CH 2 [PSI]	CH 3 [PSI]	CH 4 [PSI]	CH 5 [PSI]	CH 6 [PSI]	CH 7 [PSI]	CH 8 [PSI]	CH 13 [V]	CH 14 [V]	CH 15 [V]
	33.3481	42.1347	80.2395	49.5617	95.6099	42.6705	34.1812	28.9537	4.99985	5.00015	5.00168
Initial Pressure Arival	0.0014845	0.0014265	0.001473	0.00148	0.001536	0.001526	0.0015675	0.0015785			
Time in microsec	1484.5	1426.5	1473	1480	1536	1526	1567.5	1578.5			
Min time	1426.5										
Max time	1578.5										
arival spread	152										
max time duration	2,903.00	2,753.00	1,781.00	1,938.00	1,548.00	2,214.00	2,225.00	2,424.00			
	0.0029355	0.0028025	0.002363	0.0024485	0.0023095	0.0026325	0.0026795	0.00279			
Time in microsec	2935.5	2802.5	2363	2448.5	2309.5	2632.5	2679.5	2790			
Duration	1451	1376	890	968.5	773.5	1106.5	1112	1211.5			
Impulse (sec*psi)	1.22E-02	1.33E-02	1.64E-02	1.76E-02	1.71E-02	1.32E-02	1.26E-02	1.35E-02			
Impulse (millisec*psi)	12.24	13.26	16.43	17.65	17.10	13.19	12.64	13.54			
Time							Pressure				
Signature Sensor		1480	Microseconds				Signature Sensor		49.5617		
	Dif	Average	Dif					Dif	Average	Dif	
Channel 3	-7	43.75	56				Channel 3	161.90%	177.40%	192.91%	Channel 5
Channel 2	-53.5	-3.75	46	Channel 6			Channel 2	85.01%	85.56%	86.10%	Channel 6
Channel 1	4.5	46	87.5	Channel 7			Channel 1	67.29%	68.13%	68.97%	Channel 7

Charlie 1 - Repetition C - Pipe 1: Three 90-Gram Charges at 90-Degrees

	CH 1 [PSI]	CH 2 [PSI]	CH 3 [PSI]	CH 4 [PSI]	CH 5 [PSI]	CH 6 [PSI]	CH 7 [PSI]	CH 8 [PSI]	CH 14 [V]	CH 15 [V]	
	26.3042	43.3133	120.171	70.0323	100.814	44.4479	36.8062	36.3991	4.99985	5.00153	
Initial Pressure Arival	0.001535	0.0014935	0.00155	0.0015	0.0015235	0.001471	0.0015245	0.001651			
Time in microsec	1535	1493.5	1550	1500	1523.5	1471	1524.5	1651			
Min time	1471										
Max time	1651										
arival spread	180										
max time duration	2,767.00	2,255.00	1,537.00	1,682.00	1,498.00	1,363.00	2,461.00	2,372.00			
	0.002918	0.0026205	0.002318	0.0023405	0.002272	0.002152	0.0027545	0.0028365			
Time in microsec	2918	2620.5	2318	2340.5	2272	2152	2754.5	2836.5			
Duration	1383	1127	768	840.5	748.5	681	1230	1185.5			
Impulse (sec*psi)	1.30E-02	1.31E-02	1.85E-02	1.87E-02	1.72E-02	1.12E-02	1.14E-02	1.43E-02			
Impulse (millisec*psi)	12.97	13.07	18.46	18.67	17.20	11.16	11.42	14.29			
Time							Pressure				
Signature Sensor		1500	Microseconds				Signature Sensor		70.0323		
	Dif	Average	Dif					Dif	Average	Dif	
Channel 3	50	12.25	23.5				Channel 3	171.59%	157.77%	143.95%	Channel 5
Channel 2	-6.5	-17.75	-29	Channel 6			Channel 2	61.85%	62.66%	63.47%	Channel 6
Channel 1	35	29.75	24.5	Channel 7			Channel 1	37.56%	45.06%	52.56%	Channel 7

Charlie 2 - Repetition A - Pipe 2: Three 90-Gram Charges at 60-Degrees

	CH 1 [PSI]	CH 2 [PSI]	CH 3 [PSI]	CH 4 [PSI]	CH 5 [PSI]	CH 6 [PSI]	CH 7 [PSI]	CH 8 [PSI]	CH 9 [PSI]	CH 10 [PSI	CH 14 [V]	CH 15 [V]
	33.913	63.5481	96.6122	115.562	118.538	127.864	90.747	48.8306	30.4807	27.5267	4.99969	5.00
Initial Pressure Arival	0.001611	0.001533	0.001494	0.001473	0.001484	0.001508	0.001523	0.001546	0.001638	0.001807		
Time in microsec	1610.5	1532.5	1494	1472.5	1484	1507.5	1522.5	1545.5	1638	1806.5		
Min time	1472.5											
Max time	1806.5											
arival spread	334											
max time duration	1,009.00	892.00	1,403.00	1,663.00	1,685.00	1,602.00	1,207.00	1,010.00	946.00	2,320.00		
	0.002115	0.001978	0.002195	0.002304	0.002326	0.002308	0.002126	0.00205	0.002111	0.002966		
Time in microsec	2114.5	1978	2195	2303.5	2326	2308	2125.5	2050	2110.5	2966		
Duration	504	445.5	701	831	842	800.5	603	504.5	472.5	1159.5		
Impulse (sec*psi)	5.32E-03	9.80E-03	1.65E-02	2.29E-02	2.54E-02	2.43E-02	1.66E-02	9.81E-03	5.57E-03	1.35E-02		
Impulse (millisec*psi)	5.32	9.80	16.49	22.86	25.43	24.34	16.57	9.81	5.57	13.55		
Time							Pressure					
Signature Sensor		1484	Microseconds				Signature Sensor		118.538			
	Dif	Average	Dif					Dif	Average	Dif		
Channel 4	-11.5	30.75	23.5	Channel 6			Channel 4	97.49%	102.68%	107.87%	Channel 6	
Channel 3	10	24.25	38.5	Channel 7			Channel 3	81.50%	79.03%	76.56%	Channel 7	
Channel 2	48.5	55	61.5	Channel 8			Channel 2	53.61%	47.40%	41.19%	Channel 8	
Channel 1	126.5	140.25	154	Channel 9			Channel 1	28.61%	27.16%	25.71%	Channel 9	

Charlie 2 - Repetition B - Pipe 2: Three 90-Gram Charges at 60-Degrees

	CH 1 [PSI]	CH 2 [PSI]	CH 3 [PSI]	CH 4 [PSI]	CH 5 [PSI]	CH 6 [PSI]	CH 7 [PSI]	CH 8 [PSI]	CH 9 [PSI]	CH 10 [PSI	CH 14 [V]
	27.3222	57.593	88.8955	92.831	121.234	121.511	89.2929	45.5127	25.2858	27.7738	4.99771
Initial Pressure Arival	0.001633	0.001561	0.001493	0.001487	0.001517	0.001532	0.001548	0.001564	0.001631	0.001833	
Time in microsec	1632.5	1560.5	1493	1486.5	1516.5	1532	1547.5	1564	1630.5	1832.5	
Min time	1486.5										
Max time	1832.5										
arival spread	346										
max time duration	941.00	1,203.00	1,429.00	1,552.00	1,623.00	1,551.00	1,426.00	999.00	804.00	2,351.00	
	0.002103	0.002162	0.002207	0.002262	0.002328	0.002307	0.00226	0.002063	0.002032	0.003008	
Time in microsec	2102.5	2161.5	2207	2262	2327.5	2307	2260	2063	2032	3007.5	
Duration	470	601	714	775.5	811	775	712.5	499	401.5	1175	
Impulse (sec*psi)	5.21E-03	1.06E-02	1.57E-02	2.15E-02	2.48E-02	2.38E-02	1.61E-02	9.38E-03	5.42E-03	1.38E-02	
Impulse (millisec*psi)	5.21	10.63	15.68	21.45	24.85	23.81	16.10	9.38	5.42	13.84	
Time							Pressure				
Signature Sensor		1516.5	Microseconds				Signature Sensor		121.234		
	Dif	Average	Dif				Dif		Average	Dif	
Channel 4	-30	23.75	15.5	Channel 6			Channel 4	76.57%	88.40%	100.23%	Channel 6
Channel 3	-23.5	3.75	31	Channel 7			Channel 3	73.33%	73.49%	73.65%	Channel 7
Channel 2	44	45.75	47.5	Channel 8			Channel 2	47.51%	42.52%	37.54%	Channel 8
Channel 1	116	115	114	Channel 9			Channel 1	22.54%	21.70%	20.86%	Channel 9

Charlie 2 - Repetition C - Pipe 2: Three 90-Gram Charges at 60-Degrees

	CH 1 [PSI]	CH 2 [PSI]	CH 3 [PSI]	CH 4 [PSI]	CH 5 [PSI]	CH 6 [PSI]	CH 7 [PSI]	CH 8 [PSI]	CH 9 [PSI]	CH 10 [PSI	CH 13 [V]
	34.9134	70.819	97.9609	120.774	99.4841	132.563	103.538	49.217	31.5934	30.714	5.00015
Initial Pressure Arival	0.0016	0.001518	0.001485	0.001471	0.001491	0.001525	0.001545	0.001556	0.001623	0.0018	
Time in microsec	1599.5	1518	1484.5	1470.5	1491	1524.5	1545	1556	1623	1799.5	
Min time	1470.5										
Max time	1799.5										
arival spread	329										
max time duration	992.00	1,135.00	1,381.00	1,573.00	1,604.00	1,448.00	1,242.00	942.00	696.00	2,351.00	
	0.002095	0.002085	0.002175	0.002257	0.002293	0.002248	0.002166	0.002027	0.001971	0.002975	
Time in microsec	2095	2085	2174.5	2256.5	2292.5	2248	2165.5	2026.5	1970.5	2974.5	
Duration	495.5	567	690	786	801.5	723.5	620.5	470.5	347.5	1175	
Impulse (sec*psi)	5.56E-03	1.25E-02	1.73E-02	2.29E-02	2.43E-02	2.43E-02	1.71E-02	9.90E-03	5.48E-03	1.36E-02	
Impulse (millisec*psi)	5.56	12.54	17.29	22.85	24.28	24.33	17.07	9.90	5.48	13.56	
Time							Pressure				
Signature Sensor		1491	Microseconds				Signature Sensor		99.4841		
	Dif	Average	Dif					Dif	Average	Dif	
Channel 4	-20.5	32.5	33.5	Channel 6			Channel 4	121.40%	127.33%	133.25%	Channel 6
Channel 3	-6.5	23.75	54	Channel 7			Channel 3	98.47%	101.27%	104.07%	Channel 7
Channel 2	27	46	65	Channel 8			Channel 2	71.19%	60.33%	49.47%	Channel 8
Channel 1	108.5	120.25	132	Channel 9			Channel 1	35.09%	33.43%	31.76%	Channel 9

Charlie 3 - Repetition A - Pipe 2: Three 90-Gram Charges at 120-Degrees

	CH 1 [PSI]	CH 2 [PSI]	CH 3 [PSI]	CH 4 [PSI]	CH 5 [PSI]	CH 6 [PSI]	CH 7 [PSI]	CH 8 [PSI]	CH 9 [PSI]	CH 10 [PSI]	CH 14 [V]	CH 15 [V]
	41.816	36.9715	78.6358	38.7923	39.5594	37.781	66.5558	33.7926	38.1531	67.4099	4.99817	5.00
Initial Pressure Arival	0.001519	0.001546	0.001589	0.0015505	0.0015325	0.001563	0.0016155	0.0015545	0.001532	0.0016155		
Time in microsec	1519	1546	1589	1550.5	1532.5	1563	1615.5	1554.5	1532	1615.5		
Min time	1519											
Max time	1615.5											
arival spread	96.5											
max time duration	2,492.00	2,418.00	3,275.00	1,934.00	2,656.00	2,306.00	2,024.00	2,049.00	2,330.00	1,953.00		
	0.0027645	0.0027545	0.003226	0.002517	0.00286	0.0027155	0.002627	0.0025785	0.0026965	0.0025915		
Time in microsec	2764.5	2754.5	3226	2517	2860	2715.5	2627	2578.5	2696.5	2591.5		
Duration	1245.5	1208.5	1637	966.5	1327.5	1152.5	1011.5	1024	1164.5	976		
Impulse (sec*psi)	1.56E-02	1.57E-02	1.92E-02	1.45E-02	1.63E-02	1.53E-02	1.65E-02	1.45E-02	1.51E-02	1.60E-02		
Impulse (millisec*psi)	15.55	15.65	19.21	14.45	16.33	15.30	16.52	14.53	15.09	15.99		
Time						Pressure						
Signature Sensor		1532.5	Microseconds			Signature Sensor			39.5594			
	Dif	Average	Dif				Dif		Average	Dif		
Channel 4	18	11	30.5	Channel 6			Channel 4	98.06%	96.78%	95.50%	Channel 6	
Channel 3	56.5	69.75	83	Channel 7			Channel 3	198.78%	183.51%	168.24%	Channel 7	
Channel 2	13.5	17.75	22	Channel 8			Channel 2	93.46%	89.44%	85.42%	Channel 8	
Channel 1	-13.5	-7	-0.5	Channel 9			Channel 1	105.70%	101.07%	96.45%	Channel 9	

Charlie 3 - Repetition B - Pipe 2: Three 90-Gram Charges at 120-Degrees

	CH 1 [PSI]	CH 2 [PSI]	CH 3 [PSI]	CH 4 [PSI]	CH 5 [PSI]	CH 6 [PSI]	CH 7 [PSI]	CH 8 [PSI]	CH 9 [PSI]	CH 10 [PSI]	CH 14 [V]
	41.5865	41.0559	75.9786	38.6194	41.0785	36.6555	73.4235	39.0485	44.4239	67.5873	4.99756
Initial Pressure Arival	0.0015365	0.001562	0.001599	0.00155	0.0015275	0.0015515	0.001627	0.001577	0.0015535	0.001631	
Time in microsec	1536.5	1562	1599	1550	1527.5	1551.5	1627	1577	1553.5	1631	
Min time	1527.5										
Max time	1631										
arival spread	103.5										
max time duration	2,655.00	2,600.00	3,690.00	3,183.00	2,366.00	2,401.00	2,458.00	2,571.00	2,520.00	2,870.00	
	0.0028635	0.0028615	0.0034435	0.003141	0.00271	0.0027515	0.0028555	0.002862	0.002813	0.0030655	
Time in microsec	2863.5	2861.5	3443.5	3141	2710	2751.5	2855.5	2862	2813	3065.5	
Duration	1327	1299.5	1844.5	1591	1182.5	1200	1228.5	1285	1259.5	1434.5	
Impulse (sec*psi)	1.55E-02	1.54E-02	1.84E-02	1.54E-02	1.51E-02	1.47E-02	1.67E-02	1.50E-02	1.52E-02	1.68E-02	
Impulse (millisec*psi)	15.46	15.43	18.40	15.40	15.10	14.72	16.74	15.05	15.20	16.75	
Time							Pressure				
Signature Sensor		1527.5	Microseconds				Signature Sensor		41.0785		
	Dif	Average	Dif					Dif	Average	Dif	
Channel 4	22.5	24.75	24	Channel 6			Channel 4	94.01%	91.62%	89.23%	Channel 6
Channel 3	71.5	85.5	99.5	Channel 7			Channel 3	184.96%	181.85%	178.74%	Channel 7
Channel 2	34.5	42	49.5	Channel 8			Channel 2	99.94%	97.50%	95.06%	Channel 8
Channel 1	9	17.5	26	Channel 9			Channel 1	101.24%	104.69%	108.14%	Channel 9

Charlie 3 - Repetition C - Pipe 2: Three 90-Gram Charges at 120-Degrees

	CH 1 [PSI]	CH 2 [PSI]	CH 3 [PSI]	CH 4 [PSI]	CH 5 [PSI]	CH 6 [PSI]	CH 7 [PSI]	CH 8 [PSI]	CH 9 [PSI]	CH 10 [PSI]	CH 14 [V]
	44.1699	40.2827	68.7518	35.9208	39.0713	34.8474	72.8318	36.8529	39.4196	69.8368	4.99786
Initial Pressure Arival	0.0015275	0.0015565	0.0015925	0.0015295	0.0015135	0.001548	0.001621	0.0015615	0.001539	0.001622	
Time in microsec	1527.5	1556.5	1592.5	1529.5	1513.5	1548	1621	1561.5	1539	1622	
Min time	1513.5										
Max time	1622										
arival spread	108.5										
max time duration	2,815.00	2,419.00	2,870.00	2,960.00	3,623.00	2,932.00	2,555.00	2,751.00	2,539.00	2,713.00	
	0.0029345	0.0027655	0.003027	0.003009	0.0033245	0.0030135	0.002898	0.0029365	0.002808	0.002978	
Time in microsec	2934.5	2765.5	3027	3009	3324.5	3013.5	2898	2936.5	2808	2978	
Duration	1407	1209	1434.5	1479.5	1811	1465.5	1277	1375	1269	1356	
Impulse (sec*psi)	1.61E-02	1.60E-02	1.75E-02	1.53E-02	1.63E-02	1.50E-02	1.68E-02	1.50E-02	1.54E-02	1.72E-02	
Impulse (millisec*psi)	16.15	15.95	17.52	15.35	16.33	15.02	16.83	15.03	15.43	17.24	
Time							Pressure				
Signature Sensor		1513.5	Microseconds				Signature Sensor		39.0713		
	Dif	Average	Dif					Dif	Average	Dif	
Channel 4	16	24	34.5	Channel 6			Channel 4	91.94%	90.56%	89.19%	Channel 6
Channel 3	79	93.25	107.5	Channel 7			Channel 3	175.96%	181.19%	186.41%	Channel 7
Channel 2	43	45.5	48	Channel 8			Channel 2	103.10%	98.71%	94.32%	Channel 8
Channel 1	14	19.75	25.5	Channel 9			Channel 1	113.05%	106.97%	100.89%	Channel 9

APPENDIX N

DELTA TEST DATA SUMMARY

The data presented in this appendix is the summarized data from Delta tests detailed in Section 5.3.2. Each file highlights the signature sensor with the cells filled blue. The data presented in this appendix was extracted in accordance with the technique described in Section 5.2. The max pressure, arrival time, positive pressure duration, and impulse data was extracted from each test.

Delta 1 - Repetition A - Pipe 1: Four 90-Gram Charges at 90-Degrees

	CH 1 [PSI]	CH 2 [PSI]	CH 3 [PSI]	CH 4 [PSI]	CH 5 [PSI]	CH 6 [PSI]	CH 7 [PSI]	CH 8 [PSI]	CH 14 [V]	CH 15 [V]	CH 16 [V]
	121.505	63.6729	82.7357	60.7758	115.133	60.4632	107.875	57.0733	4.99924	5.00183	5.00641
Initial Pressure Arival	0.001542	0.001475	0.001509	0.001508	0.001563	0.001518	0.001575	0.001519			
Time in microsec	1542	1475	1508.5	1507.5	1562.5	1517.5	1574.5	1518.5			
Min time	1475										
Max time	1574.5										
arival spread	99.5										
max time duration	1,992.00	1,803.00	2,693.00	1,976.00	2,015.00	2,277.00	2,080.00	1,704.00			
	0.002538	0.002376	0.002855	0.002495	0.00257	0.002656	0.002614	0.00237			
Time in microsec	2537.5	2376	2854.5	2495	2569.5	2655.5	2614	2370			
Duration	995.5	901	1346	987.5	1007	1138	1039.5	851.5			
Impulse (sec*psi)	2.15E-02	2.00E-02	2.35E-02	2.08E-02	2.19E-02	2.12E-02	2.21E-02	1.95E-02			
Impulse (millisec*psi)	21.49	19.99	23.51	20.78	21.86	21.19	22.13	19.49			
Time							Pressure				
Signature Sensor		1507.5	Microseconds				Signature Sensor		60.7758		
	Dif	Average	Dif					Dif	Average	Dif	
Channel 3	1	33.5	55				Channel 3	136.13%	162.79%	189.44%	Channel 5
Channel 2	-32.5	-11.25	10	Channel 6			Channel 2	104.77%	102.13%	99.49%	Channel 6
Channel 1	34.5	50.75	67	Channel 7			Channel 1	199.92%	188.71%	177.50%	Channel 7

Delta 1 - Repetition B - Pipe 1: Four 90-Gram Charges at 90-Degrees

	CH 1 [PSI]	CH 2 [PSI]	CH 3 [PSI]	CH 4 [PSI]	CH 5 [PSI]	CH 6 [PSI]	CH 7 [PSI]	CH 8 [PSI]	CH 14 [V]	CH 15 [V]	CH 16 [V]
	129.044	49.6924	82.7625	74.4105	101.485	57.794	96.2928	71.3508	5.00031	5.00122	5.00626
Initial Pressure Arival	0.001548	0.0014975	0.001477	0.00147	0.001535	0.001496	0.001544	0.0015185			
Time in microsec	1548	1497.5	1477	1470	1535	1496	1544	1518.5			
Min time	1470										
Max time	1548										
arival spread	78										
max time duration	2,733.00	2,511.00	2,881.00	2,660.00	2,370.00	2,589.00	2,446.00	2,475.00			
	0.002914	0.0027525	0.002917	0.0027995	0.0027195	0.00279	0.0027665	0.0027555			
Time in microsec	2914	2752.5	2917	2799.5	2719.5	2790	2766.5	2755.5			
Duration	1366	1255	1440	1329.5	1184.5	1294	1222.5	1237			
Impulse (sec*psi)	2.37E-02	2.19E-02	2.20E-02	2.15E-02	2.19E-02	2.18E-02	2.27E-02	2.24E-02			
Impulse (millisec*psi)	23.68	21.85	22.01	21.45	21.85	21.82	22.71	22.45			
Time							Pressure				
Signature Sensor		1470	Microseconds				Signature Sensor		74.4105		
	Dif	Average	Dif					Dif	Average	Dif	
Channel 3	7	37	65				Channel 3	111.22%	123.80%	136.39%	Channel 5
Channel 2	27.5	26.75	26	Channel 6			Channel 2	66.78%	72.23%	77.67%	Channel 6
Channel 1	78	76	74	Channel 7			Channel 1	173.42%	151.41%	129.41%	Channel 7

Delta 1 - Repetition C - Pipe 1: Four 90-Gram Charges at 90-Degrees

	CH 1 [PSI]	CH 2 [PSI]	CH 3 [PSI]	CH 4 [PSI]	CH 5 [PSI]	CH 6 [PSI]	CH 7 [PSI]	CH 8 [PSI]	CH 13 [V]	CH 14 [V]	CH 15 [V]	CH 16 [V]
	115.733	55.3108	106.302	69.3346	105.298	58.9871	95.3171	64.9725	4.99985	4.99939	5.00275	5.01
Initial Pressure Arival	0.001541	0.0014945	0.001545	0.001505	0.0015505	0.001497	0.0015495	0.0015005				
Time in microsec	1541	1494.5	1545	1505	1550.5	1497	1549.5	1500.5				
Min time	1494.5											
Max time	1550.5											
arival spread	56											
max time duration	2,879.00	2,996.00	2,925.00	2,640.00	2,745.00	2,838.00	2,631.00	2,725.00				
	0.00298	0.002992	0.003007	0.0028245	0.0029225	0.0029155	0.0028645	0.0028625				
Time in microsec	2980	2992	3007	2824.5	2922.5	2915.5	2864.5	2862.5				
Duration	1439	1497.5	1462	1319.5	1372	1418.5	1315	1362				
Impulse (sec*psi)	2.28E-02	2.25E-02	2.36E-02	2.18E-02	2.26E-02	2.22E-02	2.21E-02	2.15E-02				
Impulse (millisec*psi)	22.78	22.51	23.56	21.78	22.65	22.15	22.12	21.46				
Time							Pressure					
Signature Sensor		1505	Microseconds				Signature Sensor		69.3346			
	Dif	Average	Dif				Dif	Average	Dif			
Channel 3	40	22.25	45.5			Channel 3	153.32%	152.59%	151.87%	Channel 5		
Channel 2	-10.5	-9.25	-8	Channel 6		Channel 2	79.77%	82.42%	85.08%	Channel 6		
Channel 1	36	40.25	44.5	Channel 7		Channel 1	166.92%	152.20%	137.47%	Channel 7		

Delta 2 - Repetition A - Pipe 2: Five 90-Gram Charges at 60-Degrees

	CH 1 [PSI]	CH 2 [PSI]	CH 3 [PSI]	CH 4 [PSI]	CH 5 [PSI]	CH 6 [PSI]	CH 7 [PSI]	CH 8 [PSI]	CH 9 [PSI]	CH 10 [PSI]	
	85.927	135.851	131.283	107.256	126.701	135.041	171.699	125.842	93.9319	63.95	
Initial Pressure Arival	0.0015335	0.0015235	0.001486	0.0014805	0.0015115	0.001522	0.001522	0.0015065	0.001515	0.0016065	
Time in microsec	1533.5	1523.5	1486	1480.5	1511.5	1522	1522	1506.5	1515	1606.5	
Min time	1480.5										
Max time	1606.5										
arival spread	126										
max time duration	2,362.00	1,914.00	2,040.00	1,914.00	1,989.00	1,980.00	1,694.00	2,178.00	2,100.00	2,483.00	
	0.002714	0.00248	0.0025055	0.002437	0.0025055	0.0025115	0.0023685	0.002595	0.0025645	0.0028475	
Time in microsec	2714	2480	2505.5	2437	2505.5	2511.5	2368.5	2595	2564.5	2847.5	
Duration	1180.5	956.5	1019.5	956.5	994	989.5	846.5	1088.5	1049.5	1241	
Impulse (sec*psi)	2.40E-02	2.74E-02	2.94E-02	3.08E-02	3.28E-02	3.40E-02	3.07E-02	2.72E-02	2.28E-02	2.75E-02	
Impulse (millisec*psi)	24.05	27.42	29.43	30.80	32.80	33.98	30.67	27.21	22.83	27.48	
Time							Pressure				
Signature Sensor		1511.5	Microseconds				Signature Sensor		126.701		
	Dif	Average	Dif					Dif	Average	Dif	
Channel 4	-31	-2.5	10.5	Channel 6			Channel 4	84.65%	95.62%	106.58%	Channel 6
Channel 3	-25.5	-7.5	10.5	Channel 7			Channel 3	103.62%	119.57%	135.52%	Channel 7
Channel 2	12	3.5	-5	Channel 8			Channel 2	107.22%	103.27%	99.32%	Channel 8
Channel 1	22	12.75	3.5	Channel 9			Channel 1	67.82%	70.98%	74.14%	Channel 9

Delta 2 - Repetition B - Pipe 2: Five 90-Gram Charges at 60-Degrees

	CH 1 [PSI]	CH 2 [PSI]	CH 3 [PSI]	CH 4 [PSI]	CH 5 [PSI]	CH 6 [PSI]	CH 7 [PSI]	CH 8 [PSI]	CH 9 [PSI]	CH 10 [PSI]	CH 13 [V]	CH 14 [V]
	113.367	159.104	100.605	121.447	195.771	125.342	139.57	120.525	106.449	82.1301	4.99985	5.00
Initial Pressure Arival	0.001542	0.00152	0.001488	0.0014685	0.0014815	0.0014715	0.00147	0.0014895	0.0015085	0.0016305		
Time in microsec	1542	1521.5	1488	1468.5	1481.5	1471.5	1473	1489.5	1508.5	1630.5		
Min time	1468.5											
Max time	1630.5											
arival spread	162											
max time duration	2,354.00	1,823.00	1,776.00	1,774.00	1,844.00	1,803.00	1,773.00	2,148.00	2,018.00	2,188.00		
	0.0027185	0.00243	0.0023755	0.002355	0.002403	0.0023725	0.00236	0.002563	0.002517	0.002724		
Time in microsec	2718.5	2432.5	2375.5	2355	2403	2372.5	2359	2563	2517	2724		
Duration	1176.5	911	887.5	886.5	921.5	901	886	1073.5	1008.5	1093.5		
Impulse (sec*psi)	2.55E-02	2.86E-02	3.00E-02	3.20E-02	3.49E-02	3.31E-02	3.22E-02	2.80E-02	2.41E-02	2.92E-02		
Impulse (millisec*psi)	25.48	28.63	29.99	32.02	34.91	33.10	32.22	27.98	24.10	29.18		
Time							Pressure					
Signature Sensor		1481.5	Microseconds				Signature Sensor		195.771			
	Dif	Average	Dif					Dif	Average	Dif		
Channel 4	-13	4	-10	Channel 6			Channel 4	62.04%	63.03%	64.02%	Channel 6	
Channel 3	6.5	-1	-8.5	Channel 7			Channel 3	51.39%	61.34%	71.29%	Channel 7	
Channel 2	40	24	8	Channel 8			Channel 2	81.27%	71.42%	61.56%	Channel 8	
Channel 1	60.5	43.75	27	Channel 9			Channel 1	57.91%	56.14%	54.37%	Channel 9	

Delta 2 - Repetition C - Pipe 2: Five 90-Gram Charges at 60-Degrees

	CH 1 [PSI]	CH 2 [PSI]	CH 3 [PSI]	CH 4 [PSI]	CH 5 [PSI]	CH 6 [PSI]	CH 7 [PSI]	CH 8 [PSI]	CH 9 [PSI]	CH 10 [PSI]	CH 13 [V]	CH 15 [V]
	91.5822	131.567	117.273	156.855	174.296	159.156	149.302	144.247	113.863	87.7	5	5.00
Initial Pressure Arival	0.0013815	0.0013775	0.001435	0.001497	0.001522	0.0015205	0.0014795	0.0015055	0.001523	0.001557		
Time in microsec	1381.5	1377.5	1435	1497	1522	1520.5	1479.5	1505.5	1523	1557		
Min time	1377.5											
Max time	1557											
arival spread	179.5											
max time duration	2,854.00	2,817.00	2,644.00	2,511.00	2,125.00	2,199.00	2,618.00	2,473.00	2,466.00	2,463.00		
	0.002808	0.0027855	0.0027565	0.002752	0.002584	0.0026195	0.002788	0.0027415	0.0027555	0.002788		
Time in microsec	2808	2785.5	2756.5	2752	2584	2619.5	2788	2741.5	2755.5	2788		
Duration	1426.5	1408	1321.5	1255	1062	1099	1308.5	1236	1232.5	1231		
Impulse (sec*psi)	4.95E-02	5.45E-02	5.96E-02	6.94E-02	7.25E-02	7.27E-02	6.32E-02	5.69E-02	5.23E-02	5.80E-02		
Impulse (millisec*psi)	49.50	54.53	59.57	69.41	72.51	72.74	63.21	56.90	52.30	58.02		
Time							Pressure					
Signature Sensor		1522	Microseconds				Signature Sensor		174.296			
	Dif	Average	Dif					Dif	Average	Dif		
Channel 4	-25	-8.25	-1.5	Channel 6			Channel 4	89.99%	90.65%	91.31%	Channel 6	
Channel 3	-87	-64.75	-42.5	Channel 7			Channel 3	67.28%	76.47%	85.66%	Channel 7	
Channel 2	-144.5	-80.5	-16.5	Channel 8			Channel 2	75.48%	79.12%	82.76%	Channel 8	
Channel 1	-140.5	-69.75	1	Channel 9			Channel 1	52.54%	58.94%	65.33%	Channel 9	

APPENDIX O

ECHO TEST DATA SUMMARY

The data presented in this appendix is the summarized data from Echo tests detailed in Section 5.3.2. Each file highlights the signature sensor with the cells filled blue. The data presented in this appendix was extracted in accordance with the technique described in Section 5.2. The max pressure, arrival time, positive pressure duration, and impulse data was extracted from each test.

Echo 1 - Repetition A - Pipe 3: Single 0.4 lb Charge

	CH 1 [PSI]	CH 2 [PSI]	CH 3 [PSI]	CH 4 [PSI]	CH 5 [PSI]	CH 6 [PSI]	CH 7 [PSI]	CH 8 [PSI]	CH 9 [PSI]	CH 10 [PSI	CH 11 [PSI	CH 12 [PSI	CH 13 [PSI	CH 14 [PSI	CH 15 [PSI	CH 16 [V]
	14.8763	19.7298	31.618	46.468	66.4956	75.5184	79.8705	73.6466	64.7763	47.9733	32.0059	0.928315	15.6953	13.9978	91.467	5.00595
Initial Pressure Arival	0.001455	0.001421	0.001361	0.001311	0.001271	0.001239	0.001228	0.001234	0.001261	0.001302	0.001348		0.001466	0.001686	0.001242	
Time in microsec	1454.5	1420.5	1360.5	1311	1271	1238.5	1227.5	1233.5	1260.5	1301.5	1348		1466	1686	1242	
Min time	1227.5															
Max time	1686															
arival spread	458.5															
max time duration	855.00	686.00	925.00	1,023.00	1,127.00	1,196.00	1,226.00	1,153.00	1,087.00	1,051.00	914.00		723.00	1,804.00	897.00	
	0.001882	0.001763	0.001823	0.001822	0.001834	0.001836	0.00184	0.00181	0.001804	0.001827	0.001805		0.001827	0.002588	0.00169	
Time in microsec	1881.5	1763	1822.5	1822	1834	1836	1840	1809.5	1803.5	1826.5	1804.5		1827	2587.5	1690	
Duration	427	342.5	462	511	563	597.5	612.5	576	543	525	456.5		361	901.5	448	
Impulse (sec*psi)	2.39E-03	3.08E-03	4.84E-03	7.22E-03	9.72E-03	1.21E-02	1.30E-02	1.20E-02	1.00E-02	7.22E-03	4.81E-03	0.00E+00	2.48E-03	6.05E-03	1.24E-02	
Impulse (millisec*psi)	2.39	3.08	4.84	7.22	9.72	12.06	12.96	12.03	10.00	7.22	4.81	0.00	2.48	6.05	12.37	
Time						Pressure						Impulse				
Signature Sensor		1227.5	Microseconds			Signature Sensor		79.8705				Signature Sensor		12.96		
	Dif	Average	Dif				Dif	1	Dif				Dif	Average	Dif	
Channel 6	11	8.5	6	Channel 8		Channel 6	94.55%	93.38%	92.21%	Channel 8		Channel 6	93.07%	92.94%	92.81%	Channel 8
Channel 5	43.5	38.25	33	Channel 9		Channel 5	83.25%	82.18%	81.10%	Channel 9		Channel 5	74.98%	76.08%	77.19%	Channel 9
Channel 4	83.5	78.75	74	Channel 10		Channel 4	58.18%	59.12%	60.06%	Channel 10		Channel 4	55.71%	55.71%	55.70%	Channel 10
Channel 3	133	126.75	120.5	Channel 11		Channel 3	39.59%	39.83%	40.07%	Channel 11		Channel 3	37.33%	37.22%	37.11%	Channel 11
Channel 2	193	96.5		Channel 12		Channel 2	24.70%	12.35%		Channel 12		Channel 2	23.80%	11.90%		Channel 12
Channel 1	227	232.75	238.5	Channel 13		Channel 1	18.63%	19.14%	19.65%	Channel 13		Channel 1	18.41%	18.76%	19.11%	Channel 13
Channel 14		458.5	Microseconds			Channel 14		17.53%				Channel 14		46.66%		
Flat Plate		14.5	Microseconds			Flat Plate		114.52%				Flat Plate		95.43%		

Echo 1 - Repetition B - Pipe 3: Single 0.4 lb Charge

	CH 1 [PSI]	CH 2 [PSI]	CH 3 [PSI]	CH 4 [PSI]	CH 5 [PSI]	CH 6 [PSI]	CH 7 [PSI]	CH 8 [PSI]	CH 9 [PSI]	CH 10 [PSI]	CH 11 [PSI]	CH 12 [PSI]	CH 13 [PSI]	CH 14 [PSI]	CH 15 [PSI]	CH 16 [V]
	12.59	17.93	27.12	40.29	57.5	64.36	65.12	69.25	59.39	40.41	27.3	18.98	12.99	12.7	86.63	0.07
Initial Pressure Arival	0.001449	0.001425	0.001363	0.001312	0.00127	0.001231	0.001214	0.00122	0.001246	0.001286	0.001334	0.001333	0.001455	0.00166	0.001186	
Time in microsec	1449	1425	1363	1312	1269.5	1230.5	1213.5	1220	1245.5	1285.5	1334	1332.5	1455	1659.5	1186	
Min time	1186															
Max time	1659.5															
arival spread	473.5															
max time duration	961.00	880.00	1,021.00	1,081.00	1,380.00	1,520.00	1,566.00	1,591.00	1,497.00	1,115.00	931.00	846.00	670.00	1,922.00	904.00	
	0.0019290	0.0018645	0.0018730	0.0018520	0.0019590	0.0019900	0.0019960	0.0020150	0.0019935	0.0018425	0.0017990	0.0017550	0.0017895	0.0026200	0.0016375	
Time in microsec	1929	1864.5	1873	1852	1959	1990	1996	2015	1993.5	1842.5	1799	1755	1789.5	2620	1637.5	
Duration	480	439.5	510	540	689.5	759.5	782.5	795	748	557	465	422.5	334.5	960.5	451.5	
Impulse (sec*psi)	2.37E-03	2.37E-03	3.08E-03	6.85E-03	9.53E-03	1.23E-02	1.37E-02	1.19E-02	9.90E-03	6.70E-03	4.27E-03	2.84E-03	2.27E-03	5.89E-03	1.20E-02	
Impulse (millisec*psi)	2.37	2.37	3.08	6.85	9.53	12.25	13.66	11.90	9.90	6.70	4.27	2.84	2.27	5.89	12.03	

Time					Pressure					Impulse				
Signature Sensor		1213.5	Microseconds		Signature Sensor		65.12			Signature Sensor		13.66		
	Dif	Average	Dif			Dif	Average	Dif			Dif	Average	Dif	
Channel 6	17	11.75	6.5	Channel 8	Channel 6	98.83%	102.59%	106.34%	Channel 8	Channel 6	89.72%	88.43%	87.15%	Channel 8
Channel 5	56	44	32	Channel 9	Channel 5	88.30%	89.75%	91.20%	Channel 9	Channel 5	69.77%	71.12%	72.46%	Channel 9
Channel 4	98.5	85.25	72	Channel 10	Channel 4	61.87%	61.96%	62.05%	Channel 10	Channel 4	50.15%	49.61%	49.06%	Channel 10
Channel 3	149.5	135	120.5	Channel 11	Channel 3	41.65%	41.78%	41.92%	Channel 11	Channel 3	22.53%	26.90%	31.26%	Channel 11
Channel 2	211.5	165.25	119	Channel 12	Channel 2	27.53%	28.34%	29.15%	Channel 12	Channel 2	17.38%	19.09%	20.80%	Channel 12
Channel 1	235.5	238.5	241.5	Channel 13	Channel 1	19.33%	19.64%	19.95%	Channel 13	Channel 1	17.38%	17.00%	16.63%	Channel 13
Channel 14		446	Microseconds		Channel 14		19.50%			Channel 14		43.13%		
Flat Plate		-27.5	Microseconds		Flat Plate		133.03%			Flat Plate		88.11%		

Echo 1 - Repetition C - Pipe 3: Single 0.4 lb Charge

	CH 1 [PSI]	CH 2 [PSI]	CH 3 [PSI]	CH 4 [PSI]	CH 5 [PSI]	CH 6 [PSI]	CH 7 [PSI]	CH 8 [PSI]	CH 9 [PSI]	CH 10 [PSI	CH 11 [PSI	CH 12 [PSI	CH 13 [PSI	CH 14 [PSI	CH 15 [PSI	CH 16 [V]
	22.8794	30.7919	50.9297	78.8011	104.957	134.978	154.784	128.388	111.362	69.8165	44.8415	35.0669	23.465	20.3915	151.73	5.00687
Initial Pressure Arival	0.001251	0.001198	0.001122	0.001098	0.001069	0.001042	0.001035	0.00104	0.001064	0.001099	0.00114	0.001166	0.001245	0.001449	0.001034	
Time in microsec	1251	1198	1122	1098	1068.5	1042	1034.5	1040	1063.5	1099	1140	1166	1245	1448.5	1034	
Min time	1034															
Max time	1448.5															
arival spread	414.5															
max time duration	567.00	621.00	813.00	873.00	1,042.00	1,098.00	1,127.00	1,103.00	1,054.00	993.00	730.00	690.00	532.00	1,824.00	837.00	
	0.001534	0.001508	0.001528	0.001558	0.001589	0.001591	0.001598	0.001591	0.00159	0.001595	0.001505	0.001511	0.001511	0.00236	0.001452	
Time in microsec	1534	1508	1528	1558	1589	1590.5	1597.5	1591	1590	1595	1504.5	1510.5	1510.5	2360	1452	
Duration	283	310	406	460	520.5	548.5	563	551	526.5	496	364.5	344.5	265.5	911.5	418	
Impulse (sec*psi)	2.54E-03	3.75E-03	6.38E-03	1.03E-02	1.42E-02	1.83E-02	1.99E-02	1.84E-02	1.50E-02	1.03E-02	6.39E-03	4.00E-03	2.82E-03	8.19E-03	1.89E-02	
Impulse (millisec*psi)	2.54	3.75	6.38	10.30	14.25	18.32	19.92	18.36	15.00	10.32	6.39	4.00	2.82	8.19	18.85	
Time						Pressure						Impulse				
Signature Sensor		1034.5	Microseconds			Signature Sensor		154.784				Signature Sensor		19.92		
	Dif	Average	Dif				Dif	Average	Dif				Dif	Average	Dif	
Channel 6	7.5	6.5	5.5	Channel 8		Channel 6	87.20%	85.08%	82.95%	Channel 8		Channel 6	91.98%	92.08%	92.18%	Channel 8
Channel 5	34	31.5	29	Channel 9		Channel 5	67.81%	69.88%	71.95%	Channel 9		Channel 5	71.53%	73.43%	75.33%	Channel 9
Channel 4	63.5	64	64.5	Channel 10		Channel 4	50.91%	48.01%	45.11%	Channel 10		Channel 4	51.70%	51.76%	51.81%	Channel 10
Channel 3	87.5	96.5	105.5	Channel 11		Channel 3	32.90%	30.94%	28.97%	Channel 11		Channel 3	32.01%	32.04%	32.06%	Channel 11
Channel 2	163.5	147.5	131.5	Channel 12		Channel 2	19.89%	21.27%	22.66%	Channel 12		Channel 2	18.84%	19.46%	20.09%	Channel 12
Channel 1	216.5	213.5	210.5	Channel 13		Channel 1	14.78%	14.97%	15.16%	Channel 13		Channel 1	12.75%	13.46%	14.17%	Channel 13
Channel 14		414	Microseconds			Channel 14		13.17%				Channel 14		41.14%		
Flat Plate		-0.5	Microseconds			Flat Plate		98.03%				Flat Plate		94.66%		

Echo 2 - Repetition A - Pipe 3: Single 0.6 lb Charge

	CH 1 [PSI]	CH 2 [PSI]	CH 3 [PSI]	CH 4 [PSI]	CH 5 [PSI]	CH 6 [PSI]	CH 7 [PSI]	CH 8 [PSI]	CH 9 [PSI]	CH 10 [PSI]	CH 11 [PSI]	CH 12 [PSI]	CH 13 [PSI]	CH 14 [PSI]	CH 15 [PSI]	CH 16 [V]
	22.88	30.79	50.93	78.8	104.96	134.98	154.78	128.39	111.36	69.82	44.84	35.07	23.47	20.39	151.73	0.08
Initial Pressure Arival	0.001251	0.001198	0.001122	0.001098	0.001069	0.001042	0.001035	0.00104	0.001064	0.001099	0.00114	0.001166	0.001245	0.0014485	0.0010205	
Time in microsec	1251	1198	1122	1098	1068.5	1042	1034.5	1040	1063.5	1099	1140	1166	1245	1448.5	1020.5	
Min time	1020.5															
Max time	1448.5															
arival spread	428															
max time duration	567.00	621.00	813.00	921.00	1,042.00	1,098.00	1,127.00	1,061.00	1,054.00	993.00	730.00	656.00	532.00	1,236.00	864.00	
	0.001534	0.001508	0.001528	0.001558	0.001589	0.001591	0.001598	0.00157	0.00159	0.001595	0.0015045	0.0014935	0.0015105	0.0023745	0.001452	
Time in microsec	1534	1508	1528	1558	1589	1590.5	1597.5	1570	1590	1595	1504.5	1493.5	1510.5	2374.5	1452	
Duration	283	310	406	460	520.5	548.5	563	530	526.5	496	364.5	327.5	265.5	926	431.5	
Impulse (sec*psi)	2.54E-03	2.54E-03	3.75E-03	1.03E-02	1.42E-02	1.83E-02	1.99E-02	1.83E-02	1.50E-02	1.03E-02	6.39E-03	3.99E-03	2.82E-03	8.21E-03	2.03E-02	
Impulse (millisec*psi)	2.54	2.54	3.75	10.30	14.25	18.32	19.92	18.33	15.00	10.32	6.39	3.99	2.82	8.21	20.27	

Time					Pressure					Impulse				
Signature Sensor		1034.5	Microseconds		Signature Sensor		154.78			Signature Sensor		19.92		
	Dif	Average	Dif			Dif	Average	Dif			Dif	Average	Dif	
Channel 6	7.5	6.5	5.5	Channel 8	Channel 6	87.21%	85.08%	82.95%	Channel 8	Channel 6	91.98%	92.01%	92.05%	Channel 8
Channel 5	34	31.5	29	Channel 9	Channel 5	67.81%	69.88%	71.95%	Channel 9	Channel 5	71.53%	73.43%	75.33%	Channel 9
Channel 4	63.5	64	64.5	Channel 10	Channel 4	50.91%	48.01%	45.11%	Channel 10	Channel 4	51.70%	51.76%	51.81%	Channel 10
Channel 3	87.5	96.5	105.5	Channel 11	Channel 3	32.90%	30.94%	28.97%	Channel 11	Channel 3	18.84%	25.45%	32.06%	Channel 11
Channel 2	163.5	147.5	131.5	Channel 12	Channel 2	19.89%	21.28%	22.66%	Channel 12	Channel 2	12.75%	16.40%	20.05%	Channel 12
Channel 1	216.5	213.5	210.5	Channel 13	Channel 1	14.78%	14.97%	15.16%	Channel 13	Channel 1	12.75%	13.46%	14.17%	Channel 13
Channel 14		414	Microseconds		Channel 14		13.17%			Channel 14		41.21%		
Flat Plate		-14	Microseconds		Flat Plate		98.03%			Flat Plate		101.77%		

Echo 2 - Repetition B - Pipe 3: Single 0.6 lb Charge

	CH 1 [PSI]	CH 2 [PSI]	CH 3 [PSI]	CH 4 [PSI]	CH 5 [PSI]	CH 6 [PSI]	CH 7 [PSI]	CH 8 [PSI]	CH 9 [PSI]	CH 10 [PSI	CH 11 [PSI	CH 12 [PSI	CH 13 [PSI	CH 14 [PSI	CH 15 [PSI	CH 16 [V]
	21.979	29.7069	49.3663	79.7335	110.747	130.538	144.871	126.204	115.827	84.1437	54.0608	41.5528	27.3561	20.043	90.5483	5.00641
Initial Pressure Arival	0.001242	0.001189	0.001117	0.001094	0.001063	0.001032	0.001028	0.001035	0.001057	0.00109	0.001127	0.00116	0.001226	0.001426	0.000928	
Time in microsec	1242	1189	1117	1093.5	1063	1032	1028	1034.5	1056.5	1089.5	1127	1160	1225.5	1425.5	927.5	
Min time	927.5															
Max time	1425.5															
arival spread	498															
max time duration	609.00	693.00	778.00	1,042.00	1,086.00	1,179.00	1,173.00	1,093.00	1,101.00	1,024.00	753.00	655.00	519.00	1,780.00	1,041.00	
	0.001546	0.001535	0.001506	0.001614	0.001606	0.001621	0.001614	0.001581	0.001607	0.001601	0.001503	0.001487	0.001485	0.002315	0.001448	
Time in microsec	1546	1535	1505.5	1614	1605.5	1621	1614	1580.5	1606.5	1601	1503	1487	1484.5	2315	1447.5	
Duration	304	346	388.5	520.5	542.5	589	586	546	550	511.5	376	327	259	889.5	520	
Impulse (sec*psi)	2.59E-03	2.59E-03	3.90E-03	1.01E-02	1.41E-02	1.79E-02	1.92E-02	1.75E-02	1.45E-02	1.04E-02	6.69E-03	4.43E-03	2.91E-03	8.08E-03	1.39E-02	
Impulse (millisec*psi)	2.59	2.59	3.90	10.15	14.08	17.92	19.16	17.47	14.54	10.39	6.69	4.43	2.91	8.08	13.90	
Time						Pressure						Impulse				
Signature Sensor		1028	Microseconds			Signature Sensor		144.871				Signature Sensor		19.16		
	Dif	Average	Dif				Dif	Average	Dif				Dif	Average	Dif	
Channel 6	4	5.25	6.5	Channel 8		Channel 6	90.11%	88.61%	87.11%	Channel 8		Channel 6	93.54%	92.35%	91.17%	Channel 8
Channel 5	35	31.75	28.5	Channel 9		Channel 5	76.45%	78.20%	79.95%	Channel 9		Channel 5	73.51%	74.70%	75.90%	Channel 9
Channel 4	65.5	63.5	61.5	Channel 10		Channel 4	55.04%	56.56%	58.08%	Channel 10		Channel 4	52.97%	53.59%	54.21%	Channel 10
Channel 3	89	94	99	Channel 11		Channel 3	34.08%	35.70%	37.32%	Channel 11		Channel 3	20.35%	27.63%	34.91%	Channel 11
Channel 2	161	146.5	132	Channel 12		Channel 2	20.51%	24.59%	28.68%	Channel 12		Channel 2	13.53%	18.33%	23.14%	Channel 12
Channel 1	214	205.75	197.5	Channel 13		Channel 1	15.17%	17.03%	18.88%	Channel 13		Channel 1	13.53%	14.35%	15.18%	Channel 13
Channel 14		397.5	Microseconds			Channel 14		13.84%				Channel 14		42.19%		
Flat Plate		-100.5	Microseconds			Flat Plate		62.50%				Flat Plate		72.55%		

Echo 2 - Repetition C - Pipe 3: Single 0.6 lb Charge

	CH 1 [PSI]	CH 2 [PSI]	CH 3 [PSI]	CH 4 [PSI]	CH 5 [PSI]	CH 6 [PSI]	CH 7 [PSI]	CH 8 [PSI]	CH 9 [PSI]	CH 10 [PSI]	CH 11 [PSI]	CH 12 [PSI]	CH 13 [PSI]	CH 14 [PSI]	CH 15 [PSI]	CH 16 [V]
	21.267	29.6508	51.1445	82.1233	117.562	140.574	148.373	126.414	109.369	72.1771	44.7554	35.5342	23.3902	20.626	124.202	5.00626
Initial Pressure Arival	0.001221	0.001168	0.001099	0.001043	0.001027	0.001021	0.001012	0.001018	0.001026	0.0010795	0.001119	0.0011425	0.0012255	0.0014145	0.001048	
Time in microsec	1220.5	1167.5	1098.5	1042.5	1026.5	1020.5	1012	1018	1025.5	1079.5	1119	1142.5	1225.5	1414.5	1048	
Min time	1012															
Max time	1414.5															
arival spread	402.5															
max time duration	593.00	716.00	901.00	1,090.00	1,125.00	1,098.00	1,171.00	1,096.00	1,129.00	1,033.00	923.00	697.00	571.00	1,890.00	950.00	
	0.001517	0.001525	0.001549	0.001587	0.001589	0.001569	0.001597	0.0015655	0.00159	0.0015955	0.00158	0.0014905	0.0015105	0.002359	0.0015225	
Time in microsec	1516.5	1525	1548.5	1587	1588.5	1569	1597	1565.5	1589.5	1595.5	1580	1490.5	1510.5	2359	1522.5	
Duration	296	357.5	450	544.5	562	548.5	585	547.5	564	516	461	348	285	944.5	474.5	
Impulse (sec*psi)	2.60E-03	2.60E-03	3.95E-03	1.02E-02	1.42E-02	1.82E-02	1.95E-02	1.80E-02	1.48E-02	1.03E-02	6.34E-03	3.97E-03	2.71E-03	8.27E-03	1.85E-02	
Impulse (millisec*psi)	2.60	2.60	3.95	10.16	14.22	18.15	19.55	18.05	14.80	10.30	6.34	3.97	2.71	8.27	18.52	

Time					Pressure					Impulse				
Signature Sensor		1012	Microseconds		Signature Sensor		148.373			Signature Sensor		19.55		
	Dif	Average	Dif			Dif	Average	Dif			Dif	Average	Dif	
Channel 6	8.5	7.25	6	Channel 8	Channel 6	94.74%	89.97%	85.20%	Channel 8	Channel 6	92.86%	92.59%	92.33%	Channel 8
Channel 5	14.5	14	13.5	Channel 9	Channel 5	79.23%	76.47%	73.71%	Channel 9	Channel 5	72.73%	74.22%	75.70%	Channel 9
Channel 4	30.5	49	67.5	Channel 10	Channel 4	55.35%	52.00%	48.65%	Channel 10	Channel 4	51.95%	52.33%	52.70%	Channel 10
Channel 3	86.5	96.75	107	Channel 11	Channel 3	34.47%	32.32%	30.16%	Channel 11	Channel 3	20.19%	26.31%	32.43%	Channel 11
Channel 2	155.5	143	130.5	Channel 12	Channel 2	19.98%	21.97%	23.95%	Channel 12	Channel 2	13.30%	16.80%	20.30%	Channel 12
Channel 1	208.5	211	213.5	Channel 13	Channel 1	14.33%	15.05%	15.76%	Channel 13	Channel 1	13.30%	13.59%	13.87%	Channel 13
Channel 14		402.5	Microseconds		Channel 14		13.90%			Channel 14		42.32%		
Flat Plate		36	Microseconds		Flat Plate		83.71%			Flat Plate		94.73%		

REFERENCES

A. T. Bourgoyne, K. K. Millheim, M. E. Chenevert, F. S. Young Jr. (1986). *Applied Drilling Engineering.* Richardson, Texas: Society of Petroleum Engineers.

Anderson & Emeritus. (2012). *Introduction to flight.* New York: McGraw-Hill.

B. Conway, and J. Holland. (2000, 02 21). *Pipe-collapse issues provide economic opportunities*. Retrieved from Oil and Gas Journal: http://www.ogj.com/articles/print/volume-98/issue-8/special-report/pipe-collapse-issues-provide-economic-opportunities.html

Baird, J. (2012). Symmetry Plane. (P. Mulligan, Interviewer)

Baird, J. (2016). Shockwaves. (P. Mulligan, Interviewer)

Ben-Dor, G. (1950). *Shockwave Reflection Phenomena.* New York: Springer.

Bulson, P. S. (1997). *Explosive Loading of Engineering Structures.* London, UK: E & FN Spon.

Busco, M. (1970). Optical Properties of Detonation Waves (Optics of Explosives). *International Symposium on Detonation* (pp. 513-522). Pasadena, California: Office of Naval Research - Department of the Navy.

C. T. Crowe, D. F. Elger, and J.A. Roberson. (2005). *Engineering Fluid Mechanics.* Danvers: John Wiley and Sons, Inc.

CMV Technologies, L. (2011). *Blast Calc*. Retrieved from CMV Tehnologies, LLC: http://www.cmv-tech.com/blastcalc.html

Cook, M. A. (1958). *The Science of High Explosives.* Huntington, N.Y.: Robert E. Krieger Publishing CO. INC.

Cooper, P. W. (1996). *Explosive Engineering.* New York: Wiley-VCH, INC.

D. B. Moore & T. C. Poulter. (1956). Mechanism of Wave Shaping Technques. *Detonation Wave Shaping Conference* (pp. 23-44). Pasadena, California: Picatinny Arsenal.

Department of the Army. (1974). *Engineering Design Handbook: Explosions in Air - Part 1.* Alexandria, Virginia: National Technical Information Service U.S. Department of Commerce.

Dewey, J. M. (2010). The Shape of the Blast Wave: Studies of the Friedlander Equation. *Miltary Aspects of Blast and Shock.* Jarusalem, Israel.

Glasstone, S. (1962). *The Effects of Nuclear Weapons.* Washington D.C.: United States Atomic Energy Commission.

Grulke E. A., Lusk B. T., Perry K. A. Hoffman J. M., and Saito K. (2006). *Development of Design Tools for Blast Mitigation by Layered Aluminum Mesh.*

Haxton & Haywood. (1986). Linear Elastic Response of A Ring Stiffened Cylinder to Underwater Explosion Loading. *Andvances in Marine Structures* (pp. 366-388). Dunfermline, Scotland: Elsevier Applied Science.

Henrych, J. (1979). *The Dynamics of Explosion and Its Uses.* New York: Elsevier Scientific Publishing.

Hoffman J., L. B. (2013). Shock Tube Detonator Shelf Life in Relation to Timing Accuracy. *International Society of Explosive Engineers 39th Annual Conference on Explosives and Blasting.* International Society of Explosive Engineers.

Kenward, M. (. (1986, April 17th). Explosive Tape for Tailored Demolition. *New Scientist*, p. 28.

LP, E. S. (2014). *Deepwater Horizon Blowout Preventer Failure Aalysis Report.* Engineering Experts.

M. D. Netherton & M. G. Stewart. (2009). The Effects of Explosive Blast Load Variability on Safety Hazard and Damage Risks for Monolithic Window Glazing. *International Journal of Impact Engineering*, 1346-1354.

MBI. (2016, January 25th). *Blasts / Explosions*. Retrieved from MBI Protective Building Systems: http://wm.mbindustries.com/what-we-protect-against/85-2/

Michael M Swisdak, J. (1975). *Explosion Effects and Properties Part 1 - Explosions in Air.* White Oak, Silver Spring, Maryland: Naval Surface Weapons Center.

Microsystems, L. f. (2016, May 5th). *Laboratory for Microsystems*. Retrieved from Acoustic Bubbles: http://www.labformicrosystems.com/micromechanics.html

Montgomery, D. C. (2009). *Design and Analysis of Experiments 7th Edition.* New York City, NY: John Wiley and Sons, Inc.

Needham, C. E. (2010). *Blast Waves.* Albuquerque, NM: Springer.

PCB Piezotronics. (2011). *Pressure Sensor 102B*. Retrieved from PCB Piezotronics: http://www.pcb.com/contentstore/docs/PCB_Corporate/Pressure/Products/Drawing/PDF/40707-B.pdf

Pope, A. (2013, October). *AJP Excel Information*. Retrieved from Polar Plot 2 add-in: http://www.andypope.info/charts/polarplot3.htm

R. Farnfield, W. J. Birch and G.D Rangel-Sharp. (2009). Accurate Delay Detonation with Shock-tube. *Proceedings of the International Society of Explosives Engineers. Conferences on Explosives and Blasting Technique*. International Society of Explosives Engineers.

Rinehart J. S., & Pearson J. (1963). *Explosive Working of Metals.* New York: The Macmillan Company.

Roark R. J. and Young W. C. (2012). *Formulas for Stress and Strain.* St. Louis: McGraw-Hill Book Company.

S. J. Smith, D. M. McCann, M. E. Kamara. (2009). *Blast Resistant Design Guide for Reinforced Concrete Structures.* Skikie, IL: Portland Cement Association.

S. Neddermeyer, H. Bradner, & J. F. Streib. (1943). *The Collapse of Hollow Steel Cylinders By High Explosives.* U. S. Atomic Energy Commission.

Shahriar, A. (2015). *Study and Simulation of Inviscid Supersonic Flow over a Bluff Body.* Bangladesh: Department of Mechanical Engineering - Chittagong University of Engineering & Technology.

Shanes, A. M. (1950). *Measurement on Pressure Waves in Region of Two Obliquely Intersecting Underwater Shock Waves.* Massachusetts: Office of Naval Research - Department of the Navy.

Silva L. L. & Netto T. . (2010). On the Dynamic Collapse of Cylindrical SHells Under Hydrostatic and Impulsive Pressure Loadings.

Smithsonian Ocean Protal. (2015). Retrieved from http://ocean.si.edu/gulf-oil-spill

Stiehr, J. F. (2011). *ISEE Blasters' Handbook.* Cleveland, Ohio: International Society of Explosive Engineers.

Sunden, B. (2016). *Thermopedia*. Retrieved from Crossflow over tubes: http://www.thermopedia.com/content/1216/

Swisdak, M. (1975). *Explosion Effects and Properties Part 1 - Explosions in Air.* White Oak, Silver Spring, Maryland: Naval Surface Weapons Center.

Teledyne. (2015). *RP-80 EBW Detonator* . Retrieved from Teledyne Rise: http://www.teledynerisi.com/products/0products_1ebw_page23.asp

W. P. Walters, J. A. Zukas. (1989). *Fundimentals of Shaped Charges.* New York: Wiley-Interscience.

Wall Street Journal. (2015, July 2). Retrieved from BP Agrees to Pay $18.7 Billion to Settle Deepwater Horizon Oil Spill Claims: http://www.wsj.com/articles/bp-agrees-to-pay-18-7-billion-to-settle-deepwater-horizon-oil-spill-claims-1435842739

Walters W. P. & Zukas J. A. (1989). *Fundimentals of Shaped Charges.* New York: Wiley-Interscience.

Walters, P. (2012). Blast Pressure Measurments. (P. Mulligan, Interviewer)

Worsey, P. (2005). Munroe Effect. (P. Mulligan, Interviewer)

Worsey, P. (2012). Explosive Lenses. (P. Mulligan, Interviewer)

VITA

Phillip Russell Mulligan was born in Olin, Iowa. He attended elementary school in the Olin Consolidated School District and graduated from Olin High School in June 2003. He entered the University of Missouri, Rolla in August 2003. Phillip received a degree of Bachelor of Science in Mining Engineering, with a minor in Explosives Engineering and Business from the University of Missouri-Rolla, in June 2008. Phillip received his Masters of Science Degree in Explosives Engineering from Missouri University of Science and Technology, May 2011. In June of 2011, Phillip began his Doctorate Degree in Explosive Engineering at Missouri University of Science and Technology. Phillip received his Doctorate of Philosophy degree in July 2016.

Publications

- **Mulligan P**., Ward A., Shirley A., 2016 "Novel Impulse Instrumentation of Buried Explosive Charges", Proceedings of the International Society of Explosive Engineers 42nd Annual Conference on Explosives and Blasting Technique.
- Hoffman J., Lusk B., and **Mulligan P**., 2013, "Shock Tube Detonator Shelf Life in Relation to Timing Accuracy," Proceedings of the International Society of Explosive Engineers 39th Annual Conference on Explosives and Blasting Technique
- **Mulligan P.,** and Baird J., 2013, "Mitigating Oil Disasters Via Underwater Explosive Lensing: A Preliminary Study," Proceedings of the International Society of Explosive Engineers 39th Annual Conference on Explosives and Blasting Technique
- Phelps K.., Nolan D., **Mulligan P.**, Baird J., 2013 "New Methodology in Measuring Experimental Results of Linear Shaped Charges Using Digital Software" Proceedings of the International Society of Explosive Engineers 39th Annual Conference on Explosives and Blasting Technique
- Phelps K.., Nolan D., **Mulligan P.**, Baird J., 2013 "Performance Evaluation and Effects of Standoff on 10,500 grain per foot Linear Shaped Charge" *Proceedings of the International Society of Explosive Engineers 39th Annual Conference on Explosives and Blasting Technique*
- Bookout L., **Mulligan P**., and Baird J., 2012, "Explosively Formed Projectile Soft-recovery Force Analysis" *Proceedings of the 12th Hypervelocity Impact Symposium*
- **Mulligan P**., Baird J., and Hoffman J., 2011, "The Effects of the Flyer Plate's Radius of Curvature on the Performance of an Explosively Formed Projectiles," *Proceedings of the* 17th *American Physic Society's Topical Group on Shock, Compression and Condensed Matter*
- **Mulligan P**. and Baird J., 2010, "The Effects of Run-up on Explosively Formed Projectiles" *Proceedings of the International Society of Explosive Engineers 36th Annual Conference on Explosives and Blasting Technique*